

**COMPREHENSIVE CONDITION SURVEY
AND
STORM WAVES, CIRCULATION, AND SEDIMENTATION STUDY
DANA POINT HARBOR, CALIFORNIA
FINAL REPORT**



**PREPARED FOR:
U.S. Army Corps of Engineers
Los Angeles District**



**PREPARED BY:
US Army Engineer Research & Development Center
And
Noble Consultants, Inc.**

July 2011

**COMPREHENSIVE CONDITION SURVEY
AND
STORM WAVES, CIRCULATION, AND SEDIMENTATION STUDY
DANA POINT HARBOR, CALIFORNIA**

Table of Contents

1.0	INTRODUCTION.....	1-1
1.1	Purpose and Scope	1-2
1.2	Prior Studies	1-3
2.0	PHYSICAL CONDITIONS.....	2-1
2.1	Physiographic Setting.....	2-1
2.2	Bathymetric & LiDAR Survey.....	2-1
2.3	Present-Day Breakwater Conditions.....	2-3
2.4	ADCP Current Measurements	2-4
2.4.1	Field Work.....	2-4
2.4.2	Data Process and Results.....	2-4
3.0	CMS-WAVE MODEL SIMULATIONS	3-1
3.1	Introduction.....	3-1
3.2	CMS-Wave Model Description.....	3-1
3.3	CMS-Wave Model Improvement.....	3-2
3.4	CMS-Wave Model Calibration.....	3-2
3.5	Design Storm Wave Criteria at Dana Point Harbor.....	3-5
3.5.1	General Wave Climatic Conditions.....	3-5
3.5.2	Deep Water Wave Climate.....	3-7
3.5.3	Wave Transformation.....	3-8
3.5.4	Hindcast Validation.....	3-9
3.5.5	Historical Storm Events.....	3-10
3.5.6	Storm Wave Characteristics at Dana Point Harbor	3-12
4.0	CMS-FLOW SIMULATIONS	4-1
4.1	Model Description	4-1
4.2	CMS-Flow Model Improvement	4-2
4.3	CMS-Flow Calibration and Sensitivity Analysis.....	4-3
4.4	Historical Maintenance Dredging	4-6
4.5	Simulation of Morphologic Change.....	4-7
5.0	PARTICLE TRACKING MODELING	5-1
5.1	CMS-PTM Description	5-1
5.2	CMS-PTM Simulations.....	5-2
5.3	Residence Times.....	5-3
6.0	SUMMARY AND CONCLUSIONS.....	6-1
6.1	Conditions of Breakwaters.....	6-1
6.2	Flow Field Conditions	6-2
6.3	Improvement of CMS Models	6-2
6.4	Storm Wave Characteristics	6-3
6.5	Sedimentation and Water Circulation Patterns	6-3
7.0	REFERENCES	7-1

List of Tables

Table 2-1. ADCP Locations and Depths	2-4
Table 2-2. ADCP Measurement Setup.....	2-5
Table 3-1. Calibrated Model Parameters for CMS-Wave.....	3-4
Table 3-2. Comparison of Calculated Wave Height at Outside ADCP	3-4
Table 3-3. Selected Historical Storm Wave Events.....	3-11
Table 3-4. Estimated Extreme Return Wave Heights.....	3-13
Table 4-1. Calibrated Structure Parameters and Coefficients for CMS-Flow	4-3
Table 4-2. Dredging Quantities for West Breakwater Sediment Deposition.....	4-7
Table 4-3. Comparison of Computed Annual Sedimentation	4-8
Table 5-1. Number of Particles Leaving Dana Point Harbor after Released at Baby Beach.	5-3

List of Figures

Figure 1-1	Location Map
Figure 2-1	Bathymetric Survey Area
Figure 2-2	Integration of LiDAR Scanner and Swath Bathymetry Systems
Figure 2-3	Bathymetric Contour Map
Figure 2-4	3-D Images of LiDAR Survey
Figure 2-5	Dislodged Stones at West Breakwater
Figure 2-6	Displaced Stone near Sta. 15+54
Figure 2-7	Displaced Stone at Head of West Breakwater
Figure 2-8	East Breakwater
Figure 2-9	Dislodged Stones at East Breakwater
Figure 2-10	Displaced Stone near Structure Head of East Breakwater
Figure 2-11	ADCP Gage Locations
Figure 2-12	Deployment of ADCP Instruments
Figure 2-13	Retrieval of ADCP Instruments
Figure 2-14	Unfiltered Current Profiles Collected at Inside Gage
Figure 2-15	Unfiltered Current Profiles Collected at Outside Gage
Figure 2-16	Filtered Current Profiles at Inside Gage
Figure 2-17	Filtered Current Profiles at Outside Gage
Figure 2-18	Week 1 – Bin 1 Current Measurements at Inside Gage
Figure 2-19	Week 1 – Bin 2 Current Measurements at Inside Gage
Figure 2-20	Week 1 – Bin 3 Current Measurements at Inside Gage
Figure 2-21	Week 1 – Bin 4 Current Measurements at Inside Gage
Figure 2-22	Week 1 – Bin 1 Current Measurements at Outside Gage
Figure 2-23	Week 1 – Bin 2 Current Measurements at Outside Gage
Figure 2-24	Week 1 – Bin 3 Current Measurements at Outside Gage
Figure 2-25	Week 1 – Bin 4 Current Measurements at Outside Gage
Figure 2-26	Week 1 – Bin 5 Current Measurements at Outside Gage

- Figure 2-27 Week 1 – Bin 6 Current Measurements at Outside Gage
- Figure 2-28 Week 1 – Bin 7 Current Measurements at Outside Gage
- Figure 2-29 Current Roses of Inside ADCP during Ebb Tide on November 22, 2009
- Figure 2-30 Current Roses of Inside ADCP during Flood Tide on November 22, 2009
- Figure 2-31 Current Roses of Outside ADCP during Ebb Tide on November 22, 2009
- Figure 2-32 Current Roses of Outside ADCP during Flood Tide on November 22, 2009
- Figure 2-33 Current Roses of Inside ADCP during Ebb Tide on January 5, 2010
- Figure 2-34 Current Roses of Inside ADCP during Flood Tide on January 5, 2010
- Figure 3-1 CMS-Wave Model Domain and Grid System
- Figure 3-2 CDIP 096 Wave and NOAA 9410660 Water Levels
- Figure 3-3 NDBC 46086 Wind Speed and Direction Information
- Figure 3-4 Comparison of Simulated and Measured Wave Parameters
- Figure 3-5 Comparison of Calculated Waves with and without Wind or Water Level Input
- Figure 3-6 Comparison of Calculated Waves with and without Wave Reflection or Bottom Friction
- Figure 3-7 Wave Data Station Locations
- Figure 3-8 Transformed Wave Data Station Locations
- Figure 3-9 Comparison of Significant Wave Heights from 2000 to 2008
- Figure 3-10 Scatter plot of Observed CDIP and Hindcast Significant Wave Heights
- Figure 3-11 Comparison of Significant Wave Heights during the Month of January, 2008
- Figure 3-12 CMS Observation Locations
- Figure 3-13 Maximum Significant Wave Heights during Storm Events at Locations 1, 2 & 3
- Figure 3-14 Maximum Significant Wave Heights during Storm Events at Locations 4, 5 & 6
- Figure 3-15 Deduced Extreme Wave Height Distribution at Location 1
- Figure 3-16 Deduced Extreme Wave Height Distribution at Location 2
- Figure 3-17 Deduced Extreme Wave Height Distribution at Location 3
- Figure 3-18 Deduced Extreme Wave Height Distribution at Location 4
- Figure 3-19 Deduced Extreme Wave Height Distribution at Location 5
- Figure 3-20 Deduced Extreme Wave Height Distribution at Location 6
- Figure 4-1 Sketch of Wave Transmission and Flow Penetration through a Permeable Structure
- Figure 4-2 Comparison of Simulated Water Surface Elevations and Measurements at the Outside ADCP Station
- Figure 4-3 Comparisons between Simulated and Measured Currents at the Inside and Outside ADCP Stations
- Figure 4-4 Simulated Depth Averaged Current Fields

- Figure 4-5 Wind Speed and Direction at Various Locations
- Figure 4-6 Comparisons between the Simulated and Measured Currents at the Inside and Outside ADCP Stations with Different Wind Forcing
- Figure 4-7 Comparisons between Simulated and Measured Currents at the Inside and Outside ADCP Stations with Different Permeable Breakwater Segments
- Figure 4-8 Simulated Depth Averaged Current Fields for Non-Permeable Breakwaters
- Figure 4-9 Simulated Depth Averaged Current Fields with a Developed Shoal
- Figure 4-10 Isopach of Shoal Formation from 2000-2002
- Figure 4-11 Isopach of Shoal Formation from 2002-2004
- Figure 4-12 Morphology Change at the End of a 10-day Simulation
- Figure 5-1 Water Circulation Patterns
- Figure 5-2 Local Sources of Particle Release in Dana Point Harbor
- Figure 5-3 Snapshot of Particle Distribution in Dana Point Harbor Two Days after the Particle Release at West Baby Beach
- Figure 5-4 Snapshot of Particle Distribution in Dana Point Harbor Two Days after the Particle Release at East Baby Beach
- Figure 5-5 Snapshot of Particle Distribution in Dana Point Harbor Two Days after the Particle Release in the Main Channel

1.0 INTRODUCTION

Dana Point Harbor is located in the City of Dana Point, midway between Los Angeles and San Diego, along the southern Orange County Coast of California, as depicted in **Figure 1-1**. The harbor consists of dual protective breakwaters (East and West Breakwaters), two recreational marina basins, a turning basin, two anchorage basins, a boat launch ramp area, a bathing beach, and several shallow-draft navigation channels. The development of Dana Point Harbor was initiated in 1949 and an optimal design plan was later selected after various design alternatives were formulated and evaluated. Construction of the dual breakwaters at Dana Point Harbor commenced in 1963 and was completed in 1968. The harbor operation for boat occupation and recreational purpose began after the completion of channel and basin dredging in 1970. **Table 1-1** presents the physical dimension of the dual protective breakwaters as well as various project depths in the channels and basins.

Table 1-1. Physical Dimension of Breakwaters and Project Depths at Dana Point Harbor

<i>Parameter</i>	<i>Dimension (m, (ft))</i>
<i>East Breakwater</i>	
Length	686 m (2,250 ft)
Crest Width	4.3 m (14 ft)
Crest Elevation	+4.3 m, MLLW (+14 ft, MLLW)
<i>West Breakwater</i>	
Length	1,676 m (5,500 ft)
Crest Width	4.9 m (16 ft)
Crest Elevation	+5.5 m, MLLW (+18 ft, MLLW)
<i>Project Depth</i>	
Entrance Channel	-6.0 & -4.6 m, MLLW (-20 & -15 ft, MLLW)
Main Channel	-4.6 m, MLLW (-15 ft, MLLW)
West Channel & Turning Basin	-3 m, MLLW (-10 ft, MLLW)
East Channel	-4.6 & -3.6 m, MLLW (-15 & -12 ft, MLLW)
Boat Anchorage Areas	-4.6 & -3.6 m, MLLW (-15 & -12 ft, MLLW)

At the time of construction, both the East and West Breakwaters were designed as a “semi-permeable” structure as comprised of multiple layers of riprap stones without an impermeable core layer. The weight of riprap stones in the outer layers range from 6 tons at the landward end to as heavy as 20 tons in the structure head area. Small voids were left intentionally during stone placement to allow currents partially flowing through the breakwaters, thereby promoting better water circulation within the harbor.

Sediment began to seep through the West Breakwater in the 1980's and, as a consequence, three maintenance dredging activities have been conducted by the County of Orange to remove sand material that has accumulated on the lee of the West Breakwater in the last two decades. The increased rate of shoaling in recent years necessitates a better understanding of the water and sediment exchange throughout the harbor and permeable breakwaters with specific interest on the physical processes that occur across the West Breakwater.

In addition, Dana Point Harbor was described to be "self-cleaning", defined as receiving sufficient circulation to prevent stagnation of the water within the harbor. However, since its construction, water quality issues have been regularly observed at Baby Beach located on the northwest corner of the harbor (see Figure 1-1). Several studies and field data collection have been performed to characterize the water circulation pattern and explore mitigation measures to improve the water quality, particularly at Baby Beach (SAIC, 2002 & 2003). Various mitigation measures, such as diversion of storm drain, installation of bird exclusion fencing and bird-proof trash cans, to limit sources of bacteria contamination, have been implemented that proved to be effective in significantly reducing the posting days of beach closure at Baby Beach. Nevertheless, a better understanding of water circulation within the harbor will allow for the formulation of a permanent measure to enhance the water quality in the Baby Beach area.

1.1 Purpose and Scope

The purpose of this study is 1) to conduct a comprehensive condition survey of the two breakwaters and assess the present-day structure conditions and 2) to investigate the permeability of the breakwaters via field data collection and numerical simulations. The investigation includes an assessment of the wave transmission, flow, and sediment seepage through the West Breakwater, which results in a sand shoal formed on the lee side of the West Breakwater, as well as an evaluation of water circulation pattern within the harbor, particularly in the Baby Beach area.

As part of this study, the existing Coastal Modeling System (CMS) that includes three major components of WAVE, FLOW and Partical Tracking Model (PTM) were modified and improved to depict the specific physical process of wave transmission, flow, and sediment seepage through the existing semi-permeable breakwater configuration. Using the CMS, the study also assessed the water circulation pattern within the harbor, particularly at Baby Beach. In

addition, the study applies the present-day engineering standards to characterize the oceanographic conditions at the breakwaters, based on historical storm events, and subsequently update the previously-established design criteria.

Specific tasks that were performed in this study include the following:

- A hydrographic survey using a multi-beam sonar to collect bathymetric data and to examine the underwater portion of the breakwater conditions, a LiDAR survey using a laser system for the breakwater conditions above the water level, and a visual inspection of the existing breakwater.
- An 8-week field data collection to measure currents and waves using Acoustic Doppler Current Profilers (ADCP) instruments.
- Improvement of the CMS to enhance the model capability in characterizing the permeability and functionality of breakwaters.
- Updating of oceanographic conditions for Dana Point Harbor, including estimates of the extreme design wave heights (e.g. 50 and 100-year return periods) at various locations along the breakwaters.
- Numerical modeling to identify the water circulation pattern within the harbor and characterize sediment seepage through the existing semi-permeable breakwaters.

1.2 Prior Studies

Comprehensive Condition Survey, Dana Point Harbor (USACE-LAD, 1991)

A comprehensive condition survey report was prepared by the U.S. Army Engineer District, Los Angeles (USACE-LAD), in 1991. The findings from that study concluded:

- The East Breakwater remained in excellent design condition.
- The West Breakwater had two areas showing displaced armor stones that did not warrant immediate corrective actions at that time, as both areas appeared to be functioning as designed.
- A recommendation of annual monitoring and a repeated comprehensive condition survey in 5-10 years was made.

Evaluation Studies of Bacteriological Data and Water Circulation at Baby Beach, Dana Point Harbor (SAIC, 2002-2003)

Between 2002 and 2003, a series of five (5) reports were prepared by Science Applications International Corporation (SAIC) for or in conjunction with the County of Orange Public Facilities & Resources Department (PFRD). These reports, as listed below, sought to understand the water circulation issues and related beach closures that were observed at Baby Beach.

- *Baby Beach Circulation Study Sampling and Analysis Plan (September 2002)*
- *Data Mining Task for State of the Beach Report: Evaluation of Bacteriological Data and Associated Parameters for Baby Beach (January 2003a)*
- *Baby Beach Circulation Study Final Report (March 2003b)*
- *Baby Beach Bacteriological Special Studies Report (June 2003c)*
- *State of the Beach Report, Baby Beach Region (June 2003d)*

The general findings from the abovementioned reports included the following items:

- Sources of the bacteria are limited to (a) contaminated discharges from storm drains, (b) bacteria resident (re-growth) in beach sediments, (c) weak near-beach water circulation, and (d) bacterial contamination from birds residing in the harbor area.
- Water circulation in the Baby Beach area is limited. Periodic sand replenishment efforts may be required at approximately 5-year intervals to replace the contaminated sediment.
- Storm drains are a significant source of contaminants. High bacteria levels occur inside and just outside of the storm drains, decreasing significantly within a short distance away from the pipe mouth. A practice on the storm drain plugging during the summer months showed a decrease in total coliform and fecal coliform but an increase in enterococcus. Measurable quantities of bacteria are able to enter the beachfront waters via leaks in the drain plugs and may be responsible for beach closure postings.

- Groundwater can potentially provide a transport mechanism for bacteria from various source locations into receiving waters.
- During low water levels, prevailing wind patterns appear to “pin” water within the beach area and create eddy currents near Baby Beach that may tend to restrict water flow.
- Bacteria concentrations in water vary widely at different times of the day.
- Boating activities do not contribute to a measurable quantity of bacteria. The number of beach users and turbidity do not correlate with the bacteria concentrations in the water. There is no known correlation with the tidal fluctuation; however, this could be due to field tests being conducted only once a week.
- A field study showed that large waves and swells along the outer breakwater can cause substantial disturbance and re-suspension of sediments in the Baby Beach vicinity. During this disturbance, sharp increases in bacterial concentrations were observed.
- An increase in water circulation can improve water quality near Baby Beach with greater dilution and mixing. A recommendation to conduct a demonstration project using mechanical means to improve water circulation in the Baby Beach area was made.

Circulation Improvement Pilot Project at Baby Beach, Dana Point, Final Report (Everest International Consultants, 2006)

A circulation improvement pilot project was conducted in 2005 by the collaborative efforts of the County of Orange and the City of Dana Point. The pilot project consisted of installing six circulation enhancing devices called Oloids in the immediate water zone at Baby Beach in June 2005. The layout of the Oloid deployment was chosen to enhance the existing flow conditions at Baby Beach. During this time, the adjacent storm drains were plugged to prevent various discharges onto the beach. The project was designed to provide field data in order to determine: 1) the capability of the Oloids to improve water circulation, 2) the change in bacteria levels due to water circulation improvement, and 3) the impact of the potential decrease in the bacteria levels to reduce the occurrence of the AB 411 violation. It is noted that AB 411 refers to California Assembly Bill No. 411 requiring the State Department of Health Service to adopt

regulations to test all beaches for total coliform, fecal coliform, enterococci, and streptococci bacteria, to establish minimum standards for these indicators, and to require posting at subject beaches whenever the established standards are violated. Specific findings and recommendations from this study are presented as follows:

- The current configuration of the Oloids improved water circulation in the alongshore direction from the west end towards the east, but was not effective in moving the water at the east end toward the deeper water region. Improvements in circulation were found at the west end, buoy line, and swim sampling locations. Only a slight improvement in water circulation occurred at the east end near the Youth Dock.
- Under the low wind conditions (say less than 6 mph), the Oloids can contribute more to water circulation at Baby Beach than the wind-induced drag.
- Bacteria levels at Baby Beach were low throughout the pilot project period. While there was a reduction in bacteria level at some sampling locations but not all of them during which the Oloids were operating, it is inconclusive that the reduction was due to the direct impact of the Oloids or a natural fluctuation in bacteria level.
- The limited data of bacteria sampling did not conclusively show the improvement of water quality due to the employment of the Oloids, even though the data did show some reduction in bacteria level at some locations where the Oloids were in operation.
- Winds may play a major role in water circulation at Baby Beach. It was suggested that wind data at Baby Beach be analyzed to understand the role of wind-induced circulation and mixing at Baby Beach.
- Investigation of the sources that contribute to high bacteria levels at Baby Beach should be continued and other control measures to prevent contaminated sources entering the harbor should be pursued.
- The Oloid design should be reviewed for compatibility in the marine environment.

Baby Beach in Dana Point Harbor, Orange County, Final Report, CBI Grant Nos. 19 and 260 (OC RDMD, 2006)

This report summarized a two-phase project for monitoring and improving the water quality at Baby Beach. Phase I consisted of the previously mentioned efforts by SAIC and the PFRD as described above. Also included in Phase I was the installation of a structural storm-water treatment (Stormceptor®) BMP in the site drainage system at Ocean Institute. Due to some constraints such as low hydraulic profile of the system and absence of a flap gate, the system's effectiveness was compromised approximately 45% of the days during the wet season.

Phase II of the project included the installation of sewer diversion for the Baby Beach storm drain system, bird exclusion fencing under the Baby Beach pier, and bird-proof trash cans on Baby Beach to discourage bird activity that could result in waste becoming a contaminated source. Six (6) regular sampling locations in the Baby Beach area were monitored and compared against AB411 bacteria standards. The following results were obtained from the Phase II study:

- Despite postings for various brief periods when the diversion was operational in the summer of 2005, available data demonstrates that Baby Beach was much cleaner in 2005 than in 2004. However, a direct impact associated with the diversion of the drainage water into the sanitary sewer system cannot be assessed due to the concurrent implementation of the Oloid circulation device during the pilot project period in the summer of 2005 and the extremely wet 2004-05 winter season.
- Installation of a new chain-link fence under the fishing pier proved to be effective in excluding pigeons or gulls staging underneath the pier. The bird proof trash cans also reduced the bird gathering in the Baby Beach area.

Regional Harbor Monitoring Program Pilot Project 2005-06 Final Report (Weston Solutions, Inc., 2006)

The Regional Harbor Monitoring Program (RHMP) was a comprehensive effort to survey the general water quality and condition of aquatic life in San Diego Bay, Mission Bay, Oceanside Harbor, and Dana Point Harbor. The Pilot Program for the RHMP is a scaled down version of the proposed RHMP that focused on a limited number of indicator measurements and samples in marinas

and freshwater influenced waters. Three sampling stations were located near boat slips within Dana Point Harbor. An additional station was located adjacent to a storm drain. Based on the data collected during the first year (i.e., 2005), the following general findings were established for all sampled areas:

- The copper concentration in the water column of the marinas is higher than those found in freshwater-influenced areas; and the proportion of marina samples with the elevated concentrations is higher than the historical measurements throughout the harbors.
- Concentrations of other metals and poly-aromatic hydrocarbons in the water column were below water quality objectives.
- All bacterial indicators were below the AB411 levels.
- Measurements of sediment quality were mixed as compared to the historical measurements.
- Biological indicators for benthic infauna show poor habitat quality in both the marinas and freshwater-influenced areas than was found historically throughout the harbors.
- Sediment toxicity test indicates healthier conditions than found historically.



Source: Google Earth (Dec 31, 2005)

Location Map



Figure 1-1

2.0 PHYSICAL CONDITIONS

2.1 Physiographic Setting

Dana Point Harbor is located in the City of Dana Point, Orange County, approximately midway between Los Angeles and San Diego (see Figure 1-1). The harbor is situated on an arc-shaped shoreline section of Capistrano Bay bound by the Dana Headlands on the northwest and Doheny State Beach to the south. The onshore features include the 55-meter (180-foot) high coastal bluffs that are landward of the harbor and the promontory at the base of the West Breakwater. The facilities located within the harbor are protected from ocean swells and storm wave attack by a pair of rubble mound breakwaters. The East Breakwater starting at Doheny Beach extends seawards for a total length of 686 meters (2,250 feet), while the West Breakwater originating from the Dana Cove Park stretches for 1,676 meters (5,500 feet) to the southwest toward the harbor entrance. The bedrock layers that make up the foundation of the breakwaters are part of a wave cut, submarine terrace as created by a combination of a rising sea level and an eroding shoreline. The foundation of the breakwaters consists of the hard bedrock overlaid with a thin lens of marine sands.

The harbor consists of two marina basins (the East and West Basins) containing a total of 2,500 slips for vessels of various sizes. Also included in the harbor are 50 guest slips for boats, a ten-lane launch ramp, a dry boat storage hoist, a fishing pier, a shipyard, a marine fuel dock, three yacht clubs and a commercial sports fishing operation that offers whale watching trips throughout the year (OC Parks, 2011). Recreational activities in the harbor also include an educational experience at the Orange County Ocean Institute, bathing and swimming at Baby Beach, and the water-related recreation for the youth at the County's Dana Point Harbor Youth and Group Facility.

2.2 Bathymetric & LiDAR Survey

A bathymetric & LiDAR (Light Detection and Ranging) survey was conducted in October 20-24, 2009 (Fugro, 2010) to collect basic physical data so that numerical modeling tasks can be performed to characterize the wave environment at breakwaters and water circulation within the harbor. The collected LiDAR and sonar data of the breakwaters allows for assessment of the present-day protective structure conditions. It is noted that the previous condition survey and an evaluation of the dual breakwaters were performed in 1991 (USACE-LAD, 1991). The bathymetric and side-scan sonar data below the water

surface and the LiDAR data above the water level were acquired along both sloping faces of the East and West Breakwaters extending out approximately 46 meters (150 feet) offshore on the ocean side and in the main navigation channels on the harbor side, as illustrated in **Figure 2-1**. In addition to these areas, the Baby Beach and the primary access channels within the marina basins were also surveyed.

The survey utilized the swath bathymetry system for the underwater portion and the laser scanning system for elevations above the water line, as illustrated in **Figure 2-2**. The Kongsberg GeoSwath Plus system, mounted to the port side of a survey vessel, was used to provide swath bathymetry coverage of the seabed. The system employed interferometric sonar, generating short pulses of acoustic energy which propagate out from the transducers at the speed of sound in water, insonifying a narrow strip of seabed perpendicular to the vessel track (Fugro, 2010). Horizontal positions were acquired with a POS MV and RTK system. A base station used for the survey control was set up on land to improve horizontal and vertical positioning. The survey control at the project site was logged based on the NAD83 coordinate system, California State Plane Zone 6 (i.e., the horizontal coordinates), and MLLW elevations (i.e., the vertical datum). The accuracy for the Swath bathymetry system is 0.5 meters (1.5 feet) horizontally and 0.2 meters (0.7 feet) vertically

An ILRIS 3D LiDAR Scanner system mounted on top of the vessel was utilized for obtaining above water data. The LiDAR system is an optical remote sensing technology that measures properties of scattered light to find range and/or other information of a distant target. The horizontal and vertical accuracies of the LiDAR data are approximately 0.15 meters (0.5 feet) and 0.07 meters (0.25 feet), respectively. Figure 2-2 provides a systematic sketch of the data integration that was obtained by these two measurement systems. A detailed description and survey operation of these two survey systems was presented in Fugro's survey report (Fugro, 2010).

The swath bathymetry and LiDAR data were integrated in the compilation of longitudinal profiles and cross sections along the breakwaters and bathymetric contour maps adjacent to the breakwaters and within the harbor. Topographic maps above the water line of the breakwaters and revetment along the island mole inside the harbor were also deduced from the collected data. **Figure 2-3** shows the contour plot of the breakwaters, main navigation channel and various areas within the harbor, while **Figure 2-4** illustrates the 3-D images generated from the LiDAR data at the head of the West Breakwater, the entrance area, and

in the areas of Baby Beach and Ocean Institute. A complete set of bathymetric plots including the side-scan sonar data are presented in Fugro's report (Fugro, 2010). The 2009 bathymetry combined with available bathymetric data in the nearshore region was then used to generate the modeling grid for numerical simulations to characterize the wave environment adjacent to the breakwaters and water circulation in the harbor.

2.3 Present-Day Breakwater Conditions

Since the completion of the harbor construction in 1970, the harbor only suffered damages once during the 1983 El Nino winter season when a cluster of major storms resulted in some damage to the West Breakwater from Sta. 0+61 to Sta. 3+51 (referenced to the meter unit) and from Sta. 3+51 to Sta. 7+01 as identified in Figure 2-3. The damaged areas that located on the ocean side were subsequently repaired in 1984. Another extreme storm event that occurred in January 1988 did not render any recorded damages to the protective breakwaters. A comprehensive condition survey consisting of the side-scan sonar, the image sonar profiling and topographic surveys and visual inspection was conducted in 1991. The field study indicated that the East Breakwater remained stable in excellent condition, while some armor stones were displaced on the seaward slope of the West Breakwater.

The present-day structure conditions of both breakwaters were examined via the processed 3-D LiDAR images with a visual confirmation in sections above the water line. At the West Breakwater, dislodged stones on the harbor side near Sta. 00+97 and Sta. 02+13 were detected below the water surface, as illustrated in **Figure 2-5**. This may be attributed to a slumping effect as a consequence of maintenance dredging in the past. In addition, some isolated armor stones above the water surface are also displaced from their original placement. **Figures 2-6** and **2-7** show the displaced stones at Sta. 15+54 and near the head of the West Breakwater. Nevertheless, the structure appears to function as originally designed to shelter the harbor facilities from west to northwest winter storm waves. At the East Breakwater, the structure remains intact and functions as a protective device for the harbor operation, as showing in **Figure 2-8**. However, some armor stones below the water surface on the harbor side appear to be dislodged from their original positions. **Figures 2-9** and **2-10** illustrate the processed 3-D images indicating the dislodged stones from Sta. 3+30 to 4+08 and near the head structure.

2.4 ADCP Current Measurements

Temporal currents were measured in the areas on both the harbor (inside) and ocean (outside) sides of the West Breakwater to provide the flow field information for the model calibration of the CMS. Directional wave data was also collected on the ocean side of the West Breakwater by the same outside Acoustic Doppler Current Profiler (ADCP). **Figure 2-11** shows the location map of two ADCPs that were deployed in Dana Point Harbor, while **Table 2-1** lists the coordinates of the deployed ADCPs and their respective depths.

Table 2-1. ADCP Locations and Depths

<i>Instrument ID</i>	<i>Coordinates</i>	<i>Depth (m, MLLW)</i>
Inside ADCP	N33°27'28.66",W117°42'12.28"	7.8
Outside ADCP	N33°27'25.46",W117°42'12.95"	8.4

2.4.1 Field Work

Two self-contained RDI Workhorse Sentinel 1200 kHz (RD-WHS 1200) ADCPs that have a typical depth range up to 13-16 meters (40-50 feet) for a vertical cell size of 0.5 meters (1.6 feet) were deployed on November 20, 2009 for approximately 8 weeks till January 15, 2010. A vessel named "Early Bird" equipped with an A-frame was used to carry and lower the ADCPs onto the sea floor. Prior to the deployment, divers were dispatched to inspect the sea floor in the pre-determined area and identify the appropriate location where the sea floor was flat for ADCP deployment. Each ADCP was mounted to a tripod, as illustrated in **Figure 2-12**. The tripod was anchored by a chain-link section weighed about 400 kilograms (880 lbs). The tripod was further secured on the bottom by three 10-meter (33-foot) ropes tied with metal rods that were nailed into the sea floor. **Table 2-2** presents the measurement setup of the ADCP. The two ADCPs were retrieved on January 15, 2010 using the same A-frame on the "Early Bird" vessel, as shown in **Figure 2-13**.

2.4.2 Data Process and Results

As described in Section 2.4.1, two ADCPs were deployed for eight (8) weeks from November 20, 2009 to January 15, 2010. However, the outside

ADCP collected only about one week of current and wave data as the instrument malfunctioned and failed to operate after November 26, 2009. It is noted that because the echo from the sea surface is much stronger than the echo from scatters in the water, the fault echo from the surface can overwhelm the side lobe suppression of the transducer and, consequently, contaminate the data near the surface (Teledyne, 2006). Examples of this fault-signal effect that was observed at the inside and outside ADCPs are respectively presented in **Figures 2-14** and **2-15**. Figure 2-14 shows the anomaly of current speeds measured in the upper cells that are inconsistent with the lower cells at the inside ADCP for some measurements (e.g., 11/22/09 3:25 & 11/25/09 15:20). The predominant tidal-driven currents at the inside ADCP cannot reach such a high velocity, based on tidal ranges and wave conditions outside the harbor during the measurement period. A similar data contamination near the ocean surface is also identified for the outside ADCP, as illustrated in Figure 2-15. It is suggested that the current data close to the surface not be considered representative. A personal communication with Teledyne’s engineer confirmed the potential data contamination near the surface. Consequently, current measurements that were at the upper two to three bins were rejected as the data collected are not consistent with the vertical cells below. The applicable current data from the inside ADCP is limited to Bins 1 through 4, while the outside ADCP is restricted to Bins 1 through 7. **Figures 2-16** and **2-17** show the filtered current measurements during the same time period of data shown in Figures 2-14 and 2-15, respectively, with the contaminated data being removed from the upper bins.

Table 2-2. ADCP Measurement Setup

<i>Instrument setting</i>	<i>Inside ADCP</i>	<i>Outside ADCP</i>
Current Sampling	1 minute	1 minute
Vertical Bin Width	1.5 meters	1 meter
Wave Sampling	-	2 hours with a burst duration of 20 min.
Expected S.D.	0.52 cm/sec	1.12 cm/sec

Note: S.D. denotes standard deviation

Figures 2-18 to **2-28** present the time series of current velocity and direction that were measured at the two ADCPs in Week one (i.e., November 20 to 26, 2009). Also included in these figures are the corresponding time series of wave measurements obtained from the Coastal Data Information Program (CDIP) at Dana Point (Buoy 096) as well as the predicted tides at Newport Beach, CA (Station 9410580). The measurements obtained at the inside ADCP for the

applicable bins are depicted in Figures 2-18 to 2-21, while the data collected at the outside ADCP are illustrated in Figures 2-22 to 2-28. In addition, current roses for selected periods at the two ADCPs are illustrated in **Figures 2-29 to 2-32**. The remaining data collected at the inside ADCP (i.e. Weeks 2 to 8) are presented in the Appendix A (i.e., **Figures A-1 to A-47**). It should be noted that water levels at low tides were occasionally just above the measurement elevations at Bin 4 (inside) and Bin 7 (outside) during the deployment period. The mid depths of Bins 4 and 7 are 6.55 meters (21.5 feet) and 8.15 meters (26.7 feet) above the sea floor, respectively. Therefore, current data collected at Bins 4 (inside) and 7 (outside) may be contaminated during some neap ebb tides (see Figures A-40 & A-42).

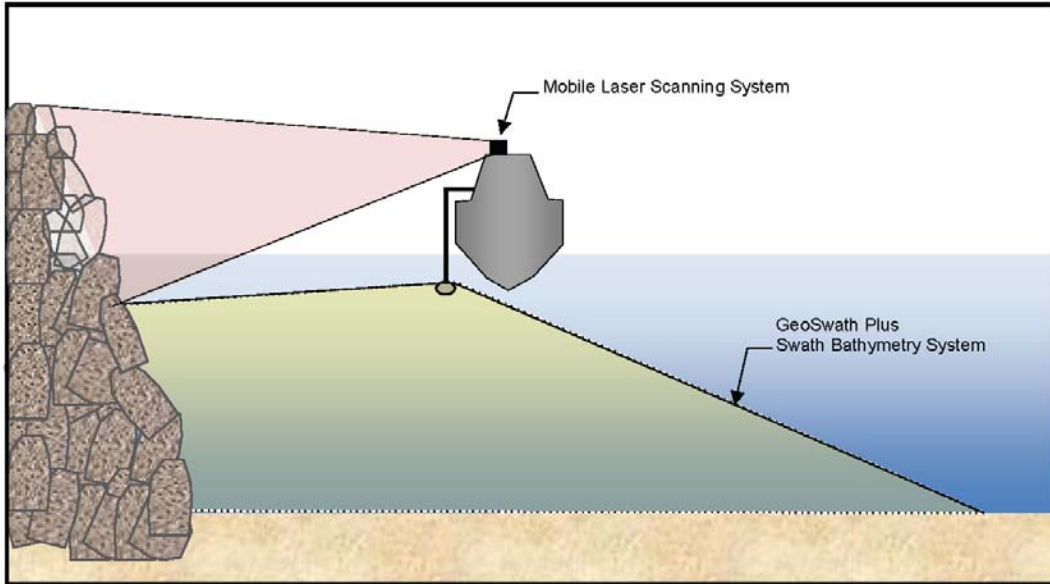
Measured instantaneous current velocities are typically less than 6 cm/sec in the main navigational channel and on the order of 10 to 20 cm/sec in the seaside area of the West Breakwater. It is evident that current flows through the rubble-mound structure occur throughout the West Breakwater, consistent with the original design of a semi-permeable rubble-mound structure. A wide range of current direction, likely resulting from current flows across the West Breakwater, were observed in the lower water column in the navigational channel during both flood and ebb tides (see current roses of Bins 1 to 3 in Figures 2-29 and 2-30). Influence of the through-breakwater currents appears to lessen near the water surface, as the measured currents with a narrower range of direction correspond well to the tide-driven flows, particularly during ebb tides (see the current rose of Bin 4). The ranges of recorded direction are in the 90° to 120° sector for ebb tides and in the 210° to 270° sector during flood tides, respectively. The current measurements in different ebb and flood cycles also exhibit a similar trend, as illustrated in **Figures 2-33 and 2-34**. For the flow field seaward of the West Breakwater, the current patterns are relatively consistent throughout the vertical water column and differ slightly for both ebb and flood tides (see Figures 2-31 and 2-32).



Bathymetric Survey Area



Figure 2-1

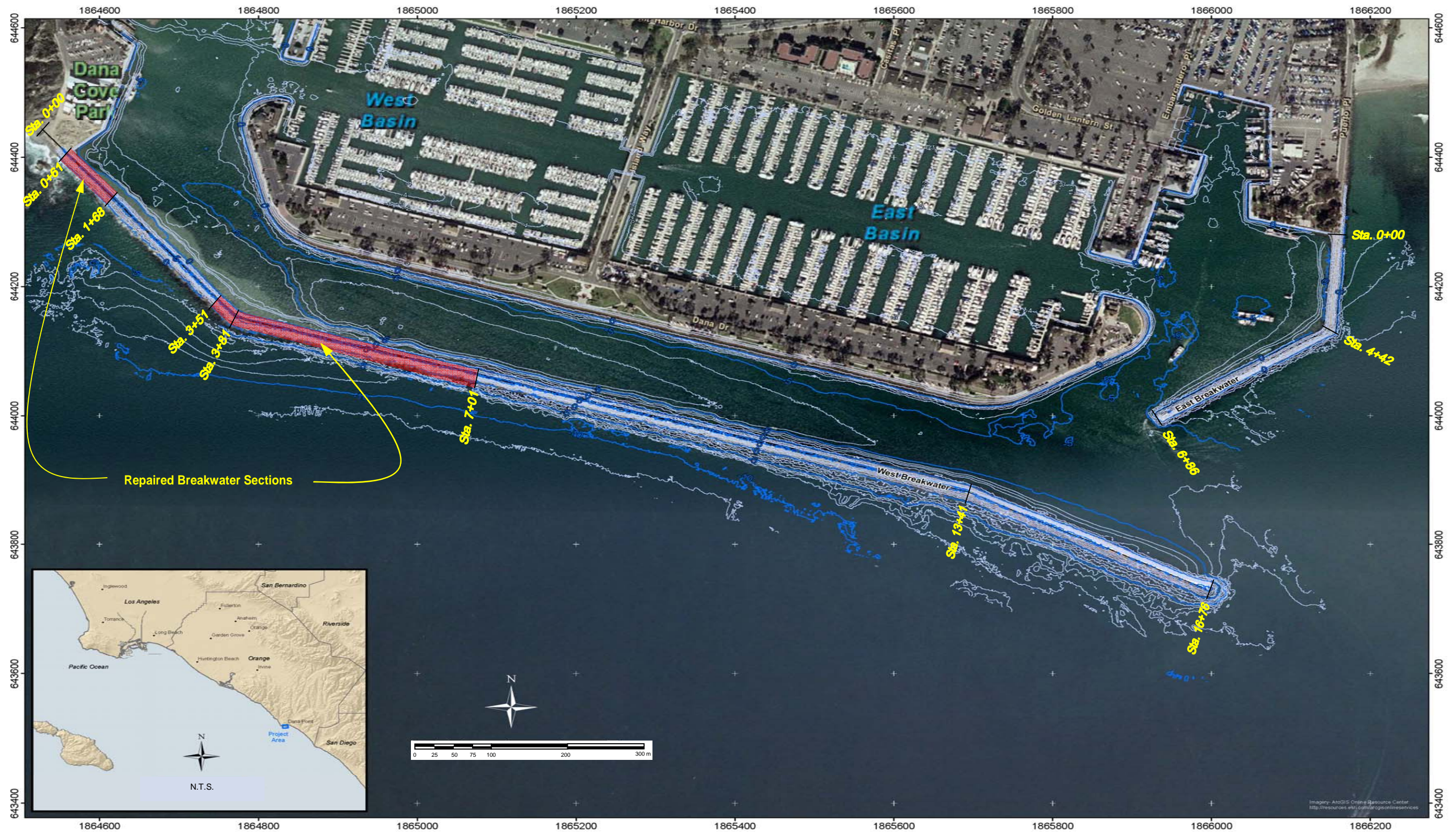


Source: Fugro, 2010

Integration of LiDAR Scanner and Swath Bathymetry Systems



Figure 2-2

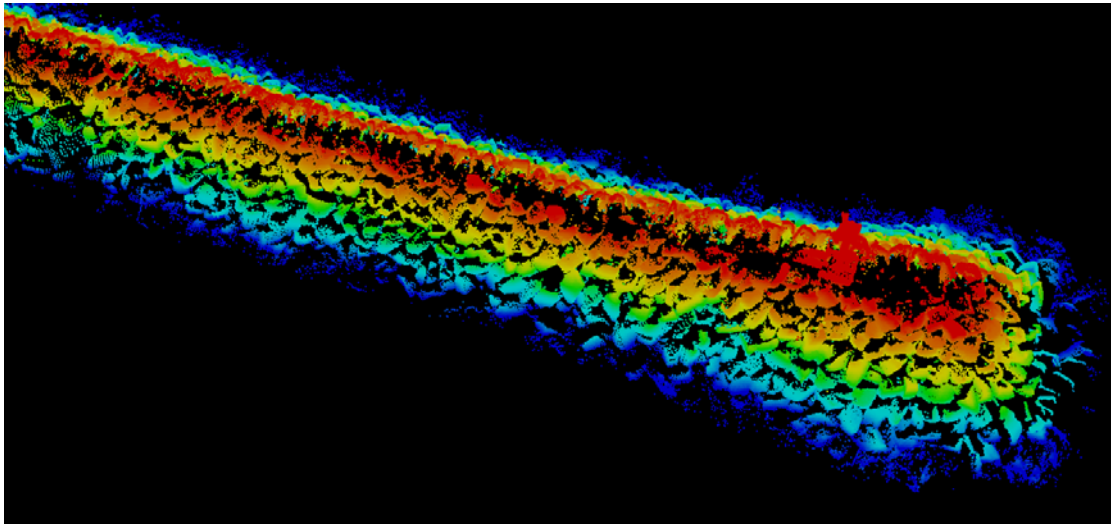


Source: Fugro, 2010

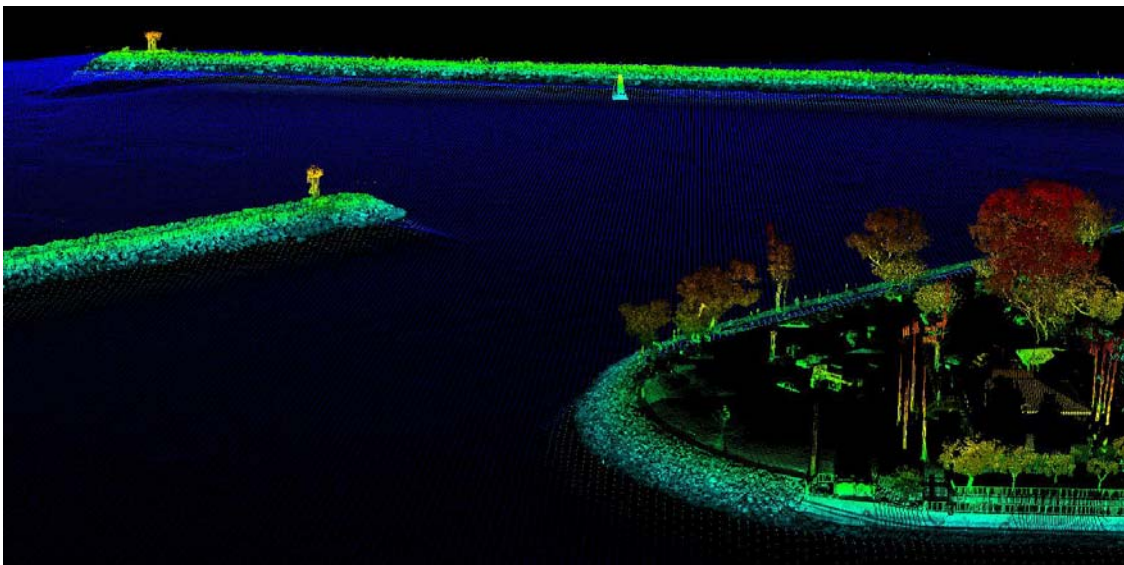
Bathymetric Contour Map



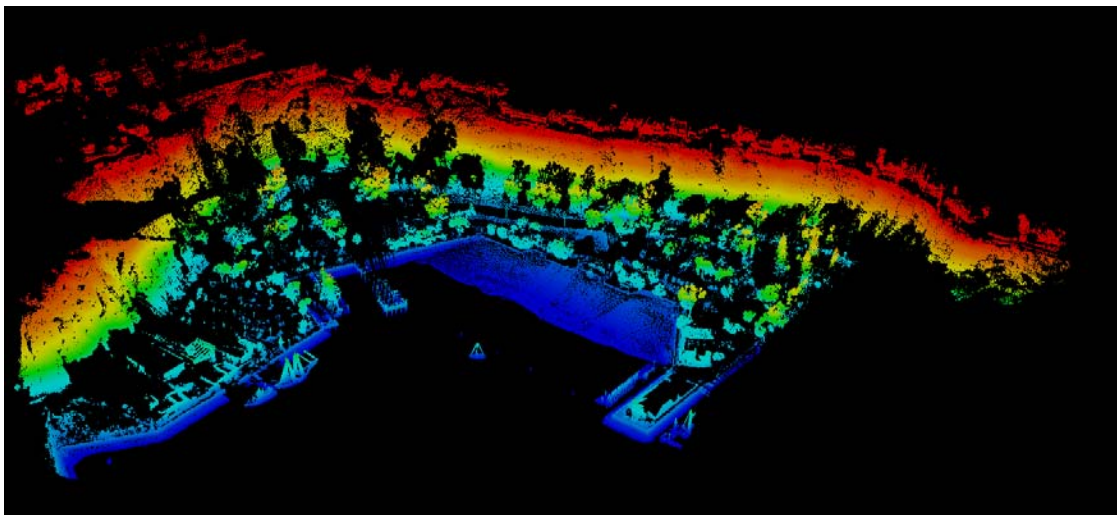
Figure 2-3



Head of West Breakwater



Harbor Entrance



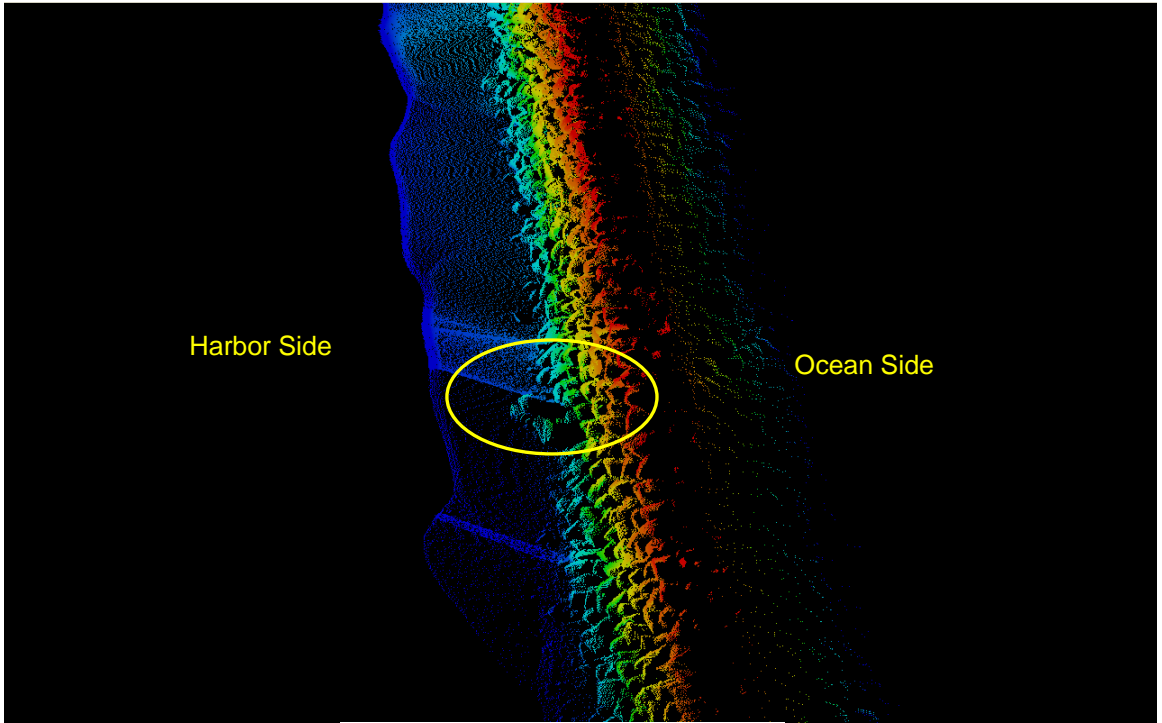
Baby Beach & Ocean Institute

Source: Fugro, 2010

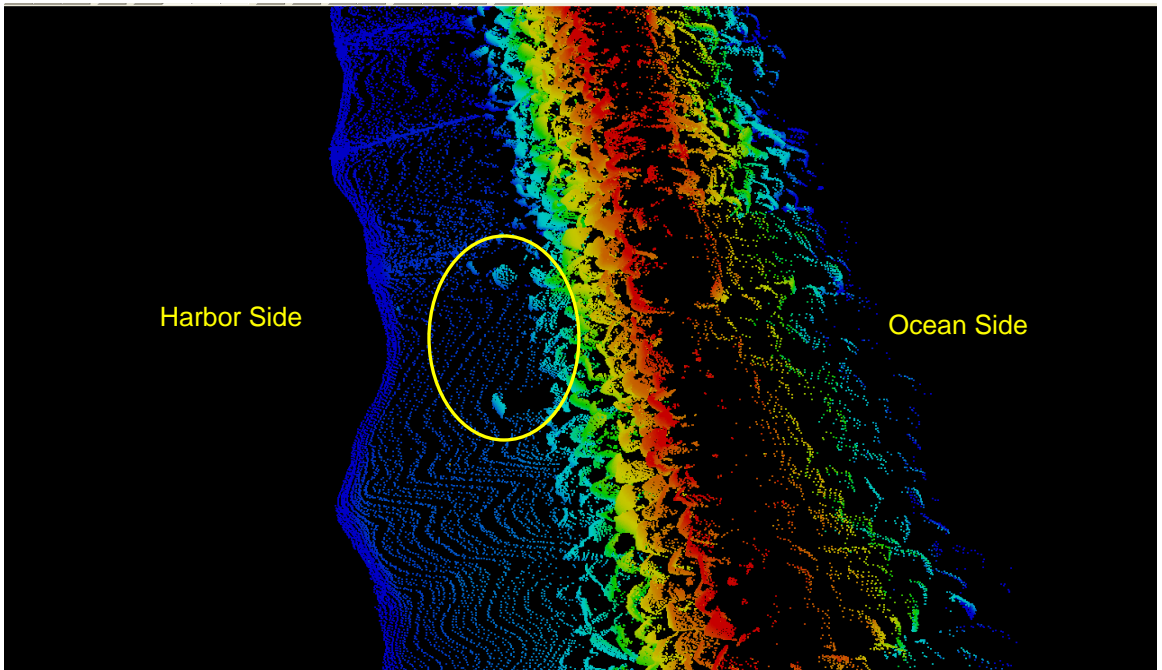
3-D Images of LiDAR Survey



Figure 2-4



Dislodged Stones near St. 00+97

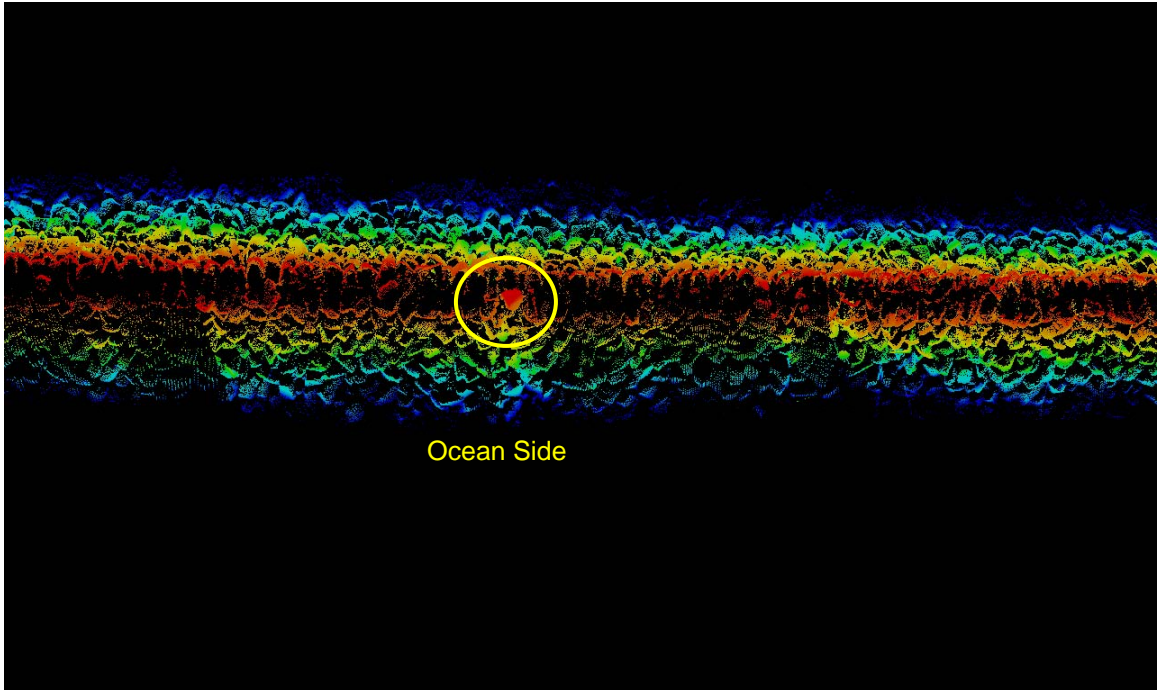


Dislodged Stones near Sta. 02+13

Dislodged Stones at West Breakwater



Figure 2-5



3_D LiDAR Image

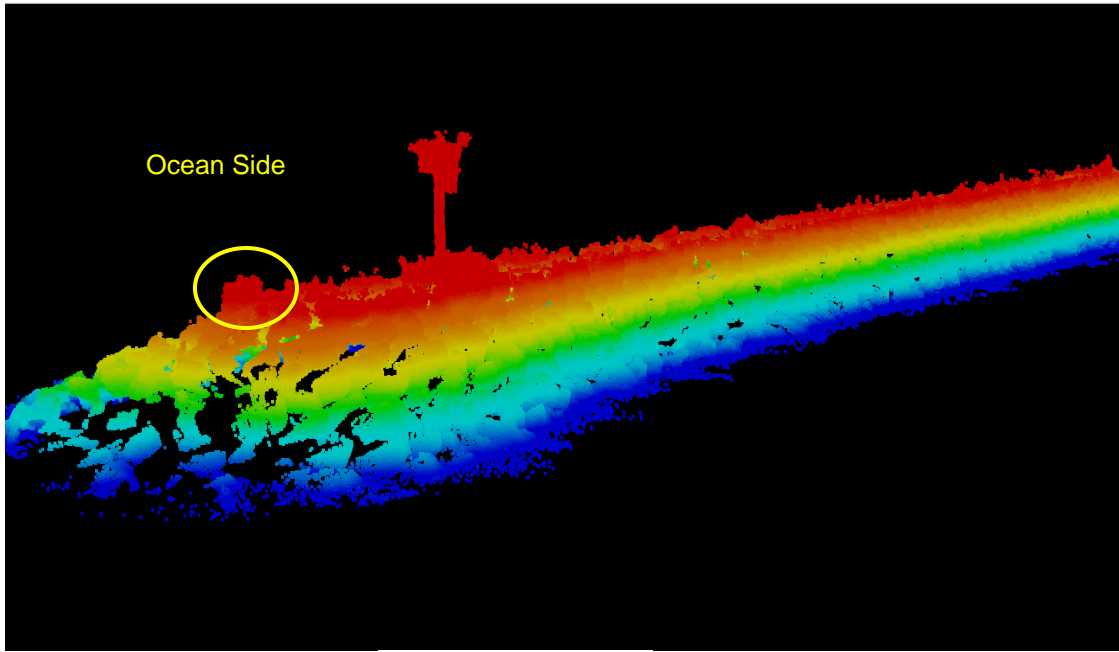


Photo Taken on 1/15/2010

Displaced Stone near Sta.15+54



Figure 2-6



3-D LiDAR Image

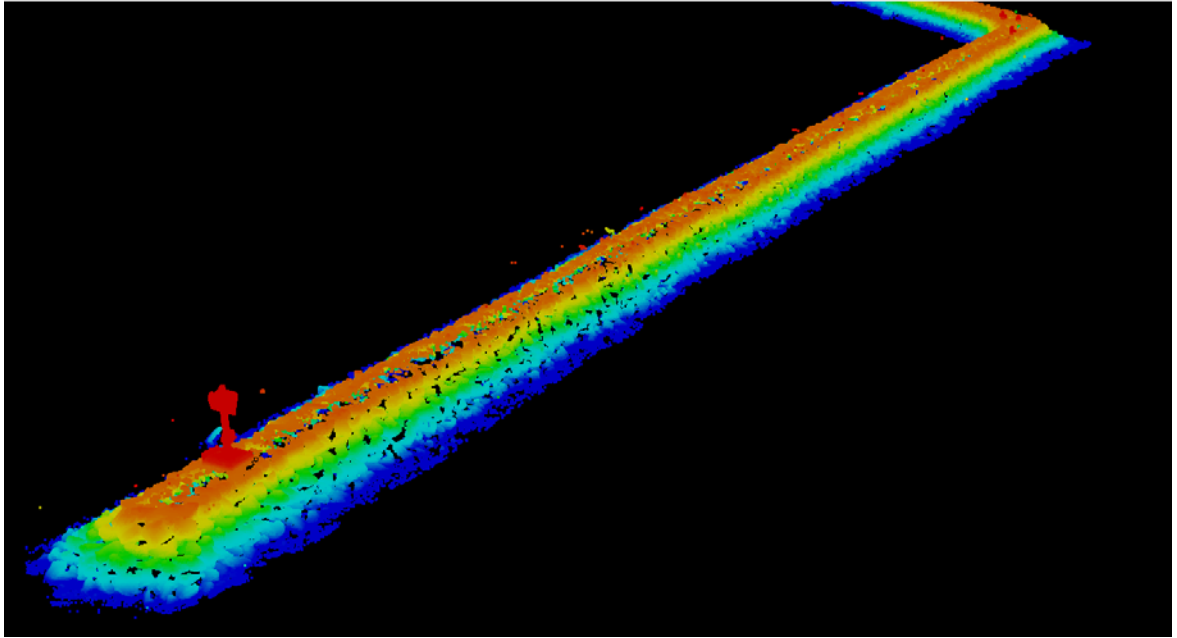


Photo Taken 1/15/2010

Displaced Stone at Structure Head of West Breakwater



Figure 2-7



3-D LiDAR Image

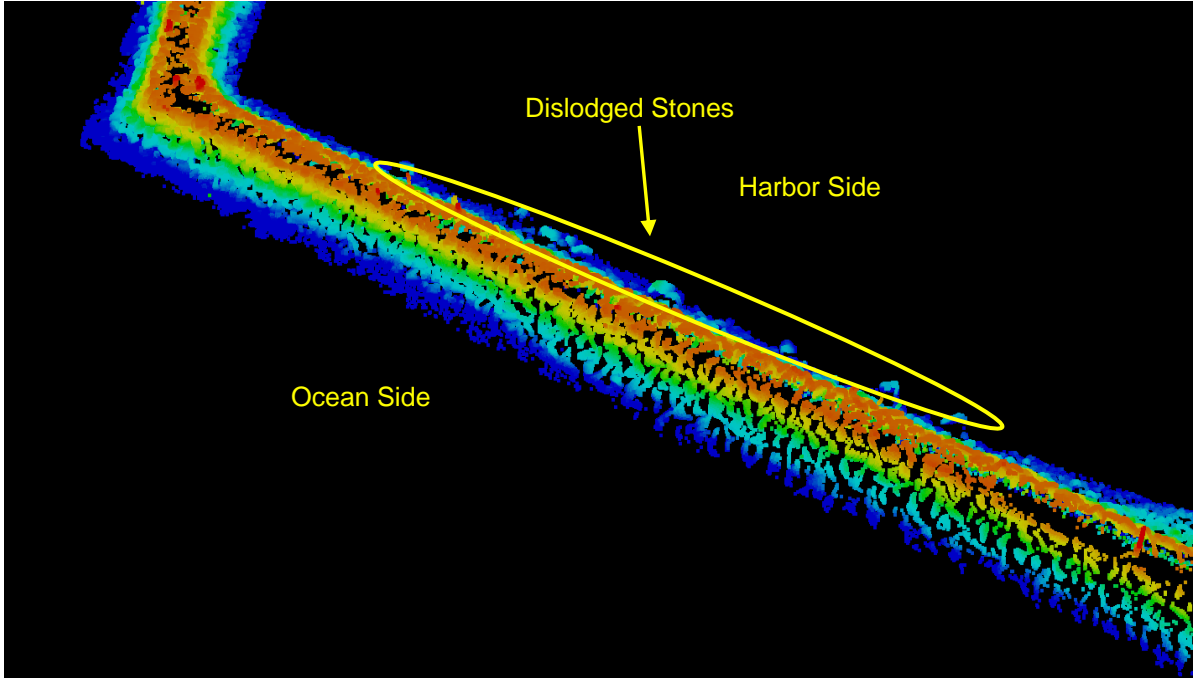
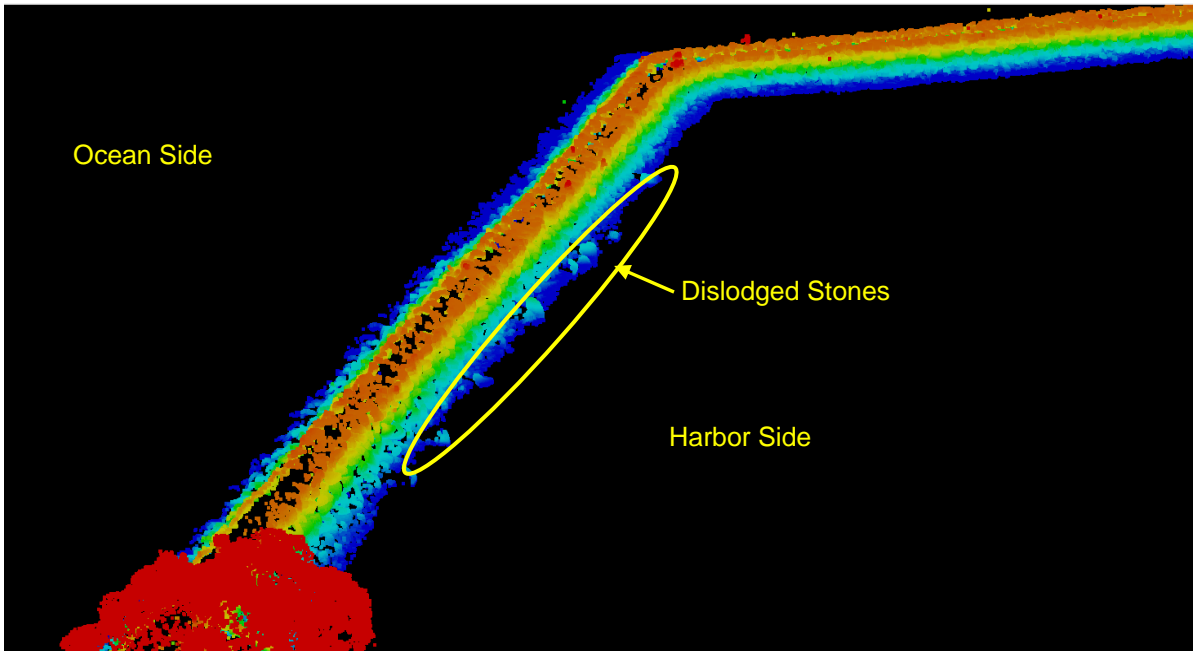


Photo Taken 1/15/2010

East Breakwater



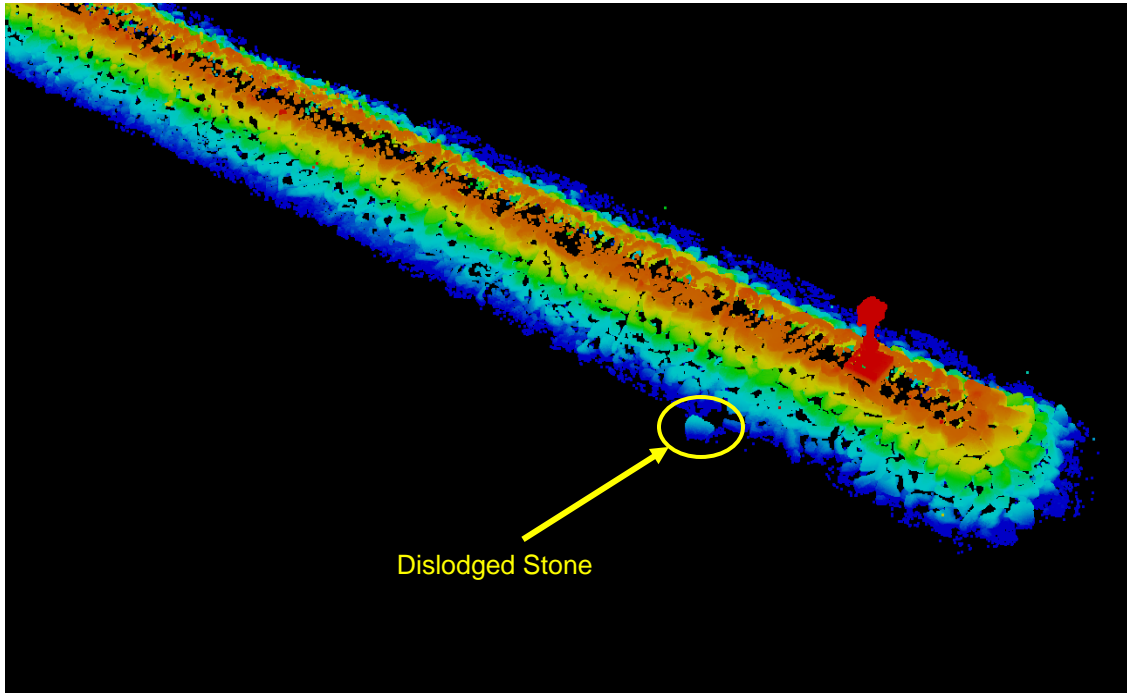
Figure 2-8



Dislodged Stones at East Breakwater



Figure 2-9



3-D LiDAR Image



Photo Taken on 1/15/2010

Displaced Stone near Structure Head of East Breakwater



Figure 2-10

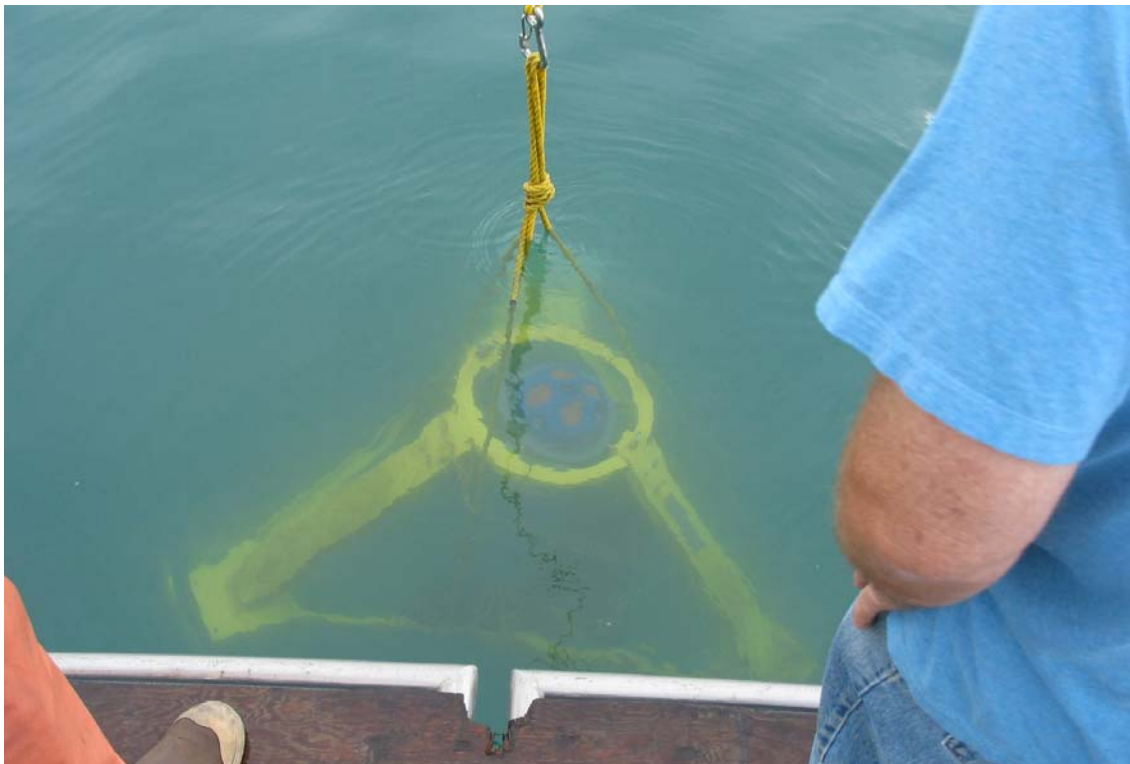
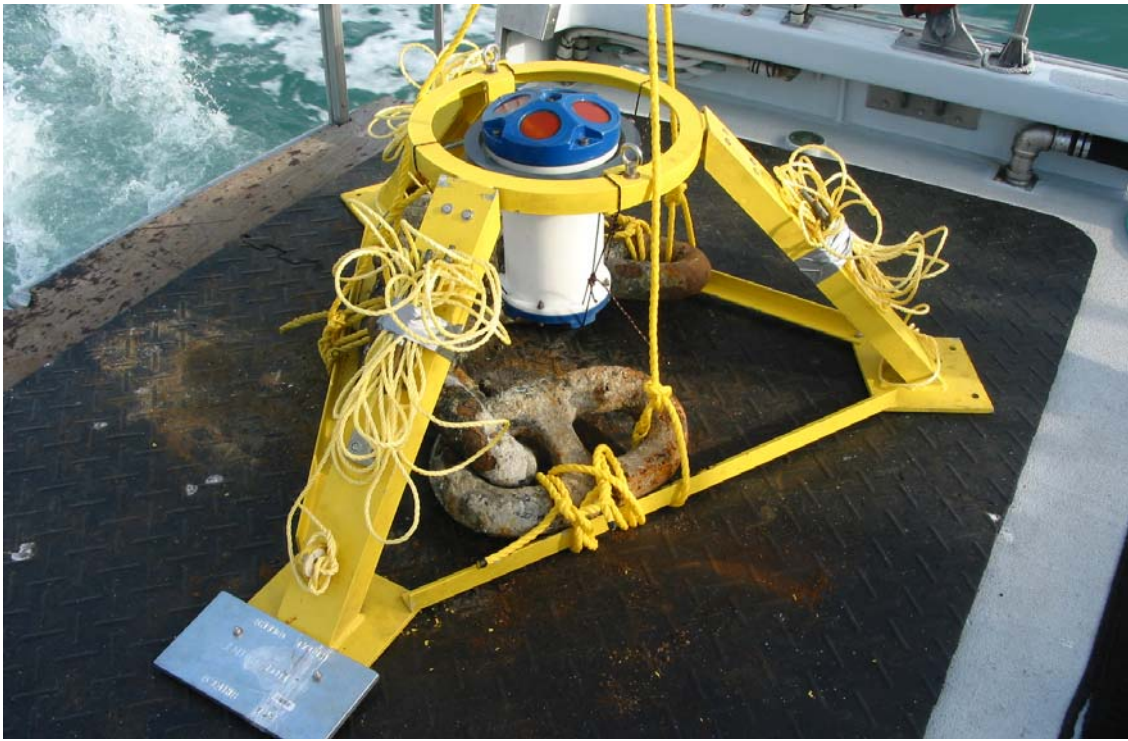


Note: Base Map from Google Earth

ADCP Gage Locations



Figure 2-11



Deployment of ADCP Instruments



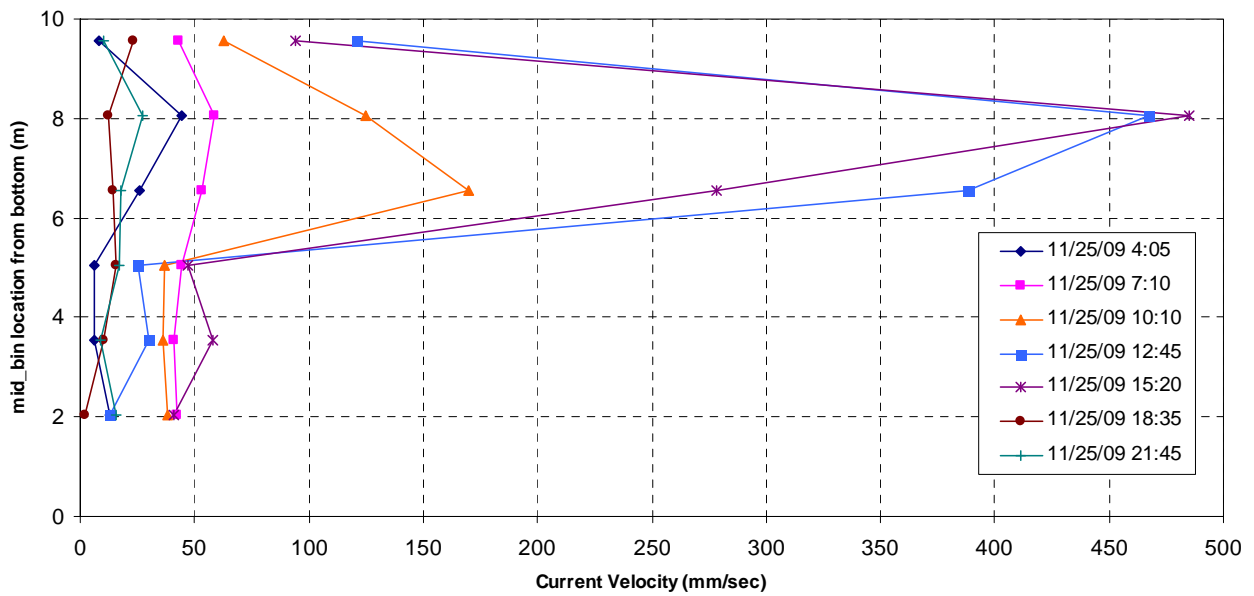
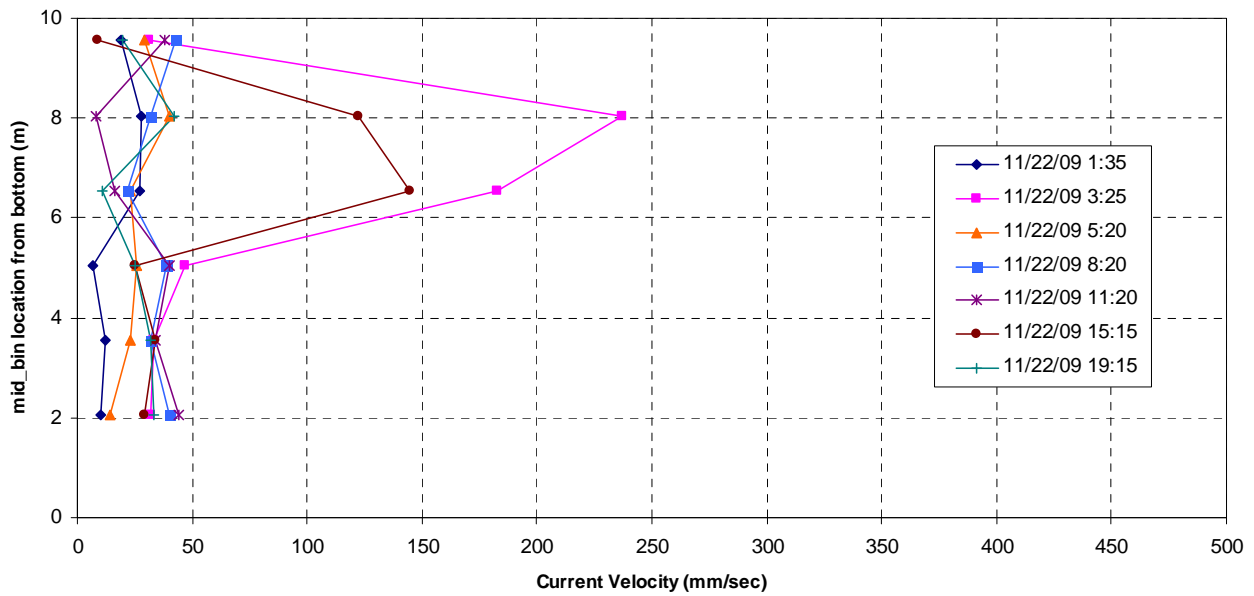
Figure 2-12



Retrieval of ADCP Instruments



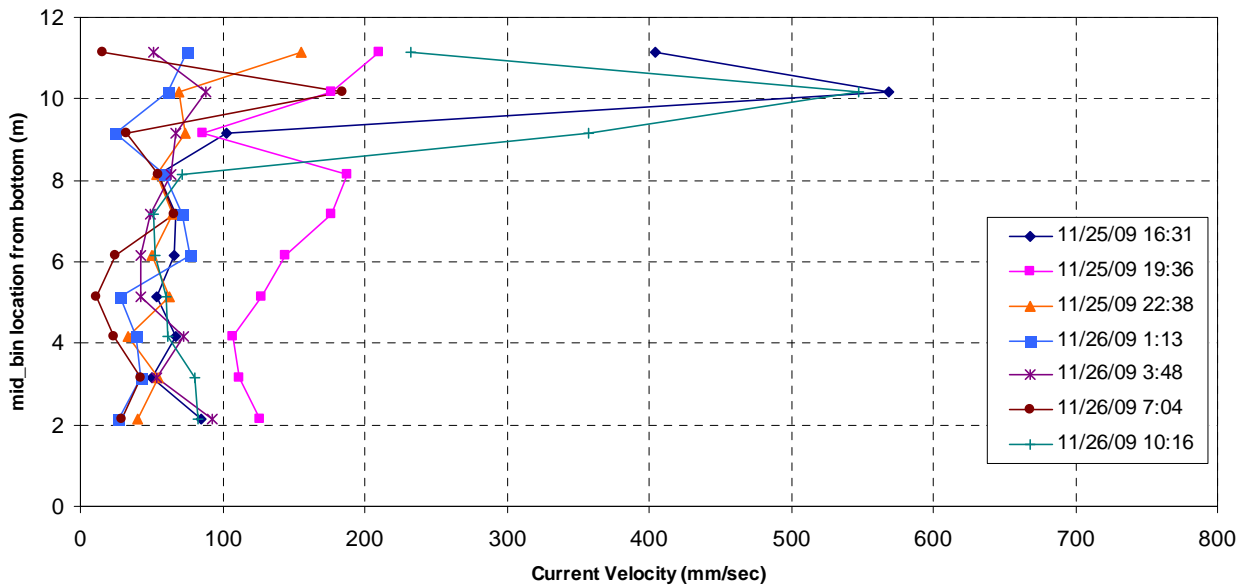
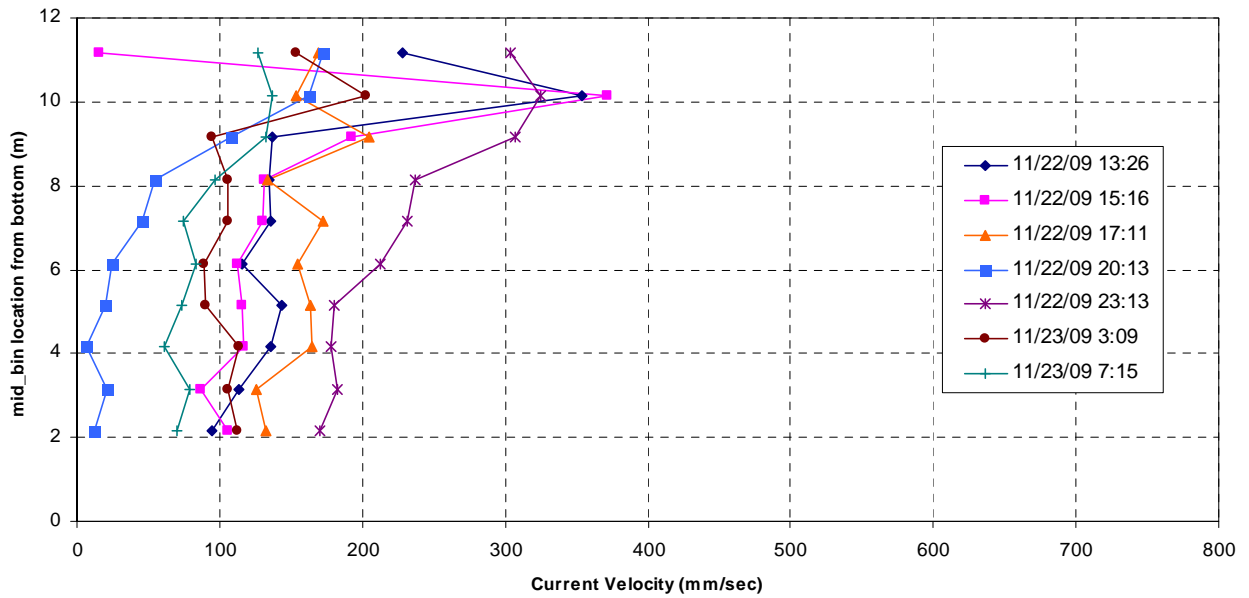
Figure 2-13



Unfiltered Current Profiles Collected at Inside Gage

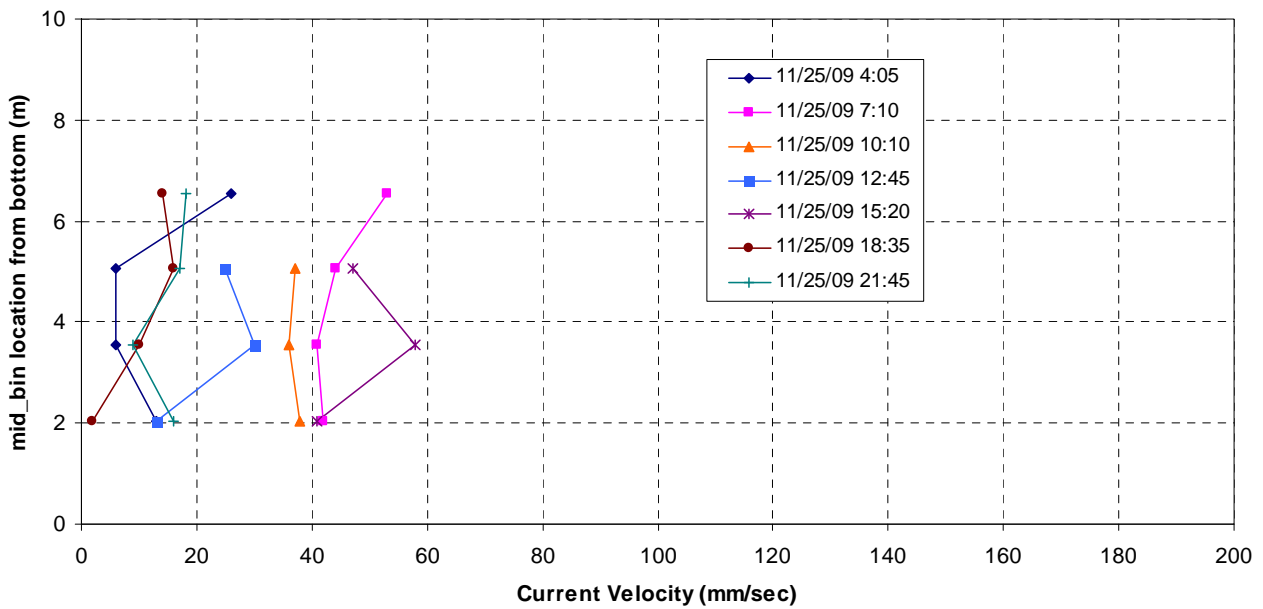
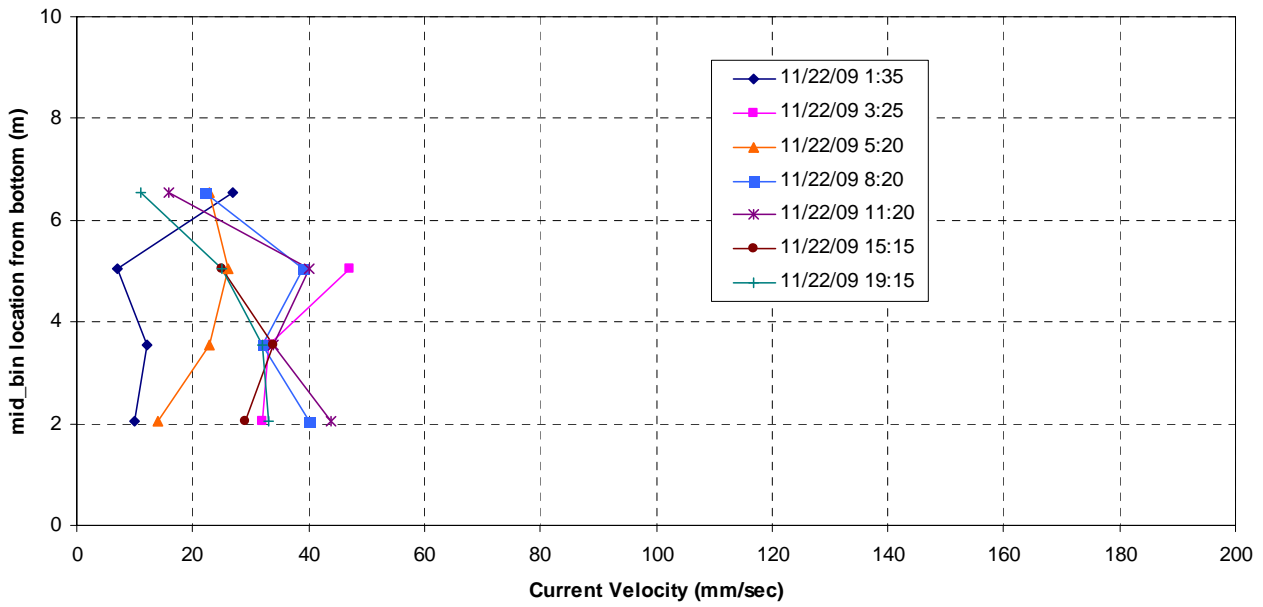


Figure 2-14



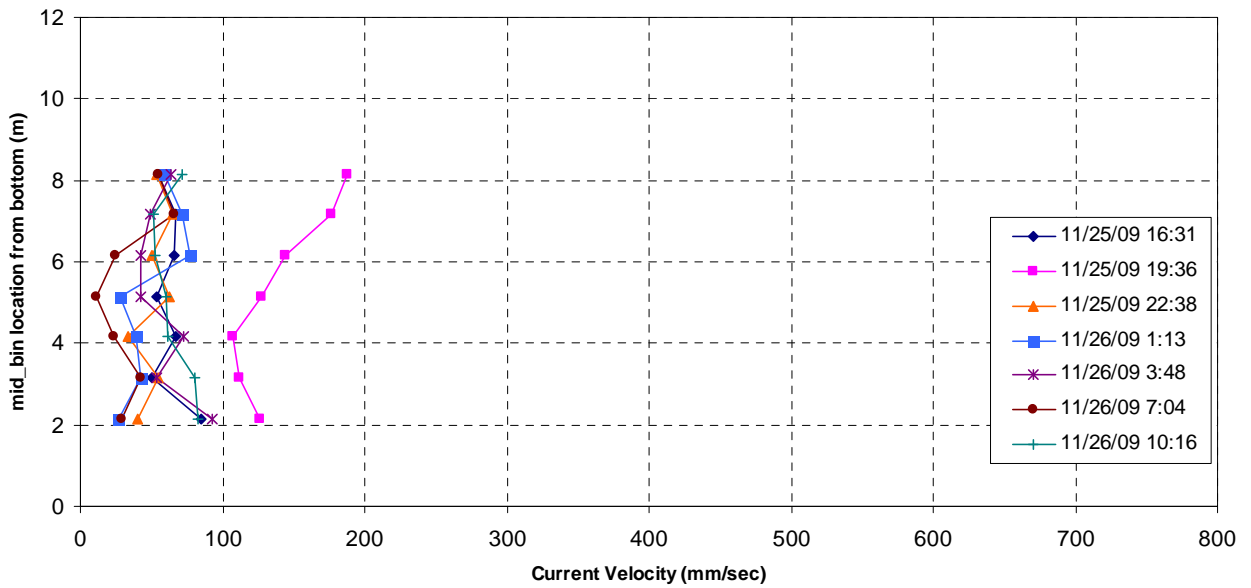
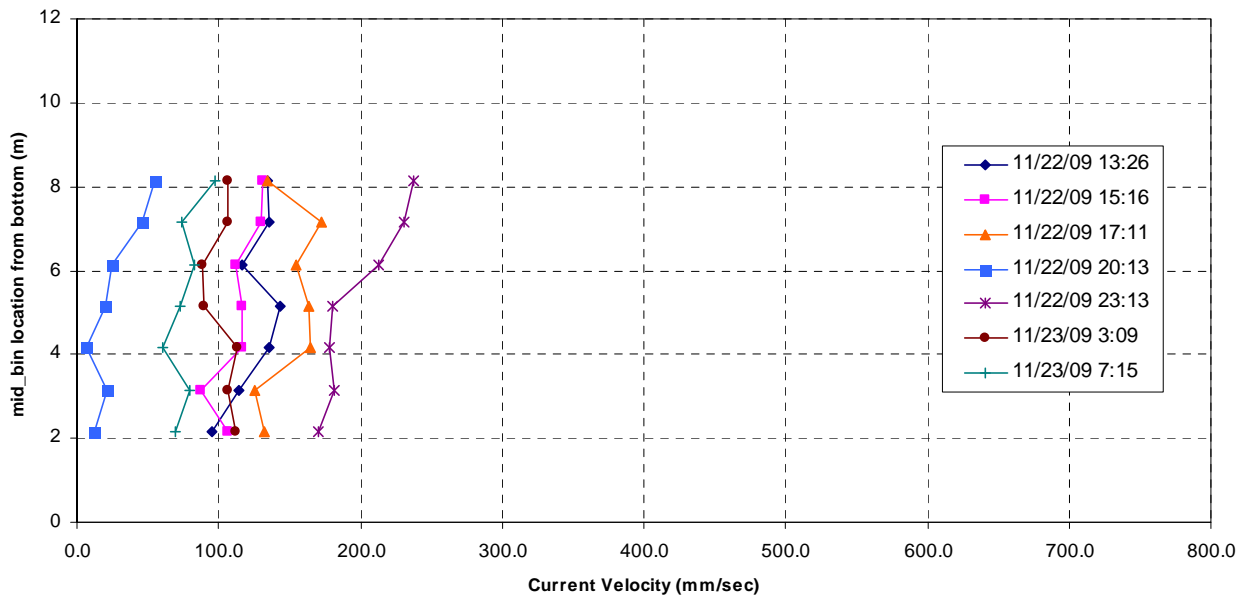
Unfiltered Current Profiles Collected at Outside Gage





Filtered Current Profiles at Inside Gage

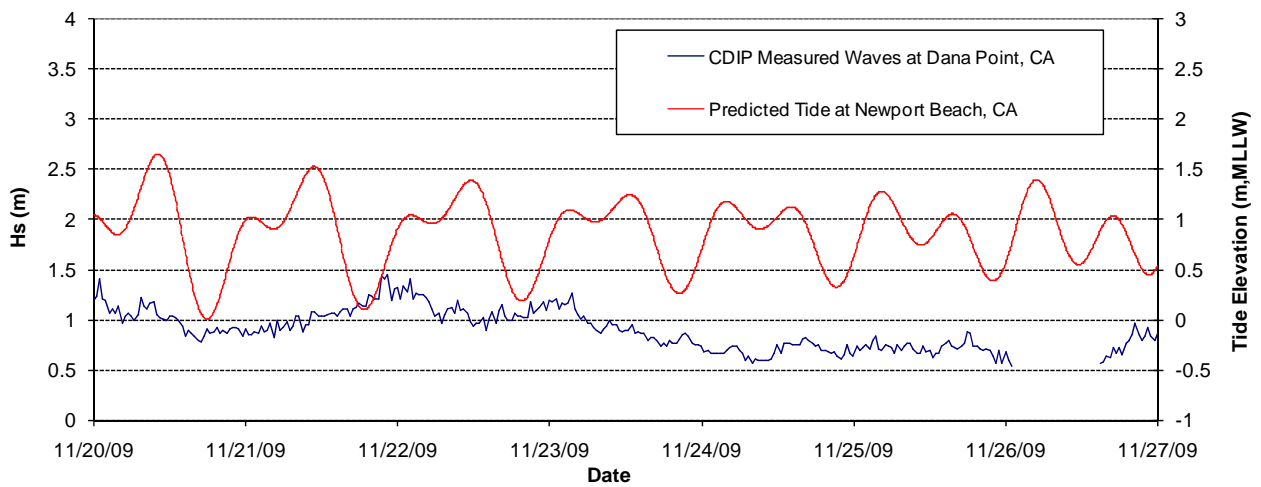
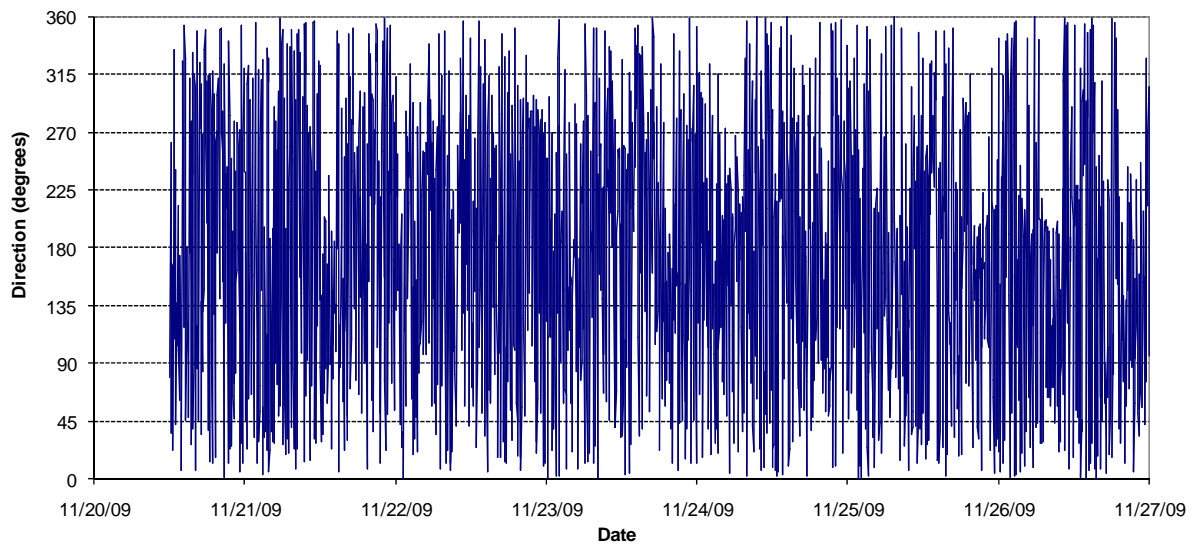
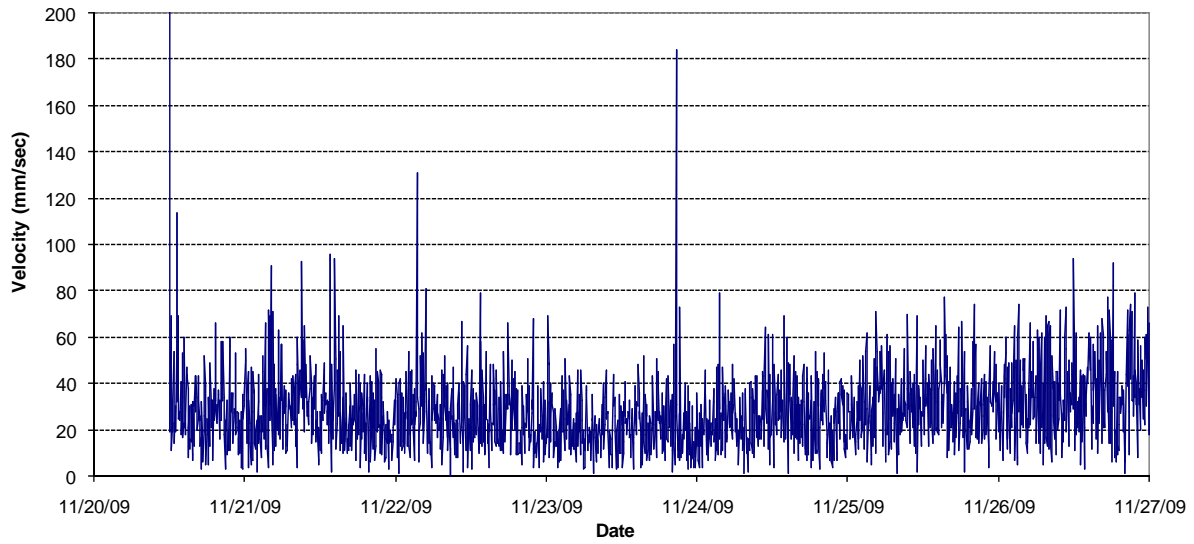




Filtered Current Profiles at Outside Gage



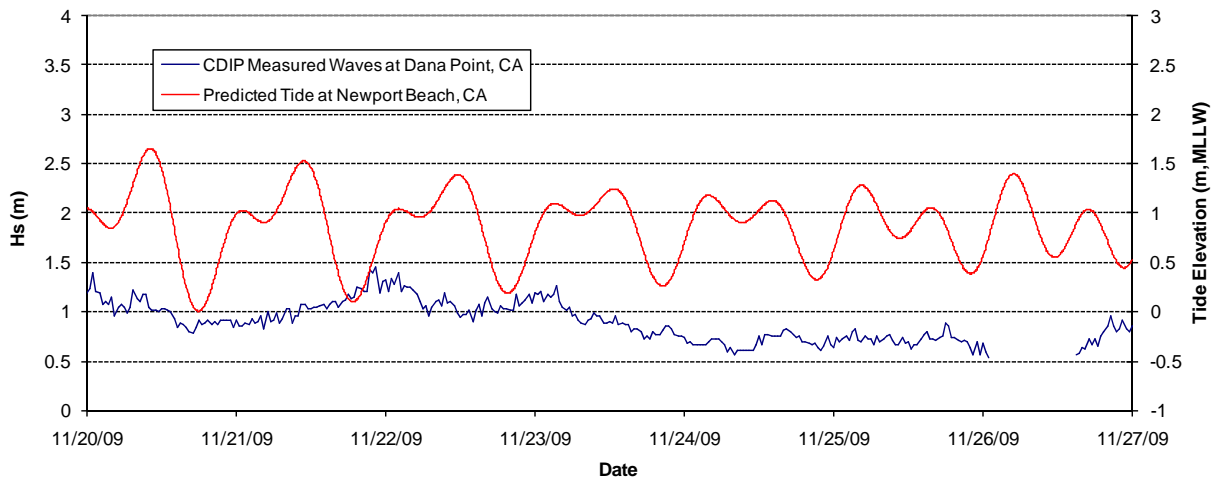
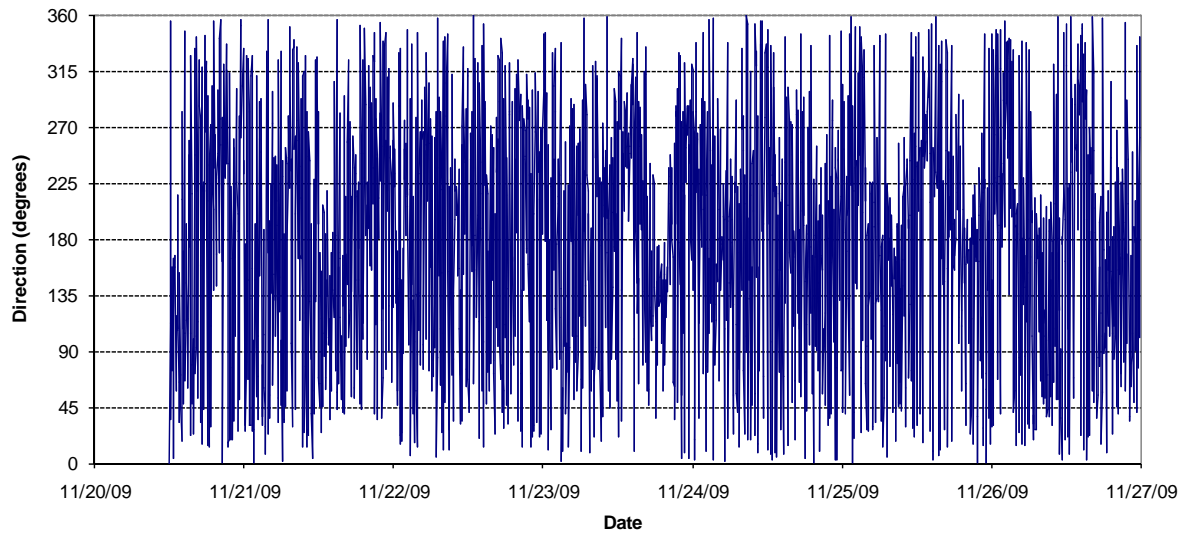
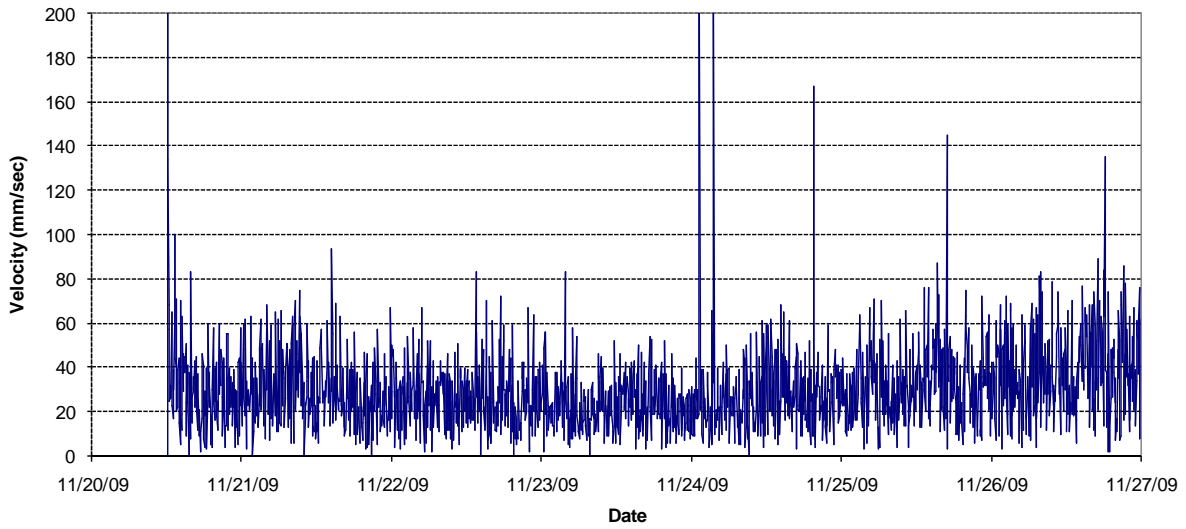
Figure 2-17



Week 1 – Bin 1 Current Measurements at Inside Gage



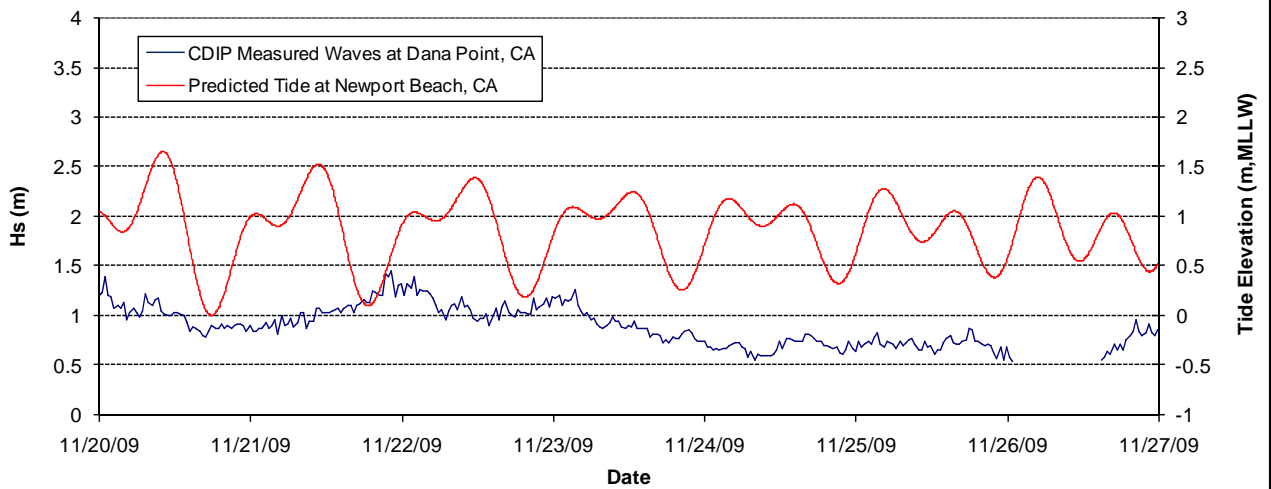
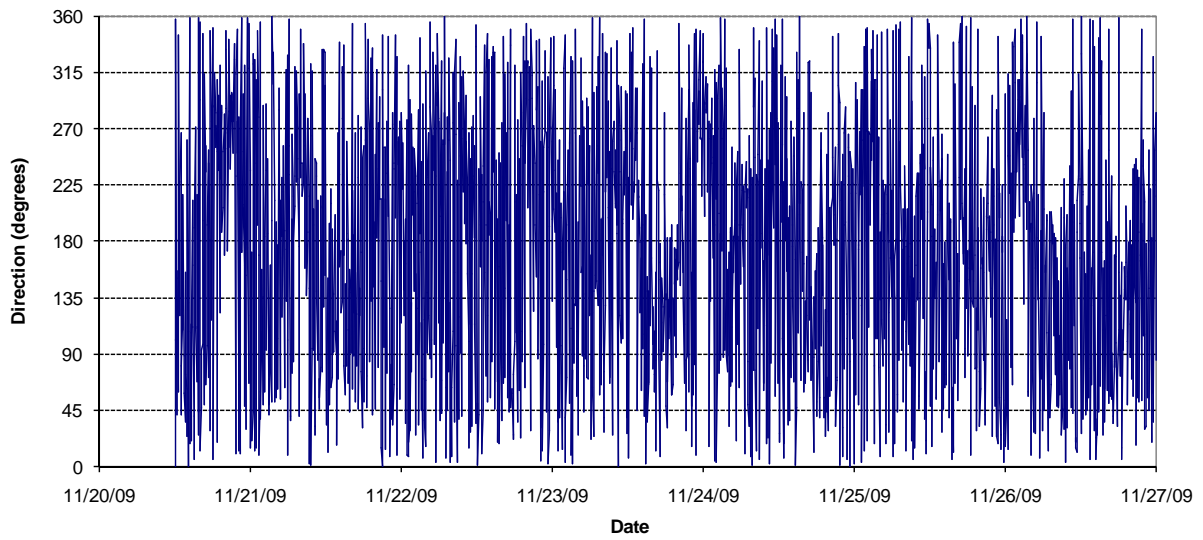
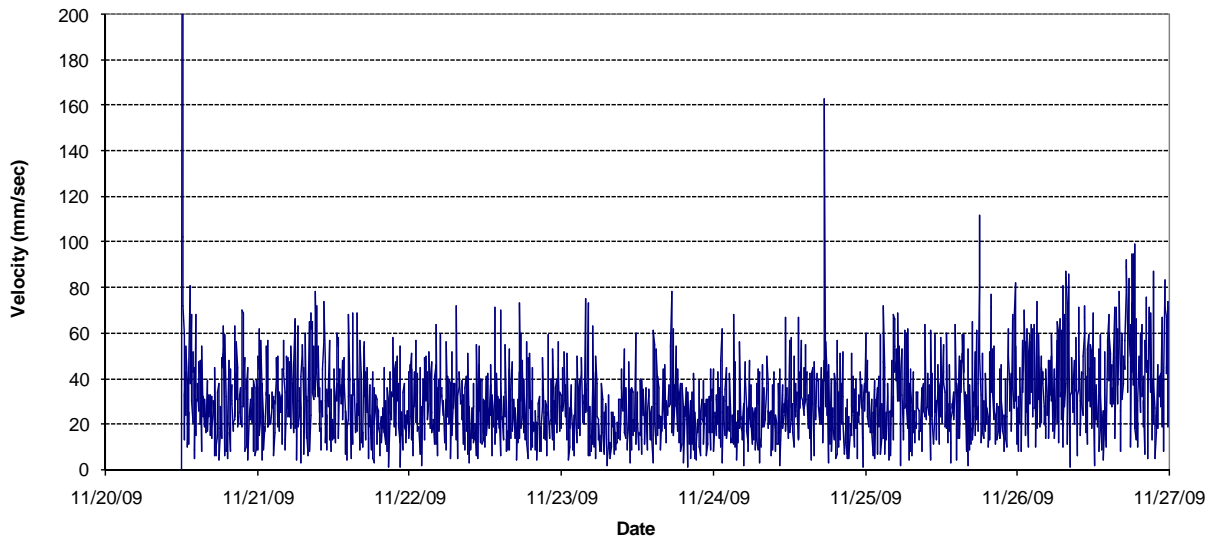
Figure 2-18



Week 1 – Bin 2 Current Measurements at Inside Gage



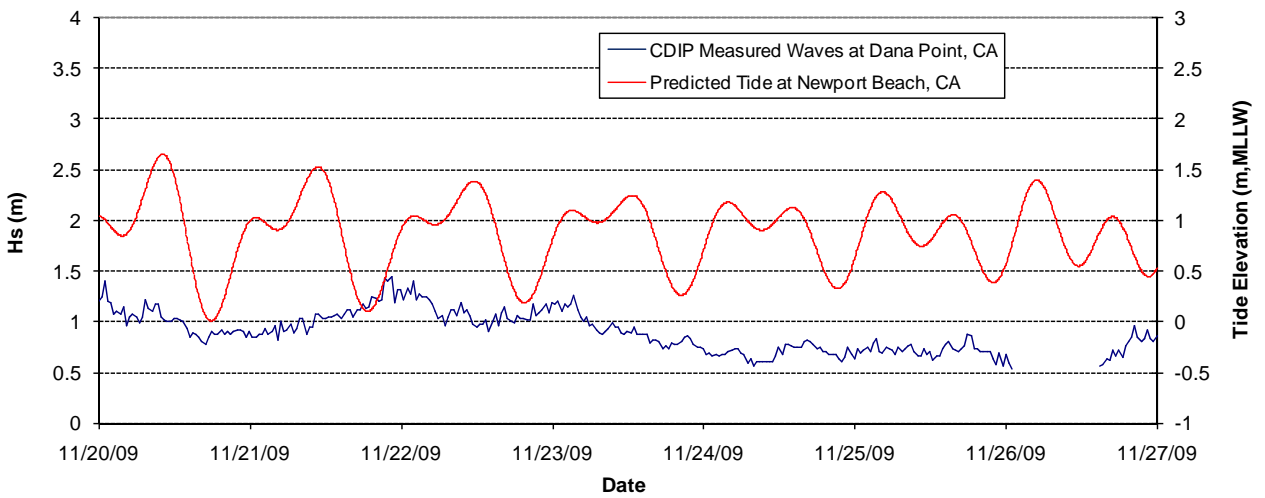
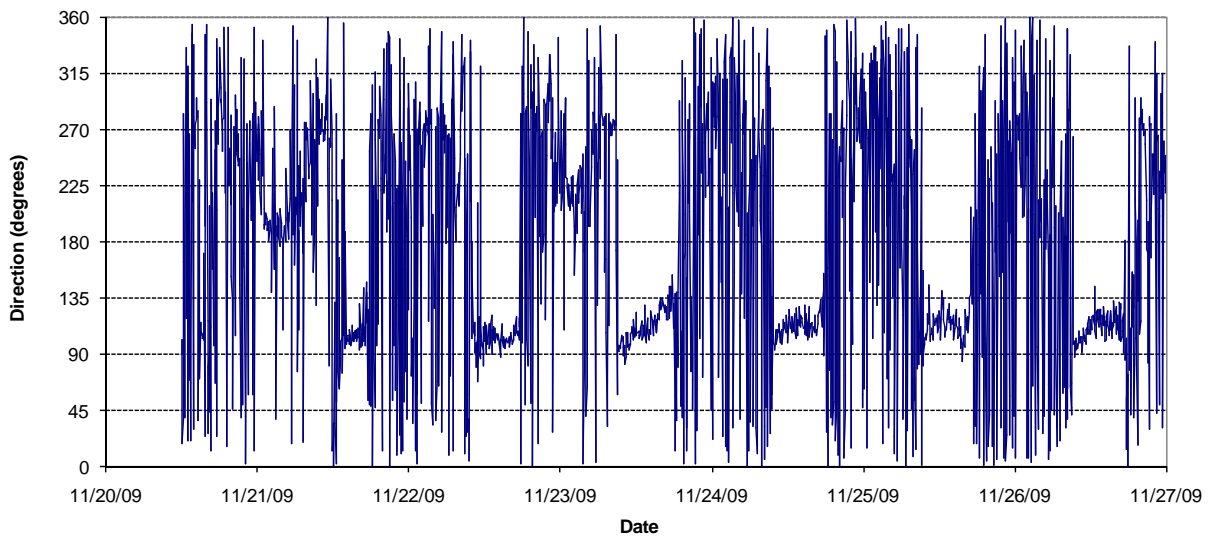
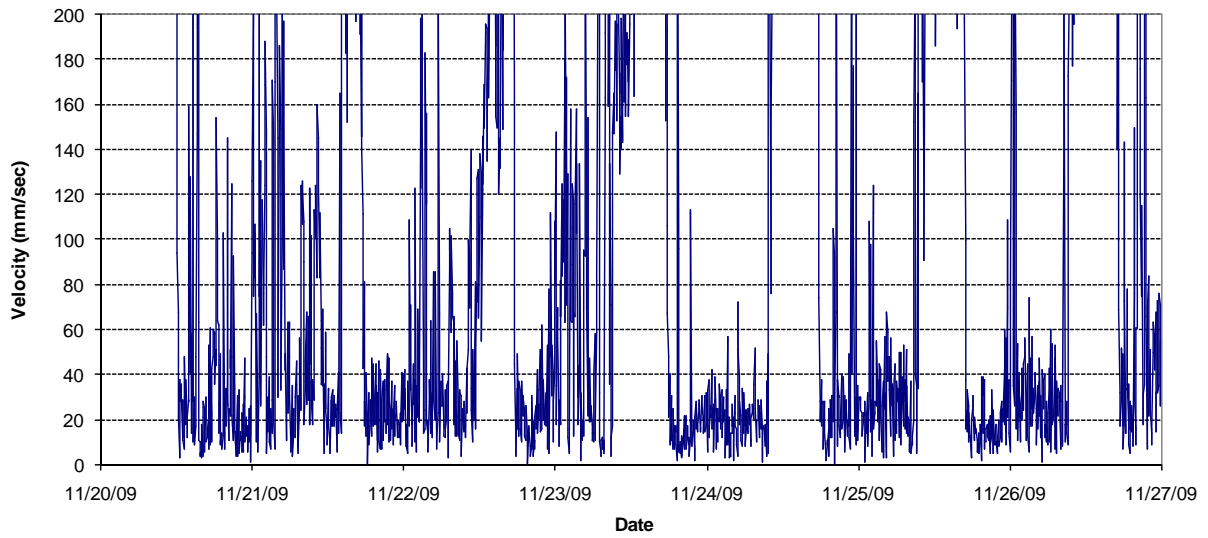
Figure 2-19



Week 1 – Bin 3 Current Measurements at Inside Gage



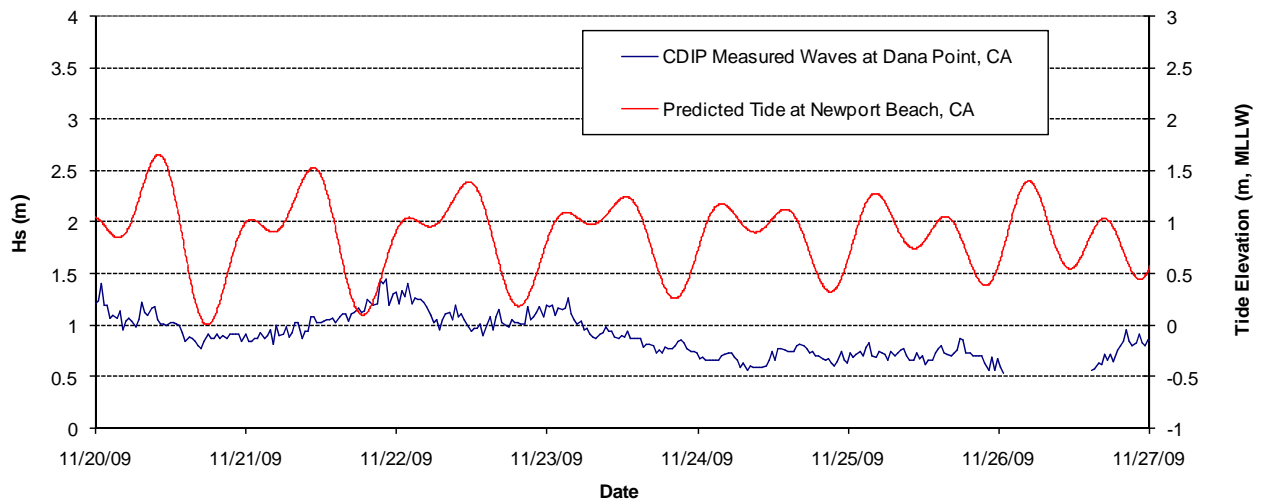
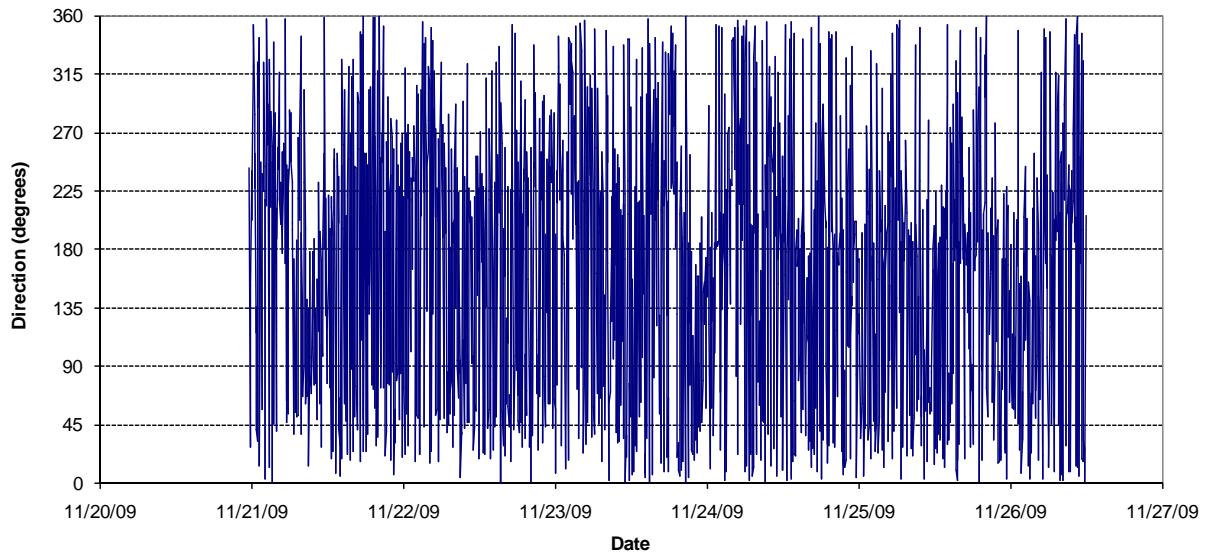
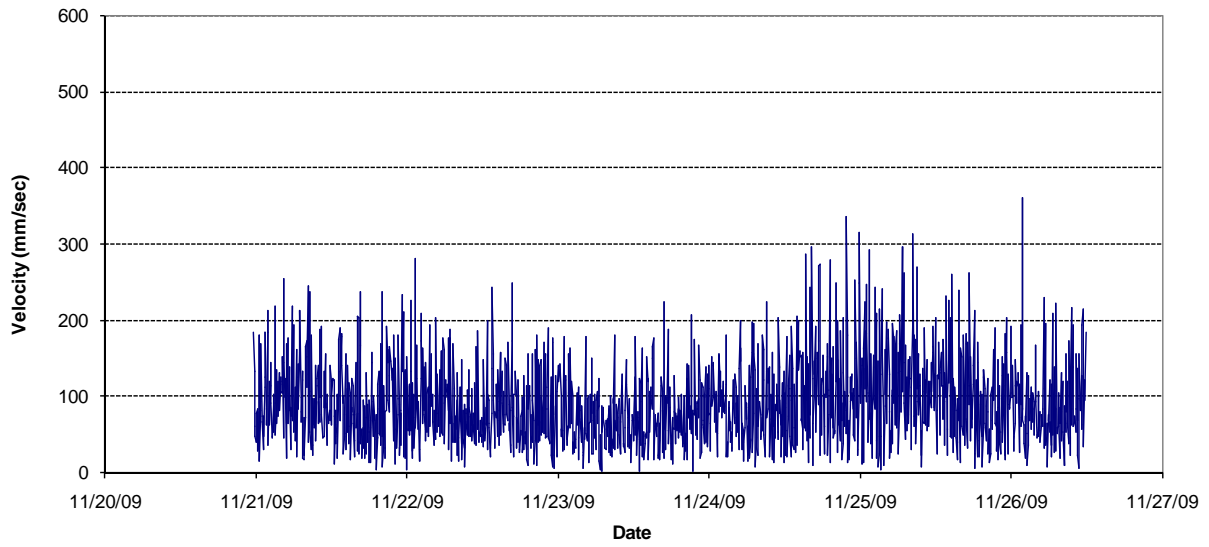
Figure 2-20



Week 1 – Bin 4 Current Measurements at Inside Gage



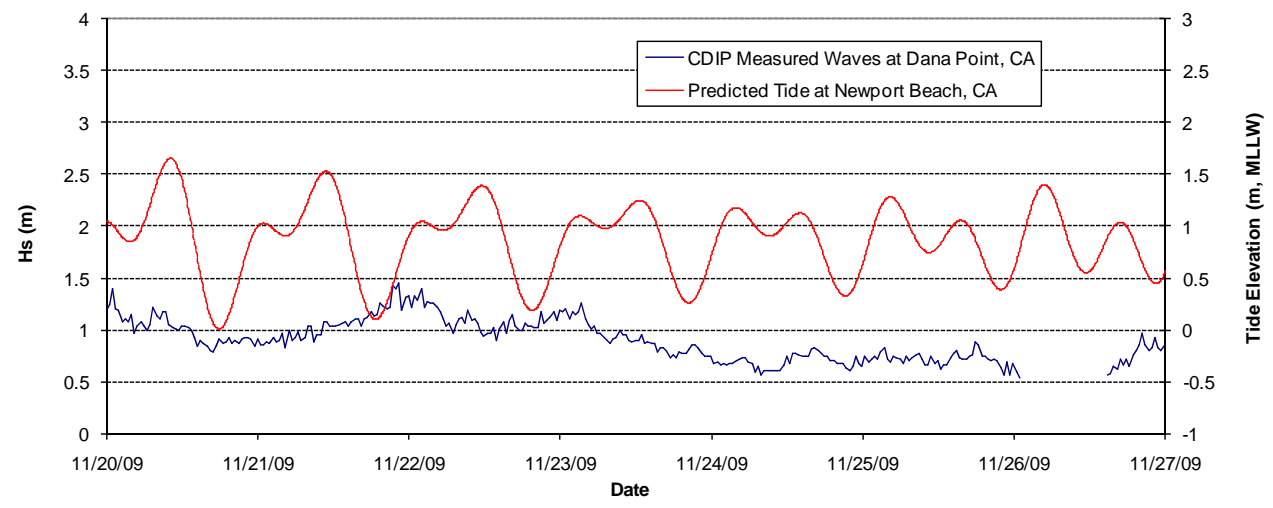
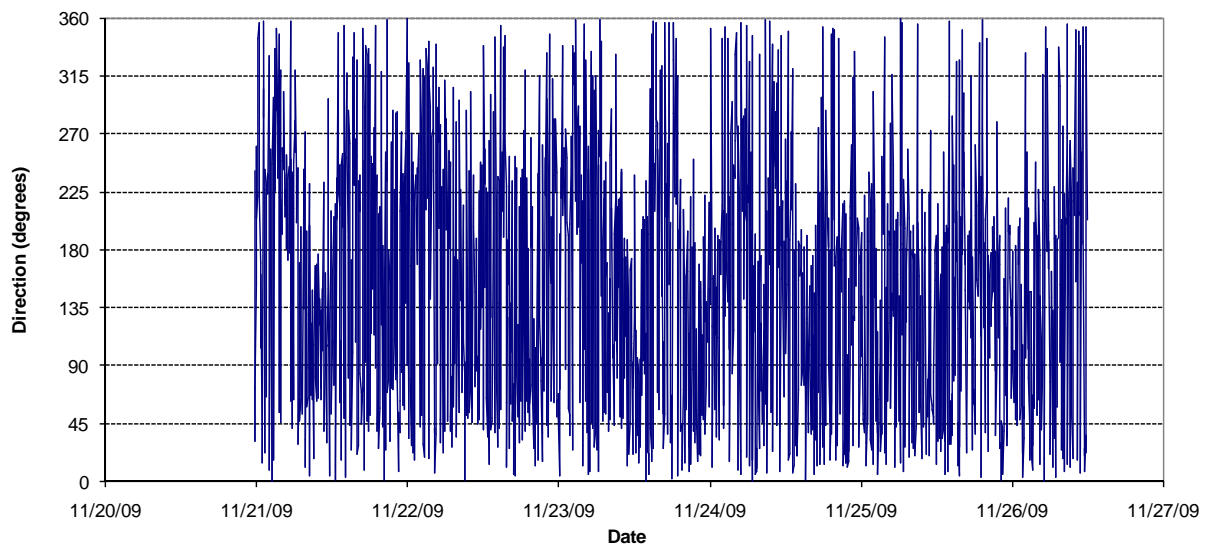
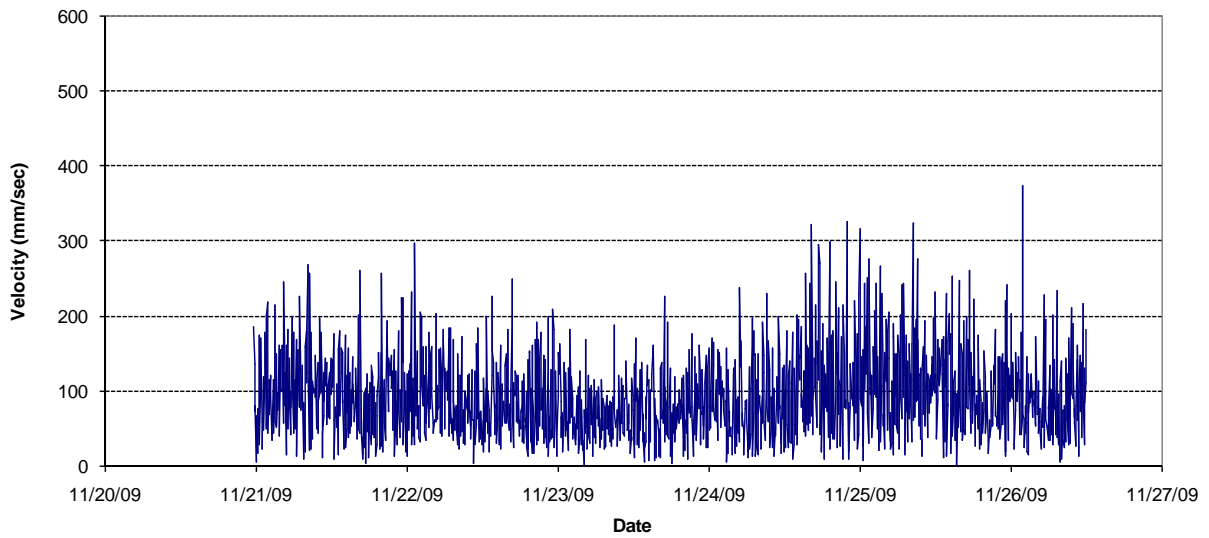
Figure 2-21



Week 1 – Bin 1 Current Measurements at Outside Gage



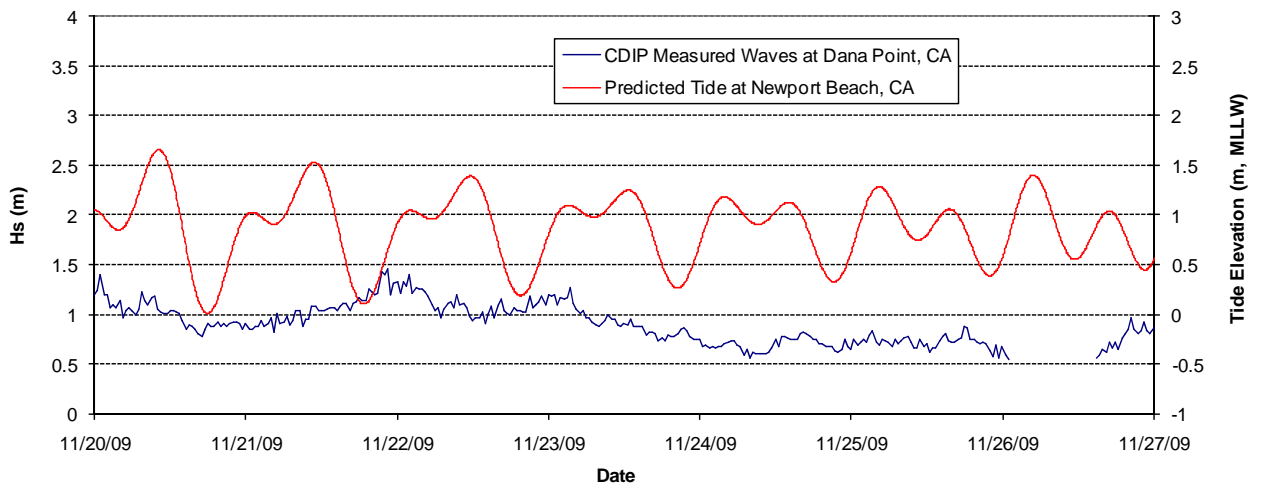
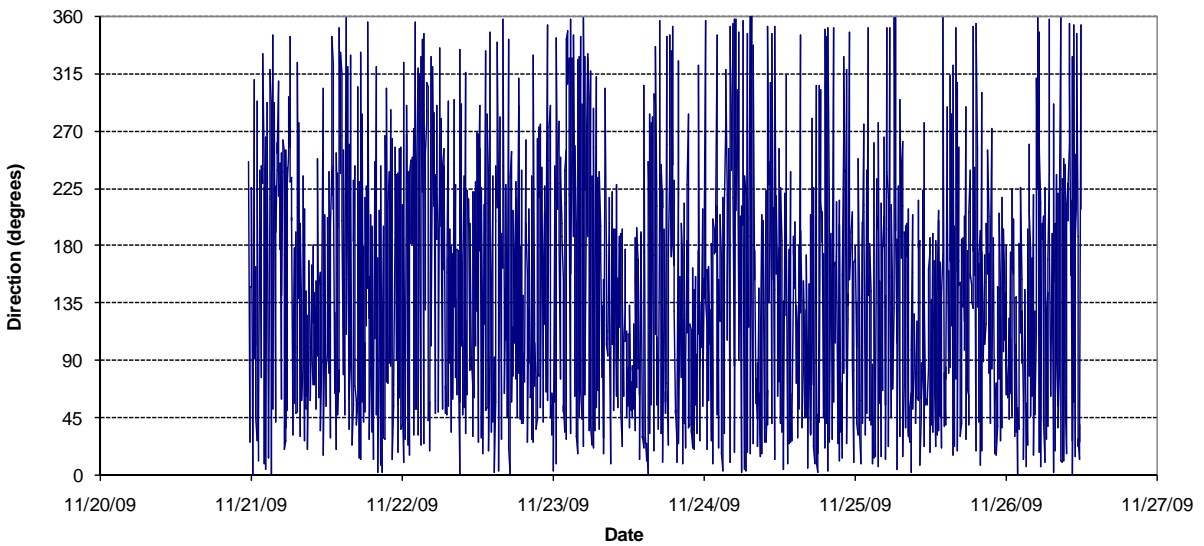
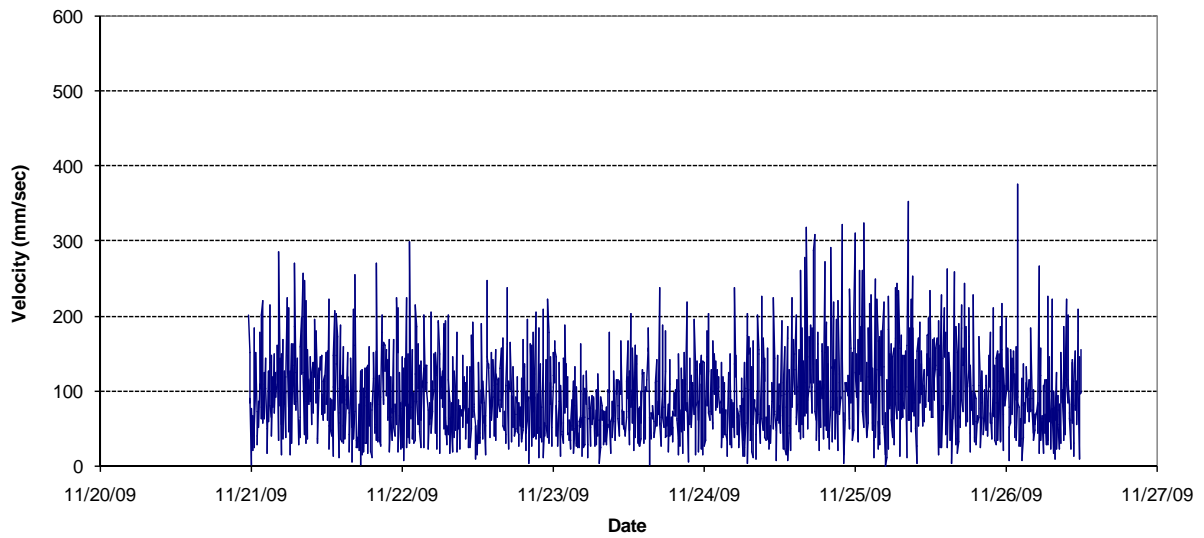
Figure 2-22



Week 1 – Bin 2 Current Measurements at Outside Gage



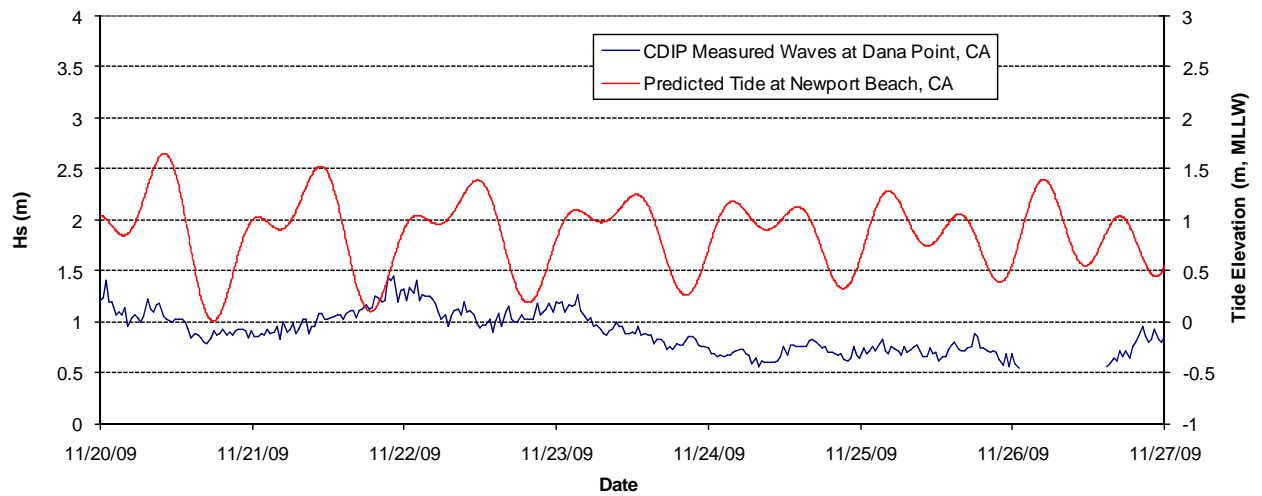
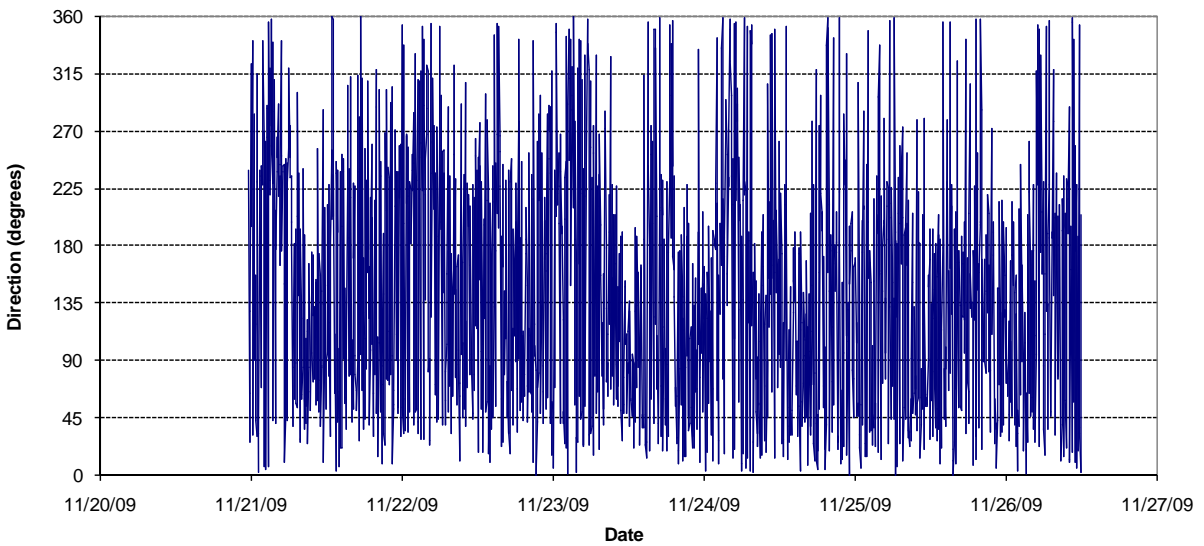
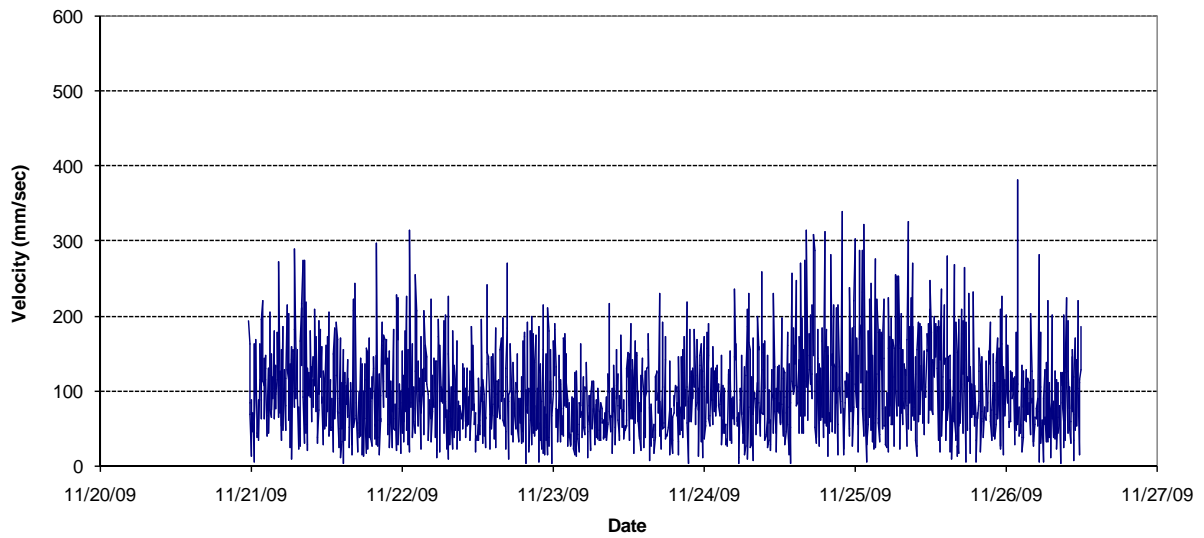
Figure 2-23



Week 1 – Bin 3 Current Measurements at Outside Gage



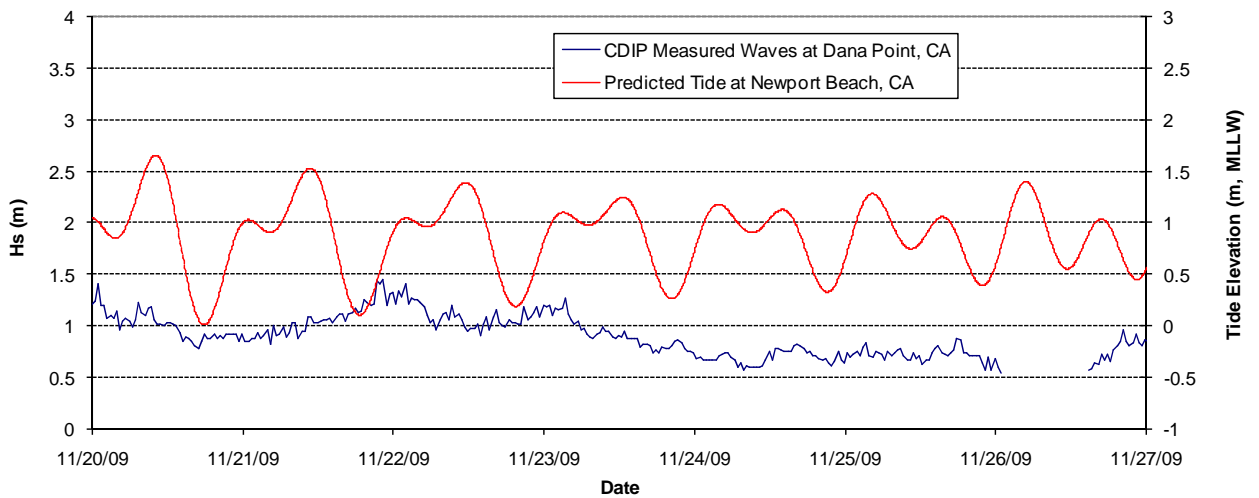
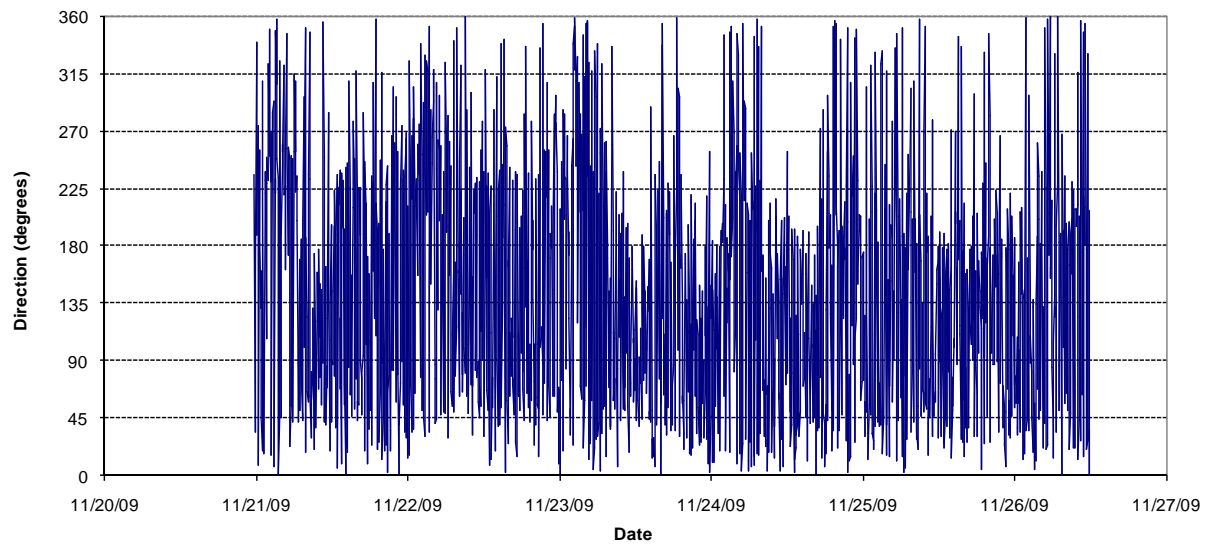
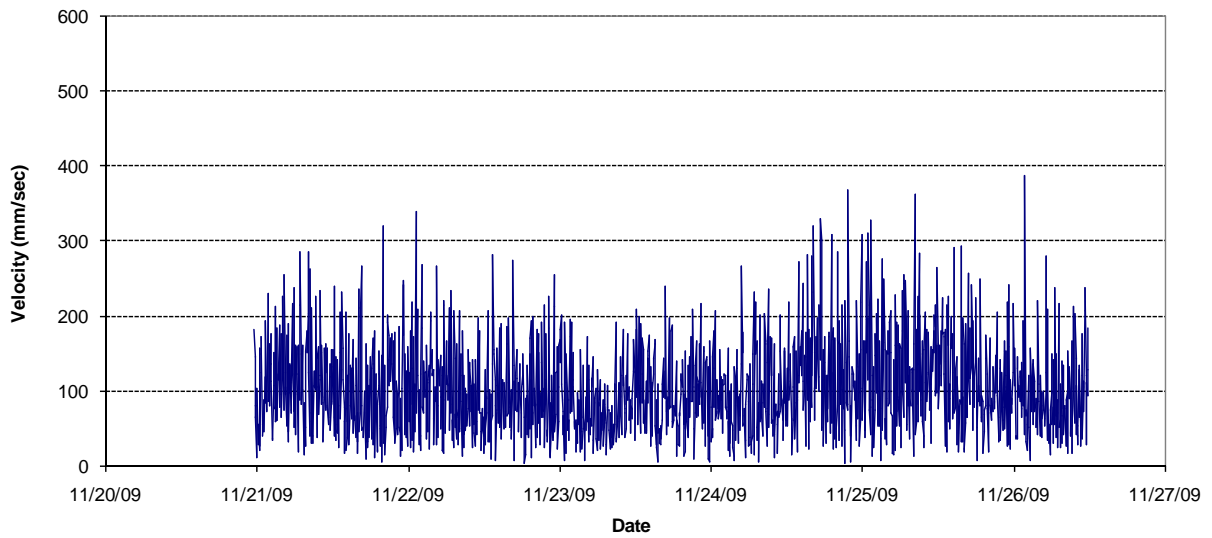
Figure 2-24



Week 1 – Bin 4 Current Measurements at Outside Gage



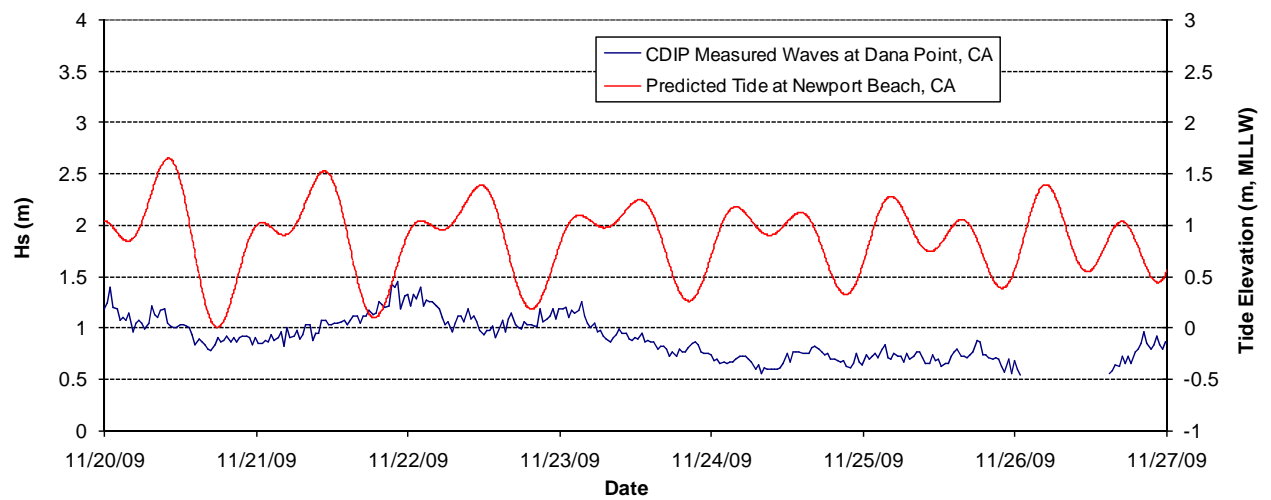
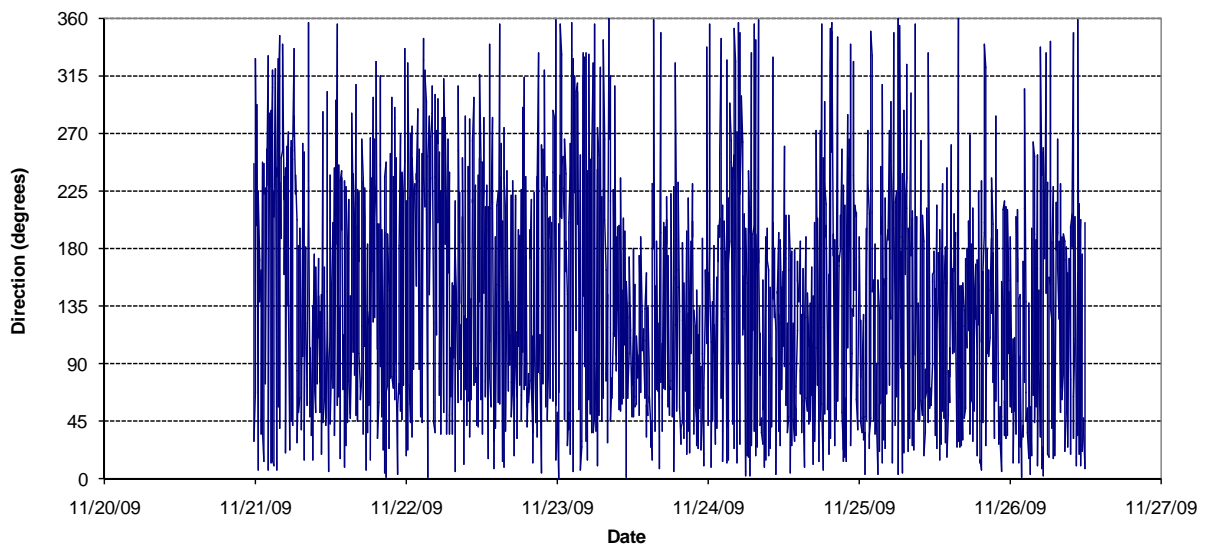
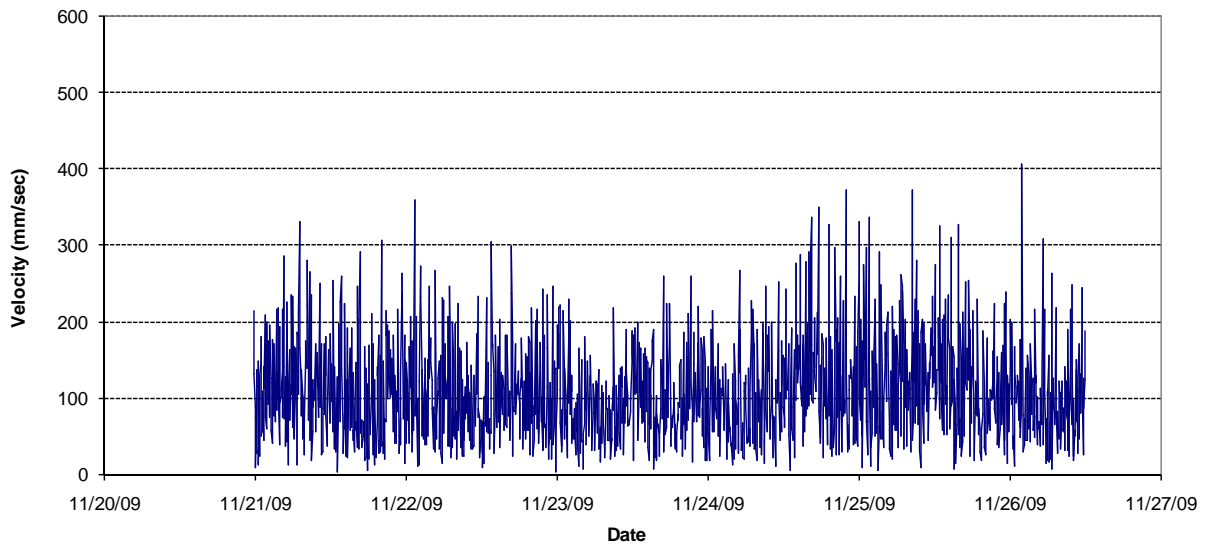
Figure 2-25



Week 1 – Bin 5 Current Measurements at Outside Gage



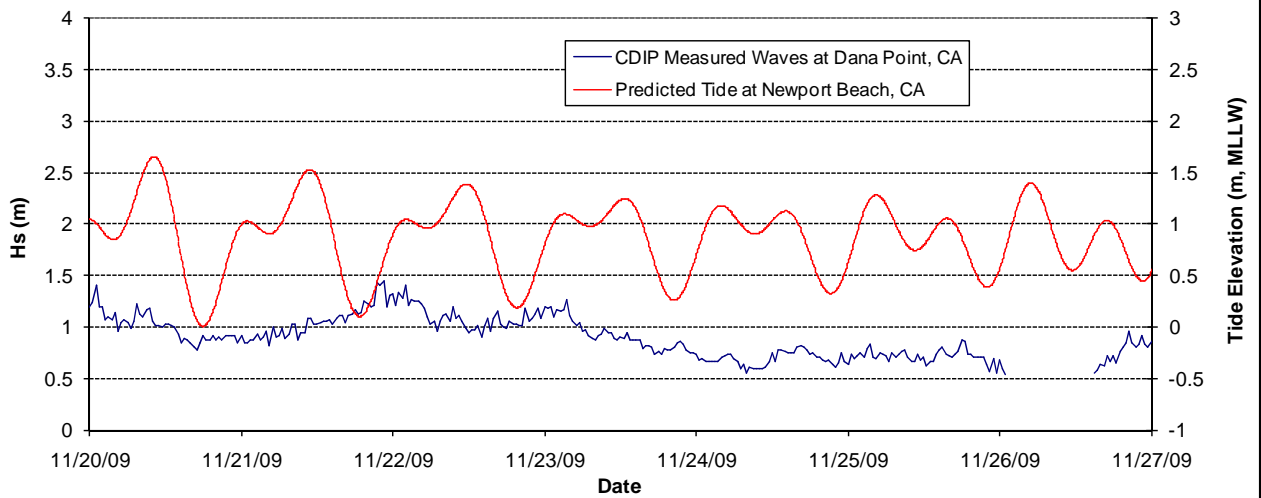
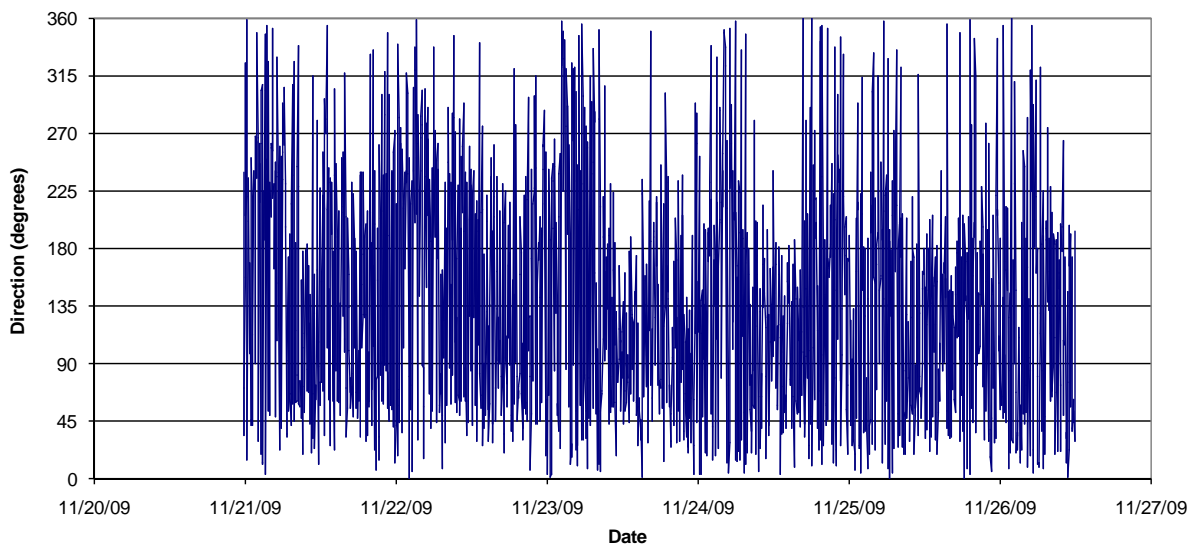
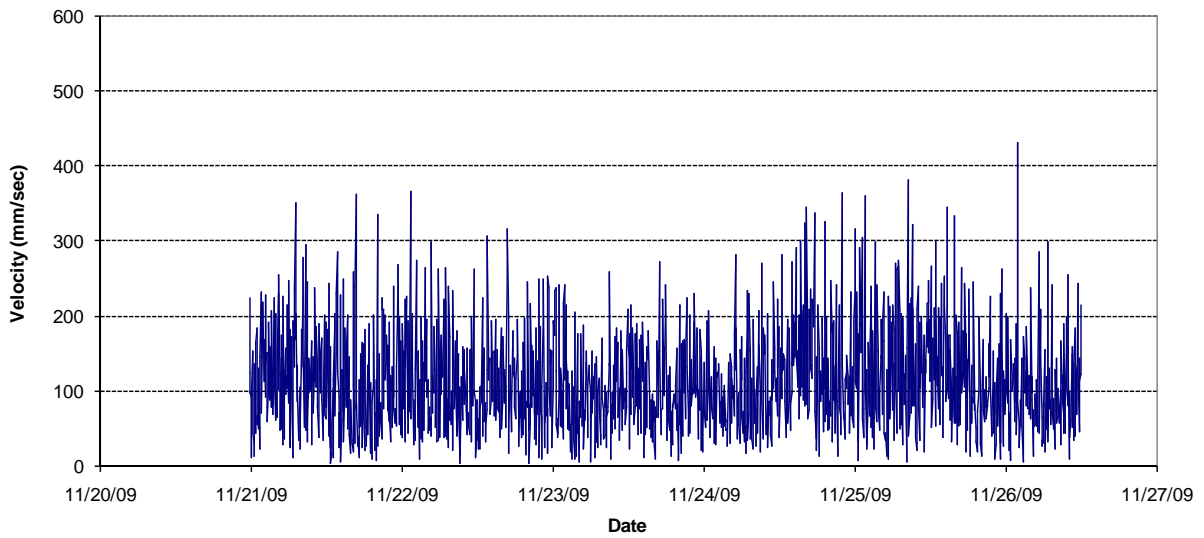
Figure 2-26



Week 1 – Bin 6 Current Measurements at Outside Gage



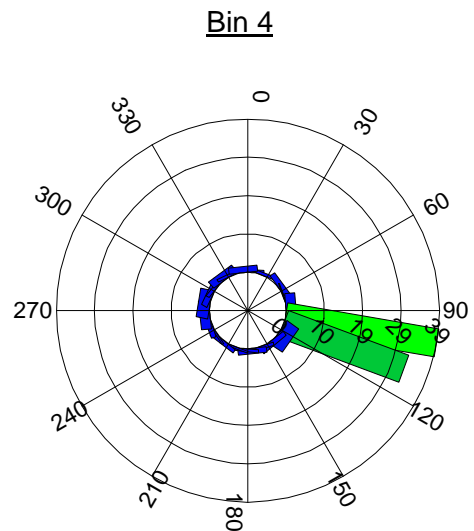
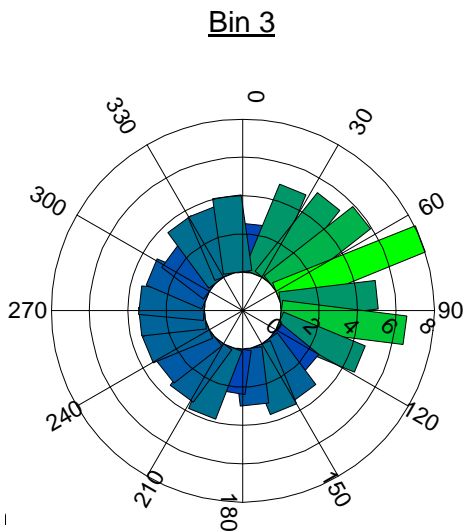
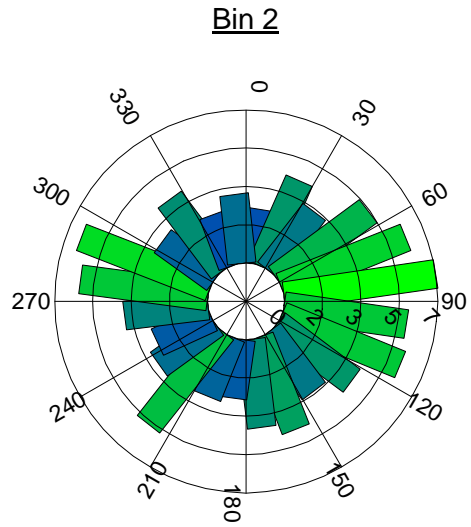
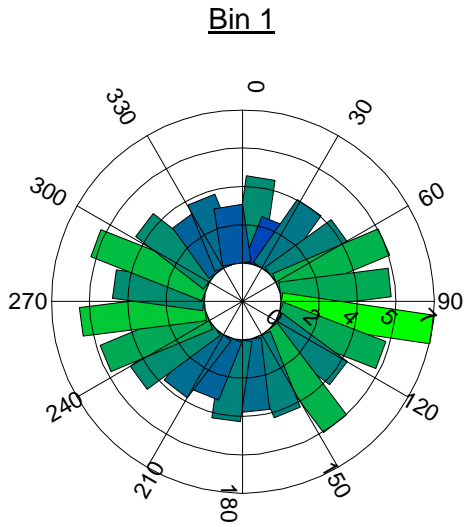
Figure 2-27



Week 1 – Bin 7 Current Measurements at Outside Gage



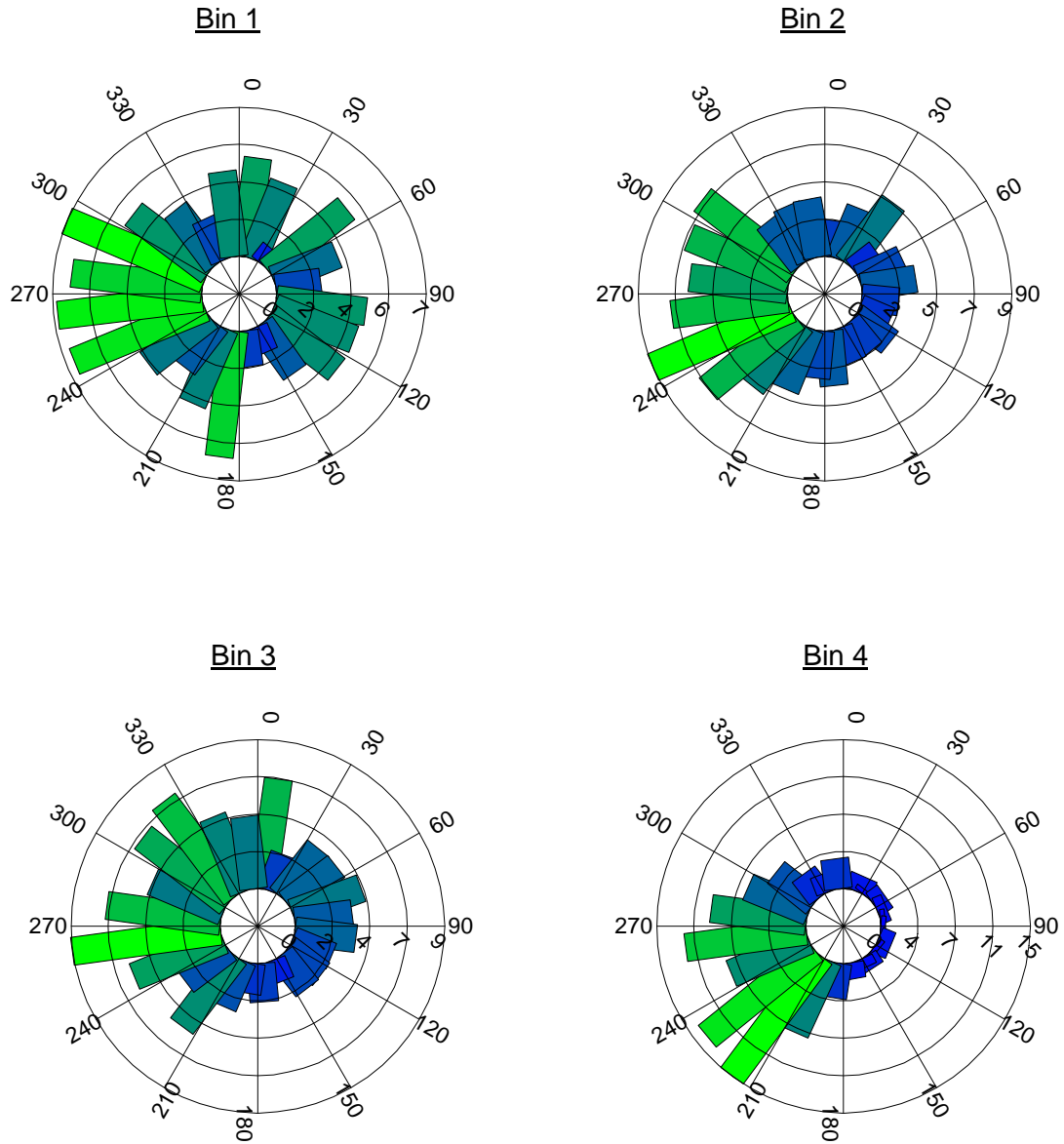
Figure 2-28



Notes: Duration from 12:00 pm to 7:30 pm, November 22, 2009
 Tidal range = 1.2 meters (3.9 feet)
 90 deg indicates current flowing toward east
 Total measurements = 451

Current Roses for Inside ADCP during Ebb Tide on November 22, 2009

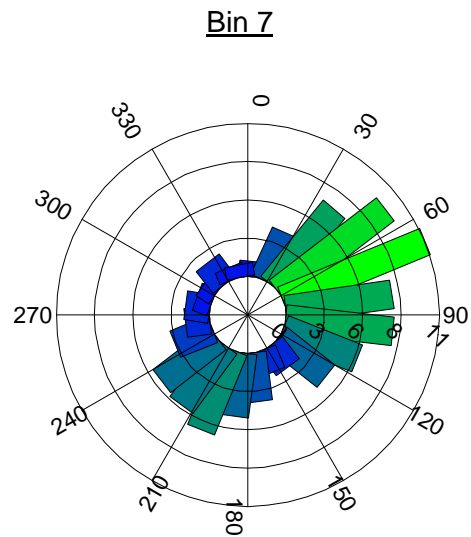
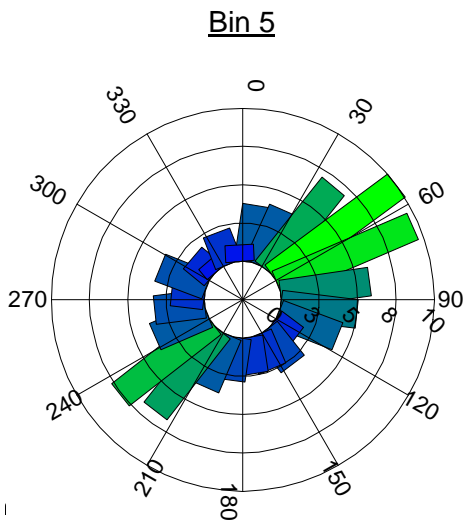
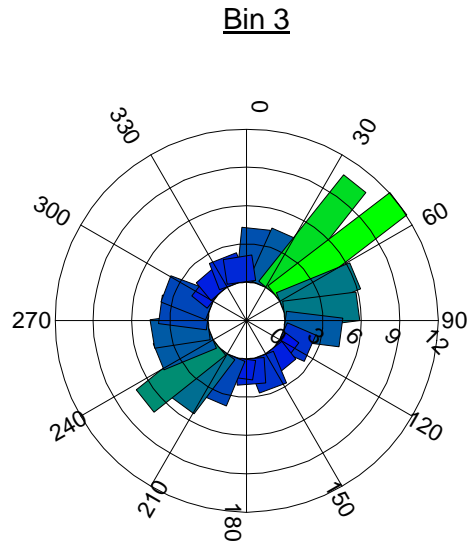
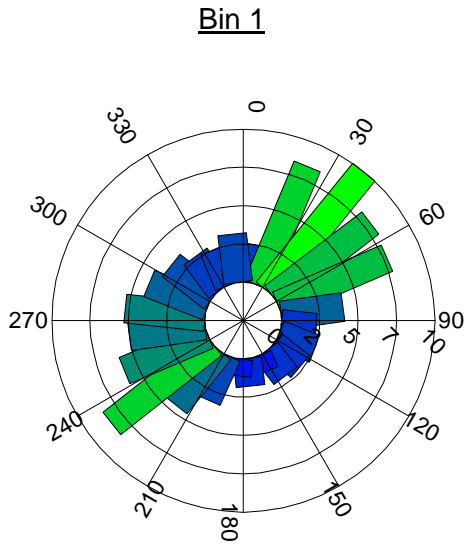




Notes: Duration from 7:35 pm, Nov. 22 to 2:55 am, Nov. 23, 2009
 Tidal range =0.9 meters (3.0 feet)
 90 deg indicates current flowing toward east
 Total measurements =441

Current Roses for Inside ADCP during Flood Tide on November 22, 2009

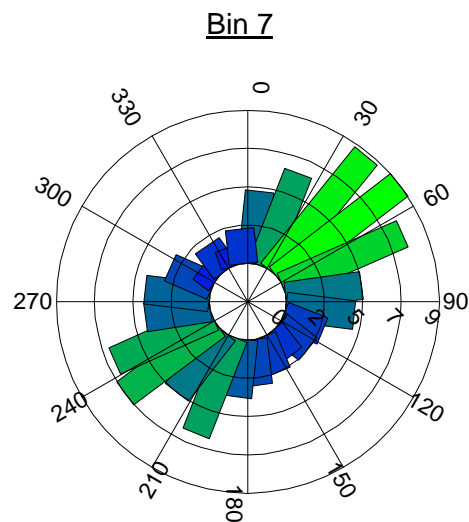
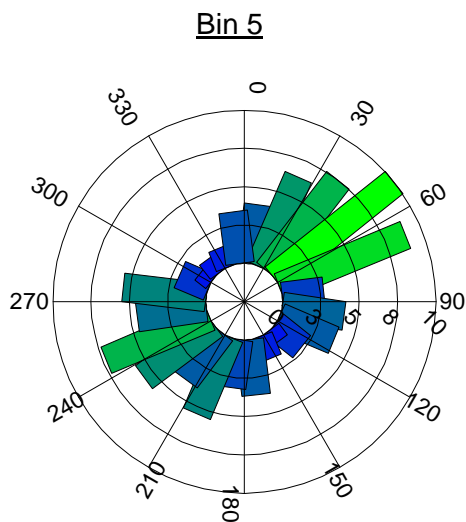
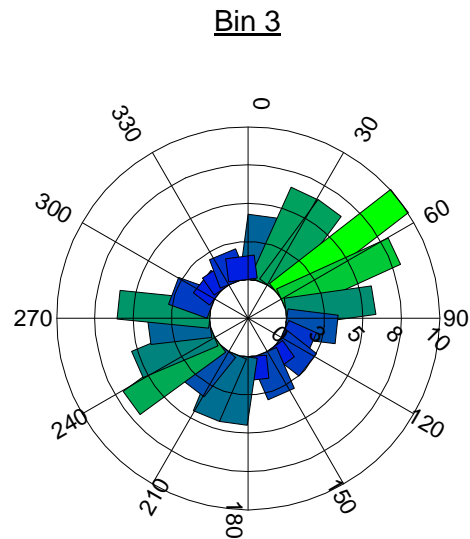
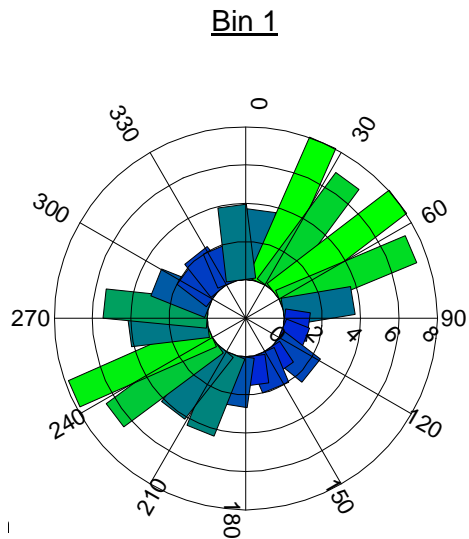




Notes: Duration from 12:00 pm to 7:30 pm, November 22, 2009
 Tidal range =1.2 meters (3.9 feet)
 90 deg indicates current flowing toward east
 Total measurements =451

Current Roses for Outside ADCP during Ebb Tide on November 22, 2009

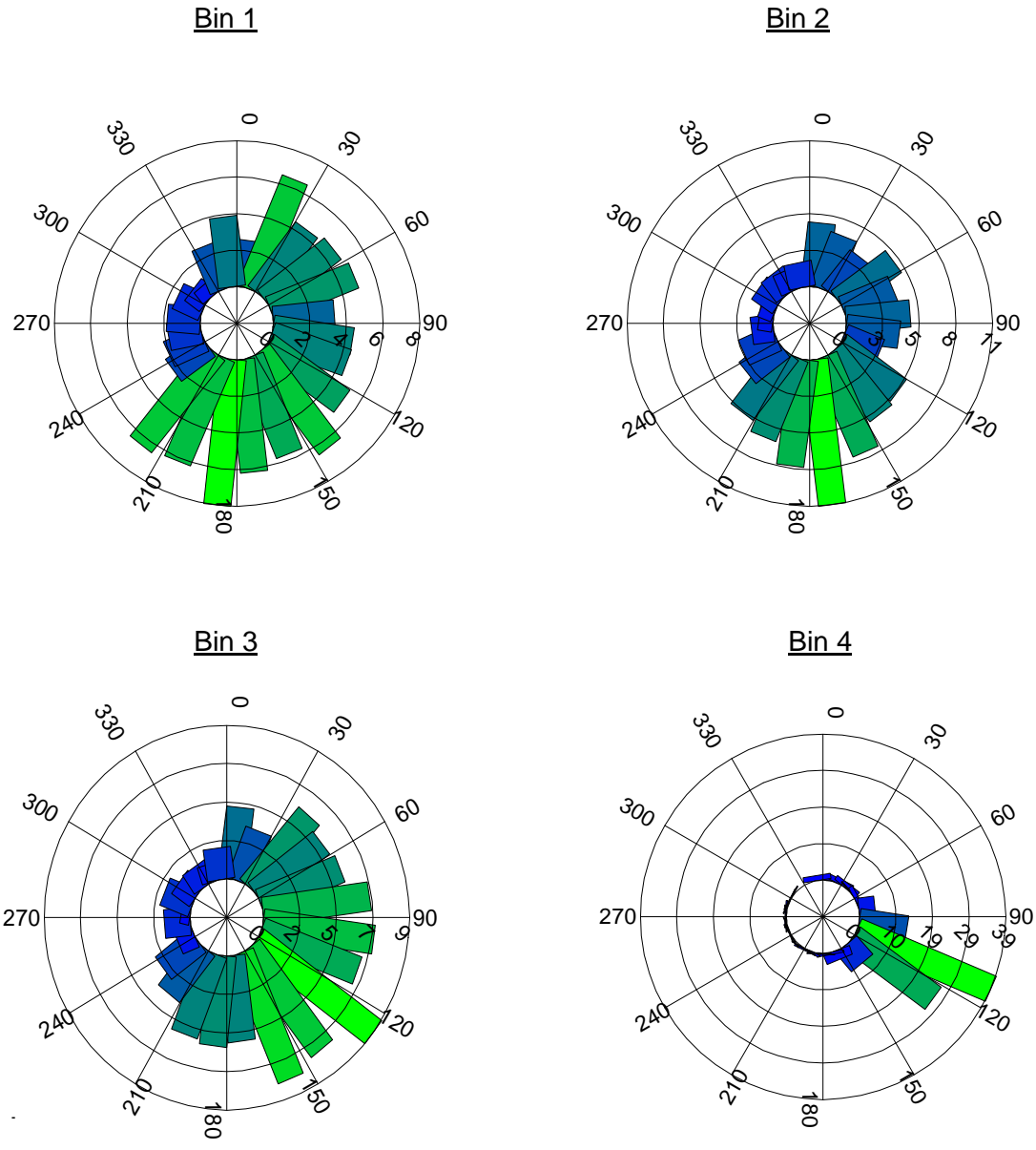




Notes: Duration from 7:35 pm, Nov. 22 to 2:55 am, Nov. 23, 2009
 Tidal range = 0.9 meters (3.0 feet)
 90 deg indicates current flowing toward east
 Total measurements = 441

Current Roses for Outside ADCP during Flood Tide on November 22, 2009

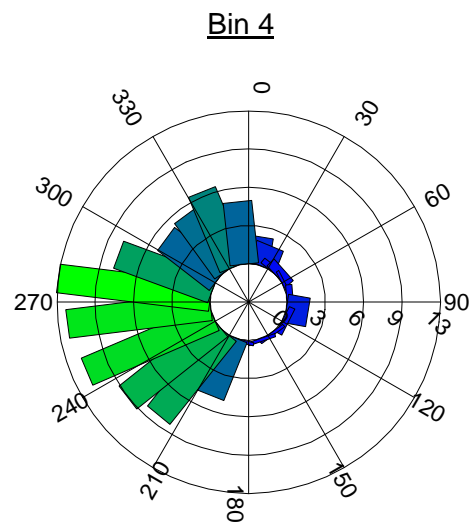
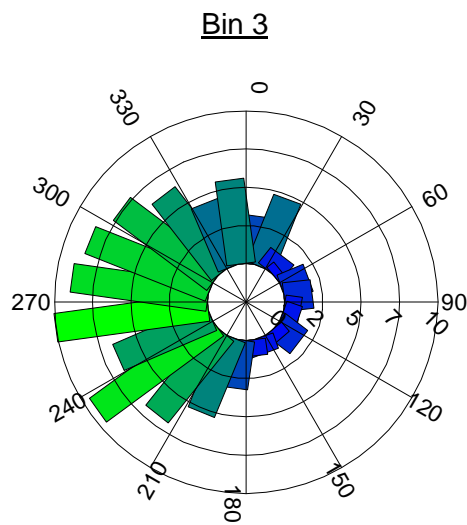
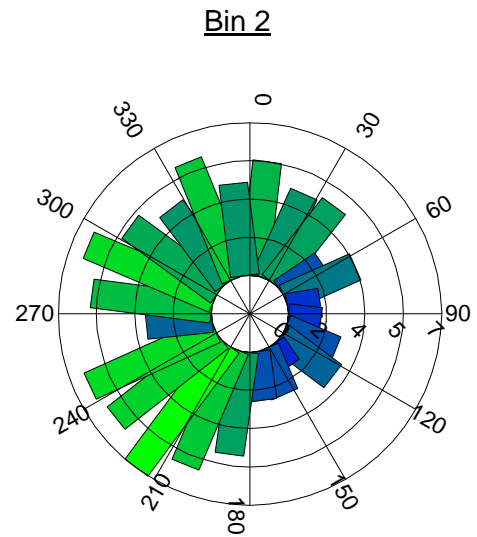
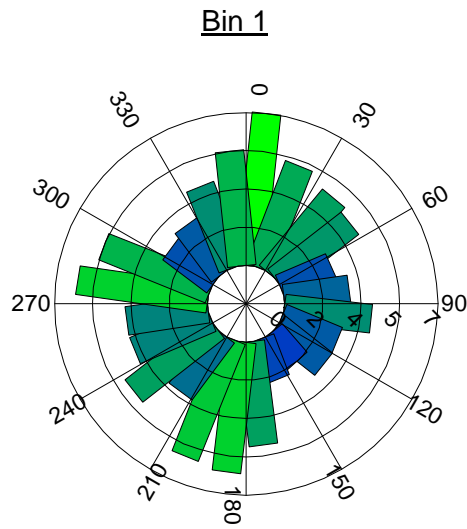




Notes: Duration from 12:30 pm to 6:45 pm, January 5, 2010
 Tidal range =1.3 meters (4.3 feet)
 90 deg indicates current flowing toward east
 Total measurements =391

Current Roses for Inside ADCP during Ebb Tide on January 5, 2010





Notes: Duration from 7:00 pm Jan. 5 to 1:30 am, Jan. 6, 2010
 Tidal range =1.4 meters (4.6 feet)
 90 deg indicates current flowing toward east
 Total measurements =387

Current Roses for Inside ADCP during Flood Tide on January 5, 2010



3.0 CMS-WAVE MODEL SIMULATIONS

3.1 Introduction

The Coastal Modeling System (CMS) is a suite of major multidimensional numerical models integrated to simulate waves, currents, water levels, sediment transport and morphology change in coastal inlets, estuaries, and harbors. The CMS, developed by the U.S. Army Corps of Engineers Coastal and Hydraulics Laboratory, consists primarily of three modeling modules, CMS-Wave, CMS-Flow and CMS-PTM. Both CMS-Flow and CMS-Wave can be coupled and operated by a steering module within the Surface-water Modeling System (Zundel, 2007) to dynamically simulate sediment transport and morphology change (Buttolph et al. 2006; Lin et al. 2008). CMS-PTM (Demirbilek et al. 2008) can be applied to compute the fate and pathways of sediment and other waterborne particles from the simulated wave environment, flow field and water exchange via CMS-Wave and CMS-Flow.

3.2 CMS-Wave Model Description

CMS-Wave is a two-dimensional (2D) wave spectral transformation model implemented in the Coastal Modeling System. The model employs a forward-marching, finite-difference method to solve the wave action conservation equation. It is a phase-averaged model, which averages changes in the wave phase to calculate wave properties and is based on the wave-action balance equation as

$$\frac{\partial(C_x N)}{\partial x} + \frac{\partial(C_y N)}{\partial y} + \frac{\partial(C_\theta N)}{\partial \theta} = \frac{\kappa}{2\sigma} [(C C_g \cos^2 \theta N_y)_y - \frac{C C_g}{2} \cos^2 \theta N_{yy}] - \varepsilon b N - S \quad (3-1)$$

where

$N = \frac{E(\sigma, \theta)}{\sigma}$ is the wave-action density that is a function of frequency σ and direction θ ;
 x and y are horizontal coordinates;
 C and C_g are wave celerity and group velocity;
 C_x , C_y and C_θ are the characteristic velocity with respect to x , y and Θ ;
 N_y and N_{yy} denote the first and second derivatives of N with respect to y ;
 κ is an empirical parameter representing the intensity of diffraction effect;

ε_b is the parameterization of wave breaking energy dissipation; and S denotes additional sources and sinks such as wind forcing, bottom friction loss.

CMS-Wave has theoretically derived approximations for wave refraction, shoaling, diffraction, reflection, and wave-current interaction, and therefore, is appropriate for conducting wave simulations at coastal inlets with jetties and in harbor entrances with breakwaters. It employs a forward-marching, finite-difference, steady-state (time-independent) Eulerian method to solve the wave action conservation equation. Wave diffraction is implemented by adding a diffraction term derived from the parabolic wave equation to the energy-balance equation (Mase et al. 2005). CMS-Wave can operate either on a coastal half-plane or full-plane with primary waves propagating from the seaward boundary toward the shore. Shoreward and seaward reflections are treated using a mirror reflection principle.

3.3 CMS-Wave Model Improvement

To improve the applicability for permeable rubble-mound breakwaters (e.g., the West and East Breakwaters at Dana Point Harbor) and allow for waves transmitting through the breakwaters, an additional component was included in the CMS-Wave to calculate the wave transmission coefficient K_t using d'Angremond et al. (1996) formula:

$$K_t = 0.64 \left[1 - \exp\left(-\frac{\xi}{2}\right) \right] \left(\frac{B}{H_i}\right)^{-0.31} - 0.4 \frac{h_c}{H_i} \quad , \quad \text{for } B < 10 H_i \quad (3-1)$$

where B is the crest width;
 ξ is the Iribarren parameter that is defined as the fore-slope of the breakwater divided by the square-root of deepwater incident wave steepness; and
 h_c is the height between the still water surface and the crest of the breakwater.

3.4 CMS-Wave Model Calibration

To ensure the applicability of the specific physical process at the breakwaters, CMS-Wave was calibrated by comparing to the directional wave data collected by the ADCP deployed outside (oceanside) the West Breakwater. **Figure 3-1** shows the CMS-Wave rectangular grid system that covers the entire harbor, the shoreline adjacent to the harbor, and the offshore region. The model

domain extends approximately 5 kilometers (3.1 miles) alongshore (expanding beyond the harbor boundary) and 4 kilometers (2.5 miles) offshore. The offshore boundary of the model domain reaches as deep as 300 meters (1,000 feet). The finite-difference grid consists of 130,473 (399×327) variable cells with the cell size ranging 5 meters (15 feet) at the harbor and 200 meters (600 feet) near the two seaward boundary corners. Both the West and East Breakwaters were specified as permeable structures that allow for waves transmission into the harbor.

The CMS-Wave calibration was performed using the collected wave data from 21 to 27 November, 2009. The model input included measurements of wind, wave, and water level at selected coastal or ocean stations. The incident wave spectra were transformed from the CDIP Dana Point Buoy 096 to the CMS-Wave grid offshore boundary using the linear wave theory with a simple assumption of shore-parallel depth contours. The measured water levels were extracted from NOAA Coastal Station 9410660 at San Pedro, Los Angeles Outer Harbor. The wind input information was acquired from the San Clemente Basin Buoy (Station 46086) of the National Data Buoy Center (NDBC). **Figure 3-2** shows the time series of wave height and water level that were collected at CDIP 096 and NOAA Station 9410660 for the calibration period (i.e., November 21 to 27, 2009). The 6-day period represents a benign wave condition with a wave approach direction typically observed in November. **Figure 3-3** illustrates the corresponding time series of wind speed and direction collected at NDBC Buoy 46086.

CMS-Wave was calibrated in a 3-hour interval with incident wave spectra and water levels specified at the sea boundary and wind input applied to the entire model domain. The bottom friction is neglected in the calibration with fully reflected waves set at the breakwaters to account for the effect of rocky outcrop bottom along the perimeter of the harbor. **Table 3-1** presents the calibrated parameters that are pertinent to CMS-Wave. **Figure 3-4** shows the comparison of wave parameters between the CMS-Wave modeled results and field measurements at the outside ADCP. The calculated wave results show a good consistency with the measured wave parameters. An underestimate of wave height during the beginning days could be related to the wind forcing as the wind input information was obtained from a NDBC offshore buoy. Strong wave refraction and reflection are evident from a comparison of the offshore (at the CDIP gage) and near-breakwater wave directions.

Table 3-1. Calibrated Model Parameters for CMS-Wave

<i>Model Parameter</i>	<i>Calibration</i>
Wave Diffraction Intensity	4.0
Backward Reflection Coefficient	1.0
Bottom Friction Coefficient	0.0

Figure 3-5 shows the comparison of CMS-Wave simulations with and without wind input as well as without tides (i.e., without the input of water level variation as a result of daily tides). **Table 3-2** presents the percent difference in model prediction compared to the oceanside ADCP measurements. The comparison indicates that the calculated wave height and direction with wind input and tides agree better with data than without the wind and water level (tide) forcing. The wave period calculation is not affected by the conditions with or without the wind and water level input. Exclusion of the wind and water level (tide) forcing in the simulations, CMS-Wave under-predicts the wave height by approximately 4% to 6% at the oceanside ADCP location.

Figure 3-6 shows the comparison of model results with and without wave reflection at breakwaters and bottom friction in the simulation. The CMS-Wave simulation with wave reflection at breakwaters agrees better with data than without the wave reflection calculation. Without invoking wave reflection of the structure, the model underprediction can be as high as 31% (see Table 3-2). It is evident that wave reflection plays an important role in accurately predicting the incident wave height near the breakwaters. On the other hand, the effect of bottom friction, using a Mannings coefficient of 0.025, appears to be insignificant (see also Figure 3-6).

Table 3-2. Comparison of Calculated Wave Height at Outside ADCP

	<i>Average Hs (m)</i>	<i>Mean Bias Hs (m)</i>	<i>Percent Difference (%)</i>
ADCP Measurement	0.67	-	-
CMS-Wave Calibration	0.64	-0.03	4.5
Excluding Wind	0.64	-0.035	5.2
Excluding Tides	0.63	-0.04	6.0
With Bottom Friction	0.64	-0.03	4.5
Without Wave Reflection	0.46	-0.21	31.3

3.5 Design Storm Wave Criteria at Dana Point Harbor

The afore-calibrated CMS-Wave was applied to establish the storm design criteria for the dual protective breakwaters at Dana Point Harbor. The storm wave criteria were derived based on the historical storm events. Peak wave heights at the dual breakwaters during individual storms were estimated by wave hindcast in deep water, wave transformation that accounts for offshore island sheltering, and the CMS-Wave simulations that includes wave refraction, diffraction, shoaling and reflection.

3.5.1 General Wave Climatic Conditions

Wind generated waves and distant swells approaching Dana Point Harbor are produced by the following six (6) meteorological patterns (USACE-LAD, 1996): i) extratropical cyclone in the northern hemisphere; ii) northwest winds in the outer coastal waters; iii) west to northwest local sea; iv) pre-frontal local sea; v) tropical storm swell; and iv) extratropical cyclone in the southern hemisphere.

Extratropical Cyclone in the Northern Hemisphere

Low pressure centers which develop along the polar front are the source of the predominant wave action along the entire California coast during the winter season. Storm swells are typically generated at some distance from the Dana Point coastline in the North Pacific. Most commonly these storms will traverse the mid-Pacific before turning northeastward toward the Gulf of Alaska with swells decaying on the average of 1,000 kilometers (660 miles) to the coast of Southern California. However, under some meteorological conditions such as during the El Nino seasons, storms can be developed in the low latitude region west of the California coast and move in much closer to the coast; and on a rare occasion these storms may move directly across Southern California, following a northeast, east or southeast trajectory. The severe winter storm occurring in January 1988 is an example of the moving close-by storm, which resulted in extremely high waves that were recorded along the Southern California coast.

Northwest Winds in the Outer Coastal Waters

The predominant wave action along the coast area within the south Orange County shoreline is due to the prevailing northwest winds. This is particularly true during the spring and summer months. Wave heights are usually low, less than one meters; but on occasion, with superposition of a strong surface high and an upper level trough, the northwesterlies increase, becoming very

strong from about Point Sal to San Nicolas Island. The inner waters of Southern California very often remain unaffected under the influence of the Catalina eddy circulation. Waves traveling at a variance to the mean wind direction reach the nearshore water with periods on the order of 6 to 10 seconds. Moderate winds from the northwest will produce breaker heights of 1 to 2 meters (3.3 to 6.6 feet), while strong events can generate heights of 2 to 3 meters (6.6 to 10 feet).

West to Northwest Local Sea

Local westerly winds can be divided into two types: 1) temperature-induced sea breezes, and 2) gradient winds. The former exhibits a pronounced seasonal and diurnal variation. The strongest sea breezes occur during the late spring and summer months, while the lightest winds are during December and January. The summer sea breezes averaging about 7.7 m/sec (15 knots) usually set in during the late morning and peak in the mid-afternoon. In winter months, sea breeze conditions are limited to a few hours during early afternoon with wind speeds on the order of 5.1 m/sec (10 knots). Gradient winds are confined largely to the months of November through May with the peak in March and early April. These typically occur following a frontal passage or with the development of a cold low pressure area over the southwestern United States.

Pre-Frontal Local Sea

The coastal zone within the south Orange County area is vulnerable under extratropical winter storm conditions (a counterclockwise wind motion) prior to frontal passage winds blowing strongly from the southeast along the coast but turning toward the south-southeast to south a short distance offshore. Wind waves, with peak energy averaging between 6 and 8 seconds, reach the shore with minimal loss. Significant wave heights are generally in the range of 1 to 2.5 meters (3.3 to 8.3 feet). Extreme wave heights are rare because the fetch to the shoreline is generally limited and the duration of the event is typically short. An example of this rare case is the storm of January 4, 1995, which generated southerly seas of 3 meters (10 feet).

Tropical Storm Swell

Tropical cyclones form regularly along the intertropical convergence zone west of Mexico from early July to early October. On the average, about 15 to 20 of them are to be expected each year. Most of the tropical cyclones travel on a westerly track, and swells generated by these storms will have little or no effect

on Southern California. A few, however, take a northwest track, thereby lengthening the effective fetch over which swells traveling toward south Orange County can be generated.

Extratropical Cyclone in the Southern Hemisphere

From the months of April through October, and to a lesser extent the remainder of the year, large South Pacific storm systems traversing the ocean between 40 and 60 degrees south from Australia to South America send swells northward to the west coast of Central and North America. The great circle approaching directions to Southern California range from about 215 degrees for storms near New Zealand to 170 degrees for South American storm systems, respectively. The decay distance ranges from about 7,200 to 11,200 kilometers (4,750 to 7,400 miles). Wave heights in deep water are usually low, on the order of less than one meter; however, since these waves are nearly monochromatic, their capacity for shoaling is greatly enhanced. Breakers of 2 to 3 meters (6.6 to 10 feet) in the south Orange County coastal region are not uncommon.

3.5.2 Deep Water Wave Climate

Because a sufficiently long-term history of direct measurements of waves and currents is generally not available, it is necessary to utilize wave hindcast that is based on meteorological data. The Global Reanalysis of Ocean Waves (GROW) data (Oceanweather, Inc., 2010) was selected to formulate long-term wave climate along the Dana Point coast, as it covers 39 years (1970-2008) of hindcast wave information.

The GROW hindcast is based on historical data consisting of background wind fields, tropical system data archives, ice edge data, and wave measurements for the validation purposes (Oceanweather, Inc., 2007). It has a global grid spacing of 0.625° in latitude by 1.25° in longitude and uses the Pierson-Moskowitz fully developed sea theory. The hindcasted sea and swell conditions were derived from a full two-dimensional (2D) spectral wind-wave generation model. Results of the GROW wave hindcast include the archived wind, wave, and spectra fields in three-hour intervals. **Figure 3-7** shows the GROW deepwater hindcast station (Station 38190) located west of San Nicholas Island at 33.125°N (latitude) and 120.0°W (longitude) in a water depth of 1,000 meters (3,300 feet). The 39-year GROW data (1970-2008) was used to establish a database of offshore deepwater wave climate.

3.5.3 Wave Transformation

To determine wave characteristics at the offshore boundary for the CMS simulations, the GROW data was transformed via the O'Reilly spectral back-refraction model (O'Reilly & Guza, 1991) to account for the island sheltering effect, wave refraction, and wave shoaling. The O'Reilly spectral back-refraction model performs a linear refraction transformation in which the transferred spectrum is established from the incident wave spectrum by back-refracting rays from the target site. Unlike more traditional forward ray refraction methods, the O'Reilly model back-refracts wave rays from the site of interest, therefore eliminating caustics which plague forward ray tracing schemes. This transformation model has been extensively validated in the field throughout the Southern California coast.

The two locations (CMS_1 and CMS_2), as shown in **Figure 3-8**, that were selected for the Dana Point study area are situated in water depths of 35 meters (115 feet) and 300 meters (984 feet), respectively. The 39-year GROW hindcast wave data in the deep water was converted to 2D wave spectra and transformed to these two locations. It is noted that the wave parameters of the GROW data include separate estimates of sea and swell energy, peak periods, and mean directions.

The 39-year (1970-2008) time series of GROW deep-water sea and swell wave parameters were transformed and propagated through the Southern California Islands to the Dana Point coast by first converting the deep-water wave parameters to a 2D JONSWAP-Mitsuyasu spectrum after Goda (1985). The JONSWAP-Mitsuyasu 2D wave spectra are characterized by a spectral peak enhancement factor, Γ , and a directional spreading parameter, S_{max} , to describe the distribution of wave energy around the peak period, T_p , and peak wave direction, D_p . Based on the observed frequency and directional spreading at the San Nicolas Island wave buoy, the following values were respectively assigned to Γ and S_{max} for different peak periods:

- $\Gamma = 3$ for $T_p < 6$ second,
- $\Gamma = T_p/2$ for $T_p > 6$ second, and
- $S_{max} = 50$ for both sea and swell.

The sea and swell spectra were estimated separately and then combined to form the final deep-water 2D spectrum prior to its transformation to the nearshore water region.

The spectral refraction wave transformation yields the same 5 spectral wave parameters that are measured by directional wave buoys: wave energy content in a frequency bin, and the first four (4) directional Fourier coefficients (a_1 , b_1 , a_2 , and b_2), as a function of the corresponding wave frequency (Kuik et. al., 1988). The directional coefficients were in turn be used with a directional estimator (e.g., Maximum Entropy Method) to estimate the 2D wave spectra time series at CMS_1 and CMS_2 (Lygre and Krogstad, 1986).

3.5.4 Hindcast Validation

Extreme winter wave events were of the greatest concern in this study, and these waves reach the Dana Point area through relatively narrow directional windows on either side of Santa Catalina Island (see Figure 3-7). As a result, wave conditions near Dana Point are considerably smaller than the offshore wave conditions on average. In addition, wave hindcast in this region can be sensitive to small directional biases in the incident offshore wave spectra, which can result in too much or too little wave energy passing through the islands.

To fine tune and validate the transformation of GROW data to the Dana Point region, the transformed wave heights were compared to measured waves at the CDIP Dana Point Buoy 096 (see Figures 3-7) from 2000 to 2008. **Figure 3-9** shows the result of the entire 8 year validation. A direct wave height time series comparison of buoy and transformed hindcast wave data shows a modest but consistent overprediction of larger winter wave events. However, by rotating the offshore swell directional spectra 5 degrees northward, a good overall peak wave height agreement between the Dana Point buoy and the transformed GROW hindcast was obtained.

The offshore GROW hindcast wave heights (GROW, green line) are significantly greater than those measured at Dana Point Buoy 096 inside the islands near the coast (Dana Buoy, red line). The GROW 2D spectra were rotated 5 degrees and transformed to the Dana Point Buoy 096 location using the spectral refraction model (GROW ADJ, blue line). Figure 3-9 illustrates that the transformation captures the overall reduction in wave heights (red and blue time series fluctuate at the same level) as well as the extreme conditions (max red and blue heights are of the same magnitude).

The unbiased nature of the Dana Point hindcast is further illustrated by the scatter plot shown in **Figure 3-10**. The transformed GROW wave heights are plotted versus the buoy observations. While there is considerable scatter, the 5 degree rotation of the offshore GROW spectra does yield relatively unbiased

estimates of larger wave events. The transformed hindcast wave tends to underpredict wave height during low wave conditions (scatter falls below the one-to-one line at low heights), that are a minor concern of more energetic wave situations.

Some scatter at larger wave heights can be attributed to small storm timing errors between the hindcast and actual wave arrivals. **Figure 3-11** shows the early 2008 comparison of time period in more detail. During this particular time period several larger peak wave heights were underpredicted by the transformed hindcast (blue line). However, the last storm (circled) of the sequence also illustrates how a good storm wave height hindcast with a timing offset can appear in the scatter plot as both overprediction (hindcast storm arrives too early) and underprediction (hindcast fades too soon). In the present study, a hindcast that reflects the proper frequency of occurrence and size of winter storm wave conditions, in a general statistical sense, is most critical. Accordingly, the 5-degree rotation of GROW offshore swell directions was applied to the entire 39-year dataset for transforming the hindcasts to the two selected nearshore locations (CMS_1 & CMS_2), which were used in the CMS simulations.

3.5.5 Historical Storm Events

Historical storm events between 1970 and 2008 were selected, based on the defined threshold criteria of wave height at CMS_1 as well as previously documented historical storm events. The 39-year wave data was sorted to satisfy the following criteria:

1. Wave height greater than a specified threshold value, and
2. Only one peak wave height is allowed for each storm event (i.e. over the 3-day interval), as it is typical for a storm event occurring in Southern California to have a duration of approximately 3 days.

In addition, previously known historical storm events were referenced to assist in determining each storm episode. In total, 42 individual historic storm events with the information of peak significant wave height, wave period and approach direction were selected at the transformed offshore CMS_1 location, as listed in **Table 3-3**. To ensure that the wave characteristics during an entire storm event was captured, 5 days of wave data for each selected event were extracted at CMS_1 and CMS_2, as the offshore boundary input for the CMS simulations.

Table 3-3. Selected Historical Storm Wave Events

<i>Date of Storm</i>	<i>Deepwater Wave Characteristics at CMS_1</i>		
	<i>Peak Hs m (ft)</i>	<i>Tp (sec)</i>	<i>Dir (deg)</i>
Jan 18, 1973	2.6 (8.5)	7.1	201.4
Dec 28, 1974	2.3 (7.5)	12.5	278.8
Jan 16, 1978	2.8 (9.2)	12.5	277.4
Mar 5, 1978	2.9 (9.5)	7.7	206.5
Dec 24, 1979	3.5 (11.5)	8.3	188.2
Feb 17, 1980	3.7 (12.1)	12.5	248.1
Jan 23, 1981	3.1 (10.2)	14.3	277.2
Jan 28, 1981	3.3 (10.8)	12.5	277.4
Dec 1, 1982	2.8 (9.2)	10.0	265.8
Jan 27, 1983	3.5 (11.5)	16.7	277.8
Feb 13, 1983	2.9 (9.5)	14.3	277.2
Mar 2, 1983	4.9 (16.1)	16.7	267.7
Mar 18, 1983	3.0 (9.8)	14.3	277.2
Dec 4, 1983	2.0 (6.6)	8.3	264.4
Dec 3, 1985	2.8 (9.2)	14.3	277.2
Feb 1, 1986	3.1 (10.2)	14.3	278.1
Feb 15, 1986	4.4 (14.4)	14.3	249.5
Mar 11, 1986	3.3 (10.8)	16.7	276.6
Mar 16, 1986	3.1 (10.2)	14.3	278.1
Dec 8, 1987	2.1 (6.9)	16.7	279.0
Dec 17, 1987	3.7 (12.1)	14.3	252.9
Jan 18, 1988	4.4 (14.4)	11.1	263.7
Mar 1, 1991	3.0 (9.8)	11.1	277.5
Jan 18, 1993	3.1 (10.2)	11.1	249.8
Jan 5, 1995	3.5 (11.5)	9.1	244.3
Jan 11, 1995	3.8 (12.5)	12.5	275.2
Mar 12, 1995	3.1 (10.2)	12.5	269.7
Dec 13, 1995	3.0 (9.8)	14.3	277.2
Nov 27, 1997	2.8 (9.2)	11.1	275.3
Feb 3, 1998	4.6 (15.1)	8.3	190.9
Feb 7, 1998	4.3 (14.1)	12.5	248.1
Feb 17, 1998	3.0 (9.8)	16.7	277.8
Feb 24, 1998	2.6 (8.5)	14.3	278.1
Feb 21, 2000	3.2 (10.5)	12.5	275.2
Jan 11, 2001	2.8 (9.2)	14.3	278.1
Dec 17, 2002	3.2 (10.5)	14.3	278.1
Feb 26, 2004	3.1 (10.2)	14.3	278.1
Jan 7, 2005	3.6 (12.0)	8.3	205.5
Jan 2, 2006	3.2 (10.5)	8.3	208.9
Dec 28, 2006	2.3 (7.5)	11.1	271.0
Jan 5, 2008	2.7 (8.9)	16.7	278.5
Feb 25, 2008	3.4 (11.2)	14.3	277.2

3.5.6 Storm Wave Characteristics at Dana Point Harbor

Nearshore storm wave characteristics were deduced at several grid locations immediately offshore of both the East and West Breakwaters via the CMS-Wave simulations. In total, eighteen (18) grid locations were chosen to represent the six (6) breakwater observation stations depicted in **Figure 3-12**. Three clustered monitoring grid cells for each breakwater location were selected to ensure a maximum wave height at each selected breakwater location was deduced. The model results include a time series of significant wave height, wave period, and wave direction at each monitoring station. The deduced maximum significant wave heights at six (6) different breakwater locations for each modeled storm event are presented in **Figures 3-13** and **3-14**. The large wave heights observed at Location 4 depict the wave conditions at the head of the West Breakwater, while the reduced wave heights at Location 5 describe sheltered wave conditions at the head of the East Breakwater.

The transformed nearshore wave conditions over a 39-year time period (1970-2008) at the selected 18 grid cells were analyzed to determine the extreme recurrence intervals using the probability distribution method provided by the Corps of Engineers (Leenknecht et. al, 1992). The maximum computed significant wave heights (refer to Figures 3-13 and 3-14) were fitted to a Fisher-Tippet Type I (FT-I) or Weibull probability distribution approximation. These curve fittings were performed through the Automated Coastal Engineering System (ACES), which was developed by the Corps of Engineers (USACE, 1991). It was observed that the data could be best described by a FT-I probability distribution function. Subsequently, the significant wave heights associated with various return periods were estimated for each selected breakwater location by selecting the maximum computed return wave height among the three grid cells. **Table 3-4** lists the deduced wave heights for the 5-, 10-, 25-, 50-, and 100-year return intervals at individual locations. The graphic representation of the data fitting for each respective station is displayed in **Figures 3-15** to **3-20**.

The deduced wave characteristics for severe extratropical storms during the 39-year time period (1970-2008) are comparable to peak storm wave heights that were previously computed for the general design of Dana Point Harbor (USACE-LAD, 1965). The deduced peak wave heights at the West Breakwater for three referred historic extratropical storm events prior to 1965, which were listed in the Design Memorandum, are 4.9 meters (16.1 feet) for the March 1904 storm, 4.9 meters (16.1 feet) for the January 1915, and 4.3 meters (14.1 feet) for the January 1943 storm, respectively. The maximum storm wave height

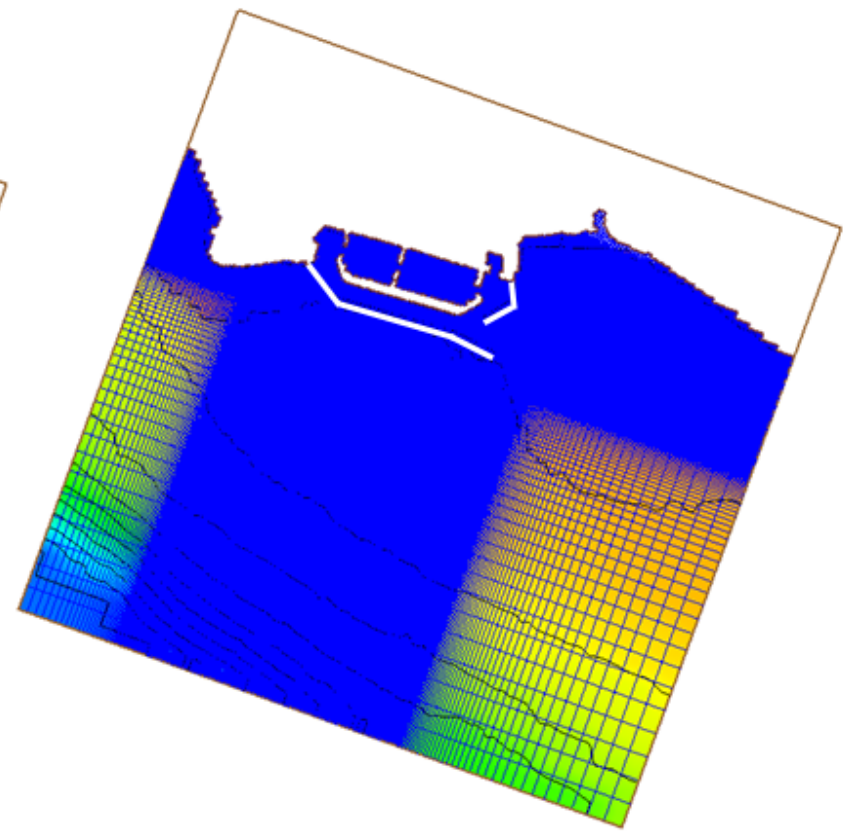
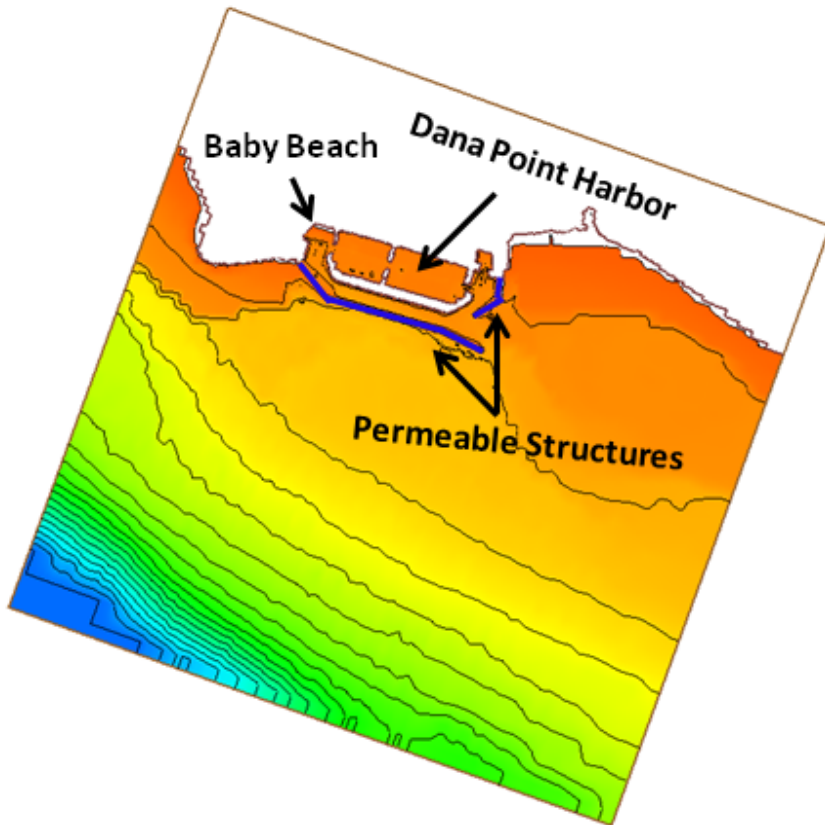
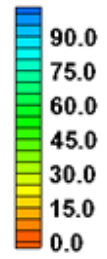
simulated by CMS-Wave is 5 meters (16.4 feet) during the February 28, 1983 storm event. The 1965 Design Memorandum called for 6 to 20 tons of riprap stones to construct the outer layers of the West breakwater from Stations 0+91 to 16+76 (Sta. 3+00 to 55+00 in feet).

Table 3-4. Estimated Extreme Return Wave Heights

<i>Breakwater Location</i>		<i>Return Wave Heights m (ft)</i>				
		<i>5-yr</i>	<i>10-yr</i>	<i>25-yr</i>	<i>50-yr</i>	<i>100-yr</i>
West Breakwater	Location 1	2.5 (8.2)	2.9 (9.5)	3.5 (11.5)	3.8 (12.5)	4.2 (13.8)
	Location 2	3.4 (11.2)	3.9 (12.8)	4.6 (15.1)	5.1 (16.7)	5.7 (18.7)
	Location 3	3.4 (11.2)	3.9 (12.8)	4.5 (14.8)	5.0 (16.4)	5.5 (18.0)
	Location 4	3.6 (11.8)	4.1 (13.5)	4.8 (15.7)	5.3 (17.4)	5.8 (19.0)
East Breakwater	Location 5	0.6 (2.0)	0.7 (2.3)	0.8 (2.6)	0.9 (3.0)	0.9 (3.0)
	Location 6	1.5 (4.9)	1.8 (5.9)	2.1 (6.9)	2.3 (7.5)	2.6 (8.5)

It is noted that a recent study was performed by the California Climate Change Center (Cayan, et al., 2009) to assess likely winter wave height changes along the California coast under various scenarios of greenhouse gas emission (i.e., sea level rise) in the future. It was concluded that the intensity of future winter storms is expected to follow a slightly negative trend within southern California, as the mean cyclone track with a warmer climate tends to move further north. Therefore, the return wave heights deduced from the 1970-2008 period should still be applicable in the future if any alteration or maintenance of the breakwaters is required.

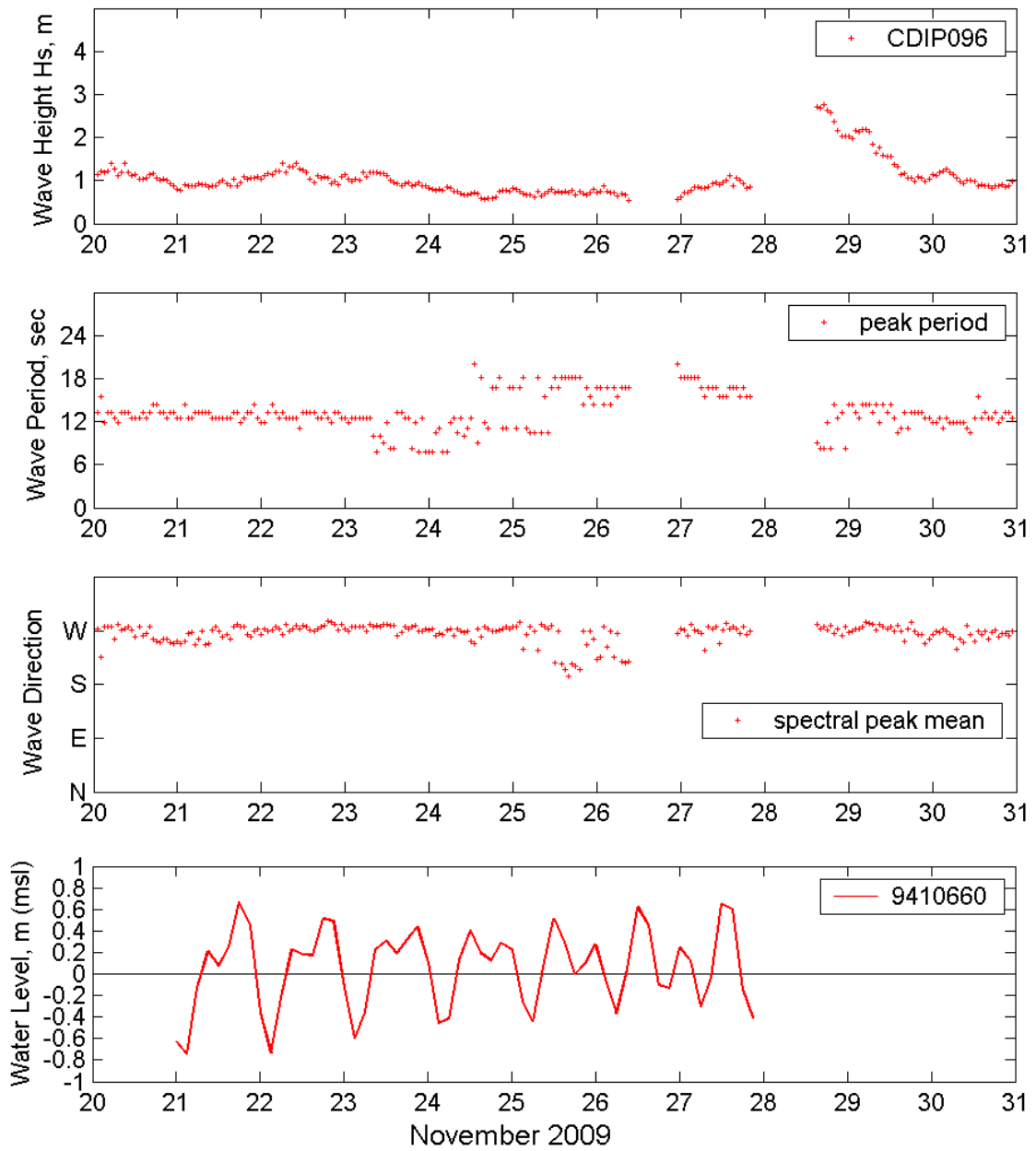
Depth (m)



CMS-Wave Model Domain and Grid System



Figure 3-1

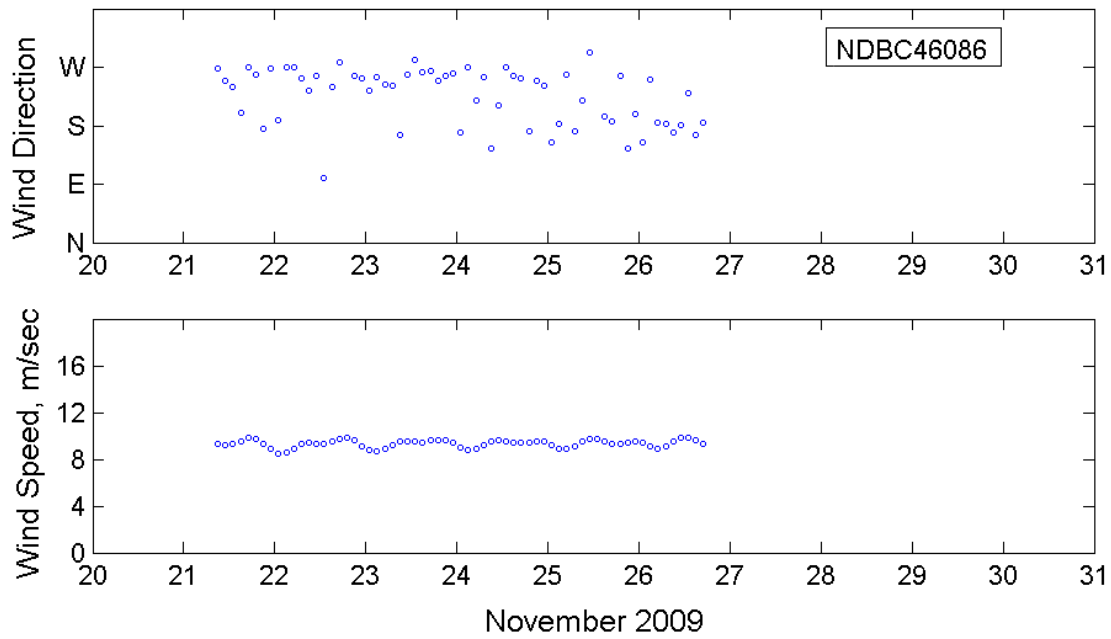


Note: Duration from November 20 to 31, 2009

CDIP 096 Wave and NOAA 9410660 Water Levels



Figure 3-2

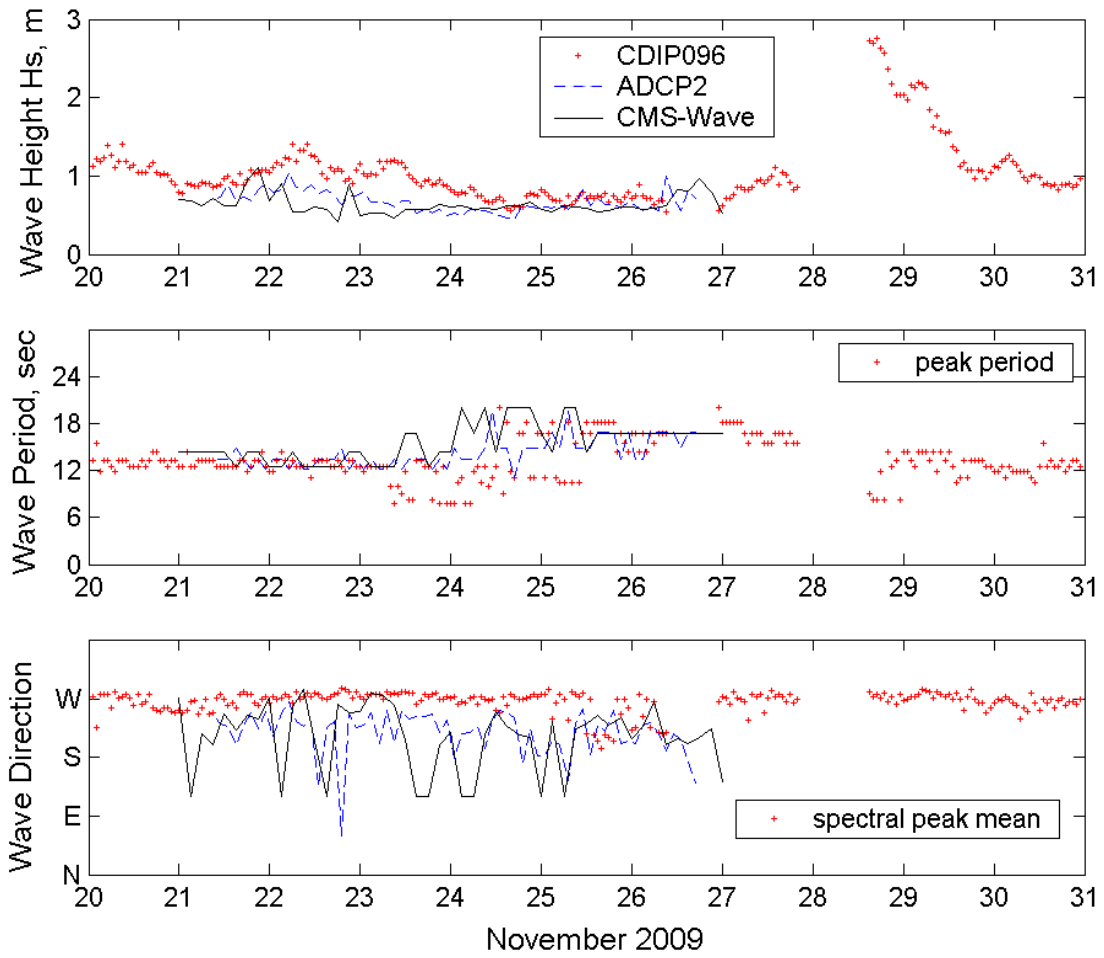


Note: Duration from November 20 to 31, 2009

NDBC 46086 Wind Speed and Direction Information



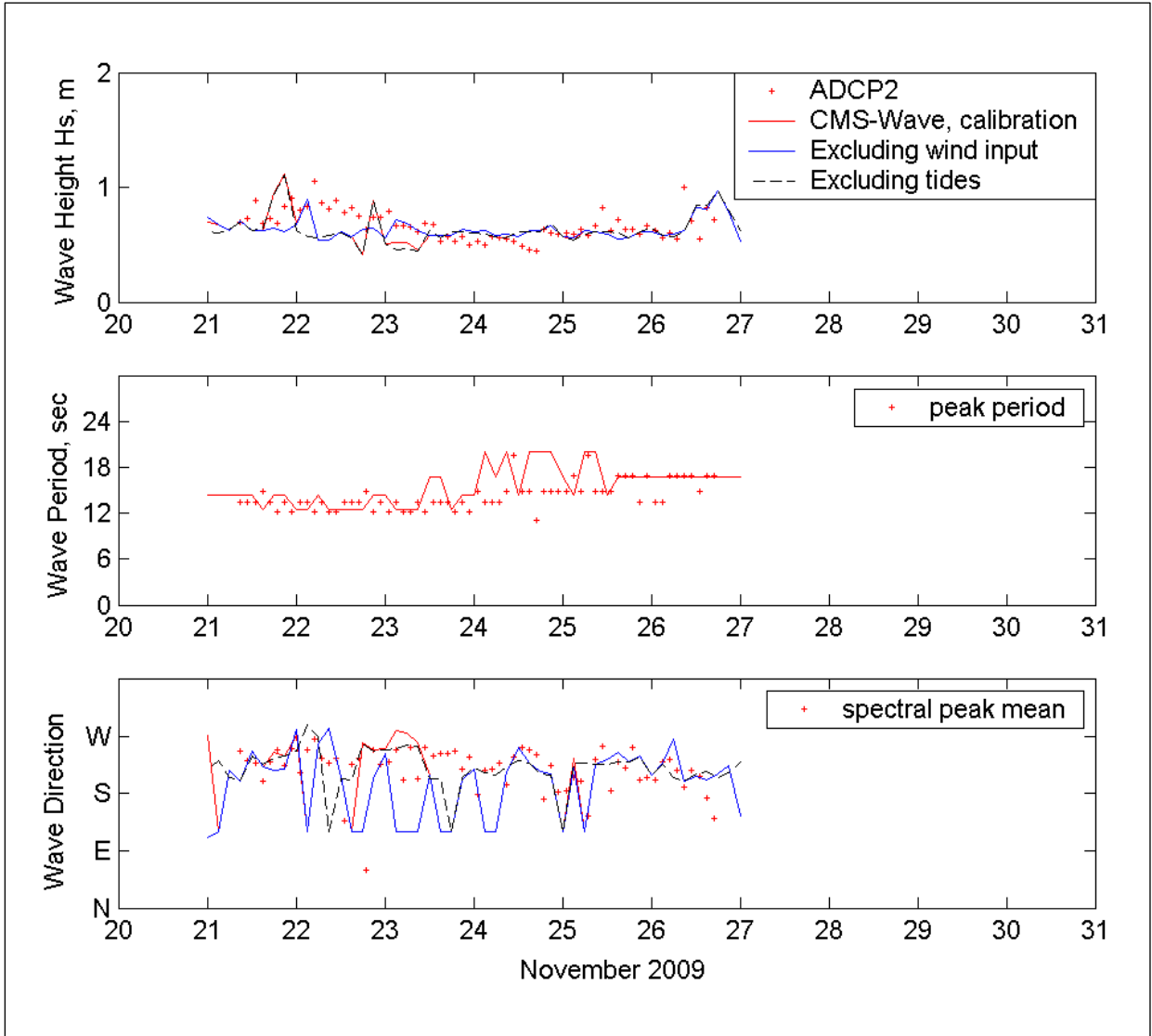
Figure 3-3



Comparison of Simulated and Measured Wave Parameters



Figure 3-4

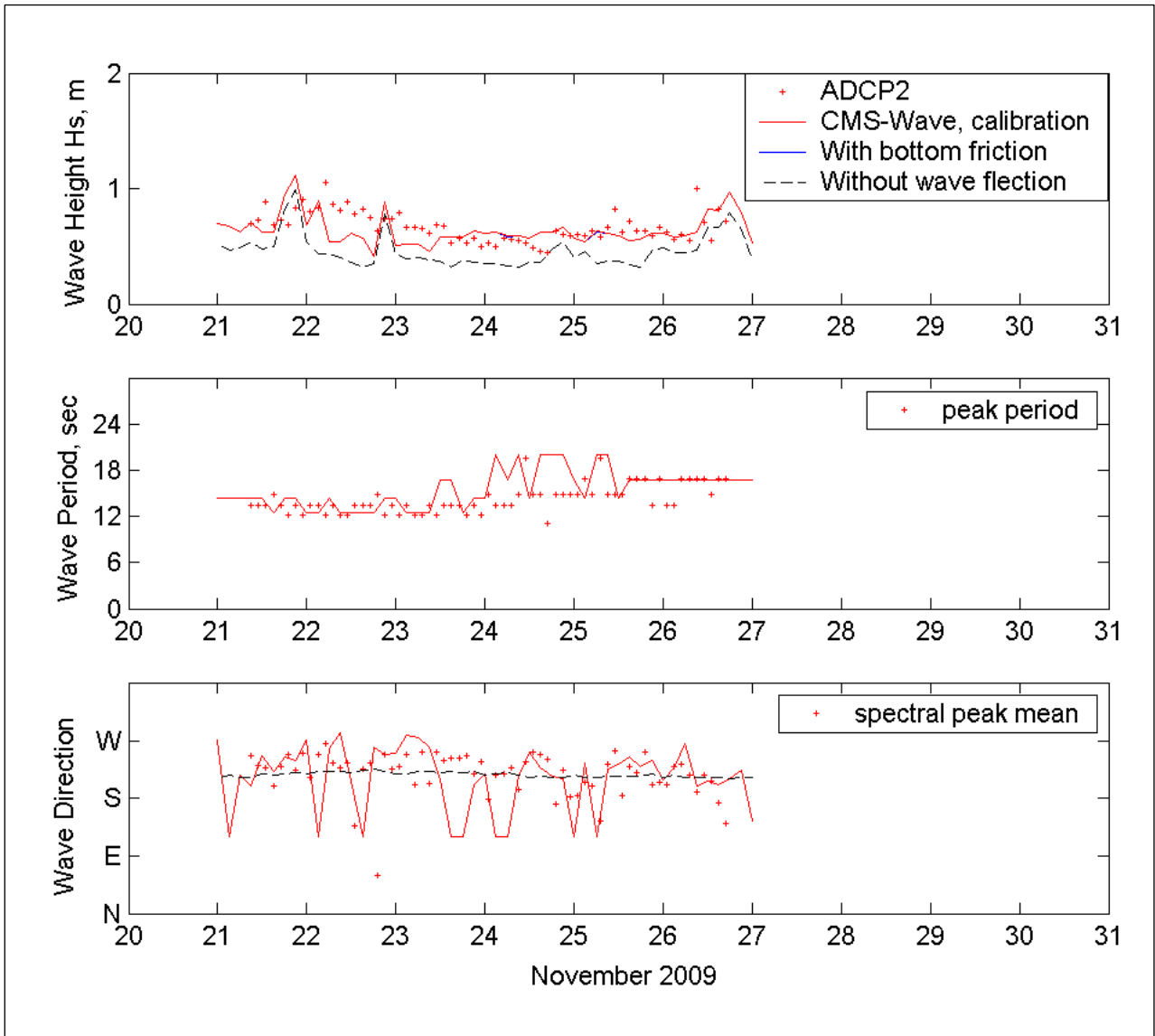


Note: Location at the seaside location of the West Breakwater

Comparison of Calculated Waves with and without Wind or Water Level Input



Figure 3-5



Note: at the seaside location of the West Breakwater

Comparison of Calculated Waves with and without Wave Reflection or Bottom Friction



Figure 3-6

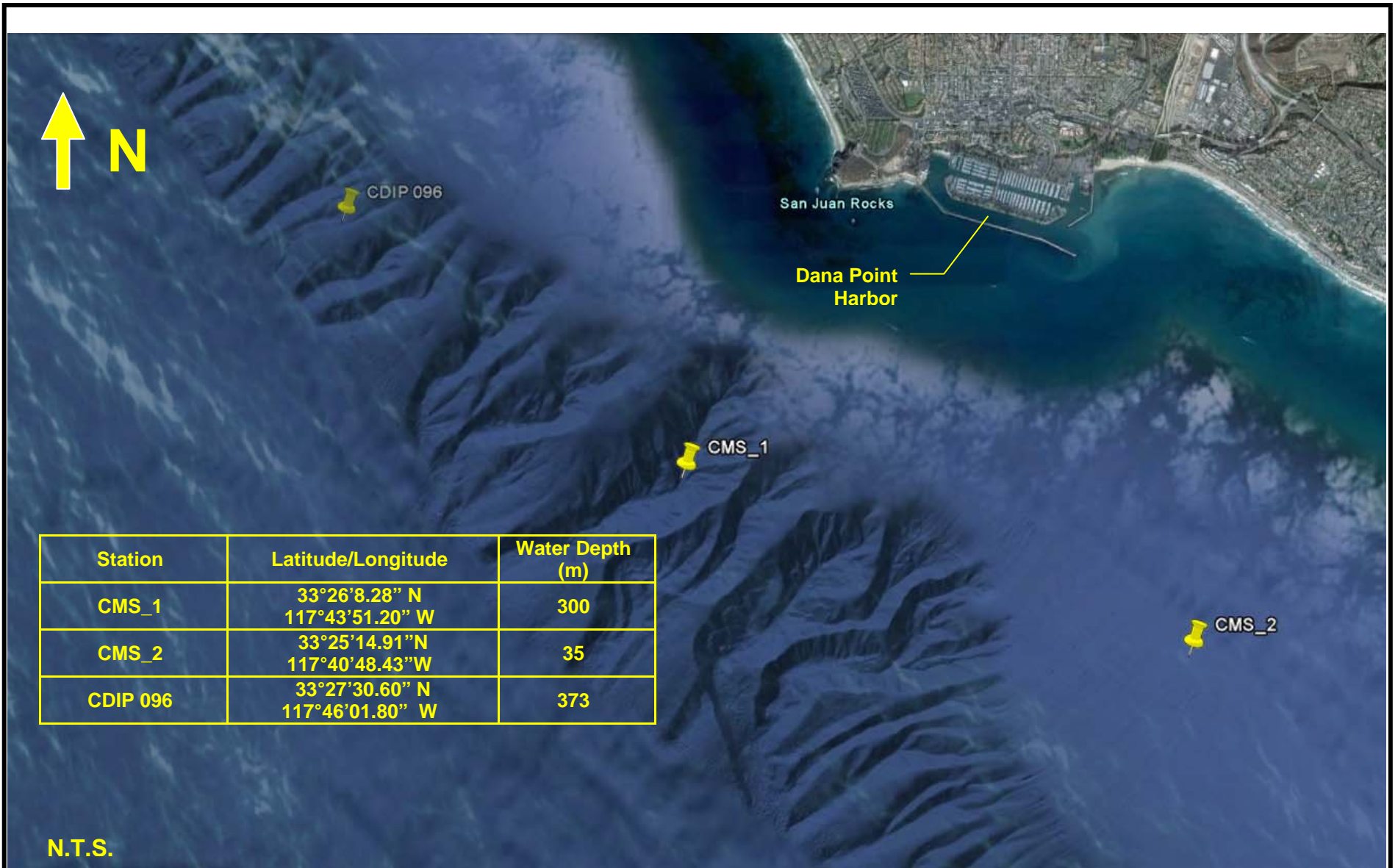


Source: Google Earth

Wave Data Station Locations



Figure 3-7

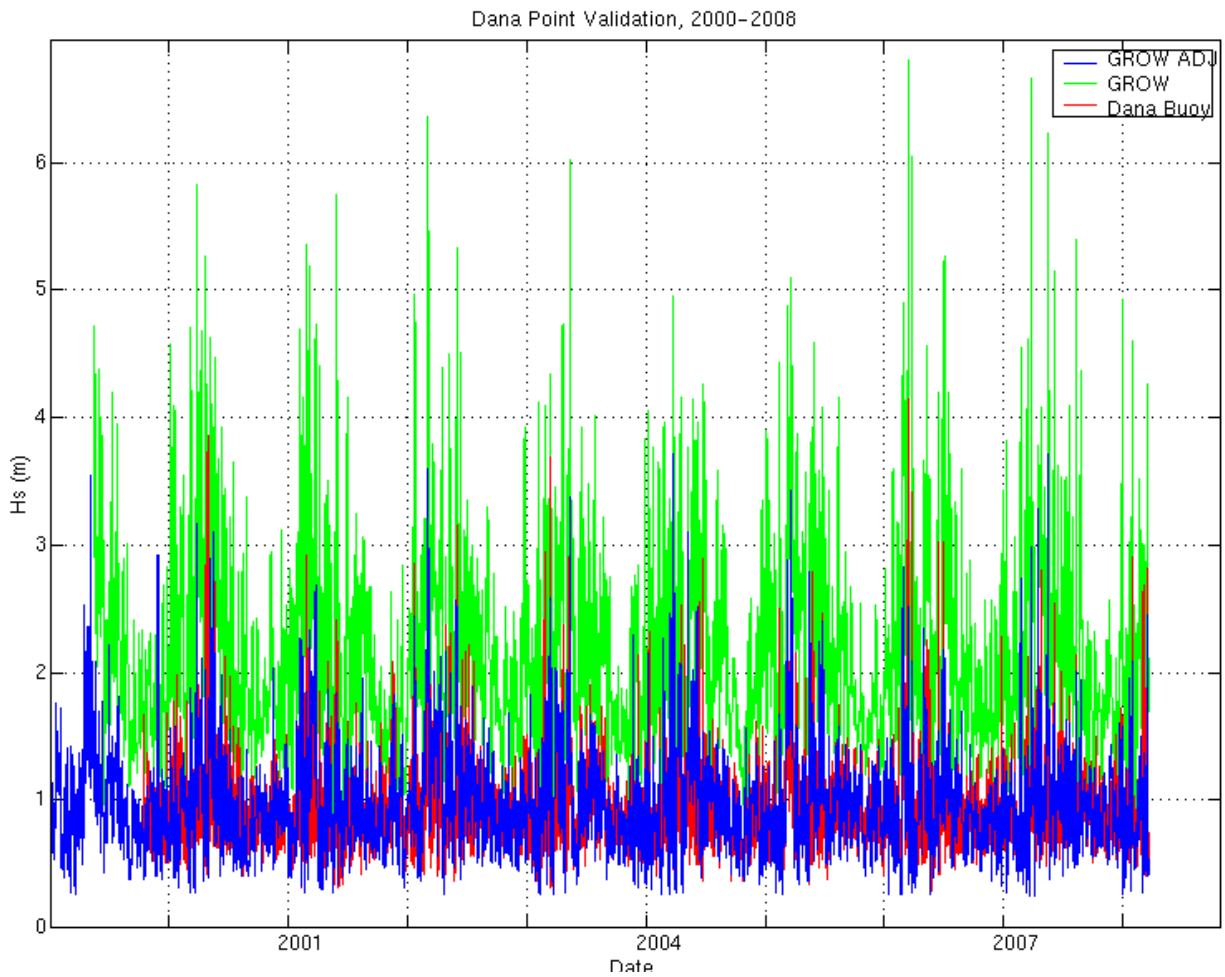


Source: Google Earth (Nov 14, 2009)

Transformed Wave Data Station Locations



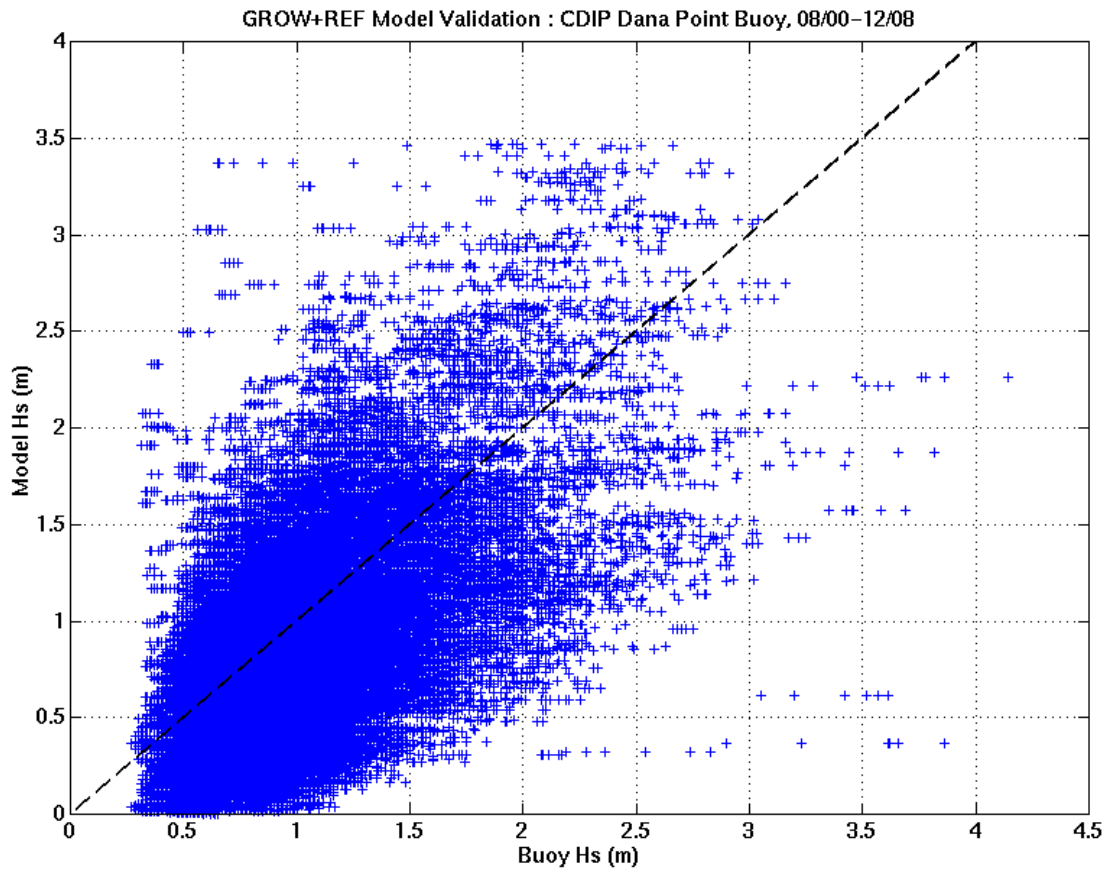
Figure 3-8



Note: The green line represents the offshore GROW hindcast significant wave heights.
 The red line represents observed significant wave heights at the Dana Point buoy.
 The blue line represents the significant wave heights of the transformed GROW hindcast waves at the Dana Point buoy location using a spectral refraction model.

Comparison of Significant Wave Heights from 2000 to 2008

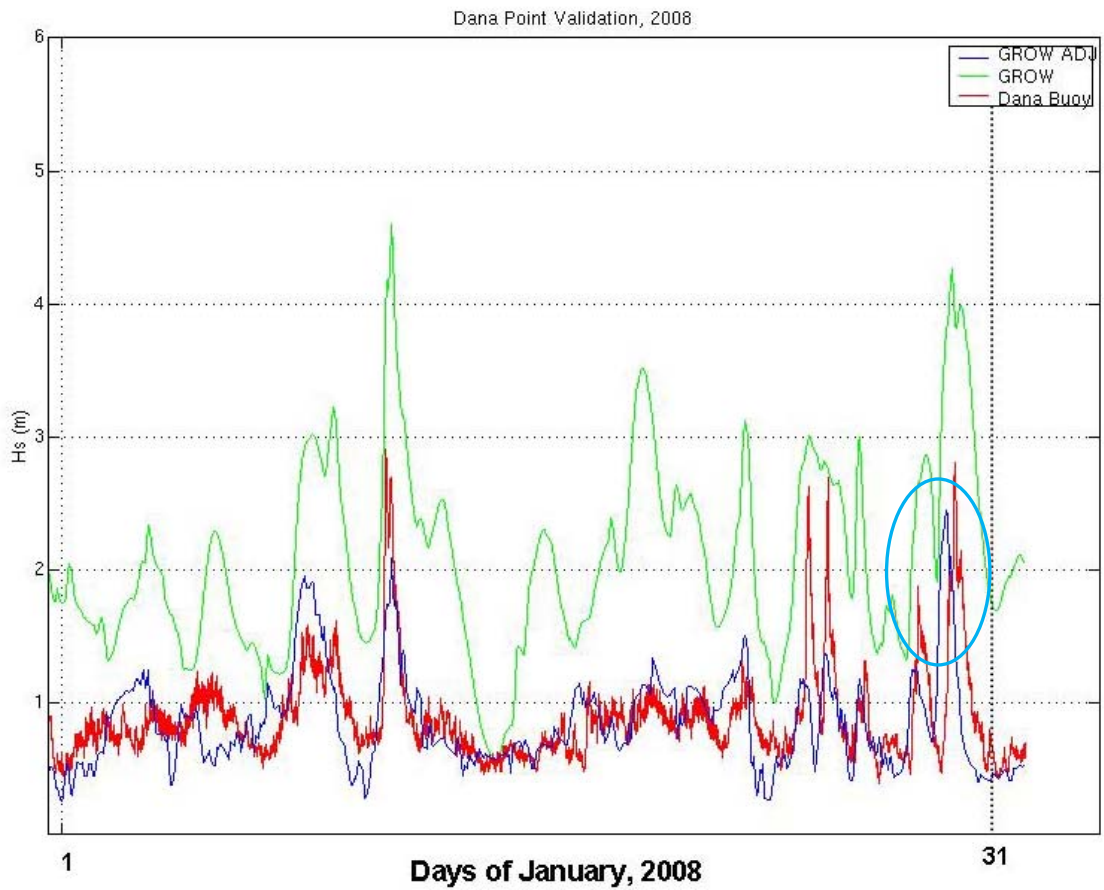




Note: Scatterplot compares observed significant wave heights at the CDIP Dana Point buoy to the transformed hindcast significant wave heights, which is based on the spectral transformation of the GROW offshore hindcast spectra to the Dana Point buoy location.

Scatterplot of Observed CDIP and Hindcast Significant Wave Heights

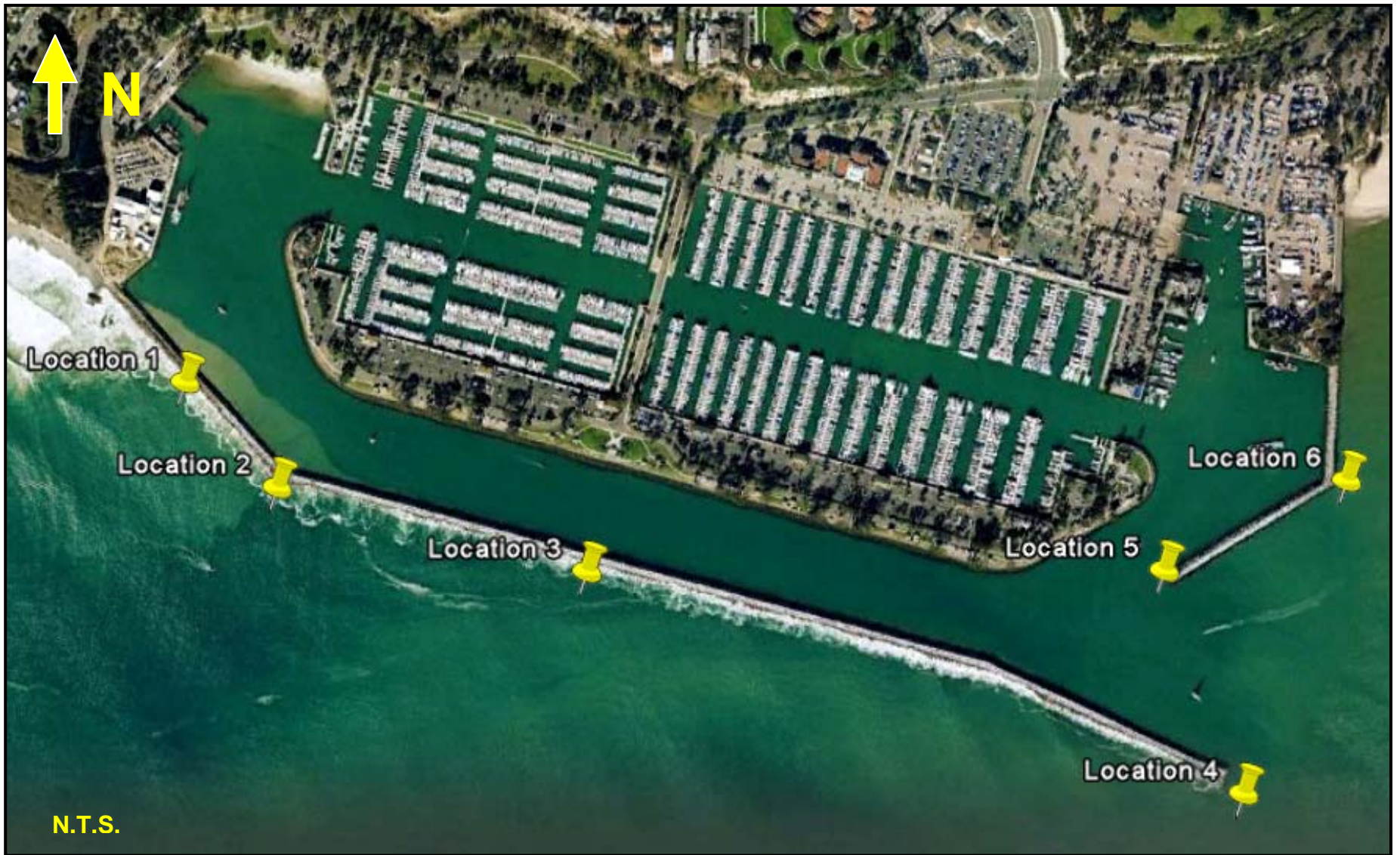




Note: The red line represents observed significant wave heights at the Dana Point buoy. The green line represents the offshore GROW hindcast significant wave heights. The blue line represents the significant wave heights of the transformed GROW hindcast waves at the Dana Point buoy location using a spectral refraction model.

Comparison of Significant Wave Heights During the Month of January, 2008





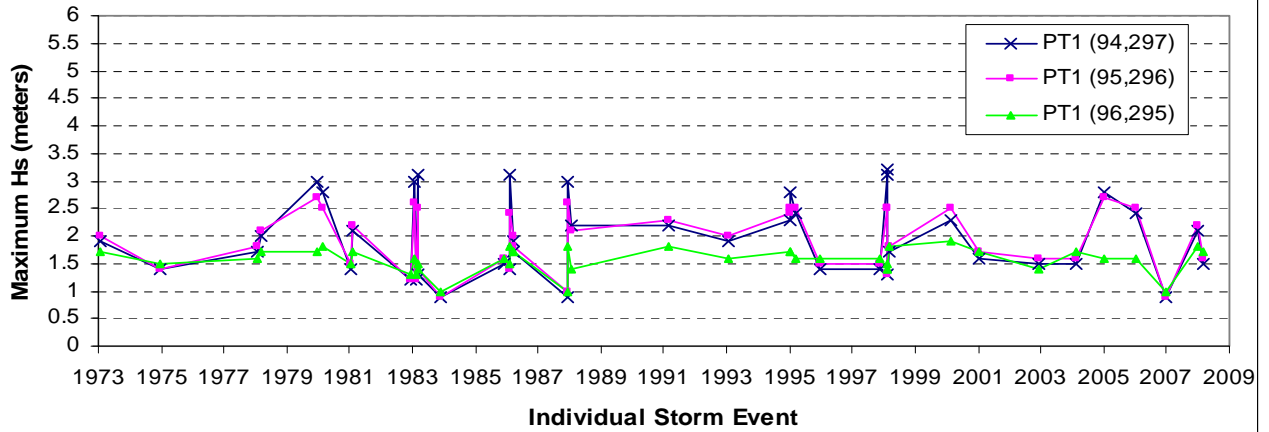
Source: Google Earth (Dec 31, 2005)

CMS Observation Locations

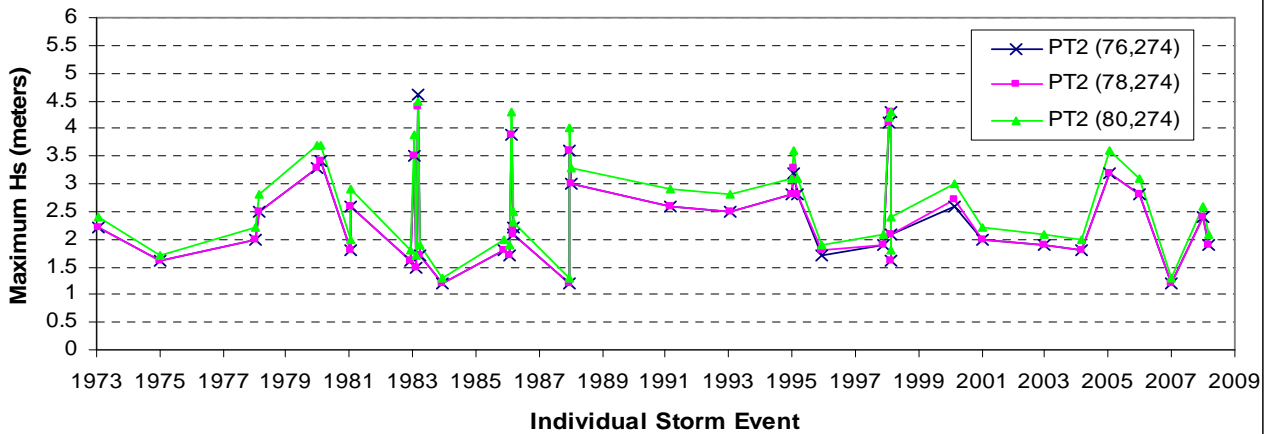


Figure 3-12

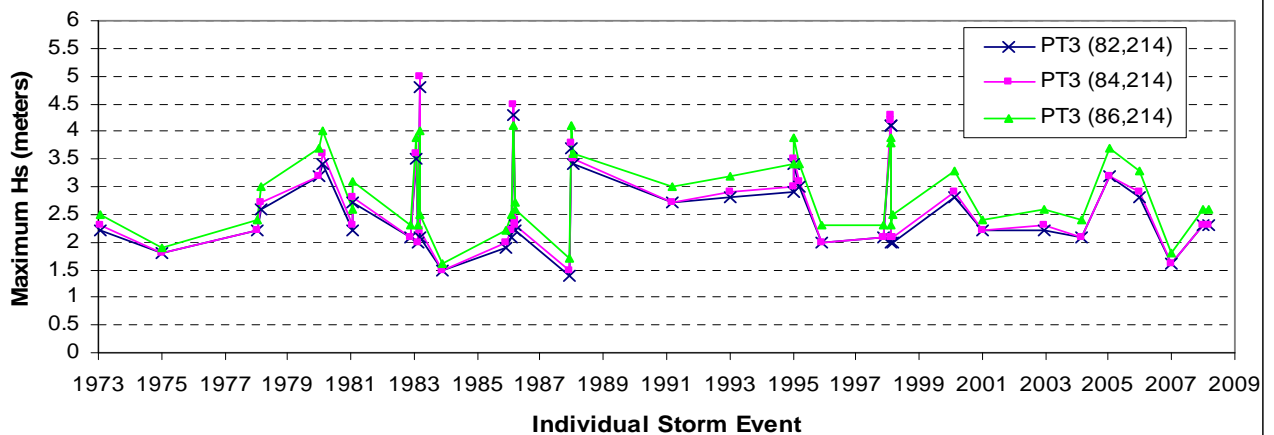
Significant Wave Heights at Breakwater Location 1



Significant Wave Heights at Breakwater Location 2



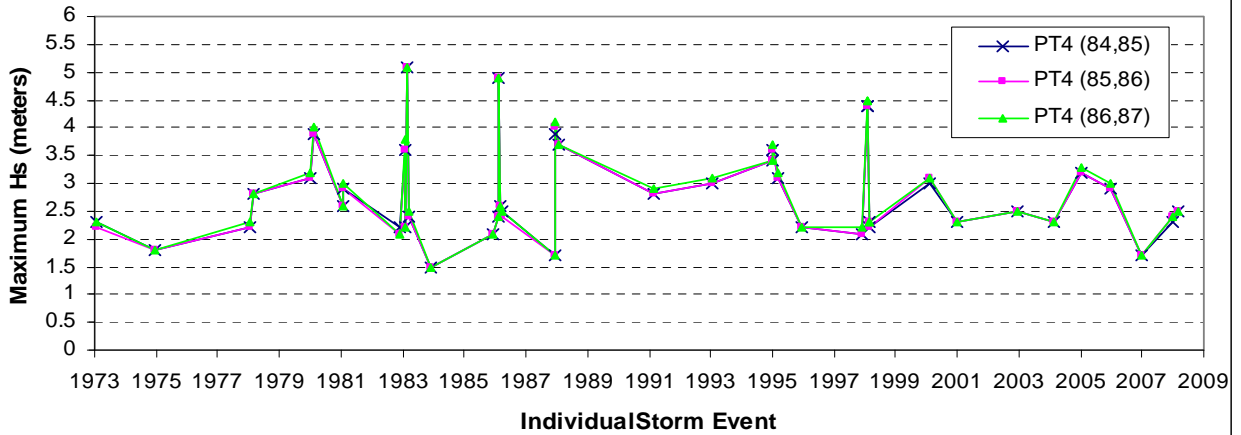
Significant Wave Heights at Breakwater Location 3



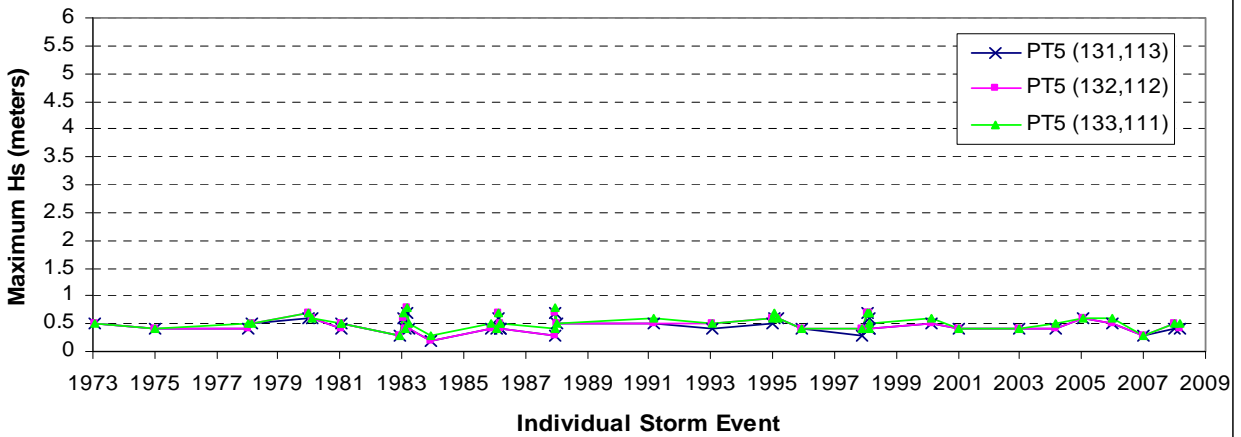
Maximum Significant Wave Heights during Storm Events at Locations 1, 2 & 3



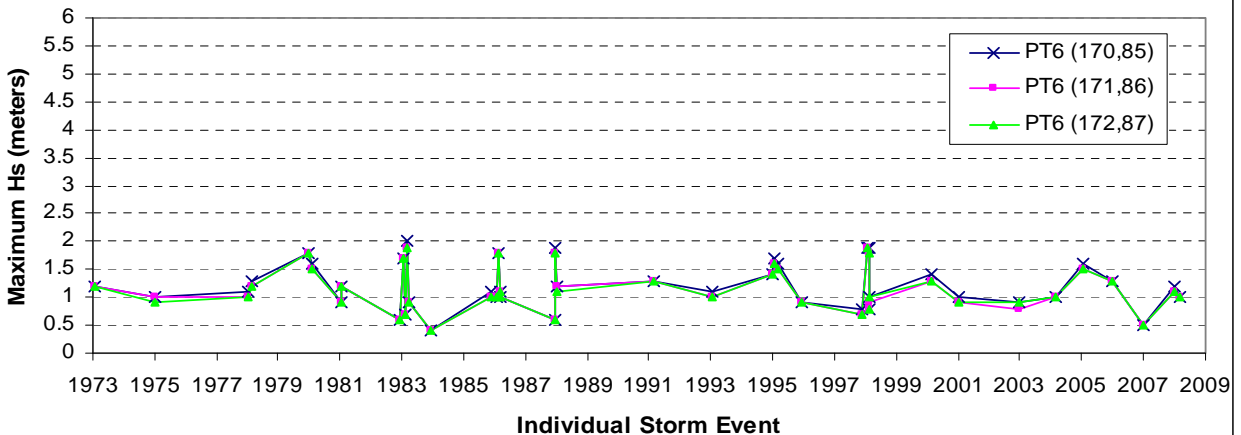
Significant Wave Heights at Breakwater Location 4



Significant Wave Heights at Breakwater Location 5



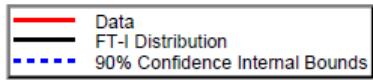
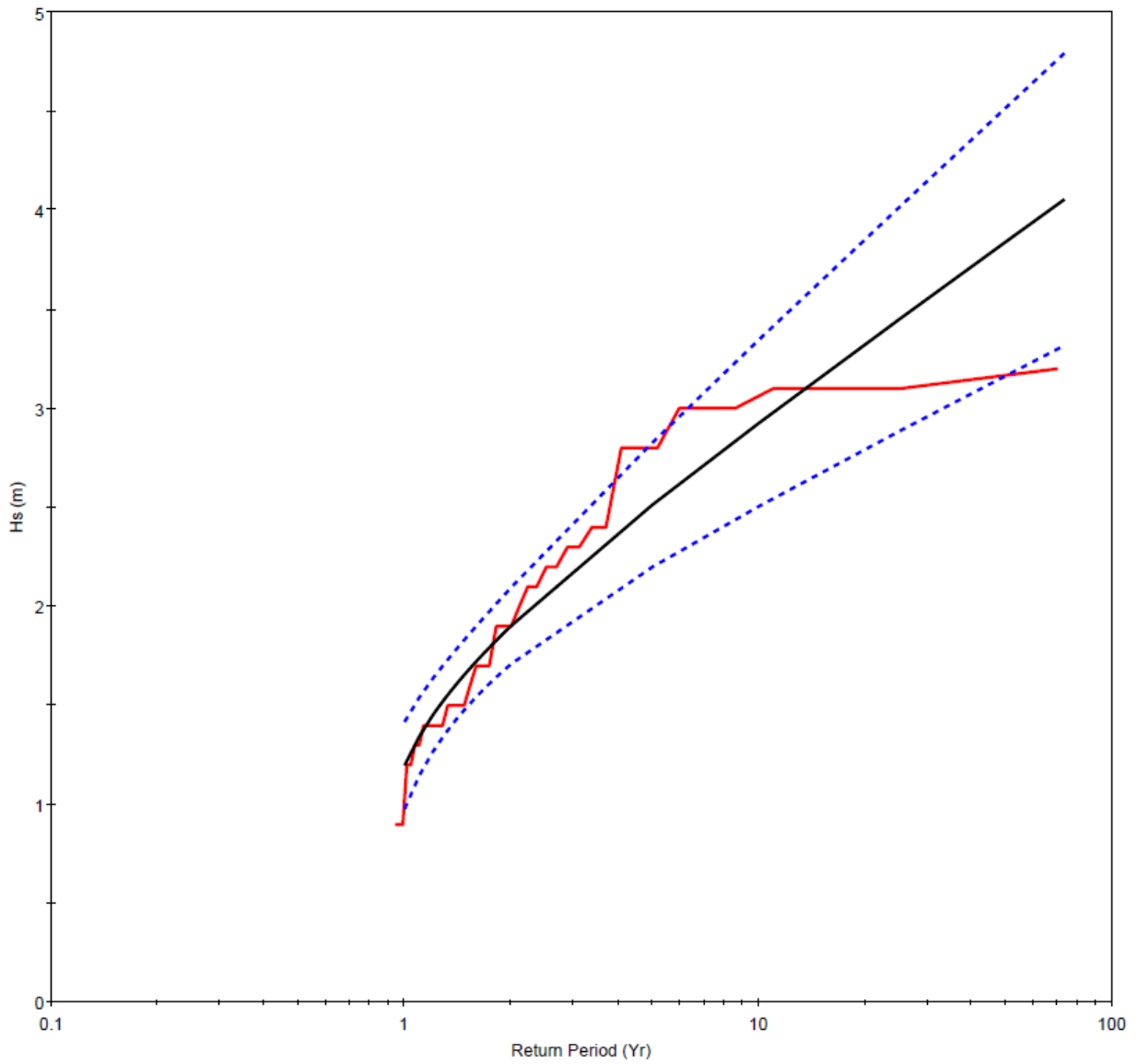
Significant Wave Heights at Breakwater Location 6



Maximum Significant Wave Heights during Storm Events at Locations 4, 5 & 6



Figure 3-14



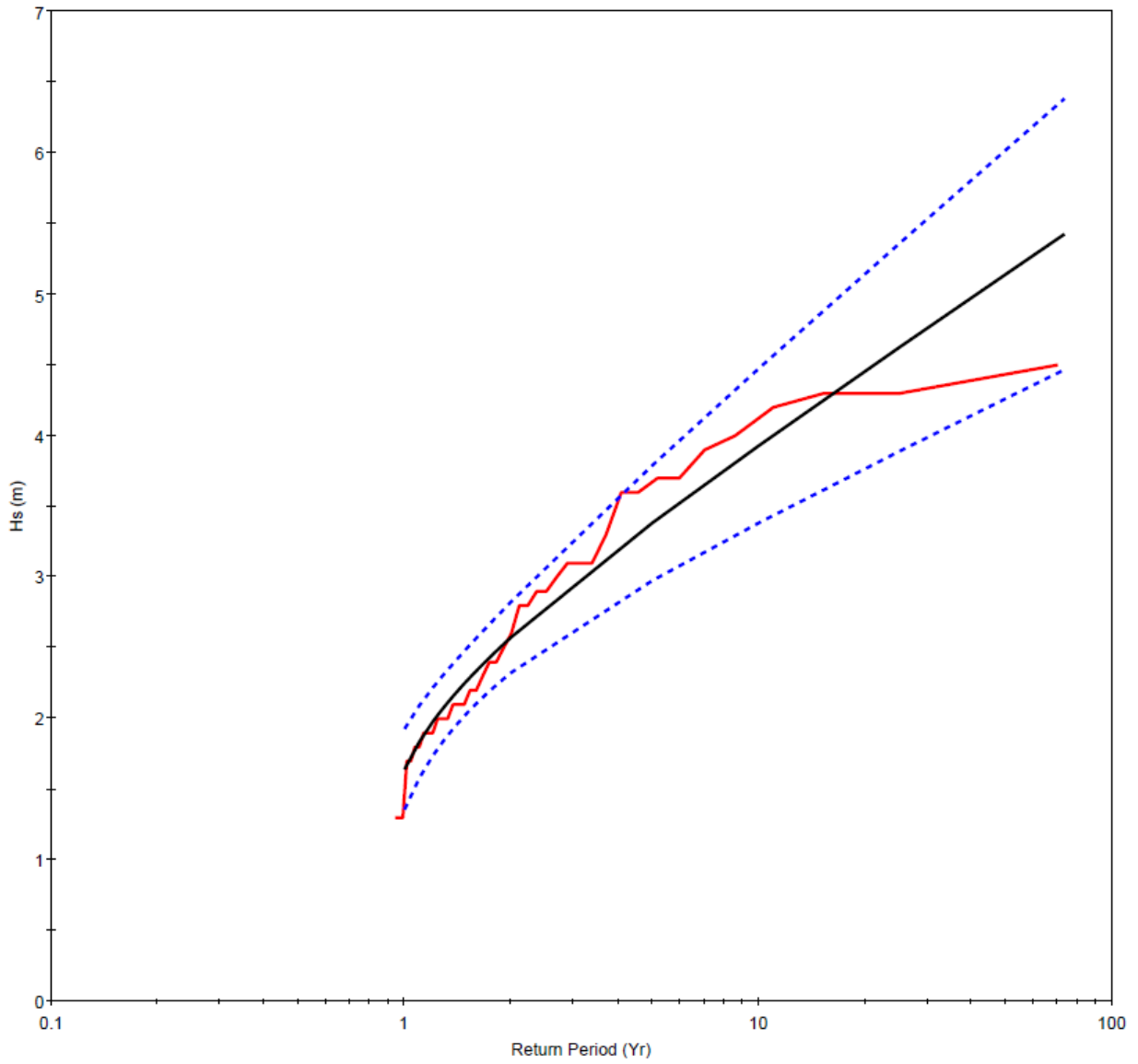
Fisher-Tippett Distribution

Note: Extreme waves estimated at
breakwater observation point PT1 (94,297)

Deduced Extreme Wave Height Distribution at Location 1



Figure 3-15



— Data
— FT-I Distribution
- - - 90% Confidence Interval Bounds

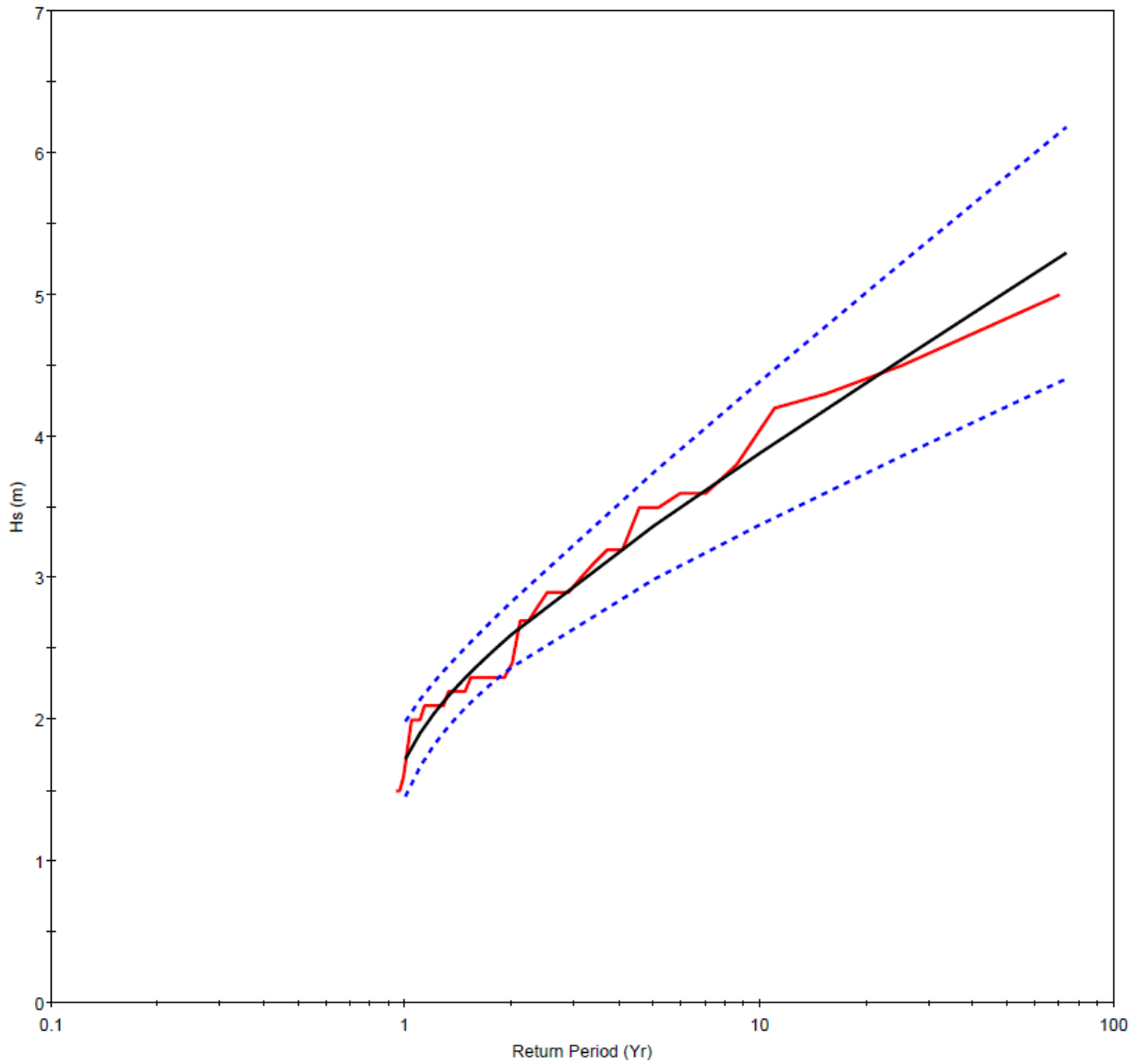
Fisher-Tippett Distribution

Note: Extreme waves estimated at breakwater observation point PT2 (80,274)

Deduced Extreme Wave Height Distribution at Location 2



Figure 3-16



— Data
— FT-I Distribution
- - - 90% Confidence Interval Bounds

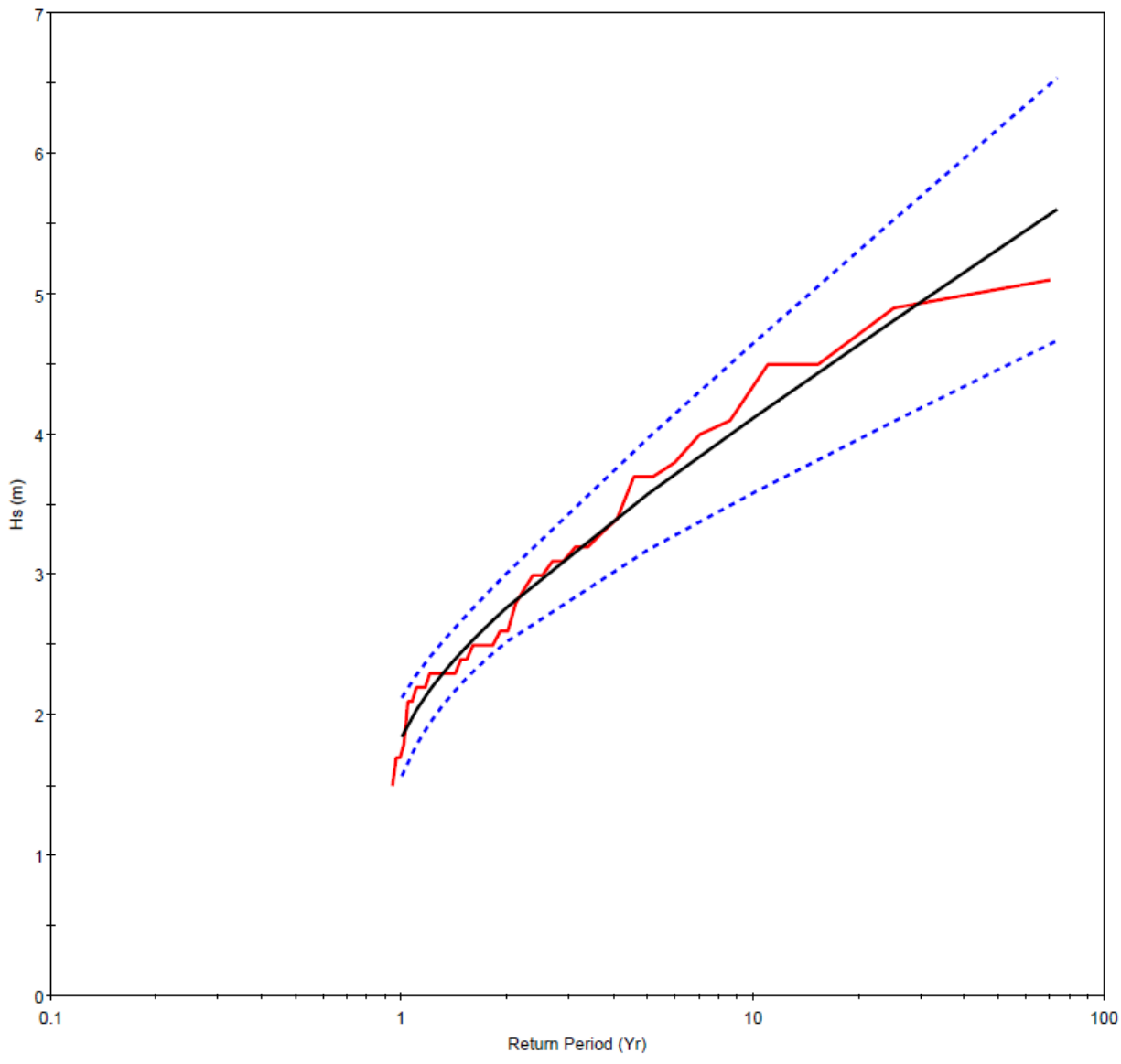
Fisher-Tippett Distribution

Note: Extreme waves estimated at breakwater observation point PT3 (84,214)

Deduced Extreme Wave Height Distribution at Location 3



Figure 3-17



— Data
— FT-I Distribution
- - - 90% Confidence Interval Bounds

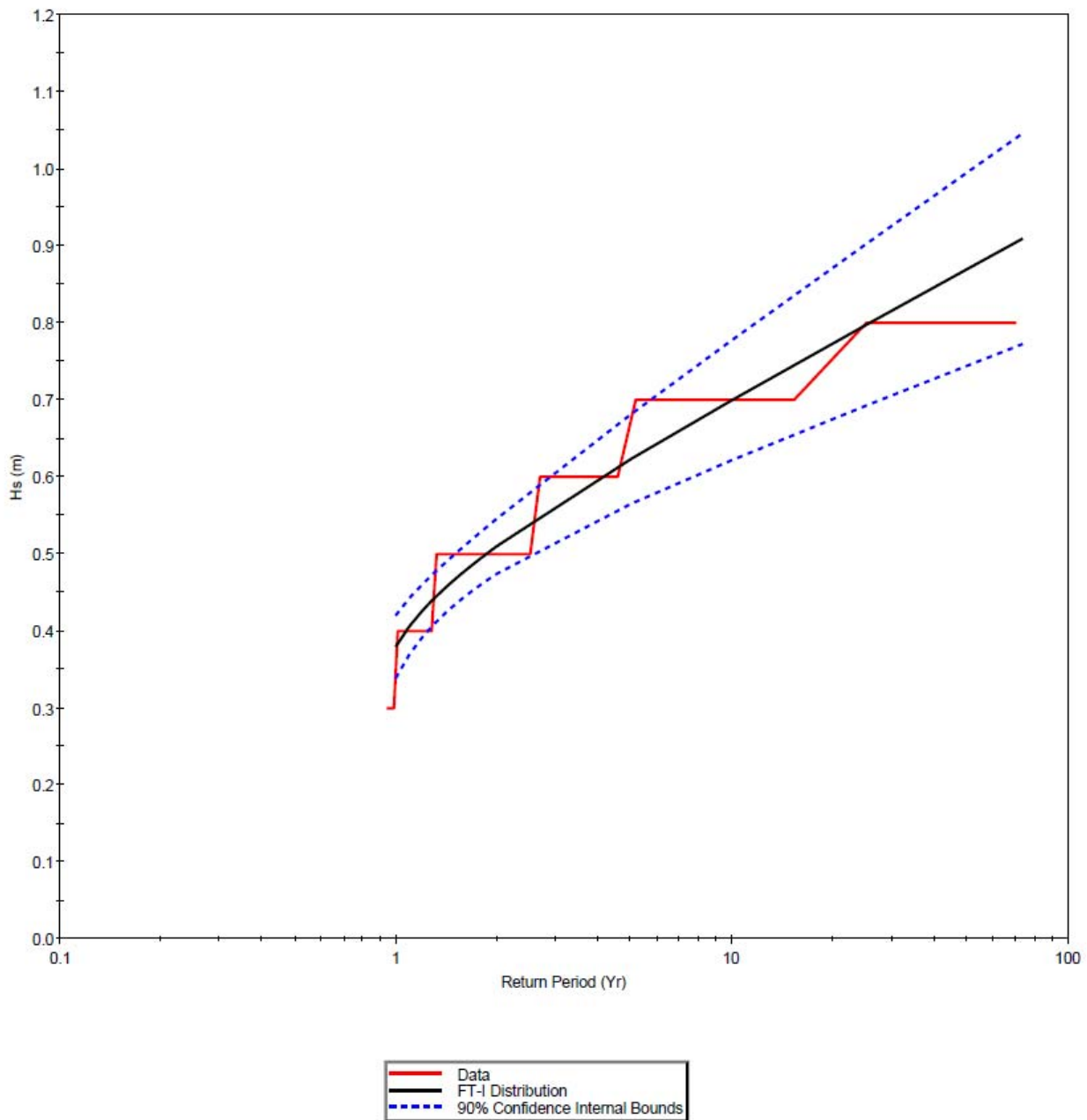
Fisher-Tippett Distribution

Note: Extreme waves estimated at breakwater observation point PT4 (86,87)

Deduced Extreme Wave Height Distribution at Location 4



Figure 3-18



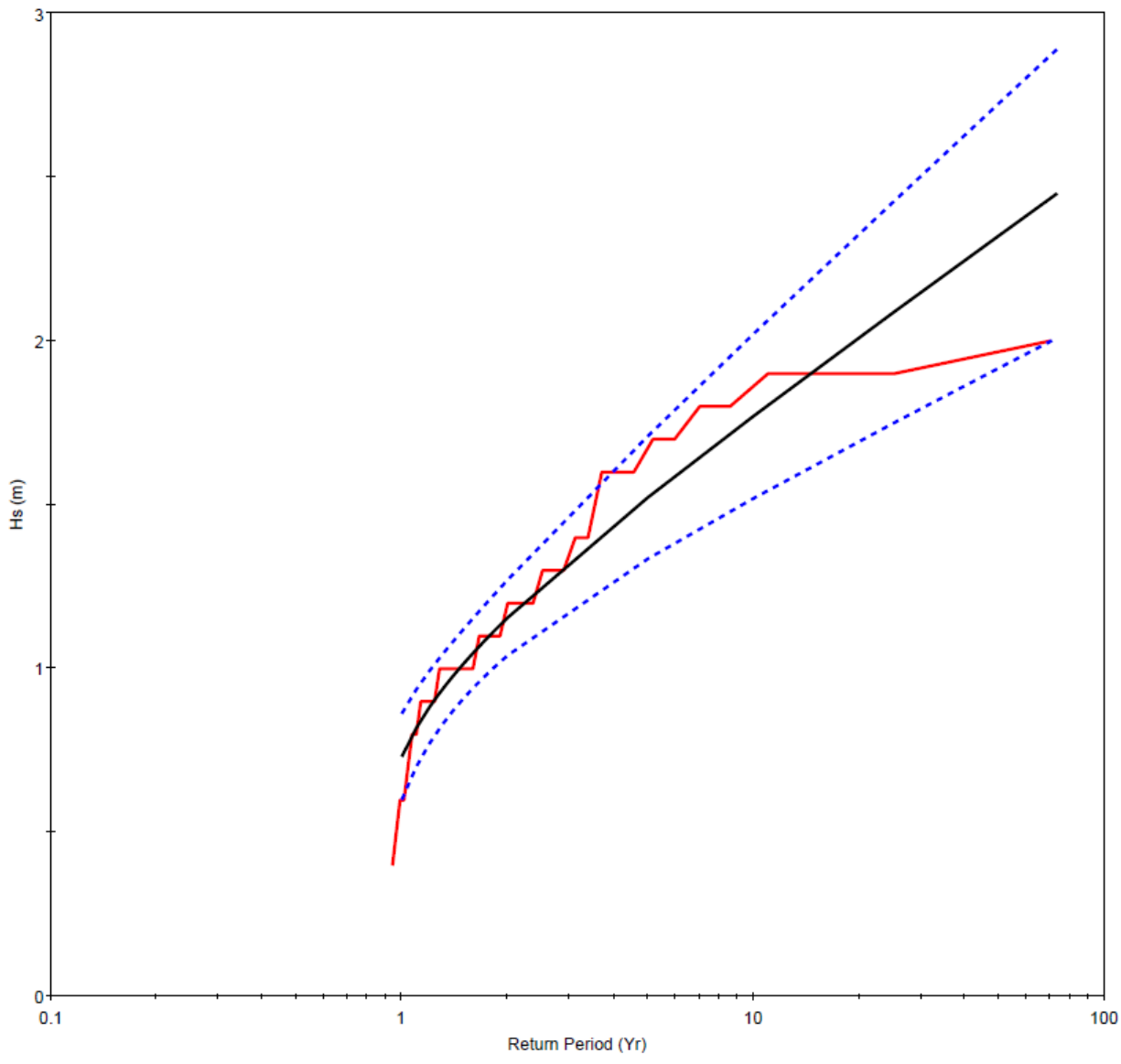
Fisher-Tippett Distribution

Note: Extreme waves estimated at breakwater observation point PT5 (133,111)

Deduced Extreme Wave Height Distribution at Location 5



Figure 3-19



— Data
— FT-I Distribution
- - - 90% Confidence Interval Bounds

Fisher-Tippett Distribution

Note: Extreme waves estimated at breakwater observation point PT6 (170,85)

Deduced Extreme Wave Height Distribution at Location 6



Figure 3-20

4.0 CMS-FLOW SIMULATIONS

4.1 Model Description

CMS-Flow is a three-dimensional (3D) finite-volume model that solves the mass conservation and shallow-water momentum equations of water motion on a non-uniform Cartesian grid. The model simulates currents, water level and sediment transport to characterize the water circulation pattern and morphologic change in the coastal zone. The model can be executed in a 2D mode based on the depth-integrated continuity equation, which was applied in the present study. The 2D depth-integrated continuity and momentum governing equations are

$$\frac{\partial(h+\eta)}{\partial t} + \frac{\partial q_x}{\partial x} + \frac{\partial q_y}{\partial y} = 0 \quad (4-1)$$

$$\begin{aligned} \frac{\partial q_x}{\partial t} + \frac{\partial uq_x}{\partial x} + \frac{\partial vq_x}{\partial y} + \frac{1}{2}g \frac{\partial(h+\eta)^2}{\partial x} = \frac{\partial}{\partial x} D_x \frac{\partial q_x}{\partial x} + \frac{\partial}{\partial y} D_y \frac{\partial q_x}{\partial y} \\ + fq_y - \tau_{bx} + \tau_{wx} + \tau_{sx} \end{aligned} \quad (4-2)$$

$$\begin{aligned} \frac{\partial q_y}{\partial t} + \frac{\partial uq_y}{\partial x} + \frac{\partial vq_y}{\partial y} + \frac{1}{2}g \frac{\partial(h+\eta)^2}{\partial y} = \frac{\partial}{\partial x} D_x \frac{\partial q_y}{\partial x} + \frac{\partial}{\partial y} D_y \frac{\partial q_y}{\partial y} \\ + fq_x - \tau_{by} + \tau_{wy} + \tau_{sy} \end{aligned} \quad (4-3)$$

where q_x and q_y are flow unit width parallel to the x and y axis;
 η is the water surface elevation from the still water level;
 h and t are the still water level and time;
 u and v are depth-average current velocities parallel to the x and y axis;
 D_x and D_y are the diffusion coefficients;
 f is the coriolis parameter;
 τ_{bx} and τ_{by} are bottom stress parallel to the x and y axis;
 τ_{wx} and τ_{wy} are surface stress parallel to the x and y axis; and
 τ_{sx} and τ_{sy} are wave stress parallel to the x and y axis.

The wave radiation stress and wave information entering the flow and sediment transport formulas are supplied to CMS-Flow through the coupling with CMS-Wave. Calculated currents and water level changes from CMS-Flow in turn provide an update flow field and water surface conditions to the wave model to

increase the accuracy of the wave transformation prediction (Buttolph et al., 2006).

4.2 CMS-Flow Model Improvement

As described in Section 3.3, both the West and East Breakwaters were specified in CMS as the permeable structures that allow for wave transmission, flow penetration, and sediment seepage. **Figure 4-1** shows the sketch of wave transmission and flow penetration through a permeable structure. Based on the Forchheimer equation (1901) with unidirectional flow, u , through a permeable structure in the x-direction, the momentum equation is

$$g(h + \eta) \frac{\partial(h + \eta)}{\partial x} = ag(h + \eta)u + bg(h + \eta)u^2 \quad (4-4)$$

where g is the gravitational acceleration;
 h is the still water depth;
 η is the water surface elevation;
 x is the x-coordinate; and
 a and b are resistance coefficients.

The left-hand side of Equation (4-4) is the hydraulic gradient, and the linear term on the right-hand side corresponds to the laminar and the non-linear term to the turbulent component of flow resistance. The resistance coefficients a and b are a function of structure permeability and the kinematic viscosity of the fluid (Sidiropoulou et al. 2007). The values of Coefficients a and b depend on the rock diameter and the hydraulic conductivity through the permeable structure. Higher values of Coefficients a and b imply less flow passing through the structure, which results in less sedimentation in the lee of the West Breakwater. The implementation of a permeable structure in the CMS requires modifications of the conservation of mass equation by introducing the structure void factor, n' . The revised equation is

$$\frac{\partial \eta}{\partial t} = \frac{1}{n'} \left[\frac{\partial q_x}{\partial x} + \frac{\partial q_y}{\partial y} \right] \quad (4-5)$$

where q_x and q_y are the mass fluxes in the x and y directions; and
 n' is the structure void factor.

In the morphologic simulation, the similar equation for the change in bed elevation is revised to account for the structure void factor:

$$\frac{\partial \zeta}{\partial t} = \frac{1}{n'} \left[\frac{\partial q_{sx}}{\partial x} + \frac{\partial q_{sy}}{\partial y} - E + D \right] \quad (4-6)$$

where ζ is the bed elevation;
 q_{sx} and q_{sy} are the bedload fluxes in the x and y directions;
 E is the erosion flux;
 D is the deposition flux.

4.3 CMS-Flow Calibration and Sensitivity Analysis

CMS-Flow was calibrated to determine various parameters such as the breakwater void factor and flow seepage rate through structures. The CMS calibration was performed for a 10-day period from November 18 to 27, 2009, during which current measurements at both the inside and outside ADCPs were available. It is noted that due to the instrument failure, the outside ADCP (i.e., the ocean side of the West Breakwater) was functional only from November 21 to 26, 2009. **Table 4-1** presents the pertinent model parameters and coefficients that were specified in the calibration process. To obtain proper flow and sediment seepage through the breakwaters, the hydraulic resistance coefficients a and b were determined by using a void factor of 0.2 and a rock size of 1.5 meters, which is approximately equivalent to a 6-ton riprap stone.

Table 4-1. Calibrated Structure Parameters and Coefficients for CMS-Flow

<i>Structure Parameter</i>	<i>Value</i>
Void Factor (Porosity)	0.2
Resistance Coefficient a	0.0016
Resistance Coefficient b	0.7304

Figure 4-2 shows the comparison of modeled and measured water surface elevations (WSEs) at the outside ADCP location from November 18 to 27, 2009. During this neap tidal period, the CMS accurately predict the WSEs measured at the ADCP outside of the West Breakwater. The current measurements exhibit different flow patterns at the inside and outside ADCP

locations. The depth averaged current over one hour had a small speed of less than 2 cm/sec, but shows a clear flood and ebb tidal current patterns in the main navigational channel inside the breakwater. The current speed at the outside ADCP location has a hourly averaged magnitude of about 4-5 cm/sec and the dominant current directions are from west northwest (i.e., traveling along the west breakwater) toward southeast under both flood and ebb conditions. **Figure 4-3** shows the comparison of the calculated currents and the measurements at both ADCP locations. The modeled results show that the harbor area experienced several short periods of relatively high currents in the first three days of model simulation during which no ADCP measurements were available. By examining all the physical forcing in the model, the relatively high tidal range is probably responsible for those speed spikes inside and outside of the harbor (Figure 4-2). Similar to the ADCP data, the model current directions at the inside ADCP location are basically corresponding to the flood (260-300°) and ebb flow (80-120°) with some discrepancies at a few occasions.

Snapshots of depth-averaged water circulation field surrounding the Dana Point Harbor at two instantaneous times were retrieved from the CMS simulations. **Figure 4-4** shows the simulated flow fields at 05:00 GMT and 22:00 GMT November 19, 2009 during the flood and ebb tide cycles, respectively. During the flood tide, strong tidal currents occur outside the harbor along the shoreline and follow the alignments of the West and East Breakwaters. The current speed can be greater than 50 cm/sec. Within the harbor, the maximum current speed ranges from 6 to 8 cm/sec and the tidal current flows into the West and East Basins through the entrance channel, respectively. Under the ebb tide condition, the alongshore current outside the harbor is much weaker. The current speeds at the northwest end of the West Breakwater and the outside (ocean side) of the East Breakwater are between 15 and 30 cm/sec. The maximum current speed along the entrance channel inside the harbor is approximately 5 cm/sec.

It is noted that the CMS-Wave is a steady-state, phase-averaged spectral wave transformation model, the time scale of the model is not applicable for an instantaneous prediction. Although the CMS-Flow is a unsteady temporal-varying model, the output of the current field via the steering-mode simulation with CMS-Wave is incapable of predicting a small time scale of instantaneous flow as recorded by ADCPs. Therefore, the comparison of CMS-Flow results was based on hourly depth-averaged current velocity.

Within the nearshore wave-dominated environment oceanside of the breakwaters, both the measured and calculated flow directions reveal that the

currents move predominantly east-southeastward parallel to the West Breakwater in accordance with the approaching wave direction. The ADCP measurements also show the same trend that the observed current patterns in both ebb and flood cycles are similar (see Figures 3-31 and 3-32). Inside the harbor, the current pattern is closely associated with tide and is also sensitive to wind though sheltered by the breakwaters from wave impingement.

A sensitivity analysis was performed to examine the CMS results in response to the variation of different forcing parameters, the permeability of the West Breakwater, and harbor shoaling. Three different sets of wind data that were collected at offshore NDBC Buoy 46048, the Ocean Institute in the Dana Point Harbor, and at the La Jolla Pier were respectively applied for the model simulations. **Figure 4-5** shows the comparison of recorded wind data for the period from November 18 to 27, 2009. Wind conditions typically vary between the offshore region and coastal zone. The wind speed is typically greater at the offshore buoy without any fetch restriction; thus, the offshore wind data is not representative for the coastal zone. It is expected that the modeled results, using the offshore wind data, would not be in a good agreement with the field measurements.

While the wind direction at La Jolla is characterized by the diurnal cycle of the sea breeze signal, the wind at the Dana Point Station does not show a clear pattern probably due to the sheltering effect of local steep seacliffs. Using the wind data collected at the offshore buoy and the Ocean Institute, calculated current speeds are overestimated although current directions show a similar east-southeastward flow outside the harbor, as illustrated in **Figure 4-6**. The wind data collected in the harbor would intuitively be considered representative of the nearshore condition. However, the Ocean Institute is significantly sheltered by the Dana Headlands that blocks the wind from west to northwest. The data collected at this site would not have a proper representation of the wind pattern within the main navigational channel. The simulation with the wind data at La Jolla (see Figures 4-3) yields a better agreement of flow field between the model predictions and actual measurements at the two ADCP locations, as compared two other wind inputs (see Figure 4-6).

A previous field circulation study at Dana Point Harbor (SAIC, 2003a) showed the evidence of flow passing through the West Breakwater and its impact on the current pattern in the navigational channel. The entire West and East Breakwaters were specified as permeable in the CMS simulations. As a sensitivity test, only incremental segment of the West Breakwater was specified

as permeable. The model and data comparisons at the two ADCPs for two different lengths of the permeable segment are shown in **Figure 4-7**. No significant changes in current speed and direction are detected at the inside and outside ADCP locations, even though the length of the permeable segment increases to allow for more water flow through the structure.

Additional sensitivity run was performed to examine the variation of flow field, if any, for non-permeable breakwaters. **Figure 4-8** shows the same depth-averaged current snapshots as in Figure 4-4 to illustrate the simulation with non-permeable breakwaters. The eddy formed outside the East Breakwater indicates a different spatial extension with a slight increase of current speed in the harbor from the non-permeable breakwaters.

As shown in Figure 1-1, harbor shoaling occurs inside the northwest end of the harbor as a result of long-term flow and sediment seepage through the West Breakwater. **Figure 4-9** presents the snapshots of flow field during the flood and ebb tides corresponding to the shoaling scenario. The sediment accumulation greatly reduces the water depth and significantly narrows the navigational channel near the northwest end of the West Breakwater. However, alteration in the flow pattern inside the harbor was not predicted, while an anticipated stronger depth-averaged current was calculated in the shoaling area.

4.4 Historical Maintenance Dredging

Maintenance dredging at Dana Point Harbor primarily focuses in the lee area of the West Breakwater as a consequence of sediment seeping through the breakwater. The shoaling area is located primarily in the area between Sta. 0+60 and Sta. 4+80 (see Figure 2-3), which results in impacts on recreational activity such as Stand Up Paddle Surfing (SUP) within the harbor. A total of three (3) maintenance dredging operations, averaging approximately 10 years per cycle, have occurred since the harbor was constructed in 1960's. Relatively small quantity of fine material that was discharged through the drainage system was also dredged in both the navigation channels and berthing basins. The dredge quantities listed in **Table 4-2** reflect only the sediment volume that was removed along the harbor-side of the West Breakwater. This particular accumulation zone, which is exemplified in Figure 1-1, accounts for the majority of the maintenance dredging requirements.

Table 4-2. Dredging Quantities for West Breakwater Sediment Deposition

<i>Year</i>	<i>Quantity of Dredged Material (cy)</i>
1990	23,500
2000	35,500
2009	541,00

Comparisons of sequential bathymetric surveys that were conducted by the Corps of Engineers reveal the general shoaling pattern that occurs along the harbor side of the West Breakwater. Isopachs of the shoal formation between two consecutive years from 2000 to 2004 are presented in **Figures 4-10** and **4-11**. The polygon shown on each plot identifies the sediment typical deposition zone that has been observed in the past. An absence of color (the white area in the polygon) on the isopach maps denotes the areas where survey data were unavailable. Between 2000 and 2001 (see the top graphic in Figure 4-10), a significant shoal was developed immediately following the maintenance dredging operation that was conducted in the spring of 2000. The sediment deposition during this post-dredging period was limited to areas immediately on the lee of the breakwater, as sediment quickly settled and deposited on the dredged channel bottom. Over time, the rising shoal formation started to expand into the main navigational channel as shown in the subsequent isopach maps.

4.5 Simulation of Morphologic Change

The aerial photograph of Google Earth taken in 2005 (see Figure 1-1) clearly shows sand seepage through the breakwater resulting in a shoal formation developed inside the West Breakwater after the previous dredging cycle in 2000. The averaged rate is approximately 4,000 cy/yr based on the maintenance dredging record in 2000; and the average annual sand deposition rate is about 6,000 cubic yards, based on the latest dredging volume that was conducted in the early 2009 (see Table 4-2).

To estimate the volume of sediment seeping through the permeable West Breakwater, sand transport through the breakwater and the morphologic change inside the breakwater (i.e., the polygon area) were modeled using the same steering mode of CMS-Flow and CMS-Wave. The structure permeability was specified by testing and adjusting the resistance parameters (see Table 4-1) in the Forchheimer equation and the structure void factor in the conservation of

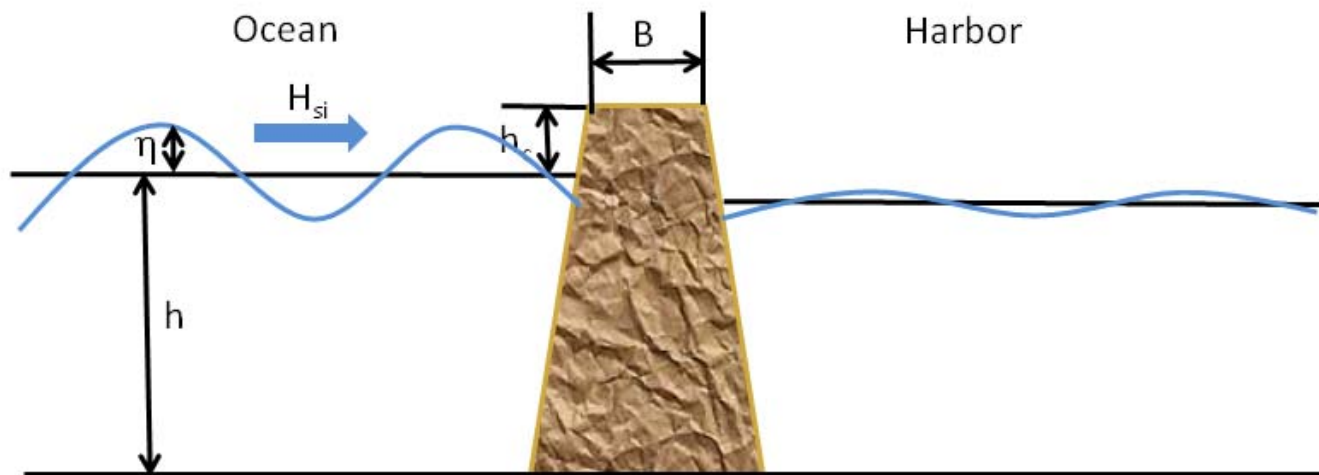
mass equation. **Figure 4-12** shows the morphologic change adjacent to the West Breakwater at the end of the 10-day simulation from November 18 to 27, 2009. Sand transport within structure cells is greatly reduced by the weaker flow velocity, lower wave energy, and subsequent smaller bottom stresses. As a result, the majority of deposition occurs within the breakwater as illustrated in Figure 4-12. Although visually insignificant, sand accretion is detectible inside the harbor along the West Breakwater.

To estimate total sediment volume changes related to the sediment seepage through the breakwater, a polygon area is drawn by the breakwater inside the harbor as shown in Figure 4-12. The morphology and bed volume change within the polygon area were estimated at the end of the 10-day simulation. By linearly extrapolating the 10-day CMS results to the entire calendar year, an approximate sediment deposition rate of 6,060 cy/yr was deduced, which is quantitatively comparable to the average annual volume that was recently dredged in the lee of the West Breakwater. By increasing the hydraulic resistance coefficients of a and b (given in Table 4-1), the anticipated sedimentation would accordingly be reduced. Conversely, increase of rock size and porosity would promote more sands seeping through the breakwater and settling in the navigational channel, and thus result in more sedimentation in the lee of the West Breakwater. Table 4-3 presents a comparison of the computed annual sedimentation for varying rock sizes and different values of porosity.

Table 4-3. Comparison of Computed Annual Sedimentation

Porosity	Size of Riprap Stones (m)	
	1.5	2.0
0.2	6,060 cy	6,830 cy
0.4	6,120 cy	7,030 cy
0.7	6,600 cy	7,560 cy

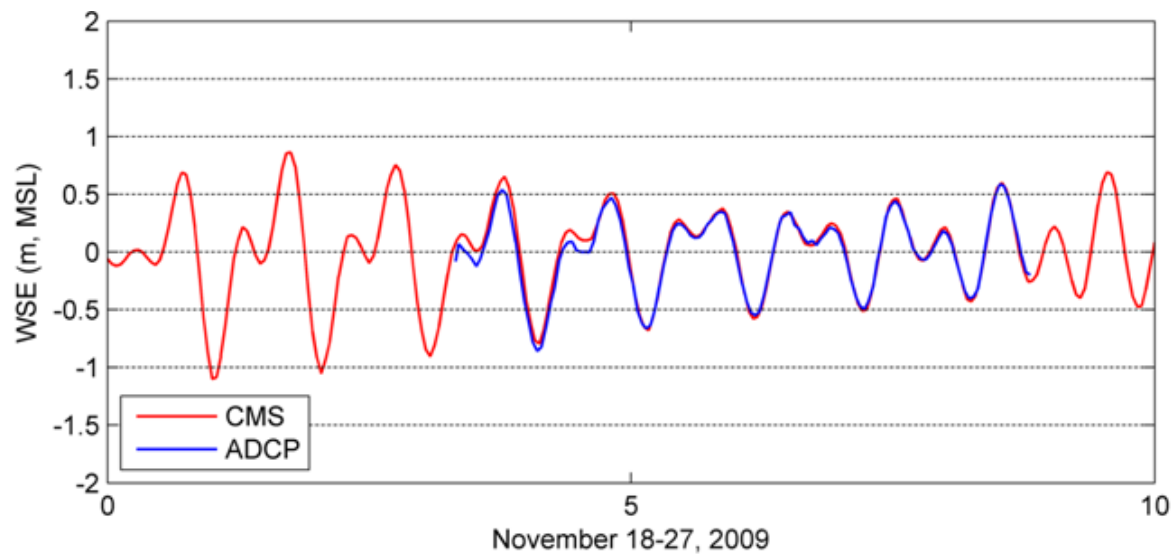
As part of the sensitivity analysis, the impact of the formed shoal on sediment transport through the breakwater was also examined using the bathymetric information prior to the 2009 dredging cycle (Figure 4-9). Following the same procedure, the sediment deposition rate in the lee of the West Breakwater was computed to be approximately 5,160 cy/yr. It is a 15-percent decrease comparing to the model simulation with the immediate post-dredging bathymetry. Therefore, the sediment seepage rate through the West Breakwater is higher in the post-dredging period than in the pre-dredging condition.



Sketch of Wave Transmission and Flow Penetration through a Porous Structure



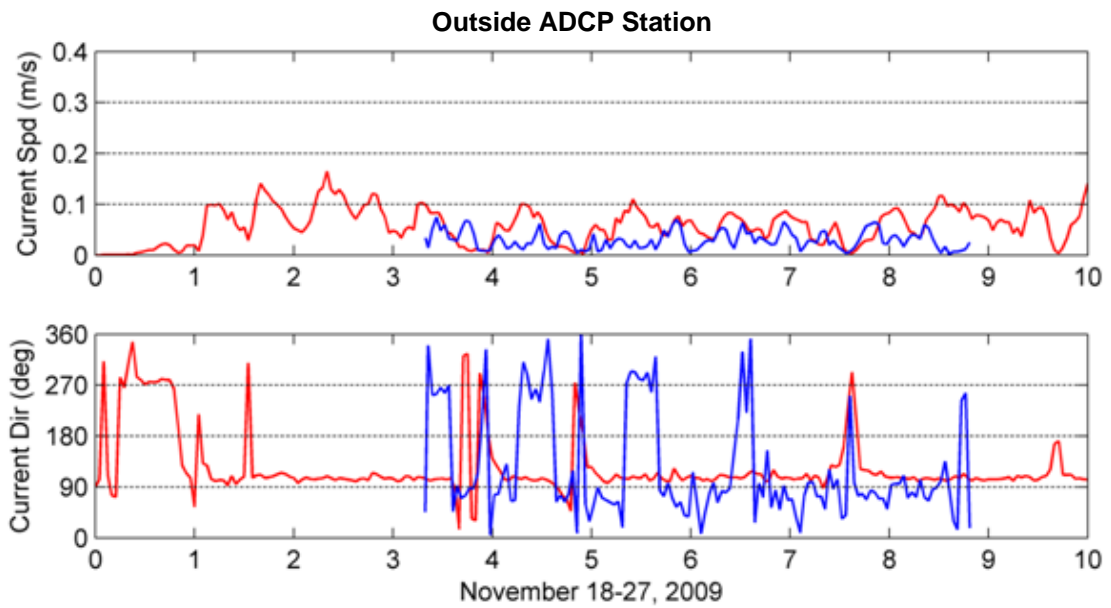
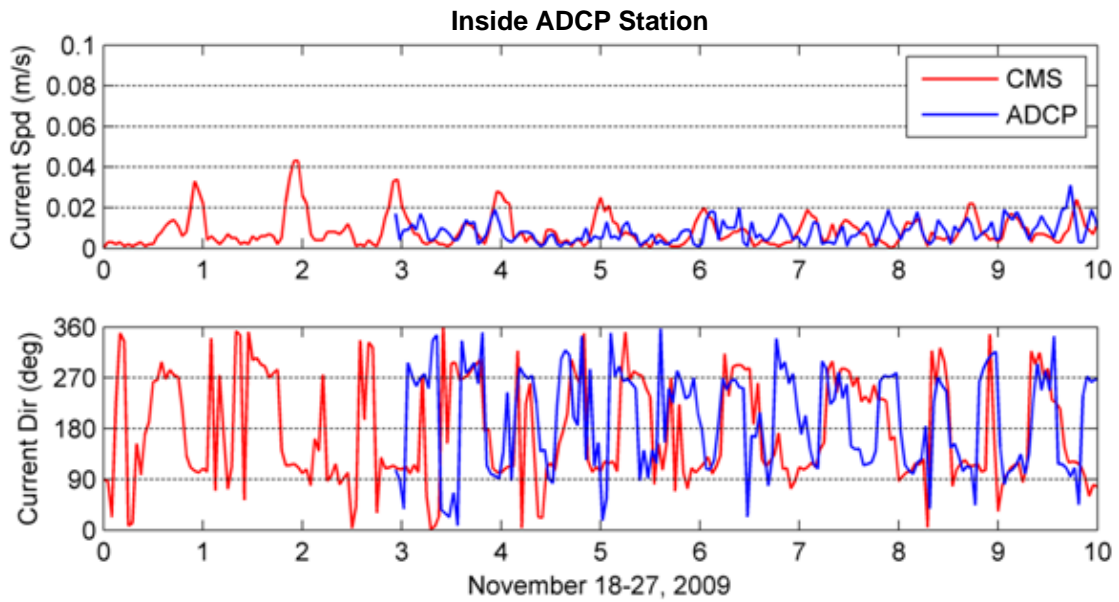
Figure 4-1



Comparison of Simulated Water Surface Elevations and Measurements at the Outside ADCP Station



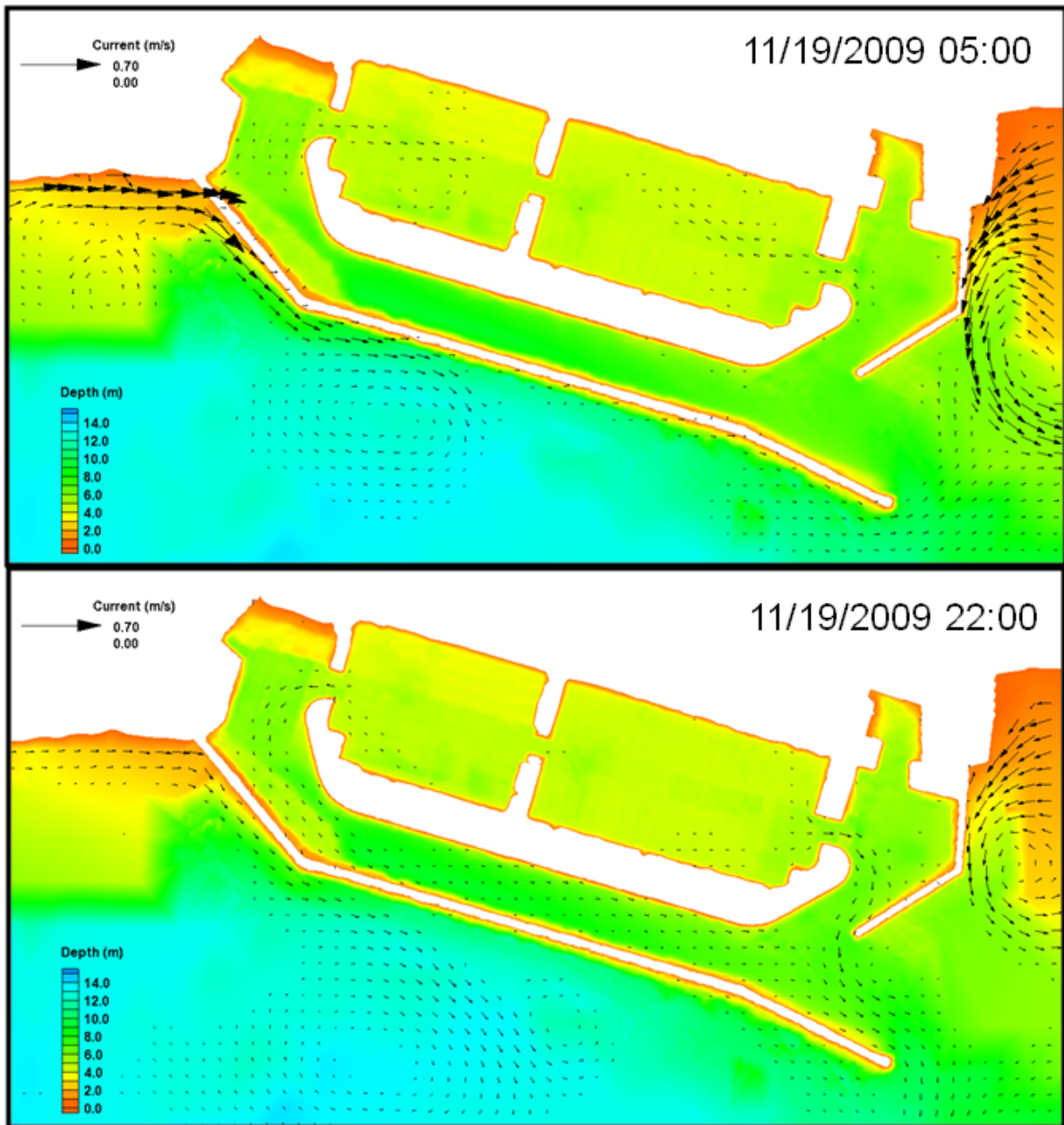
Figure 4-2



Comparisons between Simulated and Measured Currents at the Inside and Outside ADCP Stations



Figure 4-3

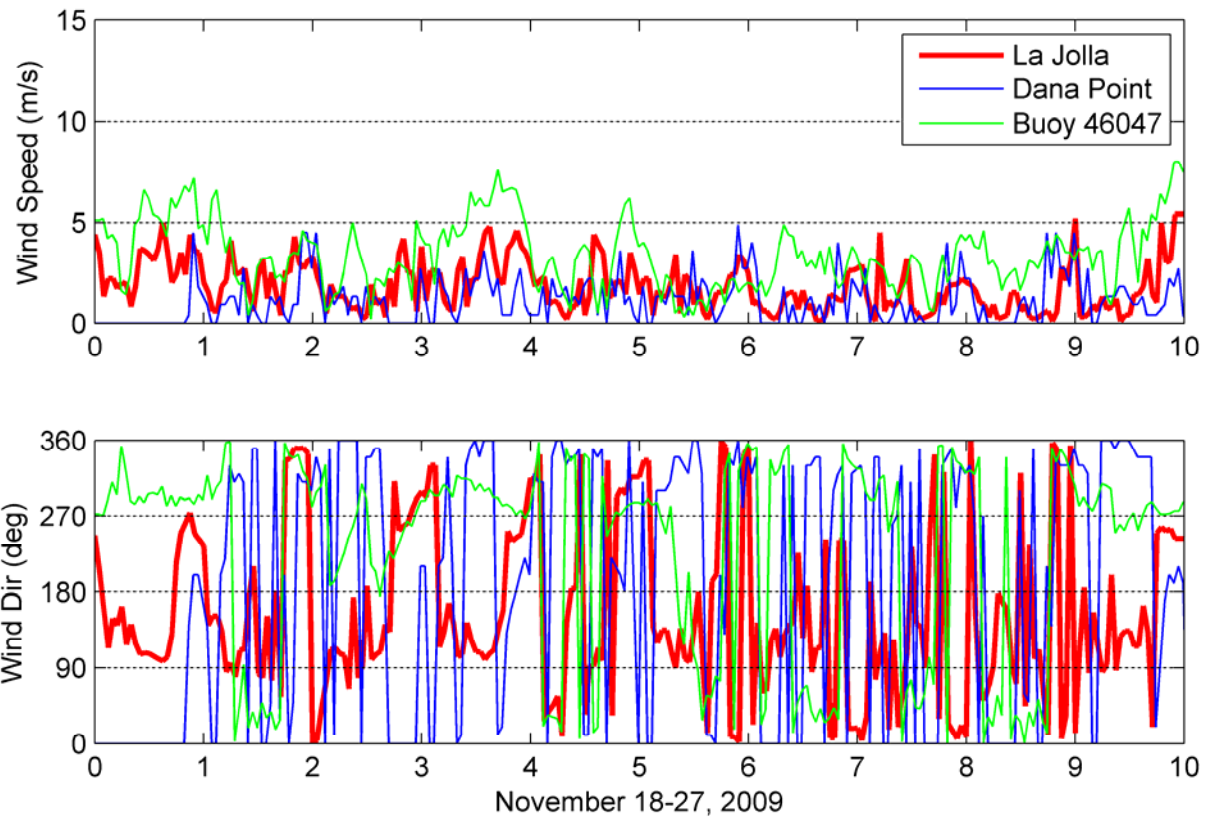


Notes: Current fields correspond to a flood tide and an ebb tide, respectively, on Nov 19, 2009 at 05:00 GMT and 22:00 GMT. Both the West and the East Breakwaters are permeable.

Simulated Depth Averaged Current Fields



Figure 4-4

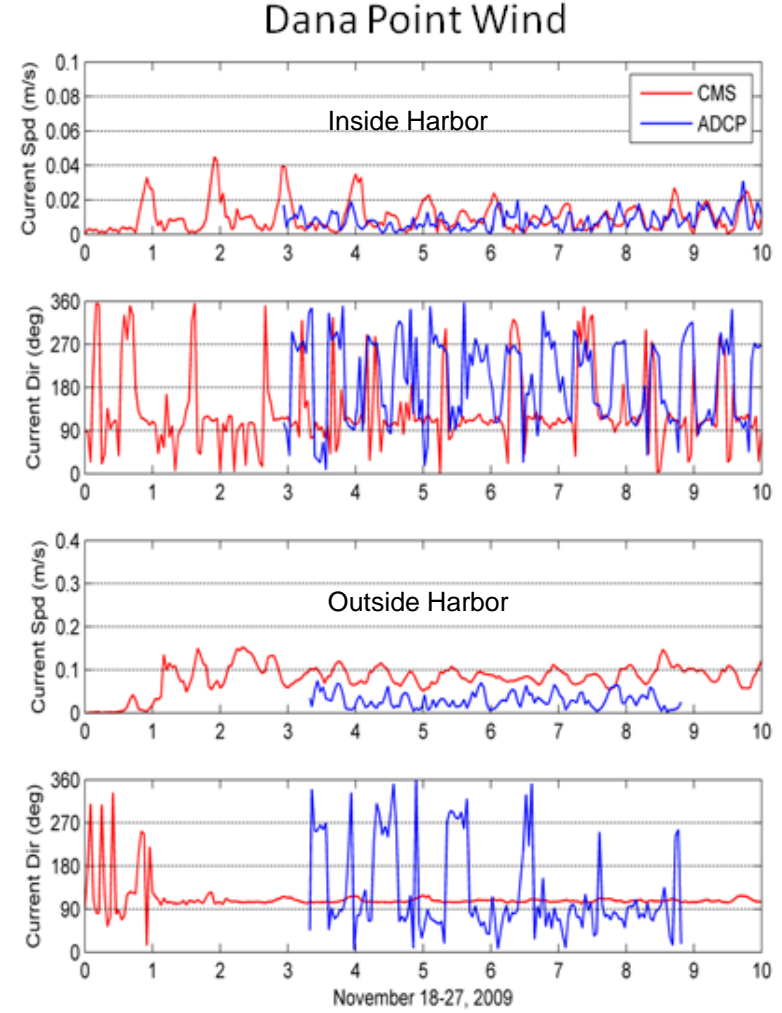
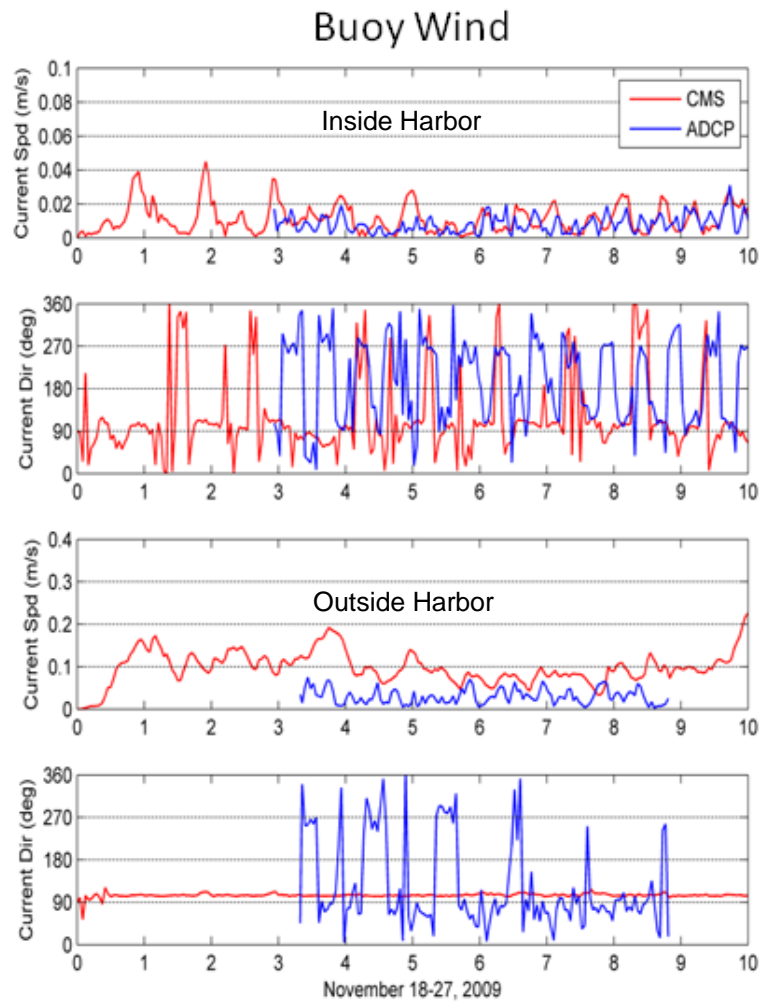


Note: The gage locations are at NOAA La Jolla Station (9419230), Dana Point Harbor (Ocean Institute), and NDBC buoy (46047), November 28-27, 2009.

Wind Speed and Direction at Various Locations



Figure 4-5



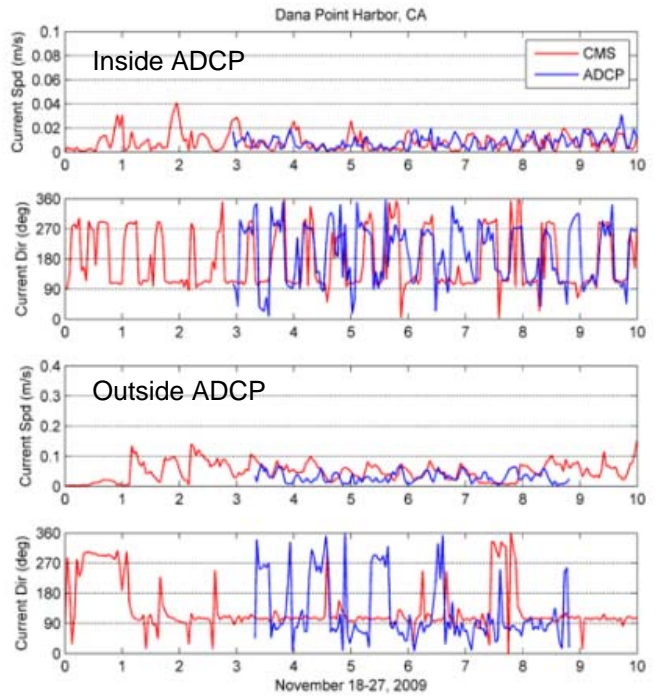
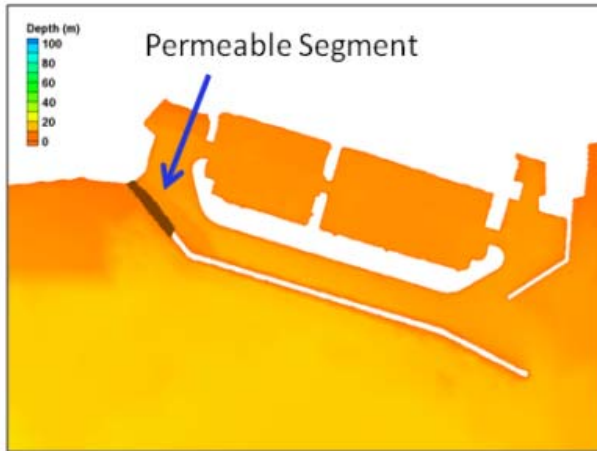
Note: The CMS was driven by the offshore buoy and the Dana Point wind, respectively.

Comparisons between the Simulated and Measured Currents at the Inside and Outside ADCP Stations with Different Wind Forcing

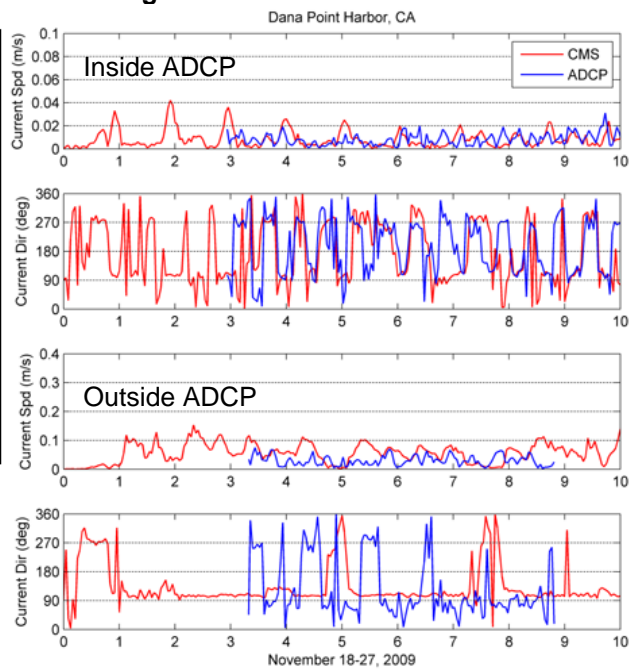
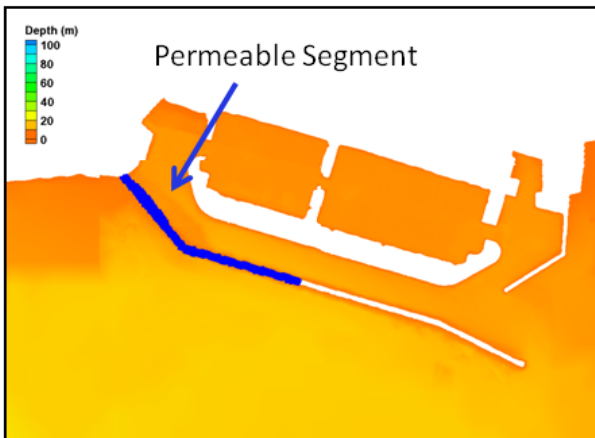


Figure 4-6

(a) Short Permeable Segment



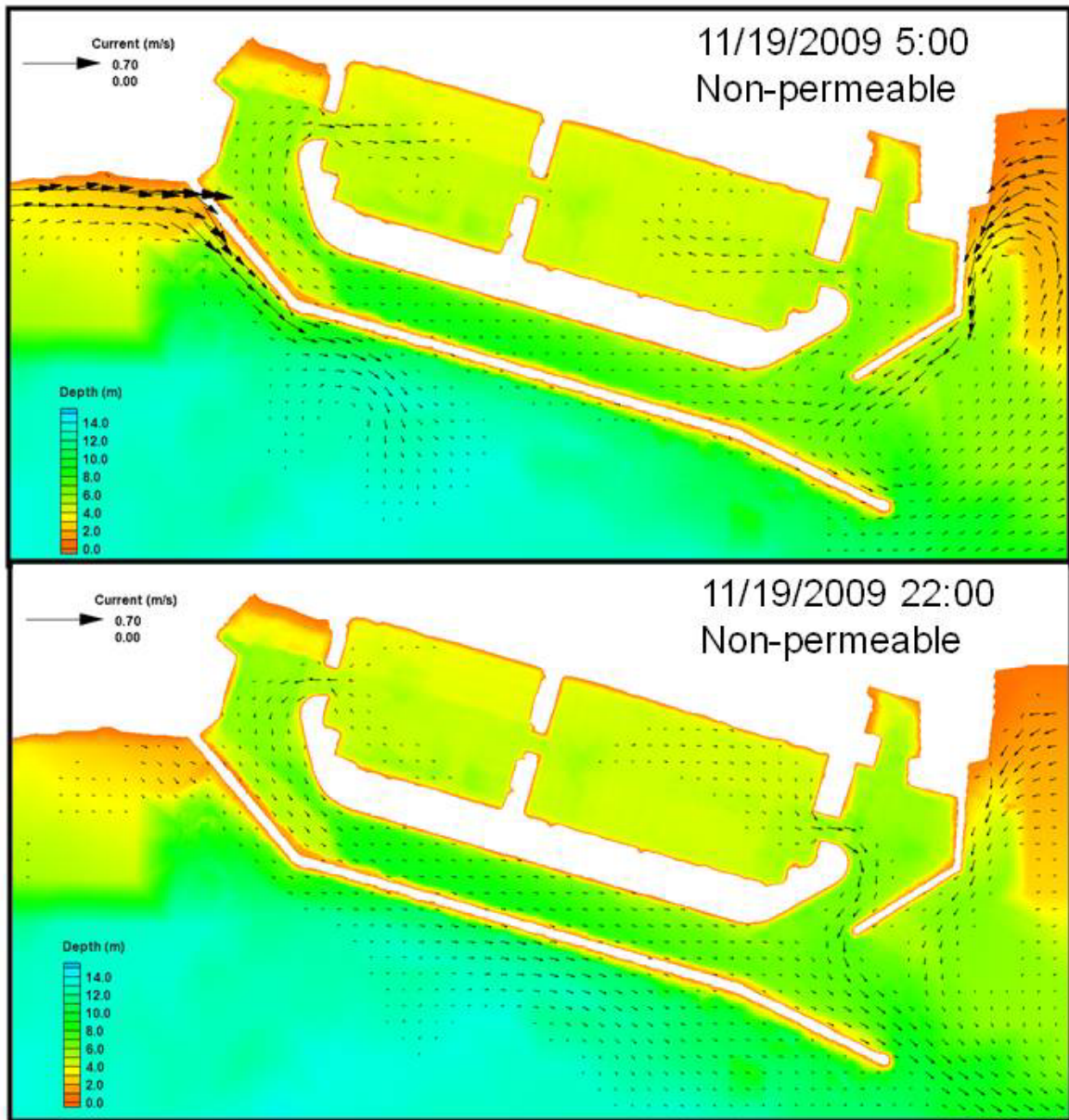
(b) Long Permeable Segment



Comparisons between Simulated and Measured Currents at the Inside and Outside ADCP Stations with Different Permeable Breakwater Segments



Figure 4-7

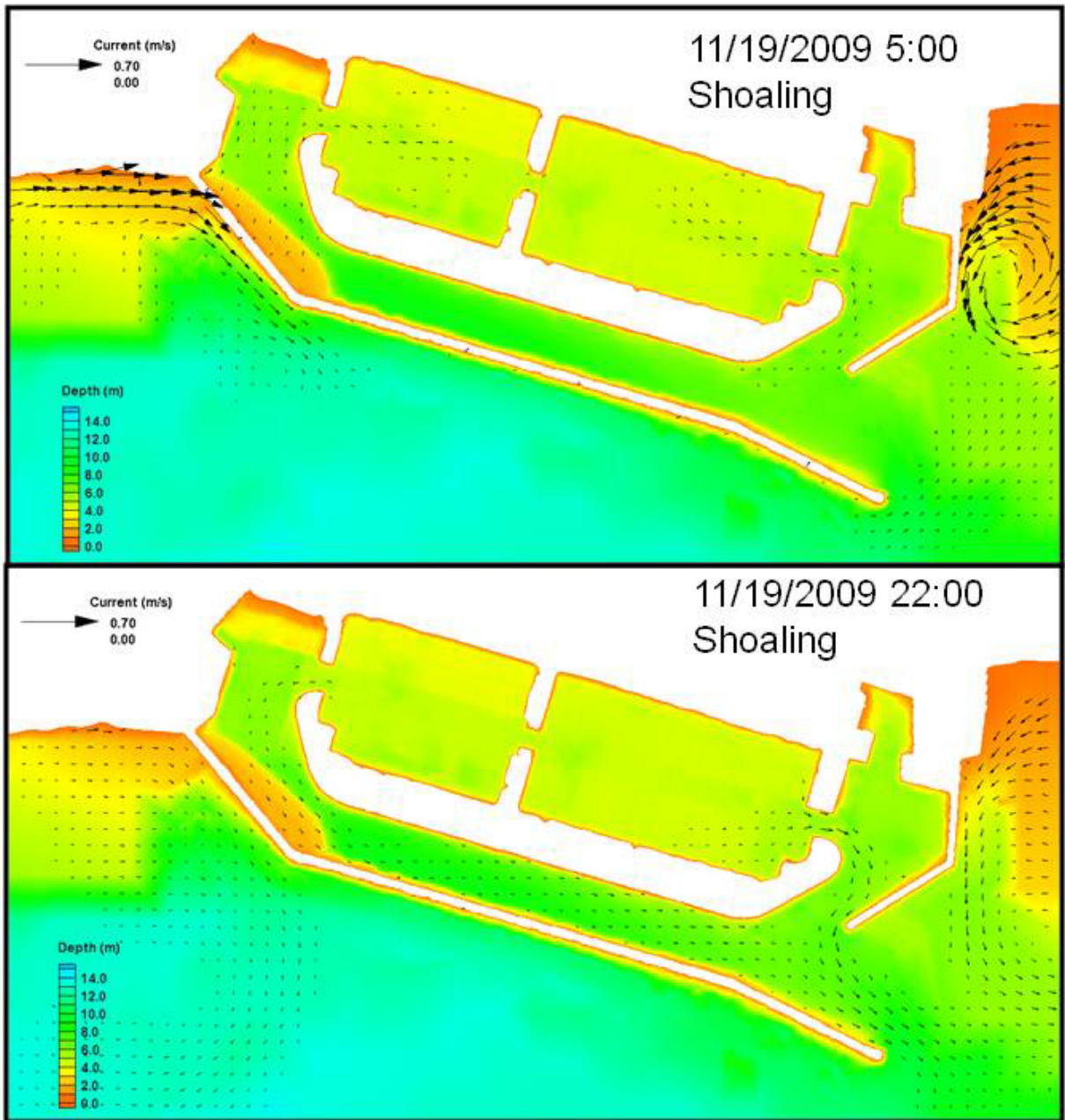


Notes: Current fields correspond to a flood tide and an ebb tide, respectively, on Nov 19, 2009 at 05:00 GMT and 22:00 GMT. Both breakwaters are non-permeable.

Simulated Depth Averaged Current Fields for Non-Permeable Breakwaters



Figure 4-8



Notes: Current fields correspond to a flood tide and an ebb tide, respectively,
on Nov 19, 2009 at 05:00 GMT and 22:00 GMT.
Both breakwaters are permeable with a shoal developed on the West Breakwater

Simulated Depth Averaged Current Fields with a Developed Shoal



Figure 4-9

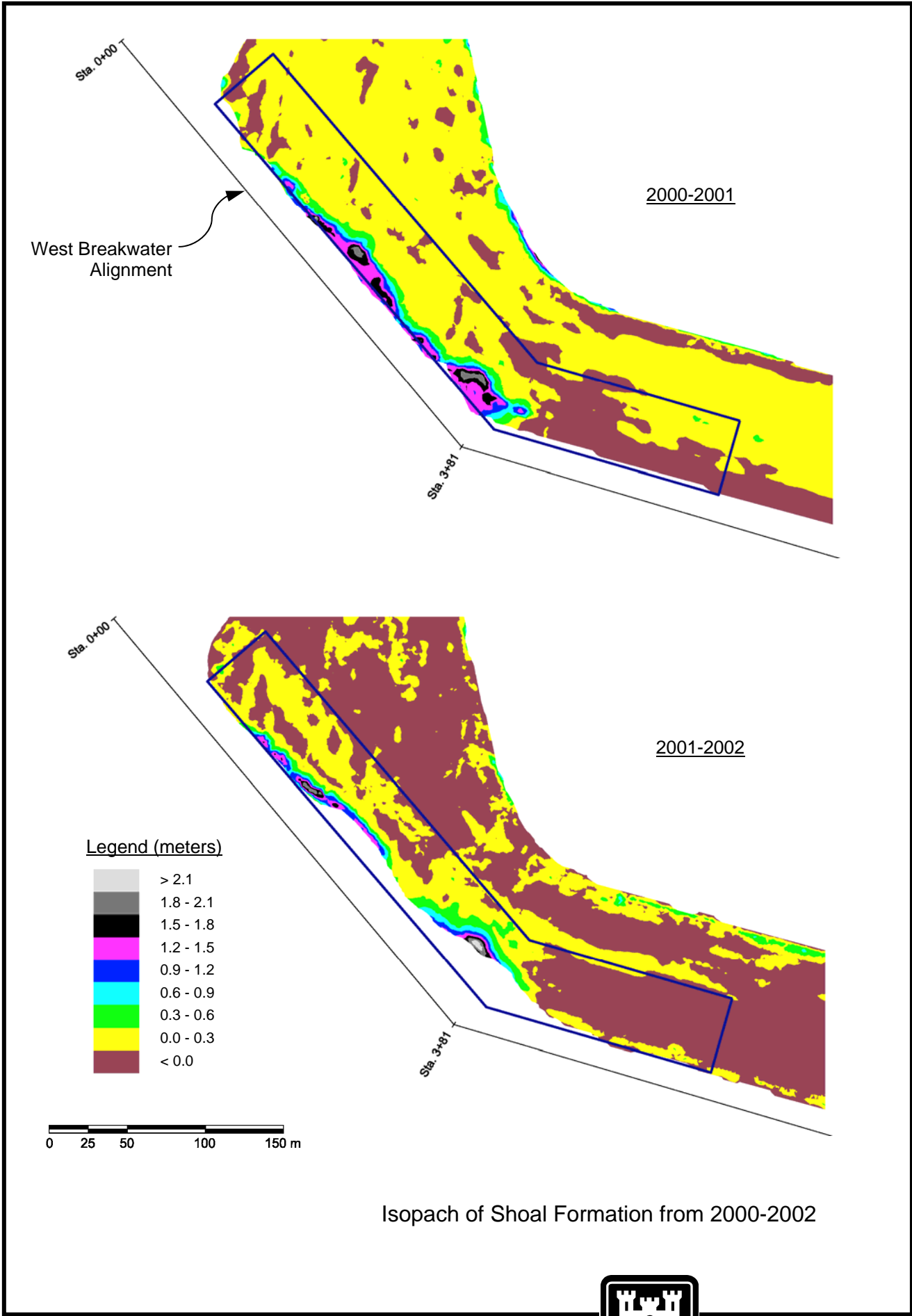


Figure 4-10

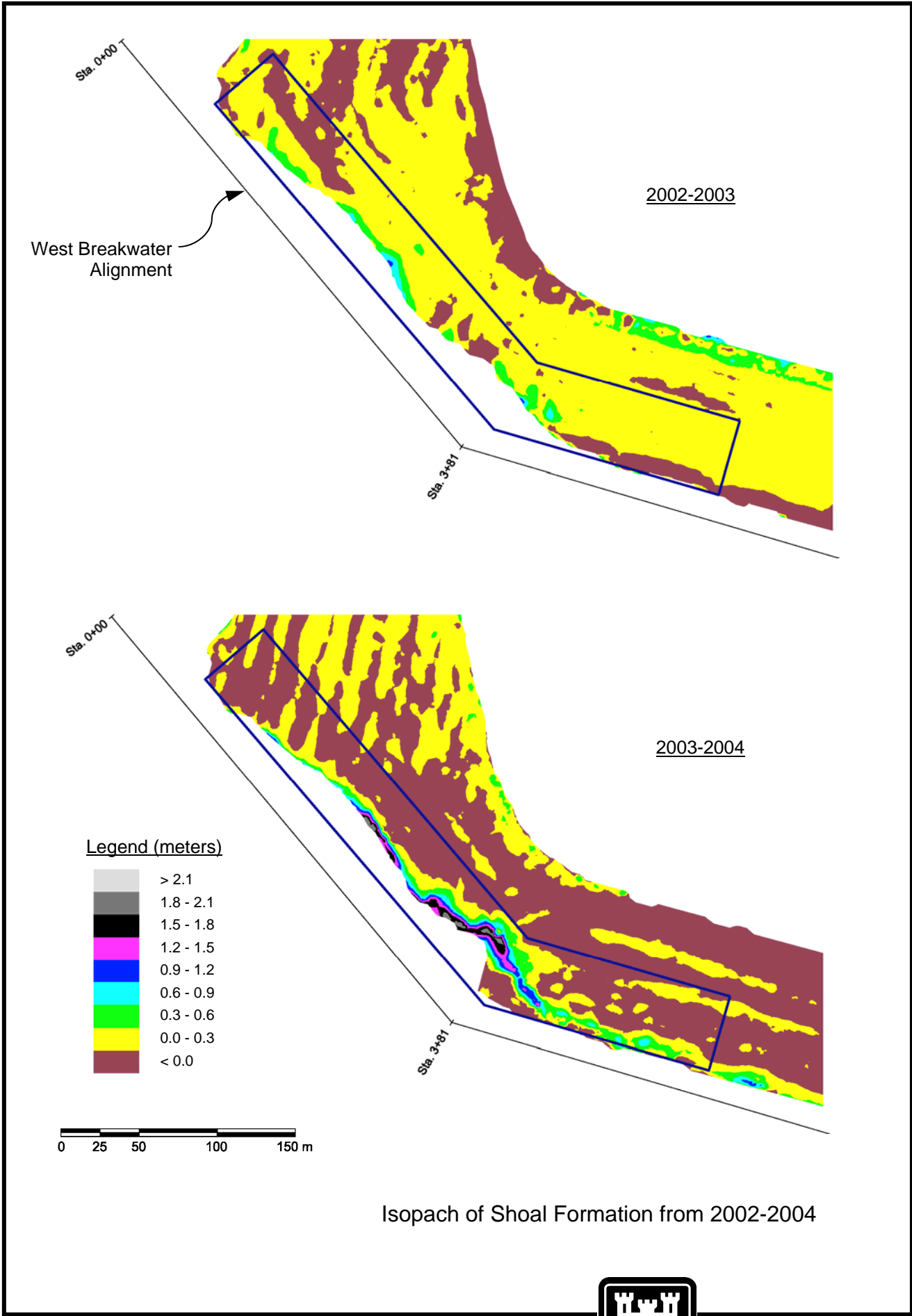
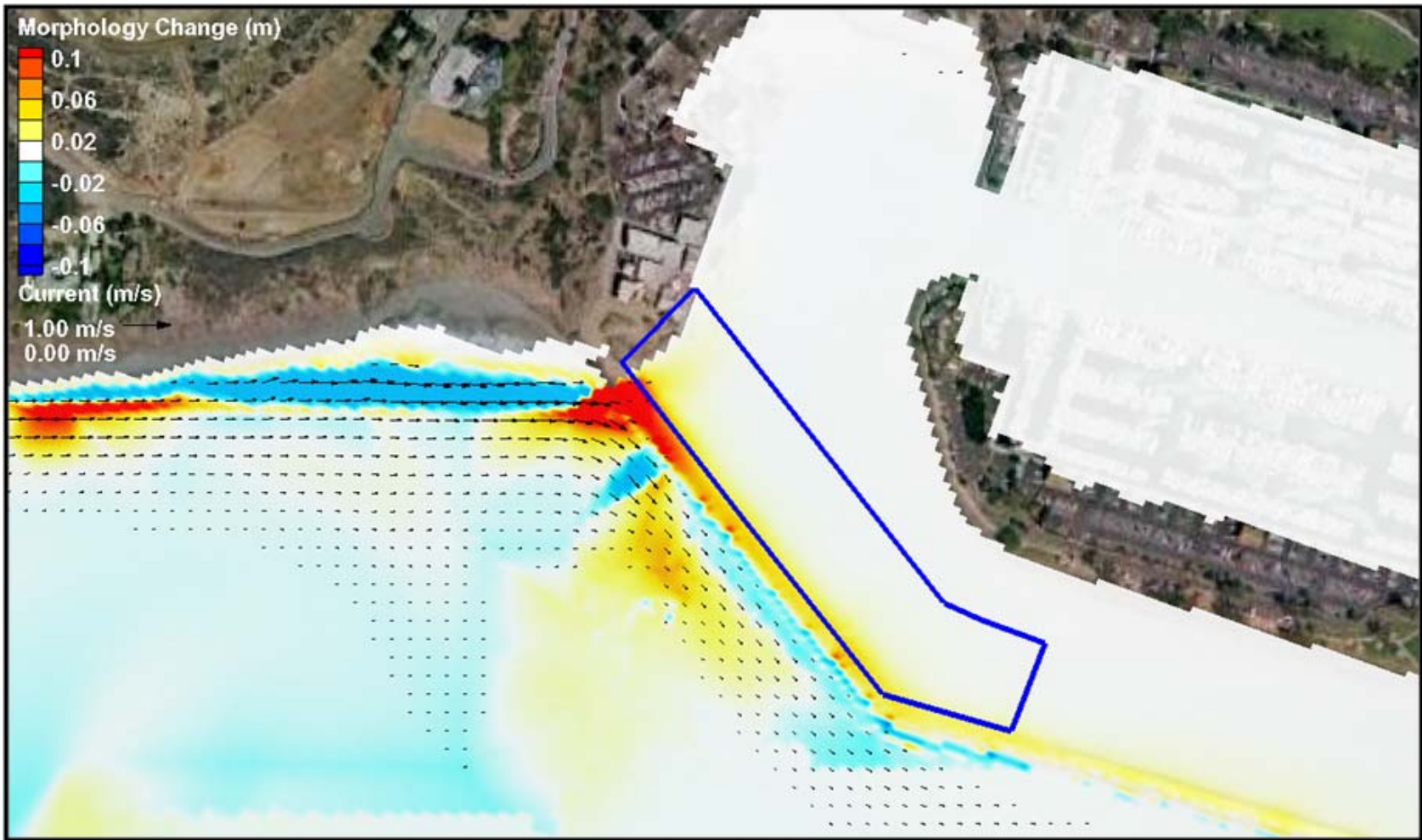


Figure 4-11



Note: The blue line denotes the area where bed volume change was estimated.

Morphology Change at the End of the 10-day Simulation



5.0 PARTICLE TRACKING MODELING

The CMS calculates water levels, currents and waves through the coupling of CMS-Flow and CMS-Wave. CMS-Flow is driven by time-dependent water surface elevation at the offshore open boundaries, and wind forcing over the surface boundary. Directional wave input spectra are specified at the seaward boundaries for CMS-Wave. **Figure 5-1** illustrates the calculated water circulation patterns in the harbor and adjacent areas during the flood and ebb cycles.

Using CMS-Flow and CMS-Wave simulation outputs, a Particle Tracking Model (CMS-PTM) can be applied to track neutrally buoyant or sediment particle movements to assess water circulation, sediment transport, and water-quality related issues. The periodically pre-calculated hydrodynamic and wave field from a CMS simulation allow for simultaneous executions of CMS-PTM.

5.1 CMS-PTM Description

The CMS-PTM is a Lagrangian-based particle transport model and designed to determine the fate and pathways of sediments and other waterborne particulates, chemicals, debris, biota, etc, for dredging operations and coastal engineering applications. In a complex hydrodynamic and wave environment, particles are released from local sources, such as dredging and placement sites, outfalls, propeller wash (MacDonald et al. 2006; Demirbilek et al. 2008).

In the PTM, particle movements are represented by the following equation:

$$\frac{dX}{dt} = U_A + U_D \quad (5-1)$$

where X , U_A , and U_D are vectors; X defines the position in three dimensions, x , y , and z , of a particle, U_A and U_D are the advection and diffusion velocities, respectively. The estimate of the turbulent diffusion coefficient in U_D is also used to drive a random walk model.

A particle position at time $t + dt$ is solved using a second-order predictor-corrector technique, which is implemented in two stages. Taking the x component in Equation 5-1 as an example, the first stage is to predict the particle position one-half time step ($n + 1/2$) into the future, $x_{n+1/2}$, based on the particle position at the present (x_n):

$$x_{n+1/2} = x_n + \frac{1}{2}(u_{Ax}dt + u_{Dx}dt) \quad (5-2)$$

where u_{Ax} and u_{Dx} are the x direction advection and diffusion velocities at the present location x_n , respectively. The second stage is to obtain the particle position at the full time step (x_{n+1}),

$$x_{n+1} = x_n + u_{Ax,n+1/2}dt + u_{Dx,n+1/2}dt \quad (5-3)$$

where $u_{Ax,n+1/2}$ and $u_{Dx,n+1/2}$ are the x direction advection and diffusion velocities at time step $n+1/2$ $x_{n+1/2}$, respectively.

The CMS-PTM also includes processes vital to sediment particle transport such as settling, deposition, re-suspension, and hiding and exposure function. Similar to CMS-Wave and CMS-Flow, CMS-PTM was operated in the Surface-water Modeling System (SMS), which provides a robust, user-friendly interface for model setup, model execution, data analysis, and post-processing.

5.2 CMS-PTM Simulations

The CMS-PTM simulations were performed using the flow field obtained from the CMS-Flow simulation during the same calibration period (i.e., November 19-27, 2009). A total of 1080 neutrally buoyant particles were released for each simulation inside the Dana Point Harbor. Because a particle pathway depends strongly on tidal conditions (flood or ebb) after its release, the hourly release lasted for 12 hours to cover the semi-diurnal tidal period. To optimize the evaluation of water quality issue at Baby Beach and the particle movement within the harbor, three (3) local particle sources where the particles were released were selected. Two are located at Baby Beach (in the east and west areas) and the third one is in the main navigation channel. **Figure 5-2** illustrates the three locations where the particles were released in the CMS-PTM simulations.

Particle pathways and fate were compared after their release at three (3) afore-mentioned locations. **Figures 5-3 to 5-5** show the particle distributions at the Dana Point Harbor two days after particles were released at west, east Baby Beach, and in the navigation channel, respectively. Figure 5-3 shows that most of the released particles at west Baby Beach are still residing inside the harbor, while a small percent of particles are moved out of the harbor and into the open water. A cluster of particles can still be detected at Baby Beach. The flood tides

bring in water/particles that subsequently are trapped in the beach area, as the previous wet cells consequently become isolated drying cells during ebb tides. Released from east Baby Beach, most of the particles are also staying inside the harbor (see Figure 5-4) although the particle distribution pattern appears to be slightly different. More particles are found in the West Basin instead of the East Basin for the releasing location at east Baby Beach. Among the three release scenarios, the channel release shows that the harbor was retaining the least number of particles after two days.

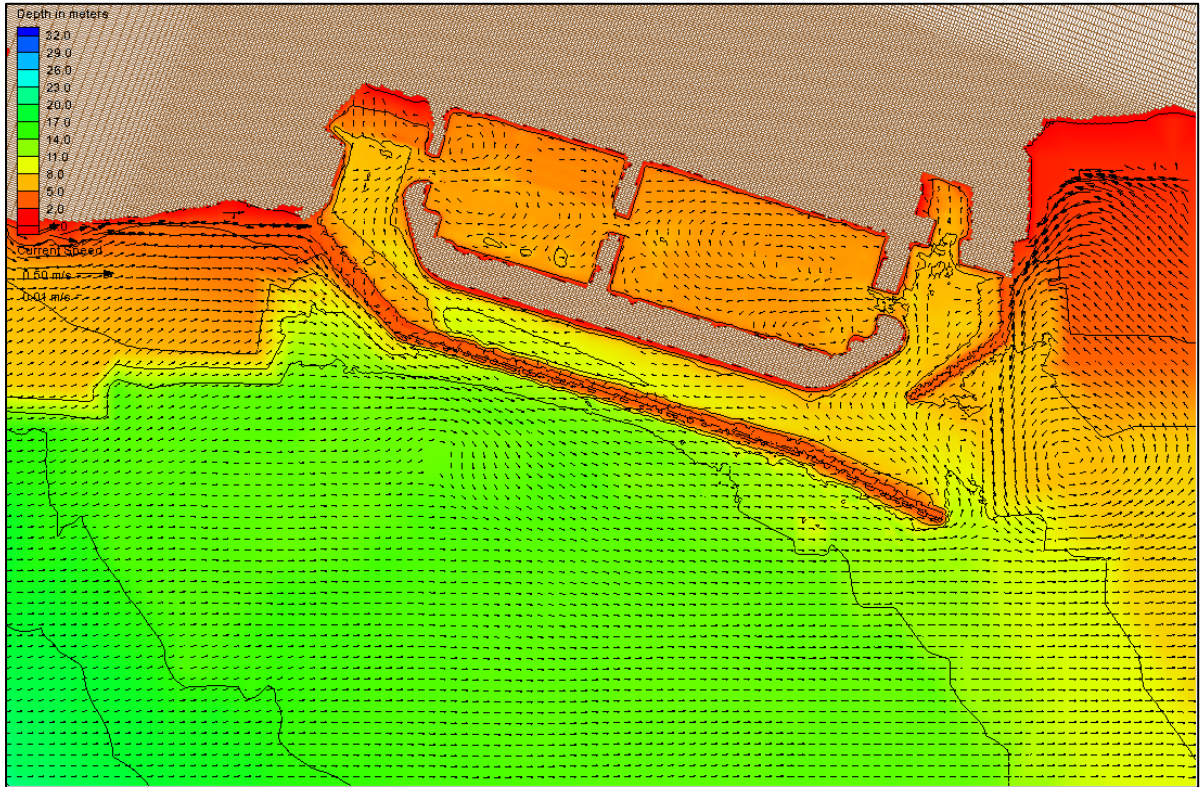
5.3 Residence Times

After the 9-day simulations, the particles released from three local sources were tracked and the residence times of particles were estimated, as presented in Table 5-1. The residence time is defined as the duration required for 67.7% of particles being moved out from the harbor into the open water. It is a common criterion used to measure the relatively tidal flushing capability within a subject harbor. For the two release locations at Baby Beach, more than 60% of particles are still in the harbor at the end of 9-day simulations. In other words, the residence time of particles released at Baby Beach would be much longer than 9 days. The residence time of particles released at the channel location is approximately 5 days. The calculated flow field in the harbor indicates relatively stronger tidal currents at this location. As a result, a much shorter residence time is expected.

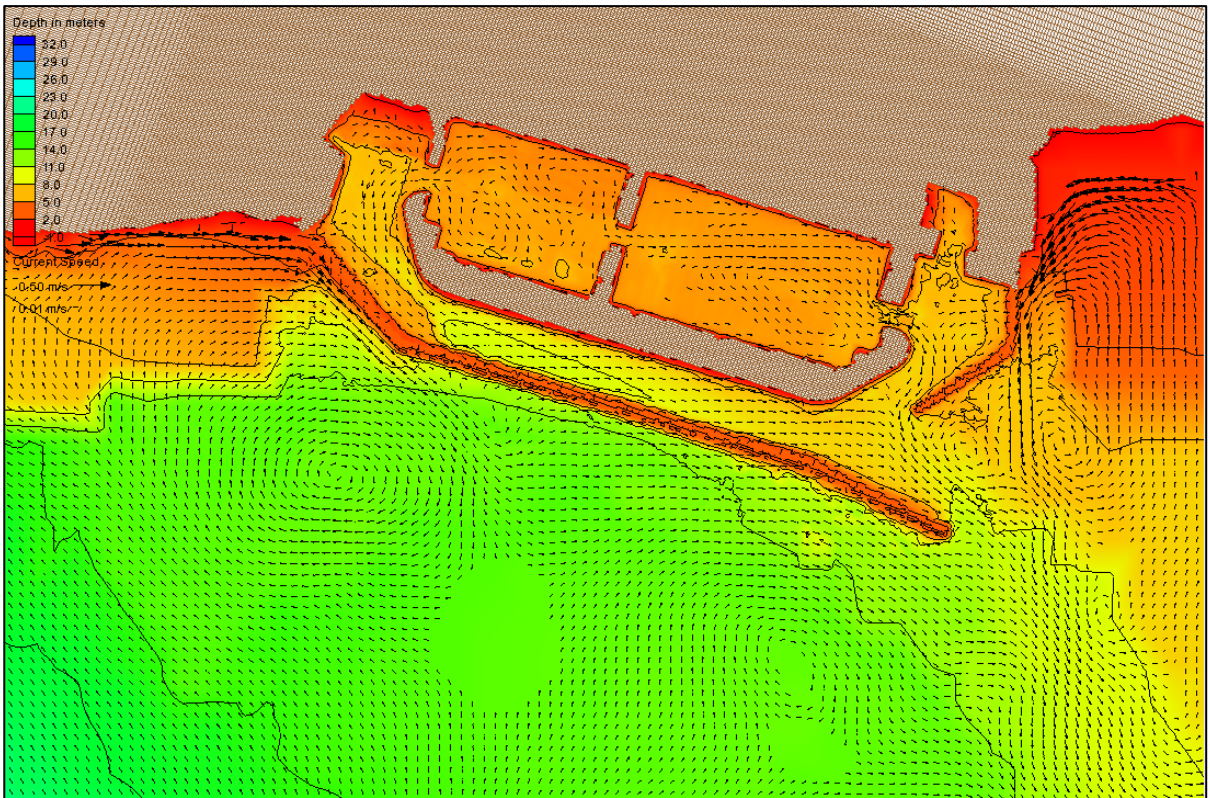
Table 5-1. Number of Particles Leaving Dana Point Harbor after Released at Baby Beach.

<i>Release Location</i>	<i>West of Baby Beach</i>				<i>East of Baby Beach</i>				<i>Navigational Channel</i>			
	<i>Particle</i>	<i>Accu. Particle</i>	<i>%</i>	<i>Accu. %</i>	<i>Particle</i>	<i>Accu. Particle</i>	<i>%</i>	<i>Accu. %</i>	<i>Particle</i>	<i>Accu. Particle</i>	<i>%</i>	<i>Accu. %</i>
1	99	99	9.2	9.2	88	88	8.1	8.1	662	662	61.3	61.3
2	120	219	11.1	20.3	84	172	7.8	15.9	33	695	3.1	64.4
3	51	270	4.7	25.0	43	215	4.0	19.9	5	700	0.5	64.9
4	50	320	4.6	29.6	41	256	3.8	23.7	18	718	1.7	66.6
5	25	345	2.3	31.9	34	290	3.1	26.8	11	729	1.0	67.6
6	27	372	2.5	34.4	35	325	3.2	30.0	7	736	0.6	68.2
7	19	391	1.8	36.2	27	352	2.5	32.5	3	739	0.3	68.5
8	5	396	0.5	36.7	10	362	0.9	33.4	3	742	0.3	68.8

Note: total released particles =1080



Flood Tide Condition

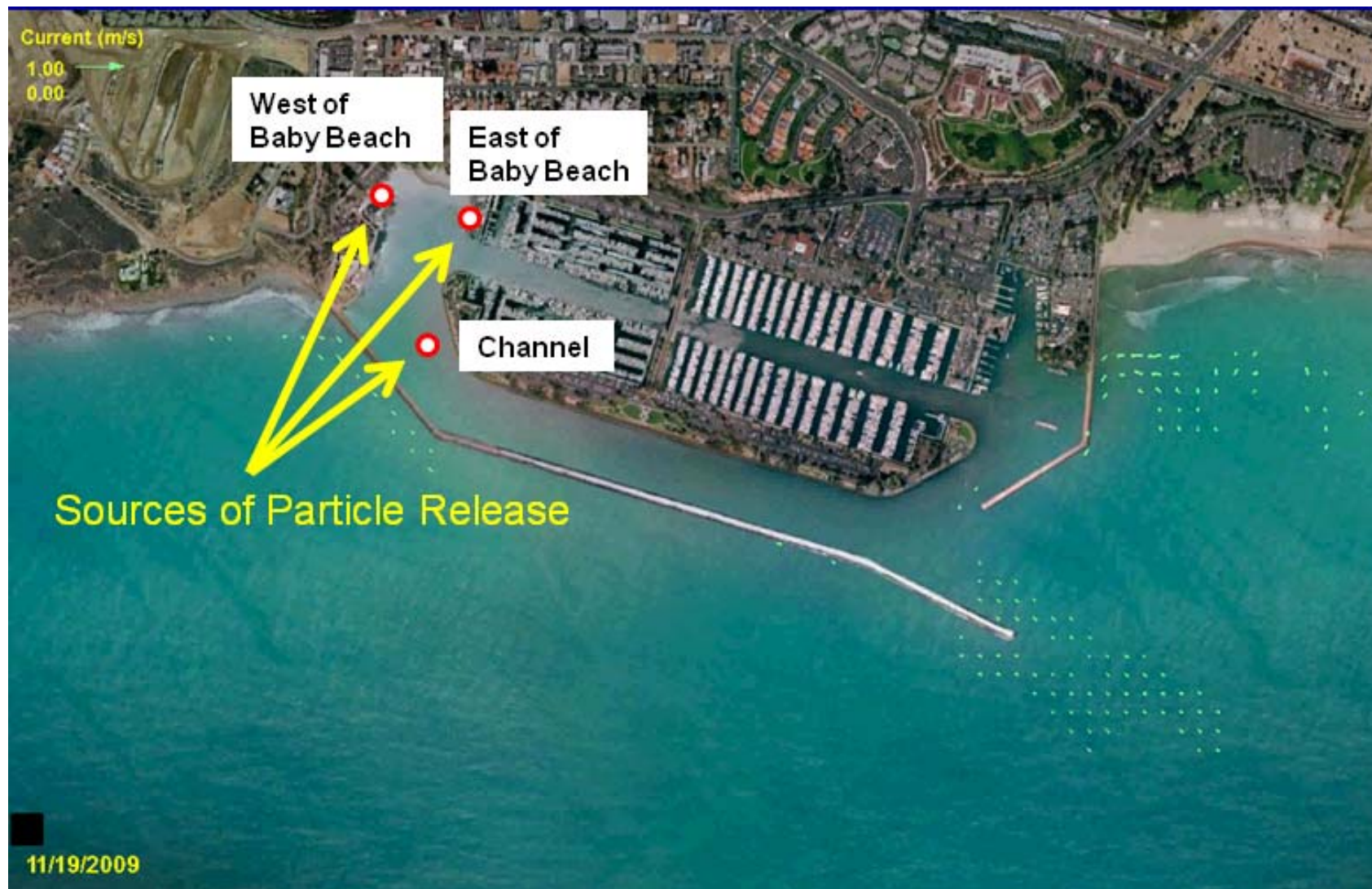


Ebb Tide Condition

Water Circulation Patterns



Figure 5-1



Local Sources of Particle Release in Dana Point Harbor



Figure 5-2



Snapshot of Particle Distribution in Dana Point Harbor Two Days after the Particle Release at West Baby Beach



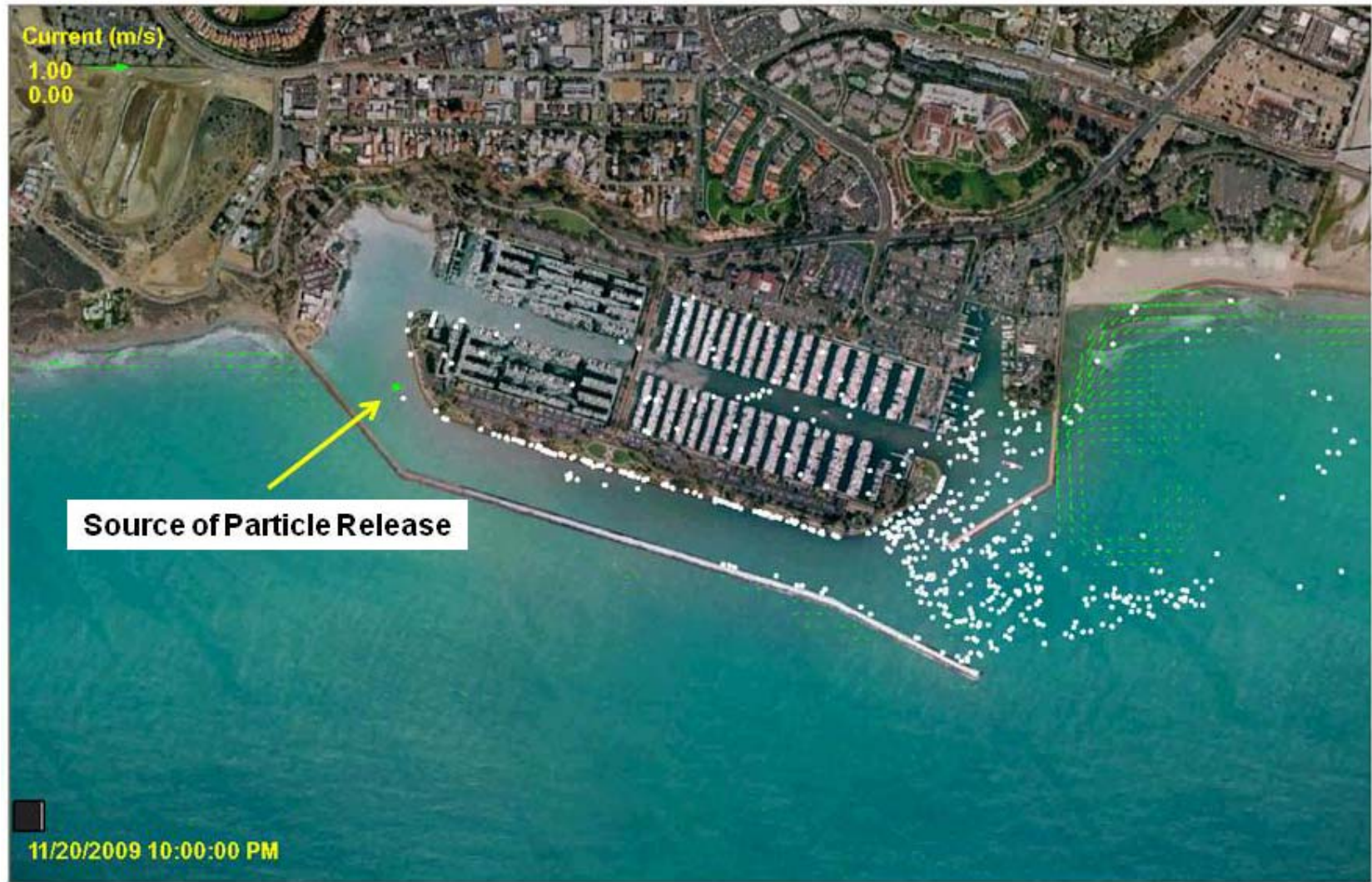
Figure 5-3



Snapshot of Particle Distribution in Dana Point Harbor Two Days after the Particle Release at East Baby Beach



Figure 5-4



Snapshot of Particle Distribution in Dana Point Harbor Two Days after the Particle Release in the Main Channel



Figure 5-5

6.0 SUMMARY AND CONCLUSIONS

A comprehensive condition survey was conducted for the dual breakwaters at Dana Point Harbor, California to assess the present-day structure conditions and their protective functionality against storm wave attack. In addition, a concurrent effort was performed to evaluate wave dynamics at the breakwaters, tidal hydrodynamics and water circulation within the harbor, and sedimentation along the lee of the West Breakwater via numerical simulations. Both numerical models CMS-Wave and CMS-Flow were improved to enhance the model capability in characterizing the permeability of the breakwaters.

A bathymetric and 3D-LiDAR (Light Detection and Ranging) survey was conducted on October 20-24, 2009 to collect basic physical data including nearshore and in-harbor bathymetry, and 3D images of breakwaters, revetments, Baby Beach and other pertinent features in the harbor. The survey utilized the swath bathymetry system for the underwater portion and the laser scanning system for elevations above the water line.

Oceanographic data collection, including current speed and direction as well as wave height, was conducted by deploying two ADCPs at both sides of the West Breakwater from November 20, 2009 to January 15, 2010. Improvement of CMS-Wave and CMS-Flow was achieved to allow the breakwaters acting as permeable structures, through which the capability of incident wave transmission, flow movement and sediment seepage was incorporated in the model. Based upon the comprehensive condition survey, oceanographic data collection and CMS numerical simulations, several findings are summarized below.

6.1 Conditions of Breakwaters

The present-day structure conditions of the dual breakwaters were examined via the combination of reviewing the processed 3-D LiDAR images and bathymetry, and visual confirmation above the water line.

At the West Breakwater, dislodged stones on the harbor side near Sta. 00+97 and Sta. 02+13 are detected below the water surface (see Figure 2-5). In addition, displaced stones above the Mean Sea Level are observed at Sta. 15+54 and near the head of the West Breakwater (see Figures 2-6 and 2-7). Nevertheless, the structure appears to function as originally designed for sheltering harbor facilities from west to northwest winter storm waves.

At the East Breakwater, the structure remains intact and functions as a protective device for the normal operation of harbor activities. Some armor stones located below the water surface on the harbor side appear to be dislodged from their original positions (see Figures 2-9 and 2-10).

6.2 Flow Field Conditions

Current data at various depths was collected from two ADCP's that were deployed at both sides of the West Breakwater for a period of 8 weeks. Measured instantaneous current velocities are typically less than 6 cm/sec in the main navigational channel (see Figures 2-18 to 2-21) and on the order of 10 to 20 cm/sec in the oceanside area of the West Breakwater (see Figures 2-22 to 2-28).

It is evident that currents moving through the rubble-mound structure occur throughout the West Breakwater, consistent with the original design of a semi-permeable rubble-mound structure. A wide range of current direction, likely resulting from current flow across the West Breakwater, was observed in the lower water column of the navigational channel during both flood and ebb tides (see Figures 2-29 and 2-30). Influence of the through-breakwater currents appears weaker near the water surface. The ranges of recorded direction near water surface (Bin 4) are in the 90° to 120° sector for ebb tides (see Figures 2-29 and 2-33) and primarily in the 210° to 270° sector during flood tides (see Figures 2-30 and 2-34), respectively. For the flow field in the ocean side of the West Breakwater, the currents that generally move toward southwest along the breakwater are relatively consistent throughout the vertical water column and differ slightly for both ebb and flood cycles (see Figures 2-31 and 2-32).

6.3 Improvement of CMS Models

The enhanced Coastal Modeling System was applied to evaluate circulation and wave conditions surrounding the Dana Point Harbor and to assess the wave transmission, flow penetration, and sediment seepage through the permeable breakwaters.

The capability of CMS-Wave was improved by allowing wave transmission through the breakwaters. Several model parameters such as forcing wind and tidal fluctuation were examined to assess their impact to the model simulations.

The model performance marginally improves with the forcing of the offshore wind condition and temporal water levels. Inclusion of the wave reflection at the breakwaters substantially increases the model accuracy of wave height prediction seaward of the breakwaters (see Table 3-2). In order to predict morphologic change and sedimentation in the main navigational channel, the capability of CMS-Flow was enhanced to account for flow penetration through the permeable breakwaters.

6.4 Storm Wave Characteristics

Storm wave conditions at the breakwaters were characterized based on the deepwater GROW wave hindcast data, spanning 39 years (1970-2008), via wave transformation through offshore islands by a back-refraction spectral model and subsequently nearshore wave propagation using CMS-Wave.

The deduced wave characteristics for severe extratropical storms from 1970 to 2008 are comparable to peak storm wave heights that were previously used in the 1965 General Design Memorandum of Dana Point Harbor. The deduced extratropical peak wave heights at the West Breakwater for three referred historic extratropical storms range from 4.3 to 4.9 meters (14.1 to 16.1 feet). The maximum storm wave height simulated by CMS-Wave is 5 meters (16.4 feet) during the February 28, 1983 storm event.

A recent study to assess likely winter wave height changes along the Southern California coast under various scenarios of future greenhouse gas emission, resulting in varying degrees of sea level rise, concluded that the intensity of future storms is expected to follow a slightly negative trend within the region, as the winter cyclone track with a warmer climate tends to move further north. Therefore, the extratropical storm wave characteristics deduced from the 1970-2008 period will be applicable in the future if any alteration or maintenance of the breakwaters is required.

6.5 Sedimentation and Water Circulation Patterns

The CMS was validated by the measured waves, currents, and water surface elevations. The implementation of the algorithms for flow penetration and sediment seepage through the permeable breakwater was verified by the historical dredging information. In the 10-day model validation during a neap tide

period between November 18 and 27, 2009, the average current speed is in the range 2-10 cm/sec in the main navigational channel.

By applying and adjusting the parameters of the breakwater void factor and flow resistance, the cumulative morphologic change due to sediment transport through the permeable West Breakwater was estimated at the end of the 10-day simulation. An annual sediment deposition rate of 6,060 cy/yr was predicted from the linear extrapolation of the CMS results. This sediment transport rate is comparable to the volumes obtained from the 2009 maintenance dredging activity at Dana Point Harbor.

Sensitivity analysis was conducted by examining model forcing, structure permeability, and harbor shoaling. The CMS results indicate that the harbor is well protected by waves with a tide-dominated environment within the harbor and a wave-dominated environment in the open ocean. The permeability of the West and East Breakwaters may slightly change the current speed inside the harbor (see Figures 4-4 and 4-8), but the circulation pattern is not affected by different specifications of the breakwater permeability. In other words, wave transmission through the West Breakwater alters the circulation pattern slightly in the main navigational channel, but the effect is localized and inconsequential in the inner harbor (e.g., Baby Beach). The permeability of the West Breakwater results in little improvement of tidal flushing in the Baby Beach area.

The presence of a shoal in the lee of the West Breakwater reduces the annual sedimentation rate by approximately 15%, as compared to the sand deposition during the immediate post-dredging period. The formed shoal results in relatively larger depth-averaged currents in the adjacent area. Nevertheless, the overall harbor circulation pattern is not altered (see Figures 4-4 and 4-9).

The residence time in the harbor was estimated by a particle tracking model (i.e., CMS-PMT). Depending on the particle release locations, the estimated residence time varies. For the two release locations at Baby Beach (i.e., the west and east ends), more than 60% of particles remain in the harbor at the end of a 9-day simulation. Therefore, any constituents situated in the Baby Beach area require much longer time than 9 days to flush approximately 67% (the residence time) out into the ocean. Conversely, the residence time of particles released in the main navigational channel is less than 5 days owing to better tidal flushing in the channel.

7.0 REFERENCES

Buttolph, A. M., Reed, C. W., Kraus, N. C., Ono, N., Larson, M., Camenen, B., Hanson, H., Wamsley, T., and Zundel, A. K. (2006). "Two-dimensional depth-averaged circulation model CMS-M2D: Version 3.0, Report 2, sediment transport and morphology change," *Coastal and Hydraulics Laboratory Technical Report ERDC/CHL-TR-06-7*. U.S. Army Engineer Research and Development Center, Vicksburg, MS.

Cayan, D., et al., 2009. "Climate Change Scenarios and Sea Level Rise Estimates for the California 2009 Climate Change Scenarios Assessment", California Climate Change Center.

County of Orange. (1990). "Plans and special provisions for the maintenance dredging at Dana Point Harbor," funded by Harbor, Beaches and Parks, County of Orange.

County of Orange. (1999). "Plans and special provisions for the maintenance dredging at Dana Point Harbor," funded by Harbor, Beaches and Parks, County of Orange.

County of Orange. (2009). "Plans and special provisions for the maintenance dredging at Dana Point Harbor," funded by Harbor, Beaches and Parks, County of Orange.

County of Orange Public Health Laboratory, Science Applications International Corporation, and County of Orange Public Facilities & Resources Department (PFRD) Watershed and Coastal Resources Division, 2003. "Baby Beach Bacteriological Special Studies Report, Dana Point Harbor, California", June 2003.

County of Orange Public Facilities & Resources Department, and Science Applications International Corporation (SAIC), 2003. "State of the Beach Report, Baby Beach Region, Dana Point Harbor, California", June 2003.

County of Orange Watershed and Coastal Resources Division, Resources and Development Management Department (RDMD), 2006. "Baby Beach in Dana Point Harbor, Orange County", Final Report, CBI Grant Nos. 19 and 260, Agreement No. 01-226-550-2, Prepared for State Water Resources Control Board, March 2006.

County of Orange Parks, 2011.

<http://www.ocparks.com/danapointharbor/default.asp?Show=History>

d'Angremond, K., Van der Meer, J. W., and de Jong, R. J. (1996). "Wave transmission at low-crested structures," *Proceedings 25th International Conference on Coastal Engineering*, Orlando, FL, USA, ASCE, 2418-2427.

Demirbilek, Z., K. J. Connell, N. J. MacDonald, and A. K. Zundel. 2008. Particle Tracking Model in the SMS10: IV. Link to Coastal Modeling System. Coastal and Hydraulics Engineering Technical Note ERDC/CHL CHETN-IV-71. Vicksburg, MS: U.S. Army Engineer Research and Development Center. <http://chl.erd.usace.army.mil/chetn>.

Everest International Consultants, Inc., 2006. "Circulation Improvement Pilot Project at Baby Beach, Dana Point", Final Report, Prepared for County of Orange, CA, January 2006.

Forchheimer, P. H. (1901). "Wasserbewegung durch Boden," *Zeitschrift des Vereines Deutscher Ingenieure* 50, 1781–1788.

Fugro West Inc., 2010. "USACE Dana Point Harbor Breakwater Comprehensive Condition Survey, Field Operation Report. May 2010.

Goda, Y., 1985, "Random Seas and the Design of Maritime Structures", University of Tokyo Press, 323pp.

Kinnetic Laboratories, Inc., 2006. "Sampling and Analysis Plan, Dredge Material Evaluation, Dana Point Harbor Maintenance Dredging," Prepared for Moffatt & Nichol and County of Orange Dana Point Harbor Department, June 2006.

Kuik, A. J., G. Ph. van Vledder, and L.H. Holthuijsen, "A method for routine analysis of pitch-and-roll buoy data" *J. Phys. Oceanogr.*, 18, 1020-1034, 1988.

Lin, L., Z. Demirbilek, H. Mase, J. Zheng, and F. Yamada. 2008. CMS-Wave: A nearshore spectral wave processes model for coastal inlets and navigation projects. Coastal and Hydraulics Laboratory Technical Report ERDC/CHL-TR-08-13. Vicksburg, MS: U.S. Army Engineer Research and Development Center.

Lygre A., H. E. Krogstad, 1986, "Maximum Entropy Estimation of the Directional Distribution of Ocean Wave Spectra", *Journ. Of Phys. Ocean.*, Vol. 16, No. 12, 1986.

MacDonald, N. J., M. H. Davies, A. K. Zundel, J. D. Howlett, T. C. Lackey, Z. Demirbilek, and J. Z. Gailani. 2006. *PTM: Particle Tracking Model; Report 1: Model theory, implementation, and example applications*. Coastal and Hydraulics Laboratory Technical Report ERDC/CHL-TR-06-20. Vicksburg, MS: U.S. Army Engineer Research and Development Center.

Mase, H., H. Amamori, and T. Takayama. 2005. Wave prediction model in wave-current coexisting field. *Proceedings 12th Canadian Coastal Conference* (CD-ROM).

O'Reilly, W.C., and R.T. Guza, 1991. "Modeling Surface Gravity Waves in the Southern California Bight", SIO reference Series No. 19-25, September 1991.

O'Reilly W. C., and R. T. Guza, 1993, "A comparison of spectral wave models in the Southern California Bight", *Coastal Engineering*, 19(3), 263-282.

Science Application International Corporation (SAIC) and County of Orange Public Facilities and Resources Department, 2002. "Baby Beach Circulation Study Sampling and Analysis Plan (SAP)", September 2002.

Science Application International Corporation (SAIC), 2003a. "Circulation Study Report, Baby Beach Region, Dana Point Harbor, California", Prepared for the County of Orange Public Facilities and Resources Department. March 2003.

Science Application International Corporation (SAIC), 2003b. "Data Mining Task for State of the Beach Report: Evaluation of Bacteriological Data and Associated Parameters for Baby Beach, Dana Point Harbor, CA", Prepared for County of Orange Public Facilities & Resources Department, January 2003.

Teledyne, 2006. "Acoustic Doppler Current Profile, Principal of Operation, A Practical Primer", P/N 951-6069-00, November 2006.

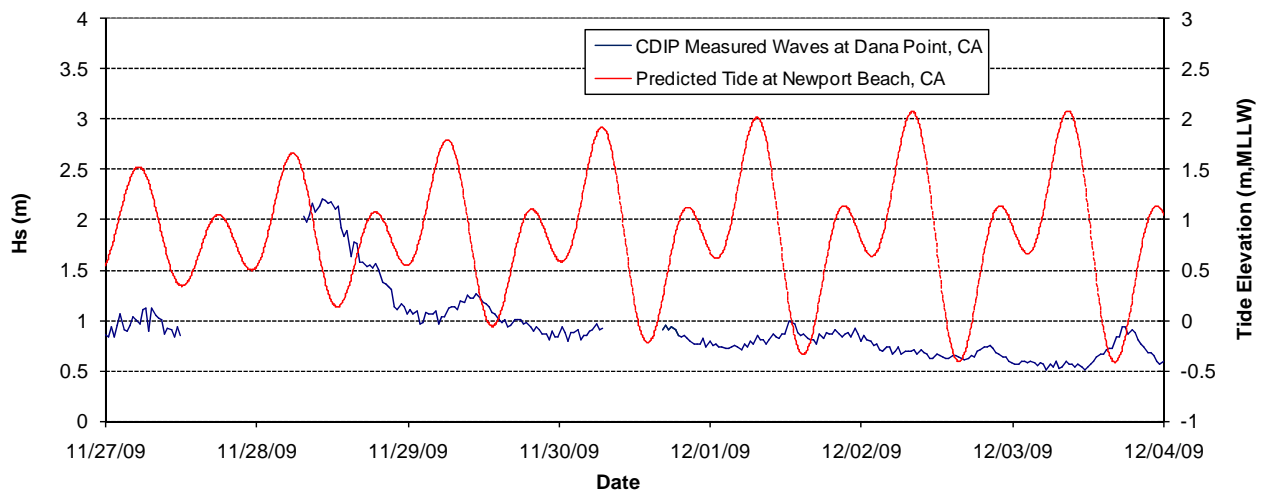
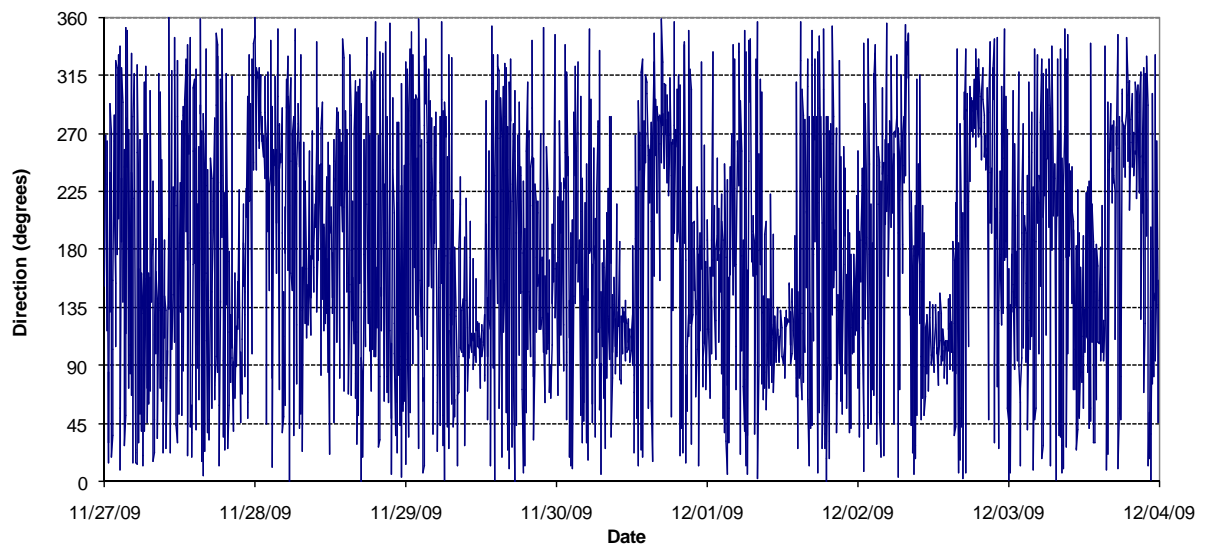
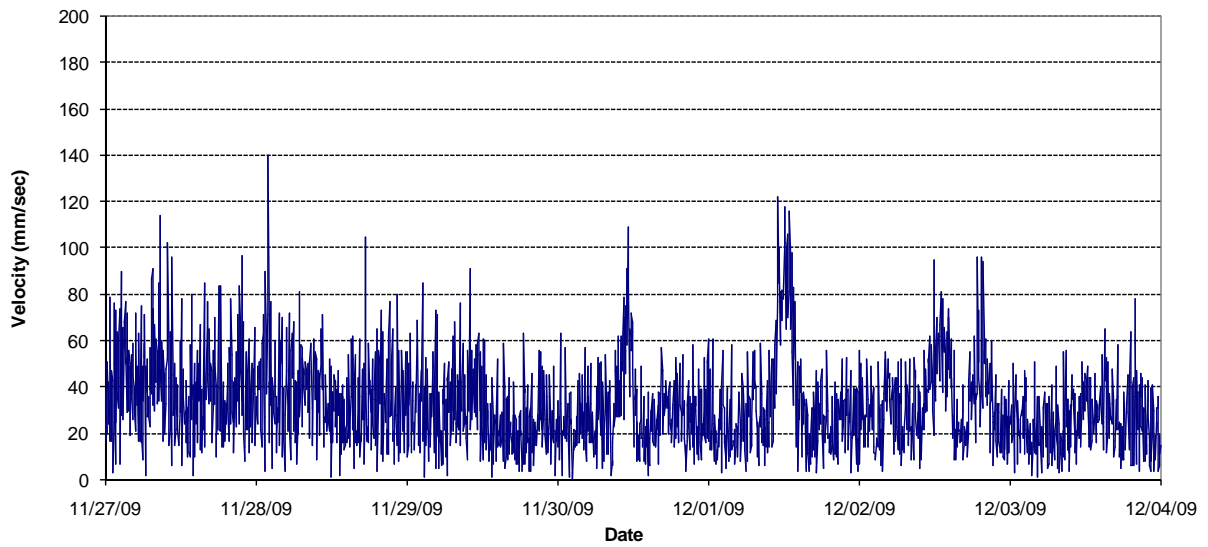
USACE-LAD, 1996. "Nearshore Hydrodynamic Factors and Wave Study of the Orange County Coast", Coast of California Storm and Tidal Wave Study South Coast Region, Orange County, Final Report No. 96-3.

USACE_LAD, 1991. "Comprehensive Condition Survey, Dana Point Harbor" Final Report, December 1991.

USACE-LAD, 1965. "Design Memorandum No. 1, General Design for Dana Point Harbor, Dana Point, California, September 1965.

Zundel, A. K. 2007. *Surface-water modeling system reference manual, Version 10.0*. Provo, UT: Brigham Young University Environmental Modeling Research Laboratory. http://www.ems-i.com/SMS/SMS_Overview/sms_overview.html.

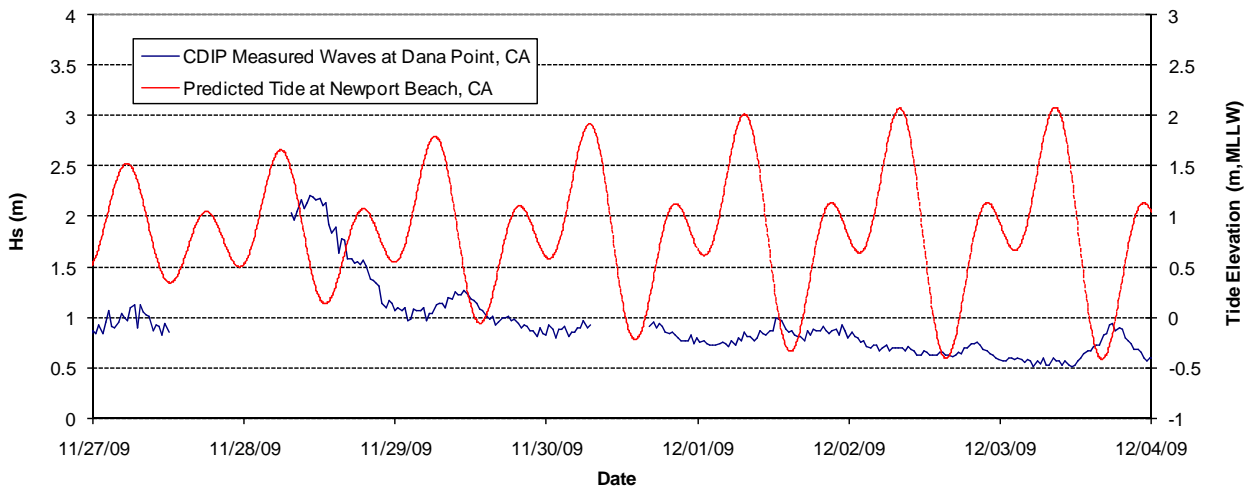
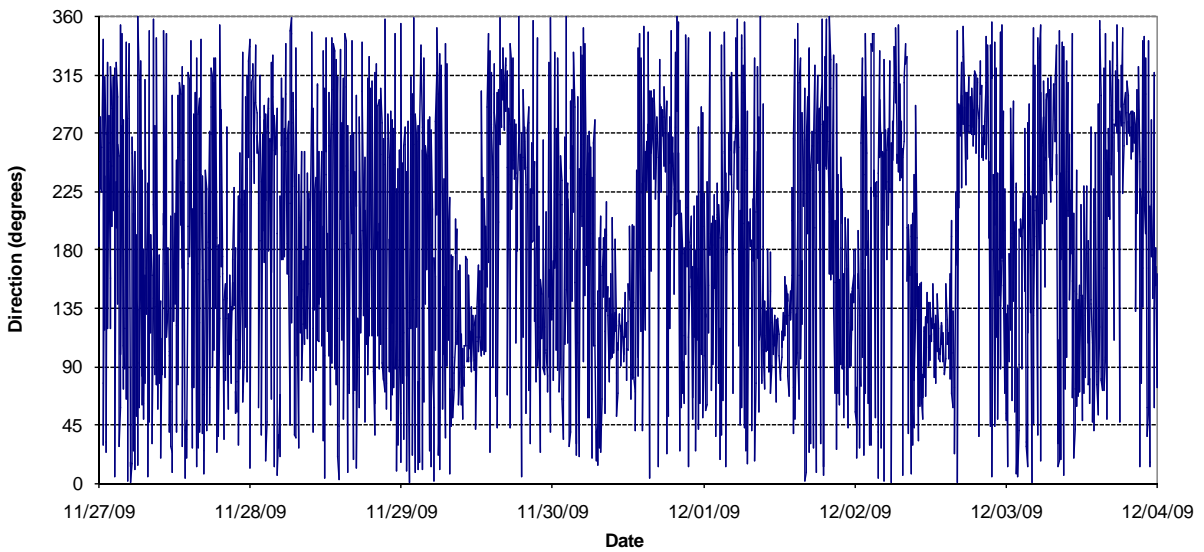
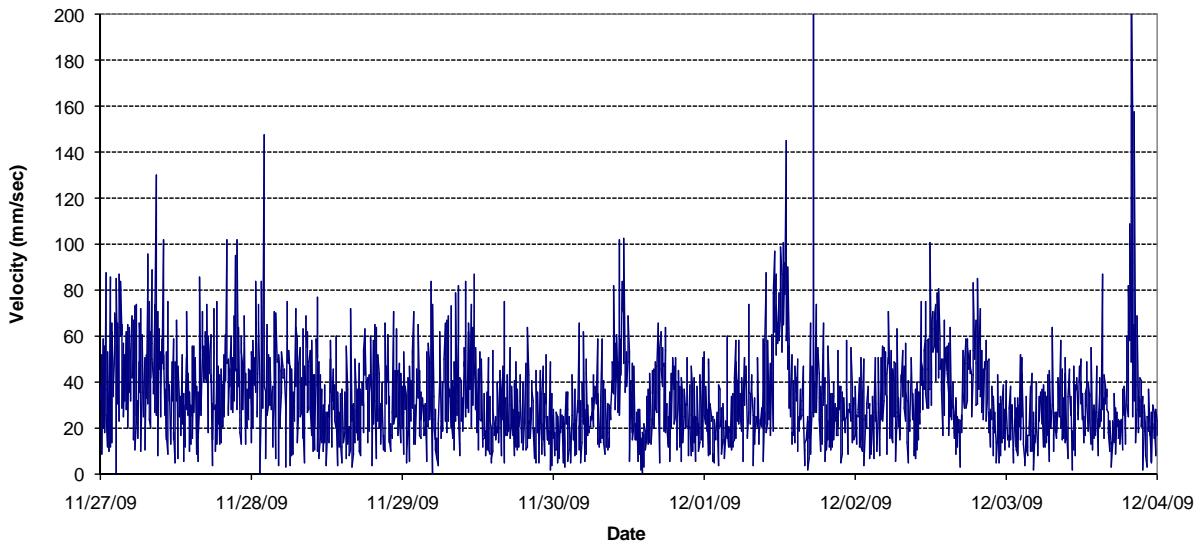
APPENDIX A
ADCP MEASUREMENTS



Week 2 – Bin 1 Current Measurements at Inside Gage



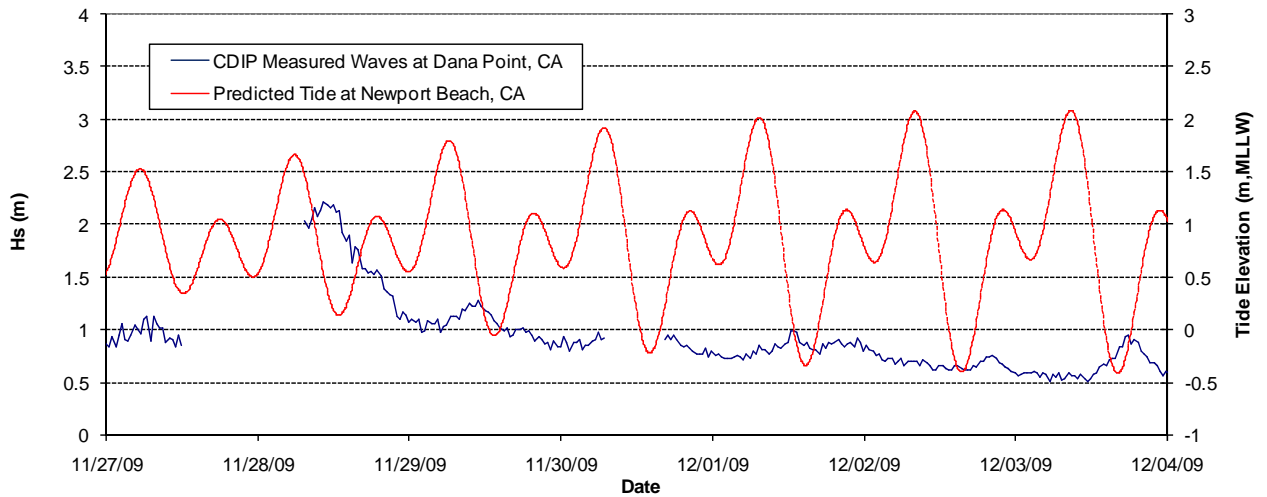
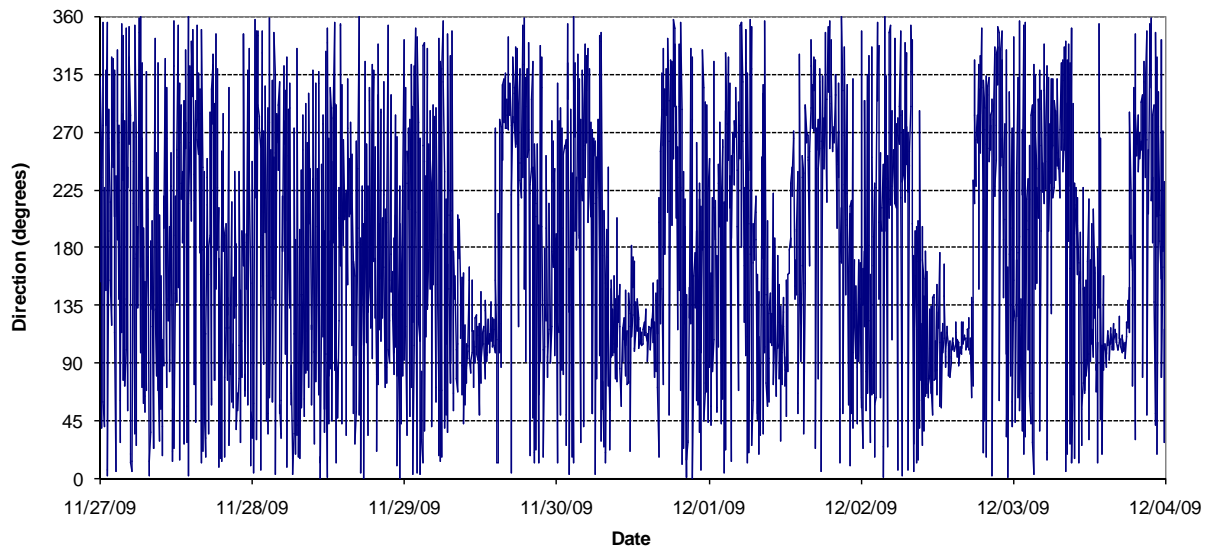
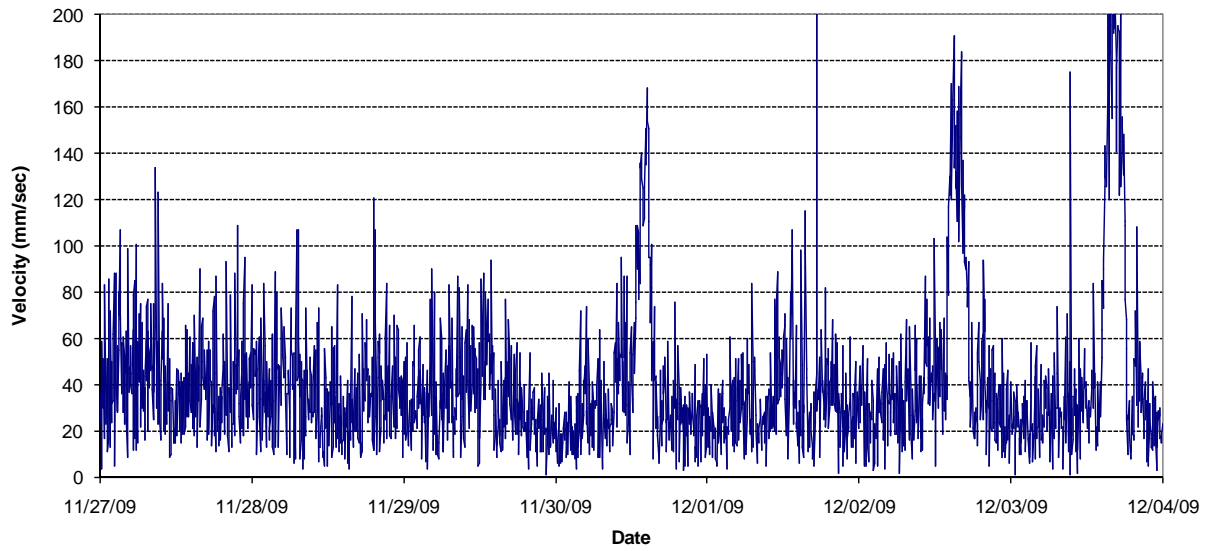
Figure A-1



Week 2 – Bin 2 Current Measurements at Inside Gage



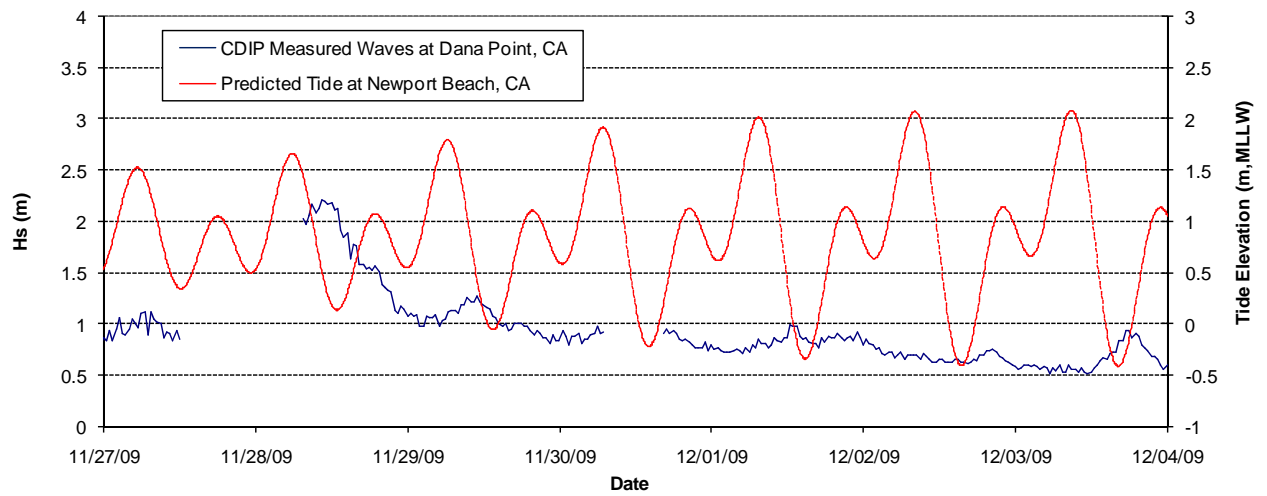
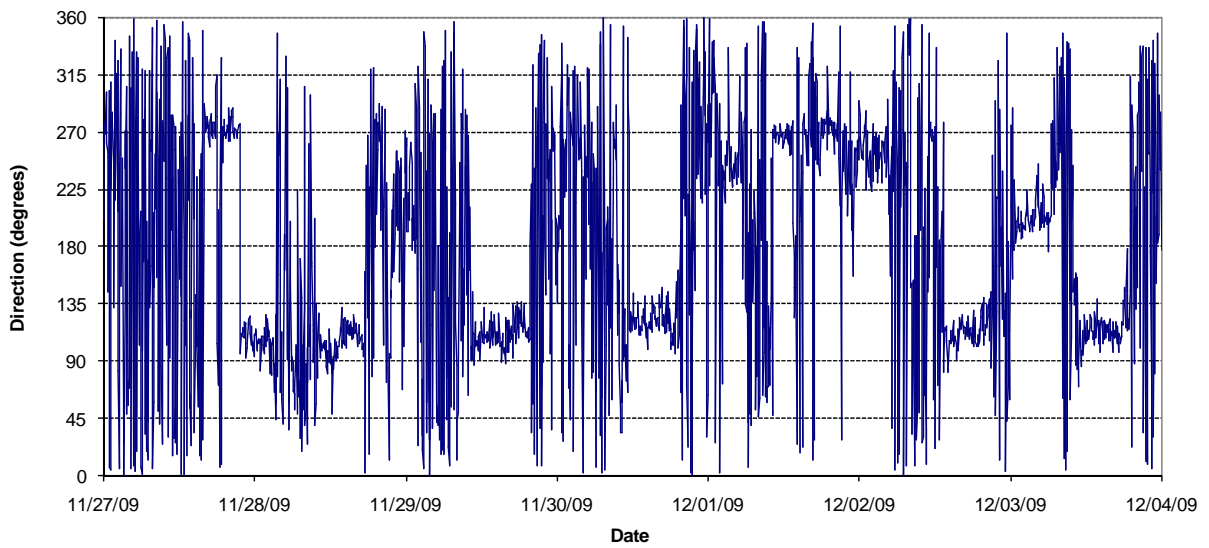
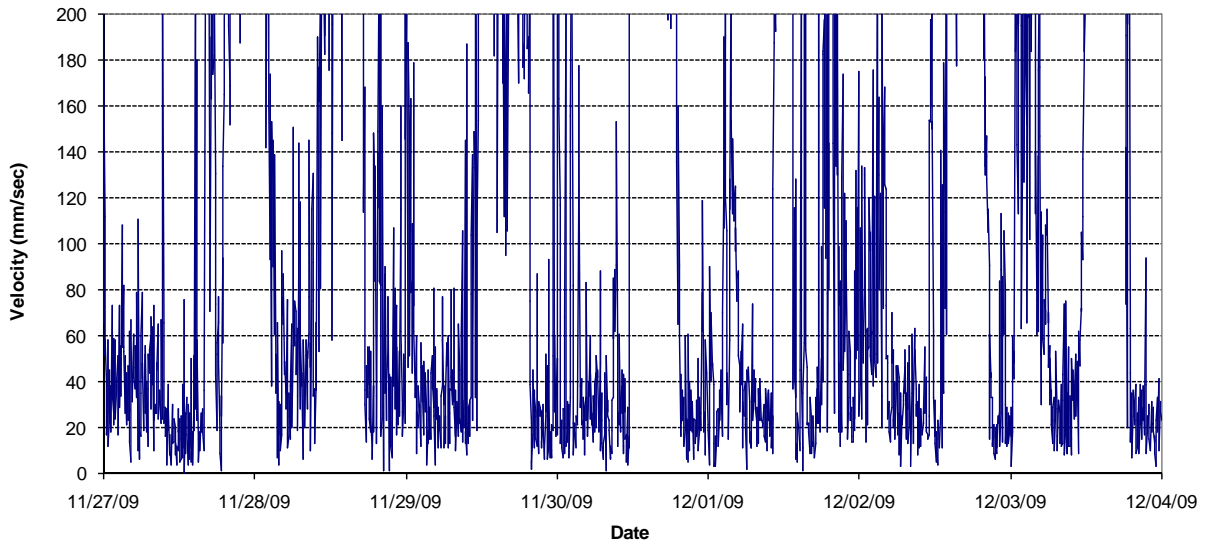
Figure A-2



Week 2 – Bin 3 Current Measurements at Inside Gage



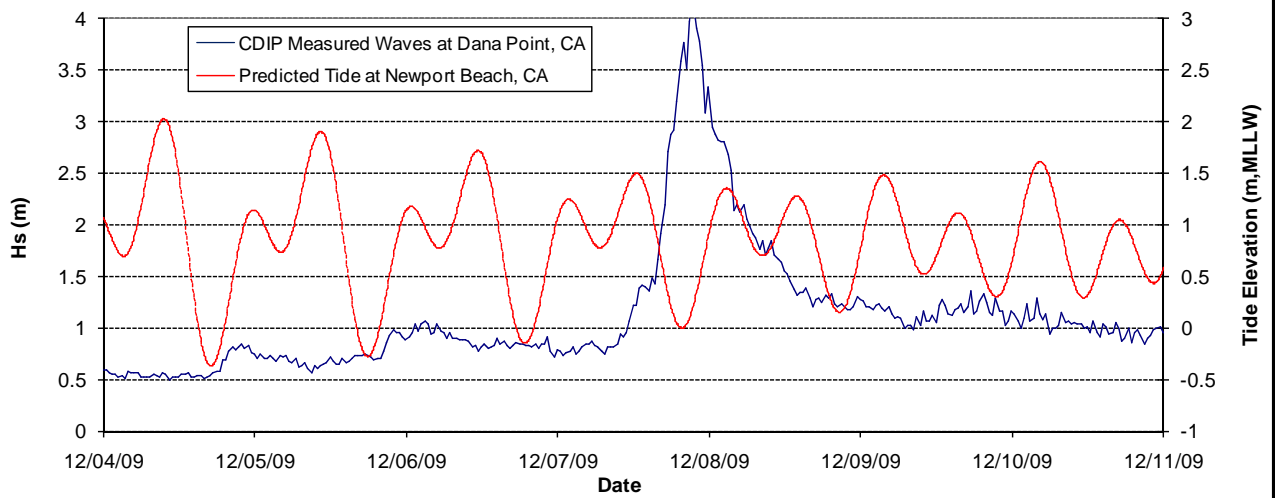
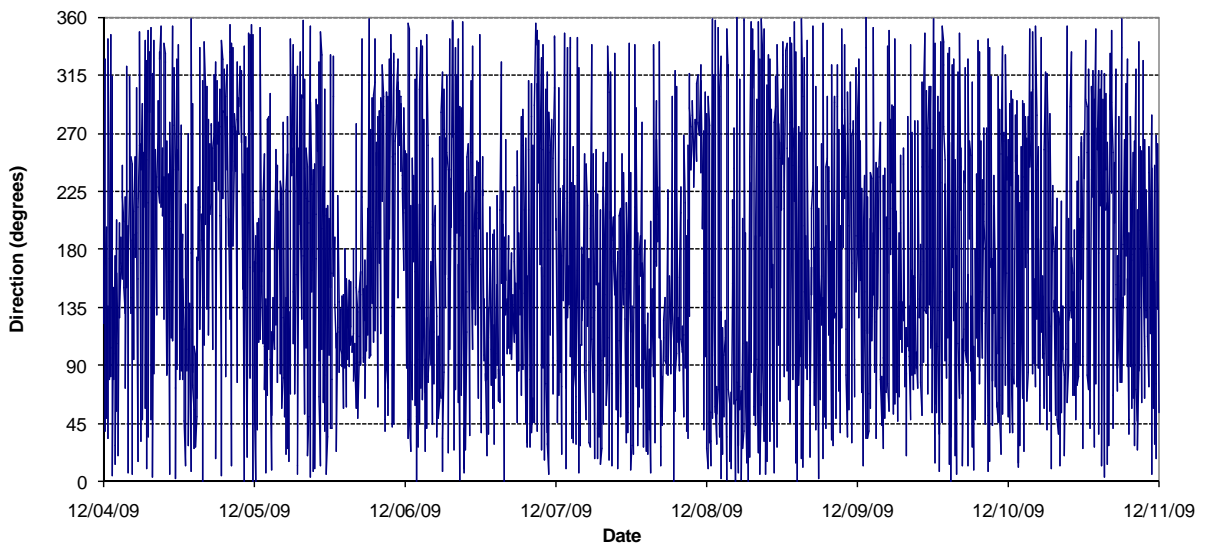
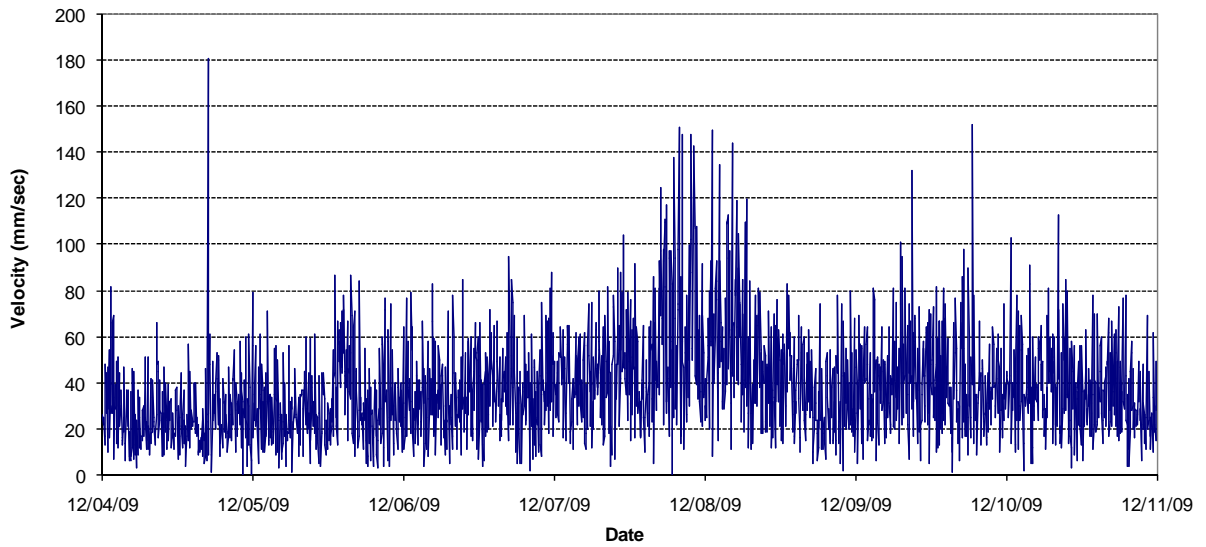
Figure A-3



Week 2 – Bin 4 Current Measurements at Inside Gage



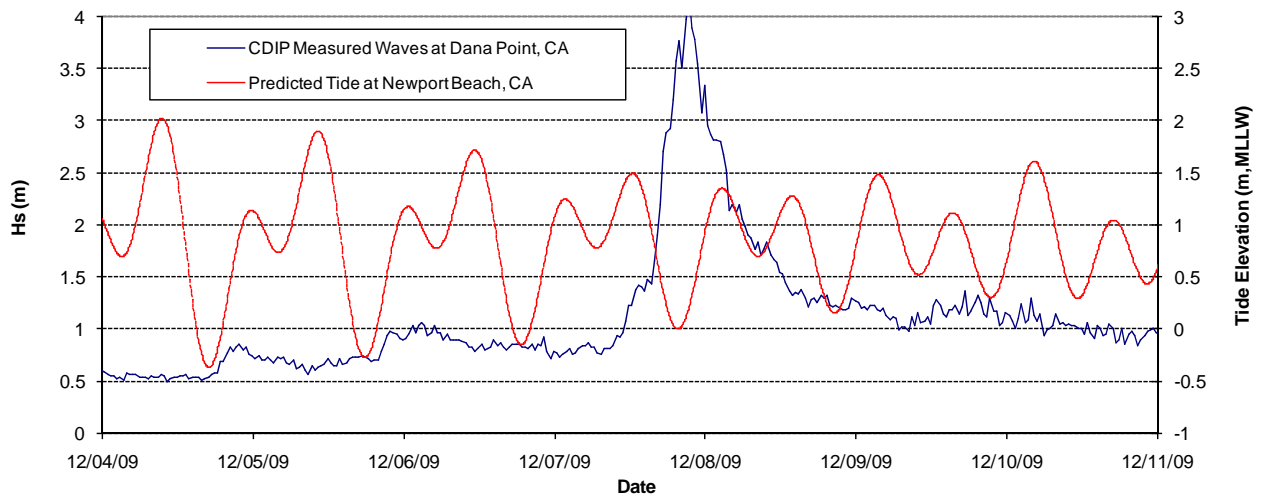
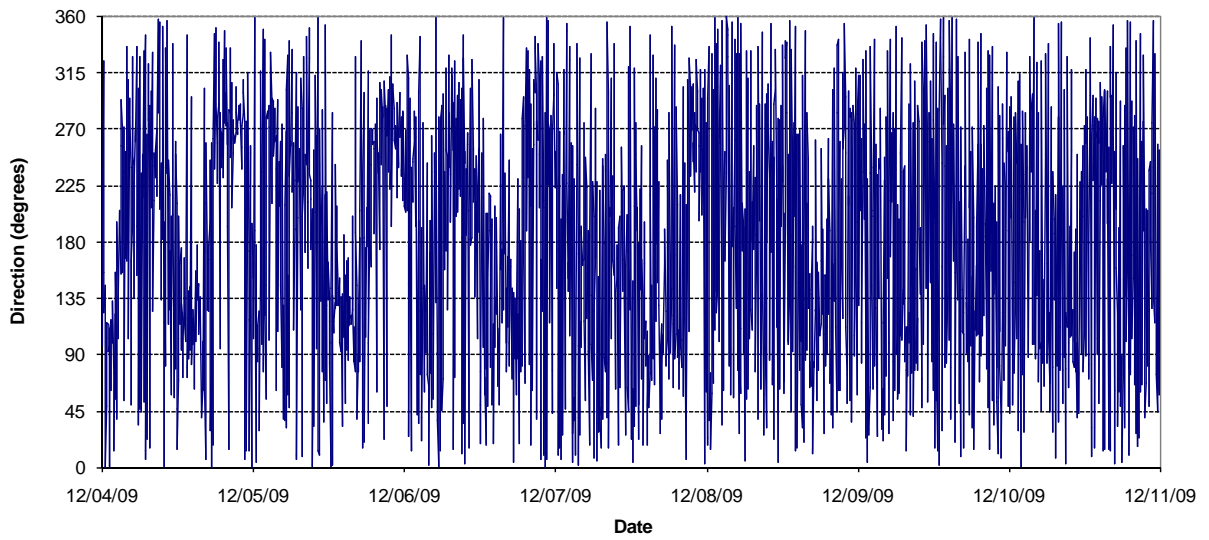
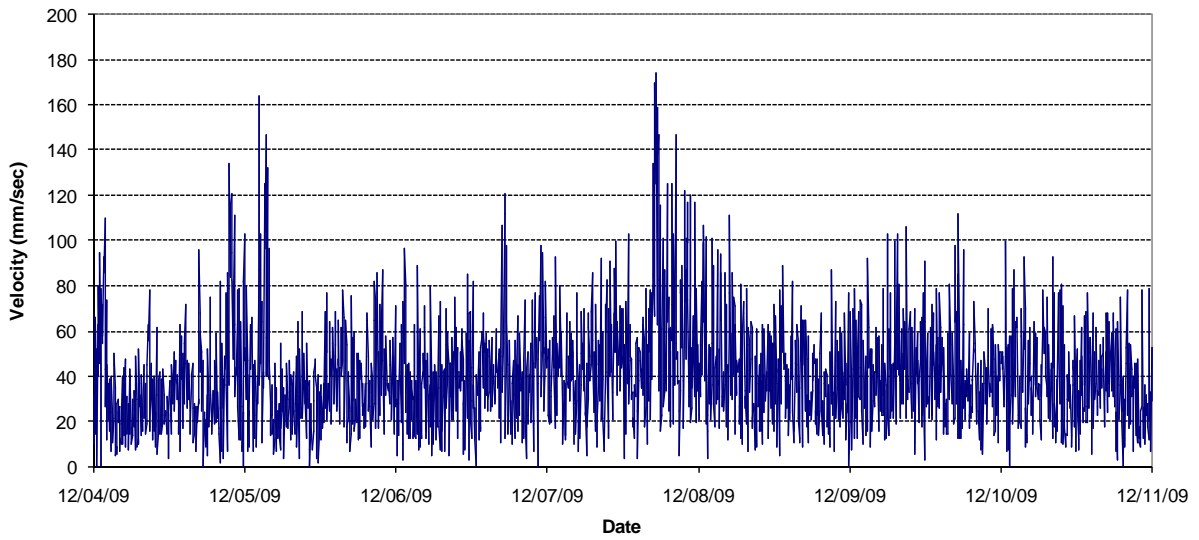
Figure A-4



Week 3 – Bin 1 Current Measurements at Inside Gage



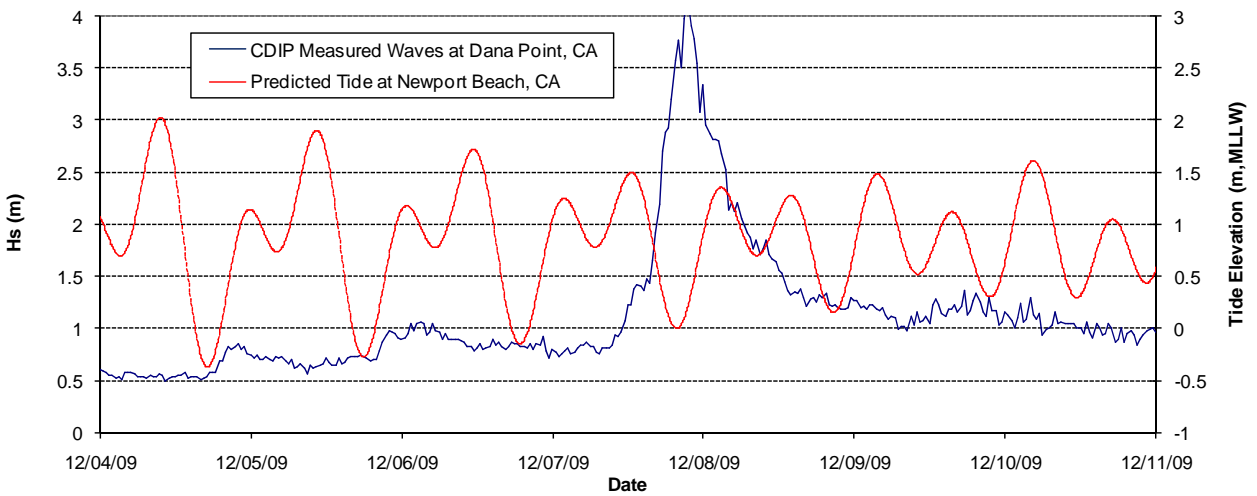
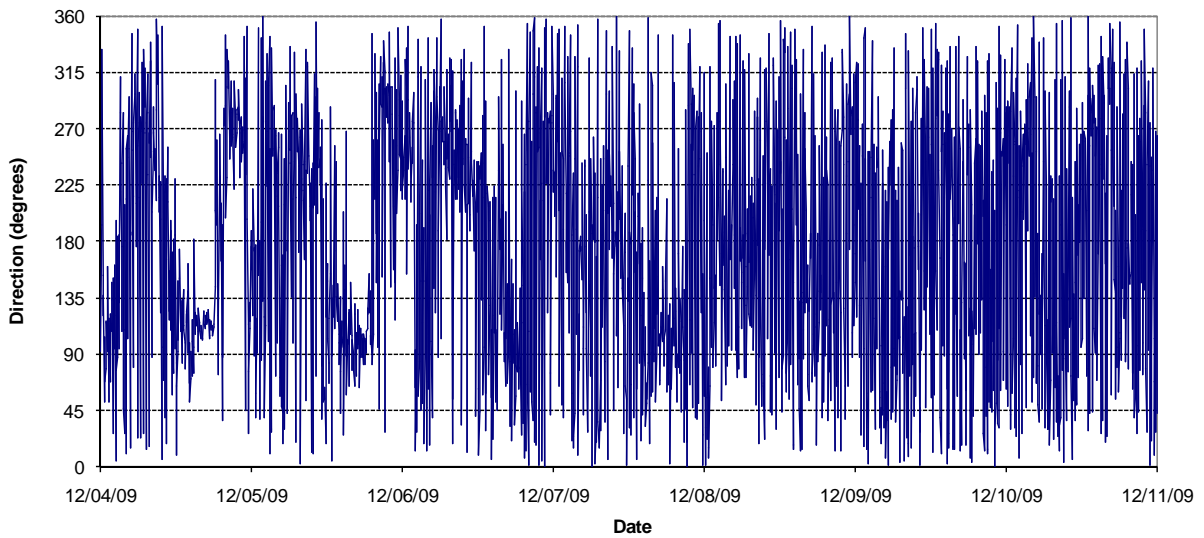
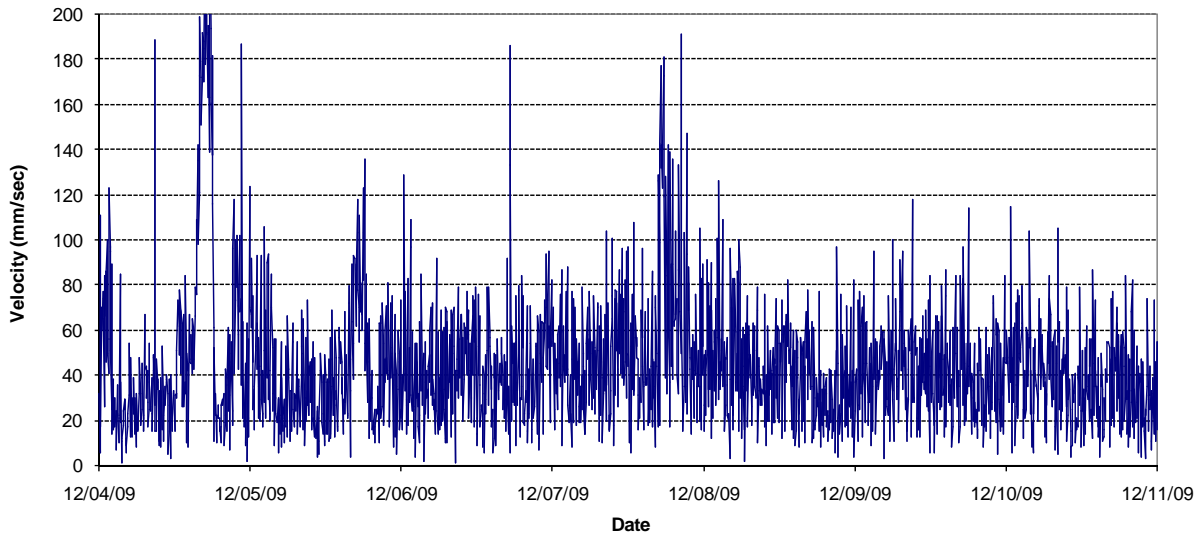
Figure A-5



Week 3 – Bin 2 Current Measurements at Inside Gage



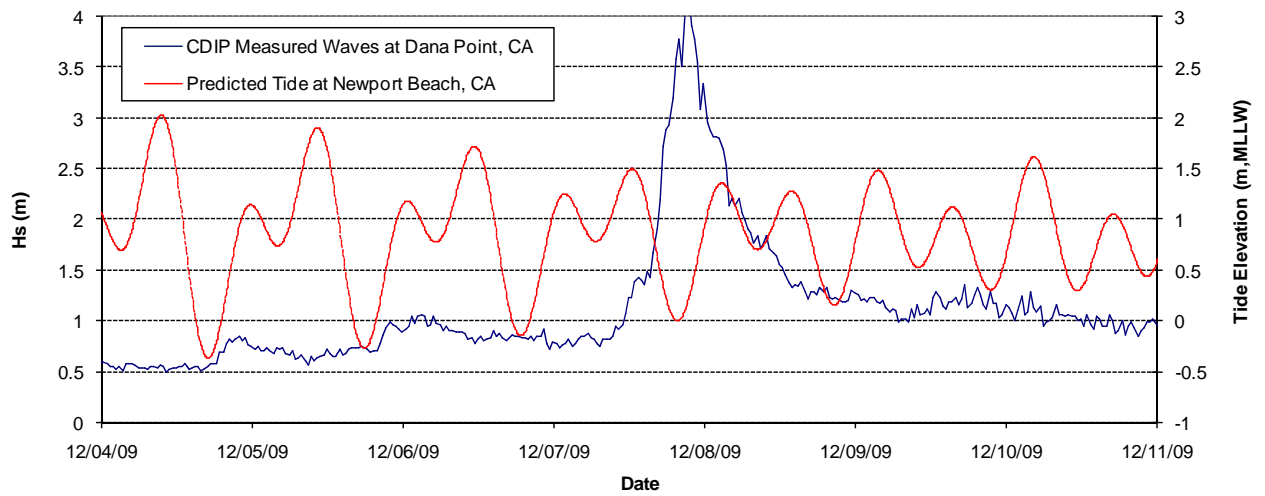
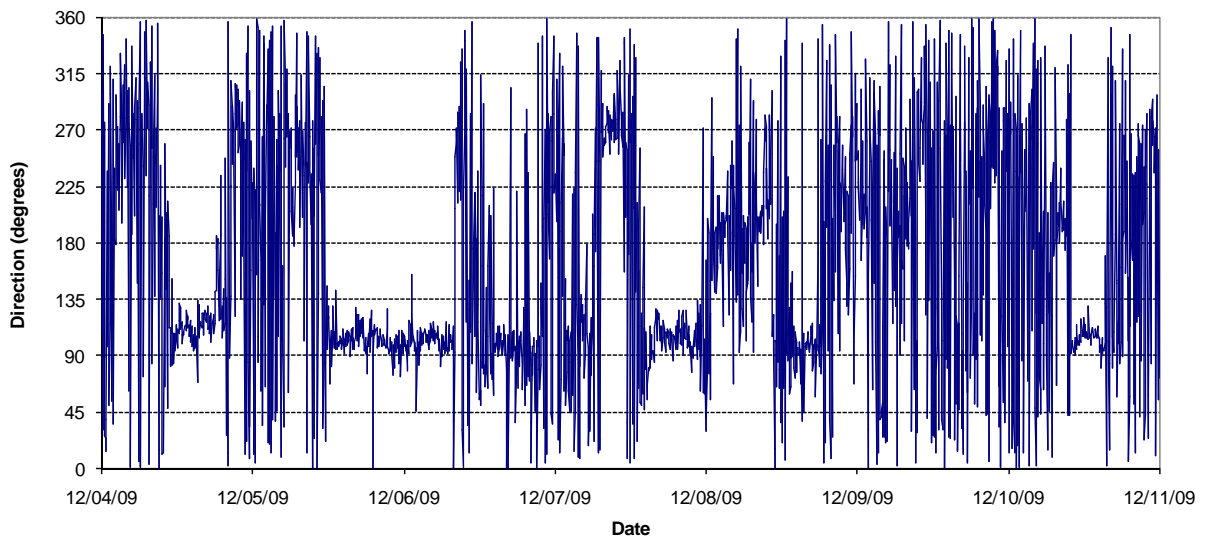
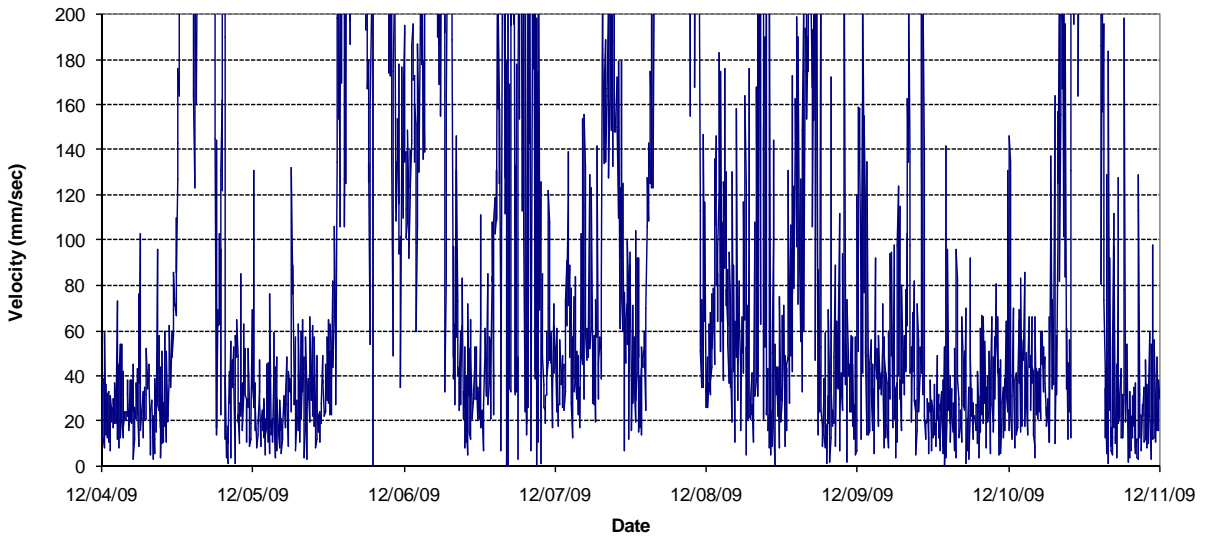
Figure A-6



Week 3 – Bin 3 Current Measurements at Inside Gage



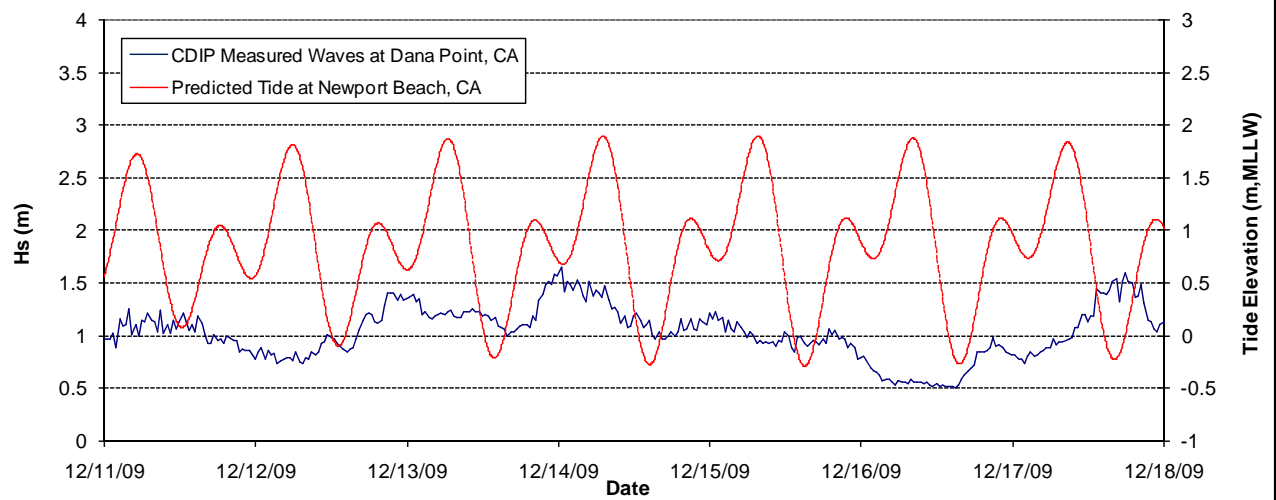
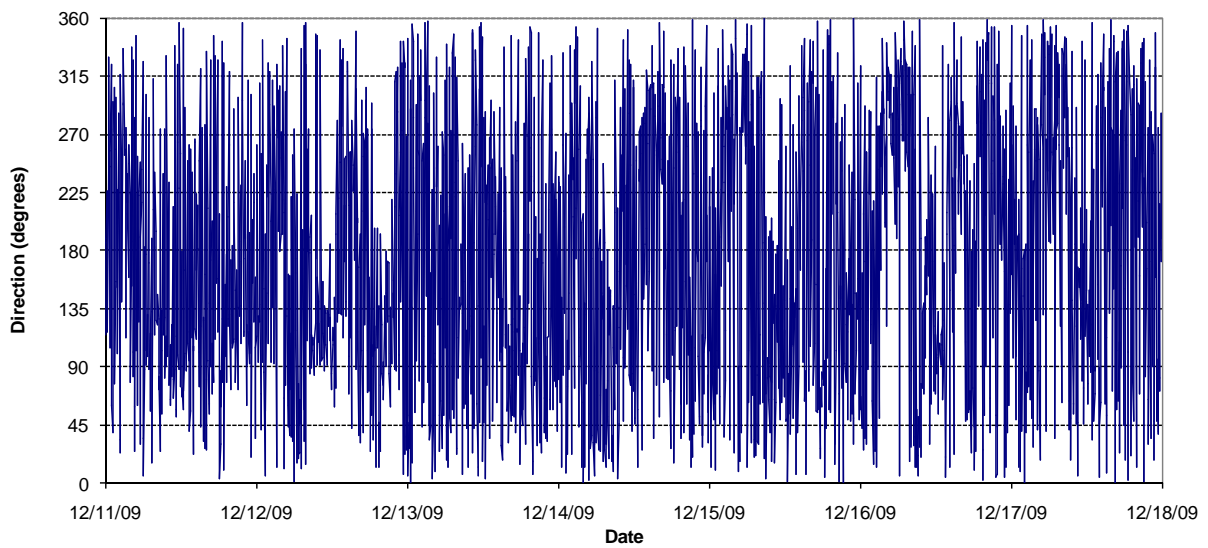
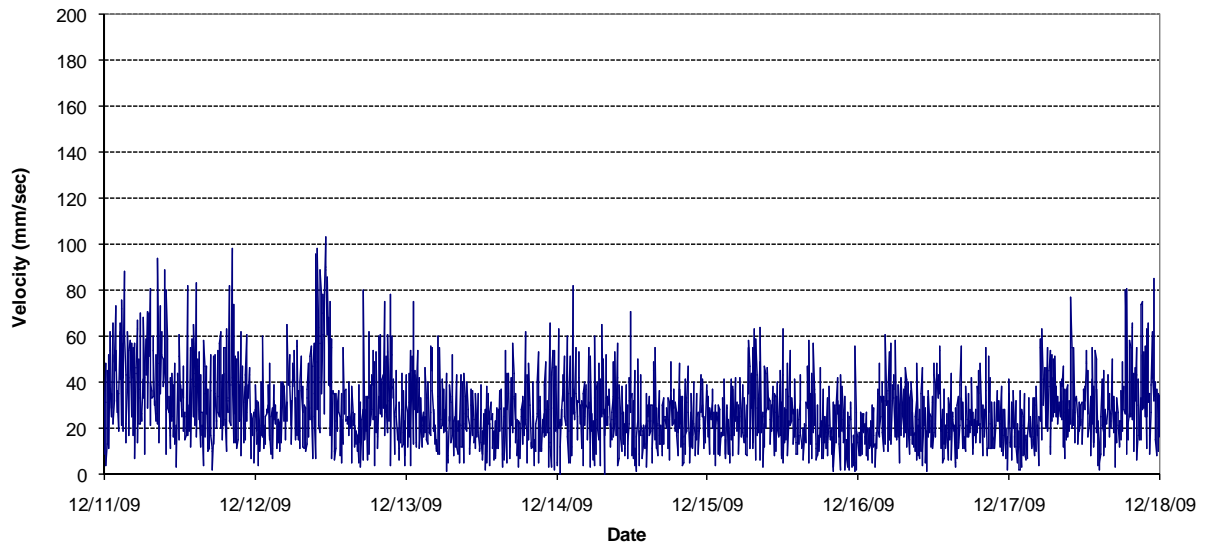
Figure A-7



Week 3 – Bin 4 Current Measurements at Inside Gage



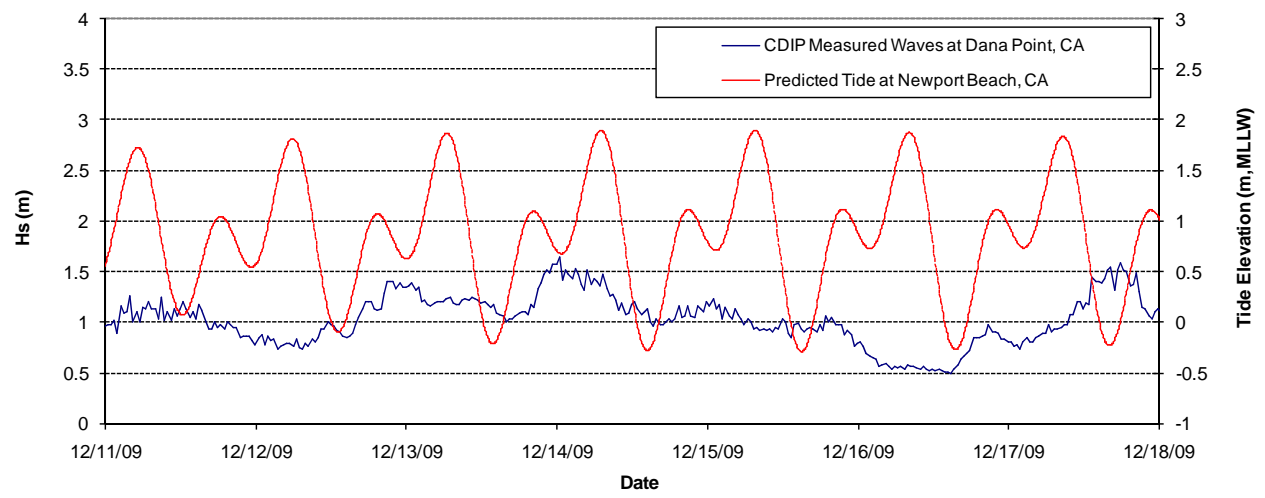
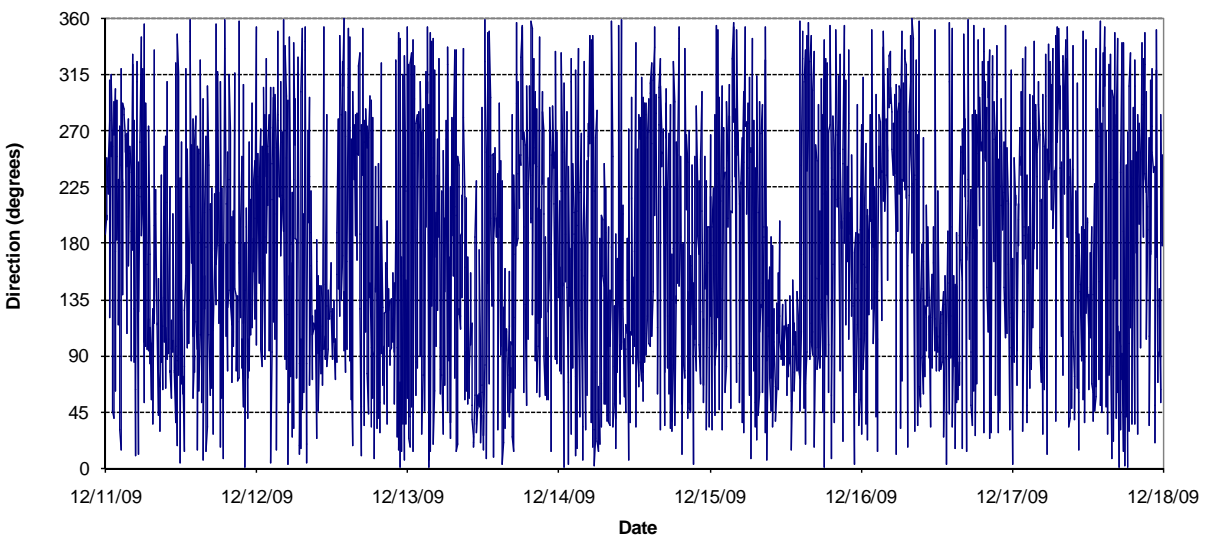
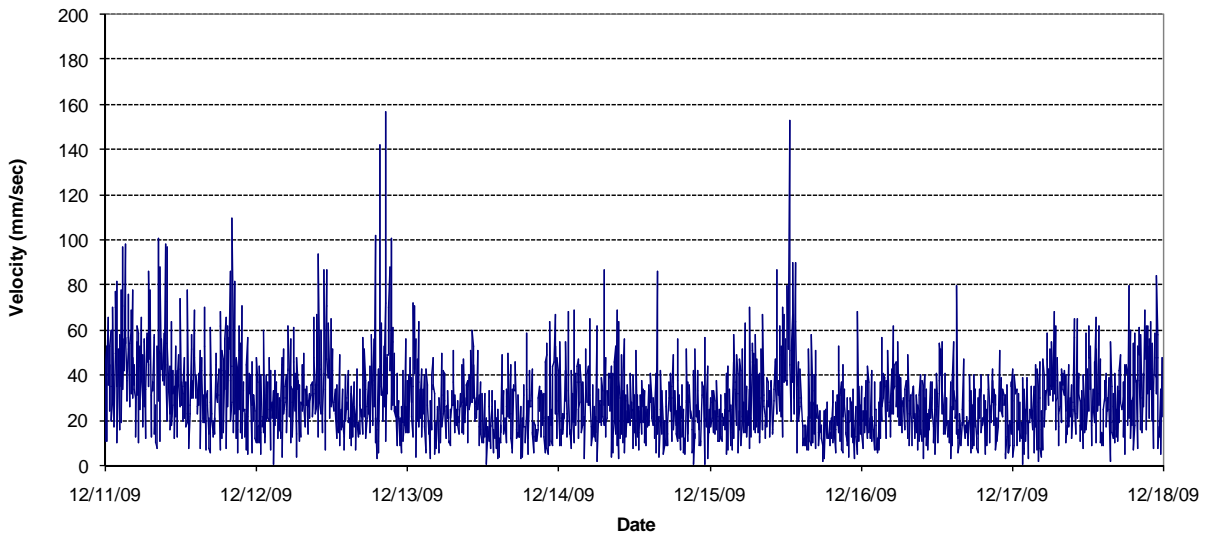
Figure A-8



Week 4 – Bin 1 Current Measurements at Inside Gage



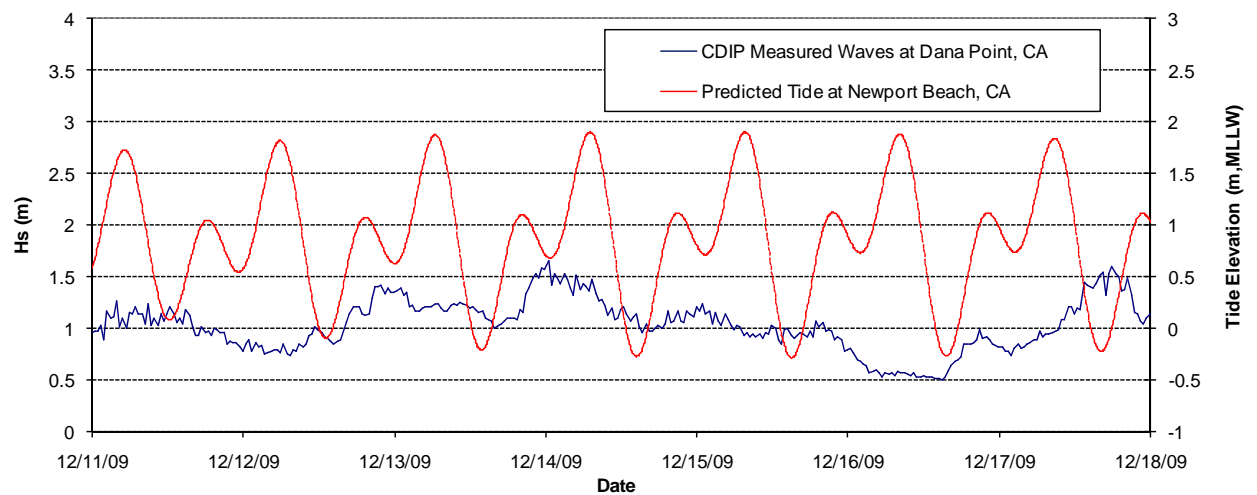
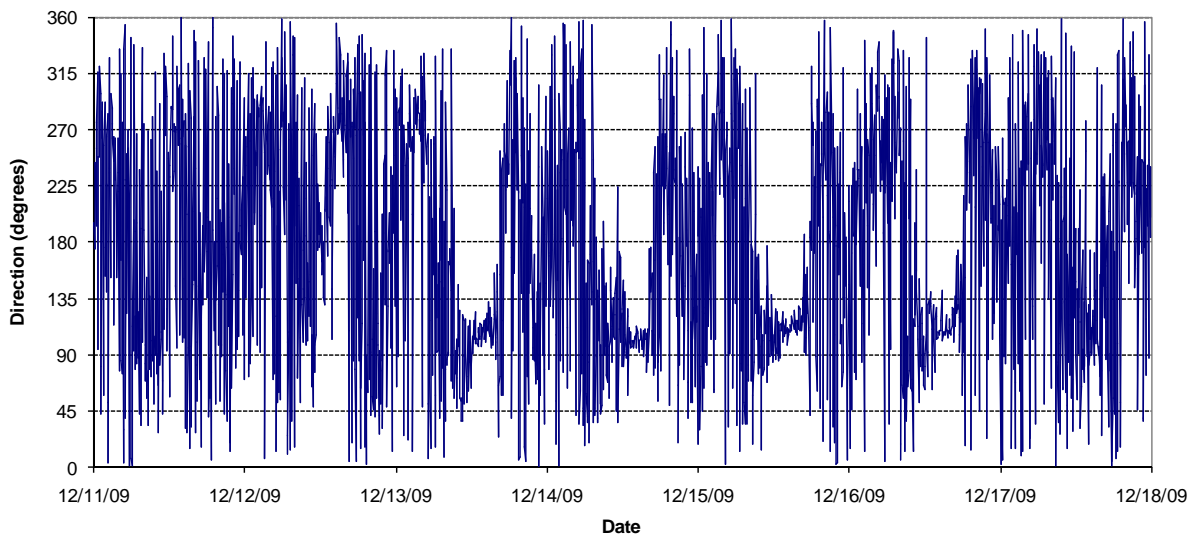
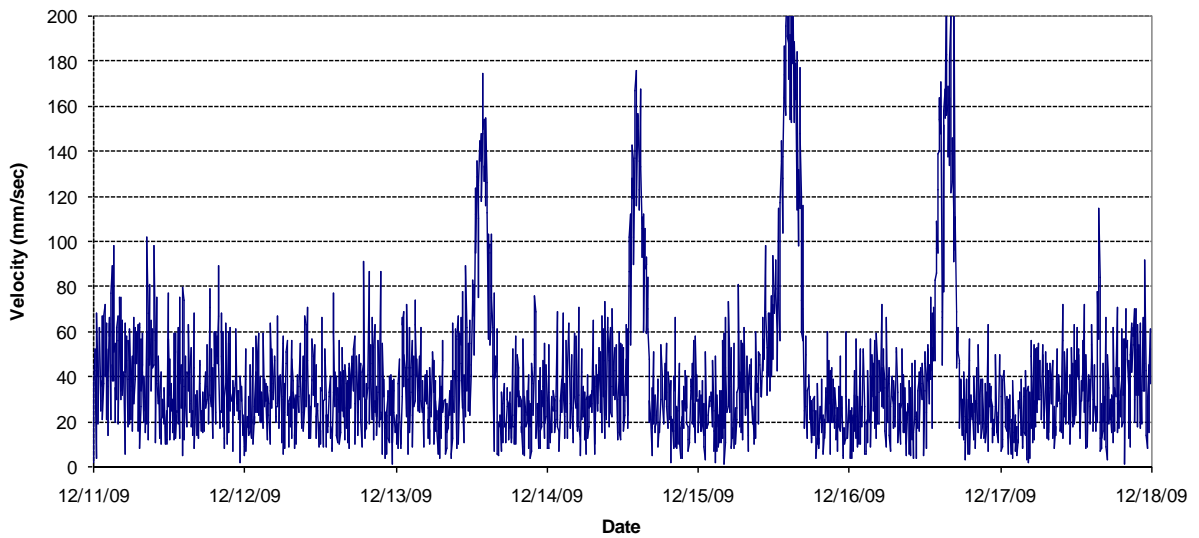
Figure A-9



Week 4 – Bin 2 Current Measurements at Inside Gage



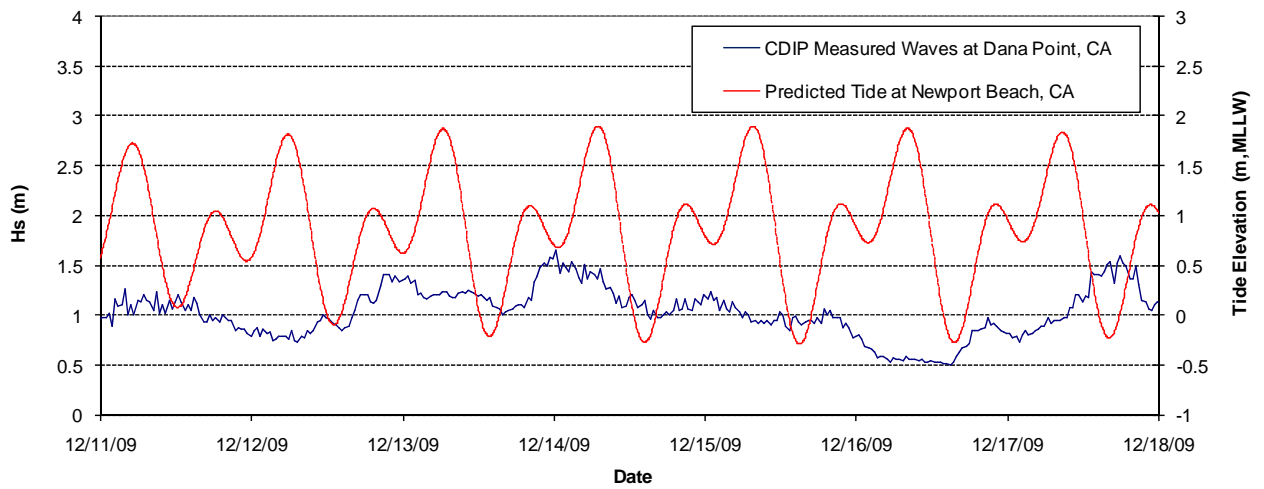
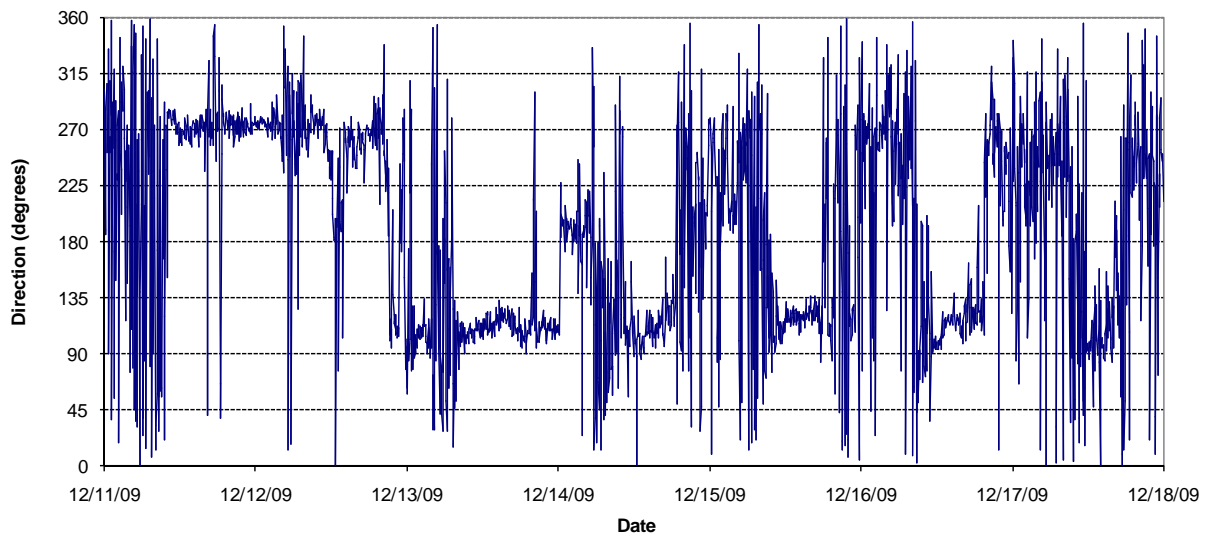
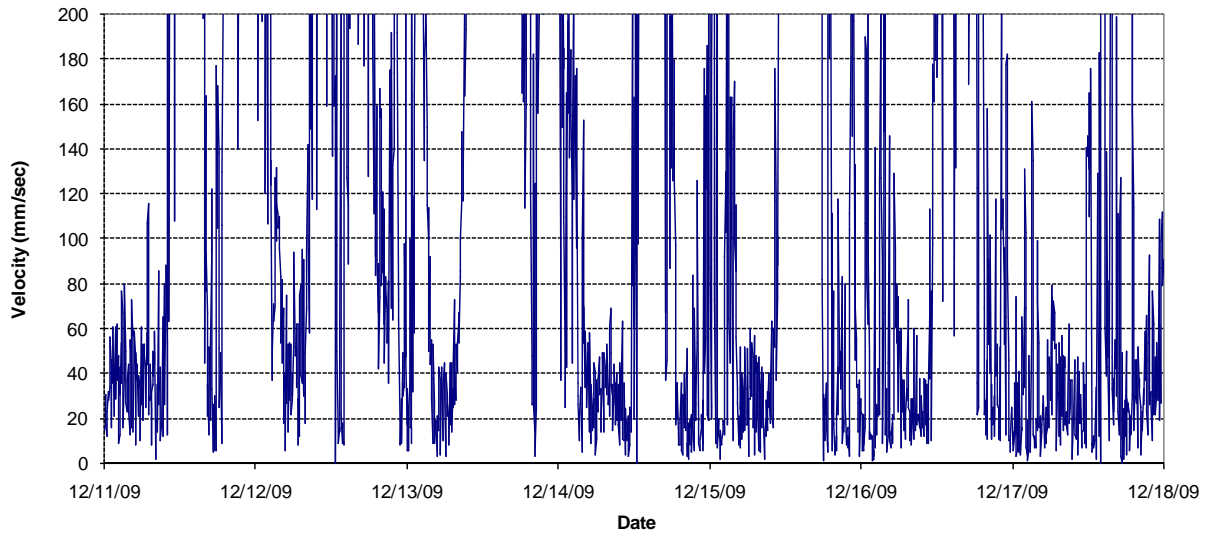
Figure A-10



Week 4 – Bin 3 Current Measurements at Inside Gage



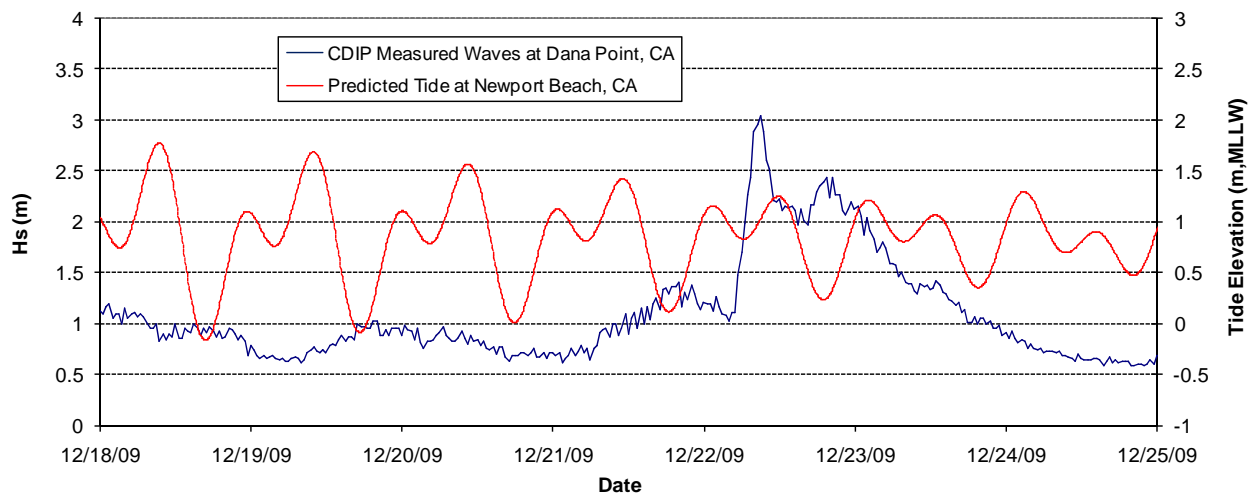
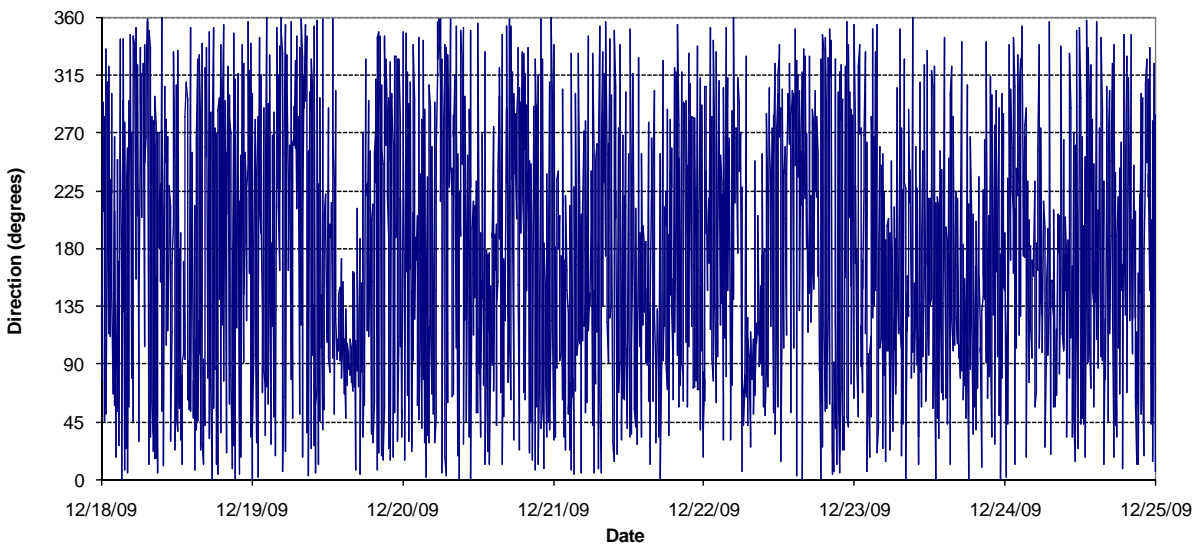
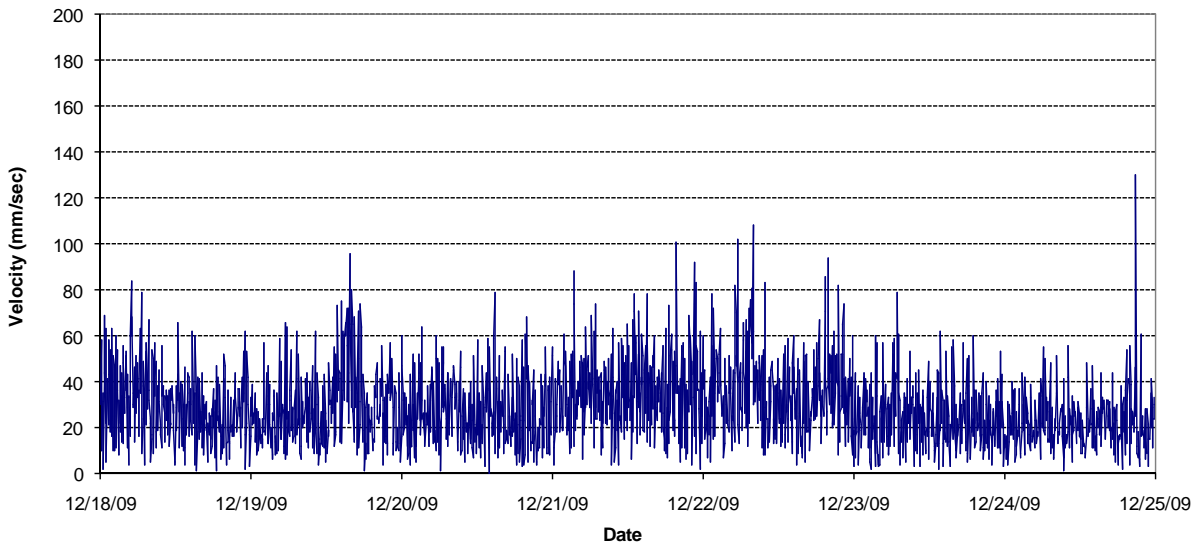
Figure A-11



Week 4 – Bin 4 Current Measurements at Inside Gage



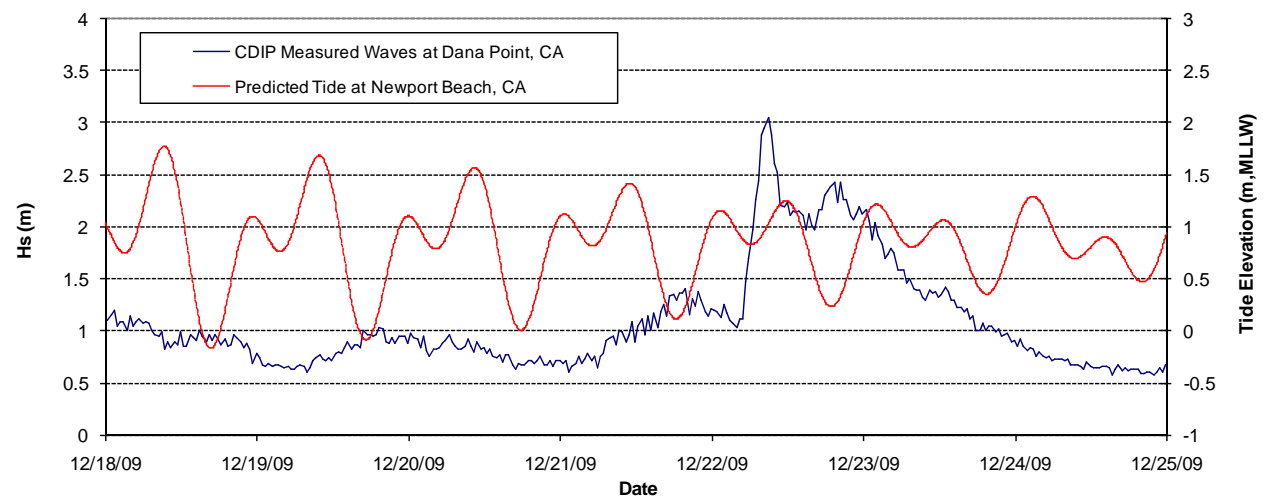
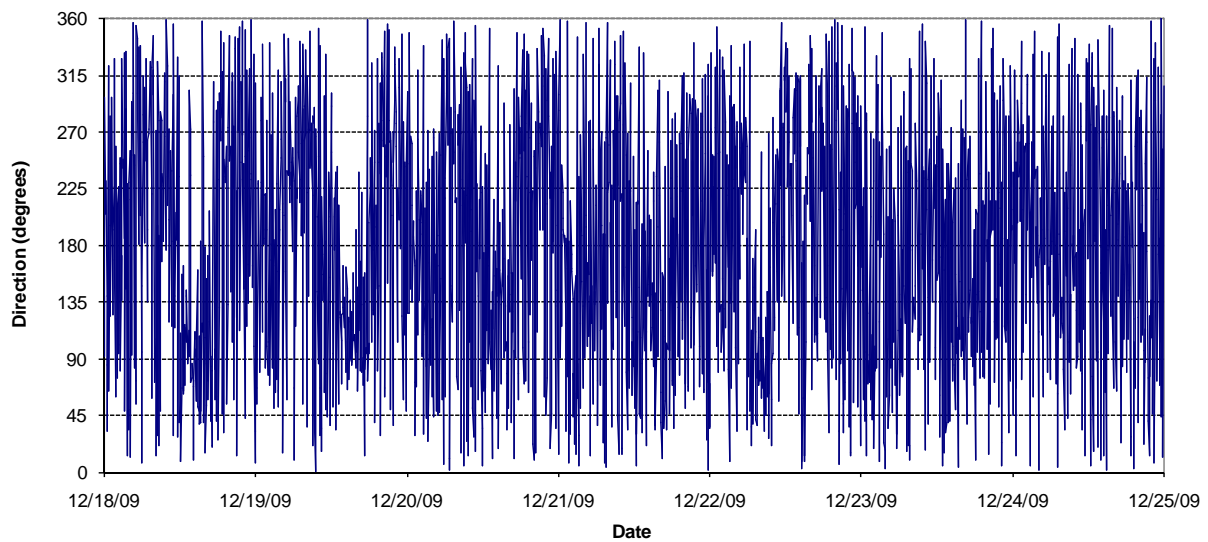
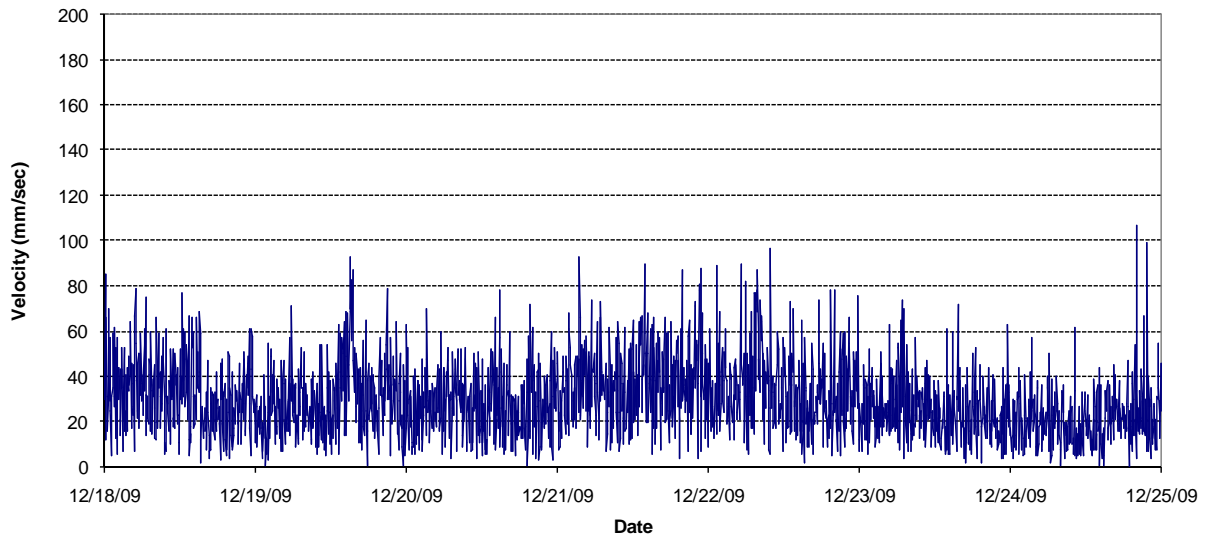
Figure A-12



Week 5 – Bin 1 Current Measurements at Inside Gage



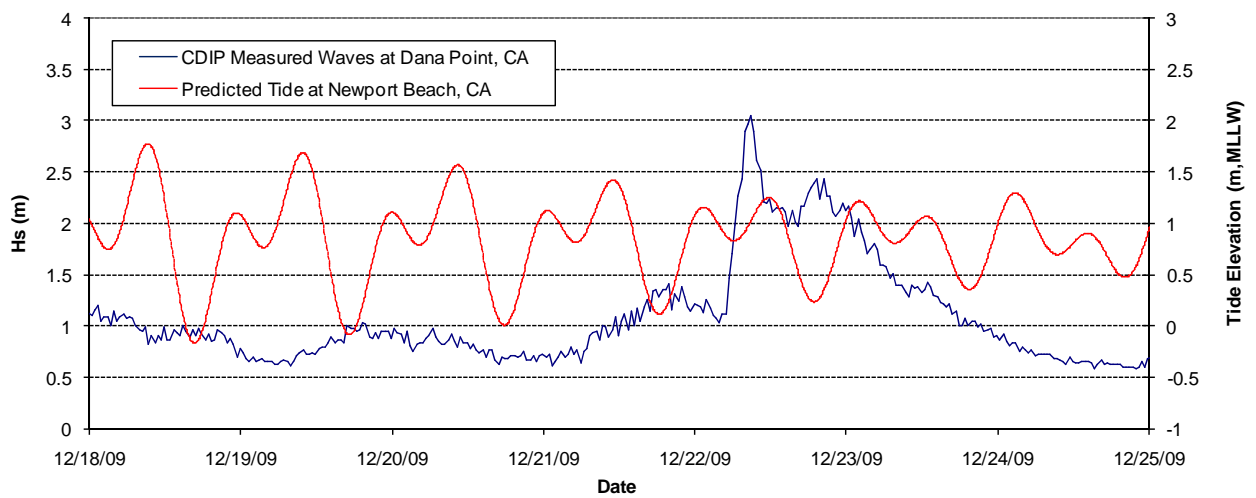
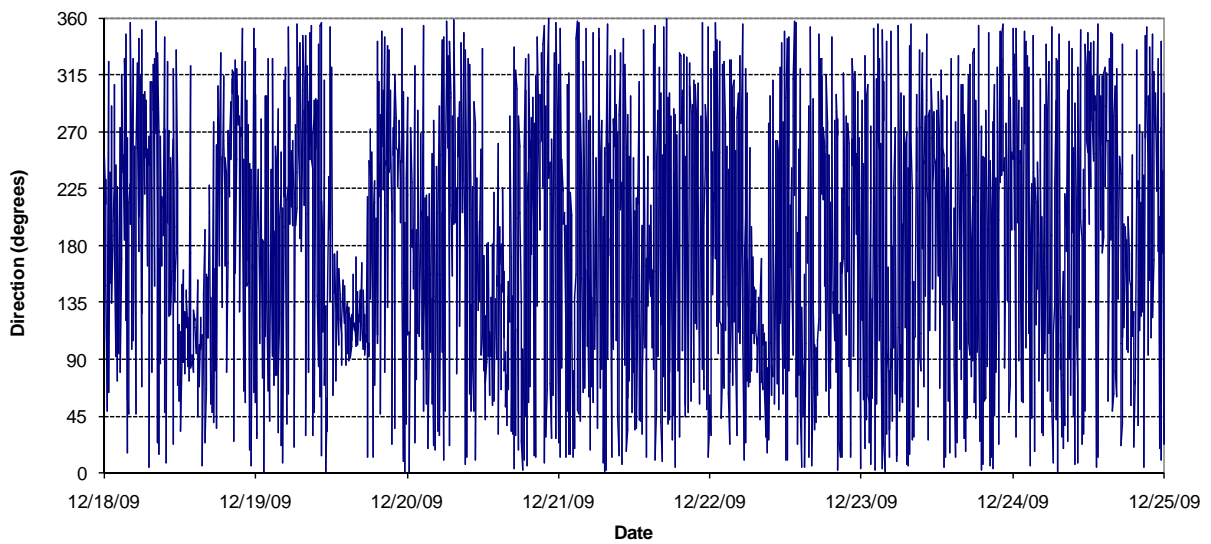
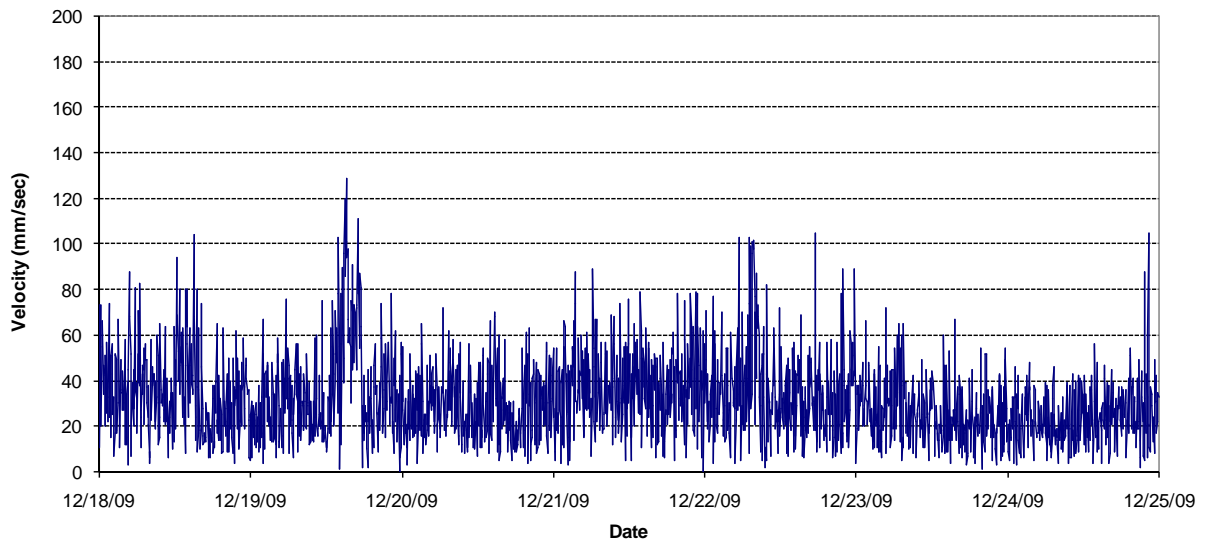
Figure A-13



Week 5 – Bin 2 Current Measurements at Inside Gage



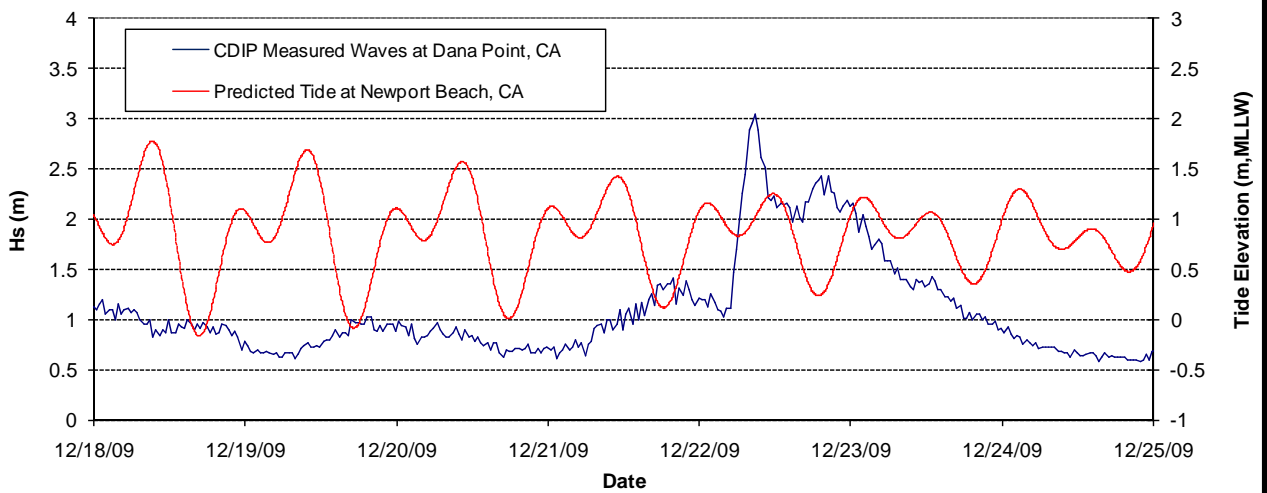
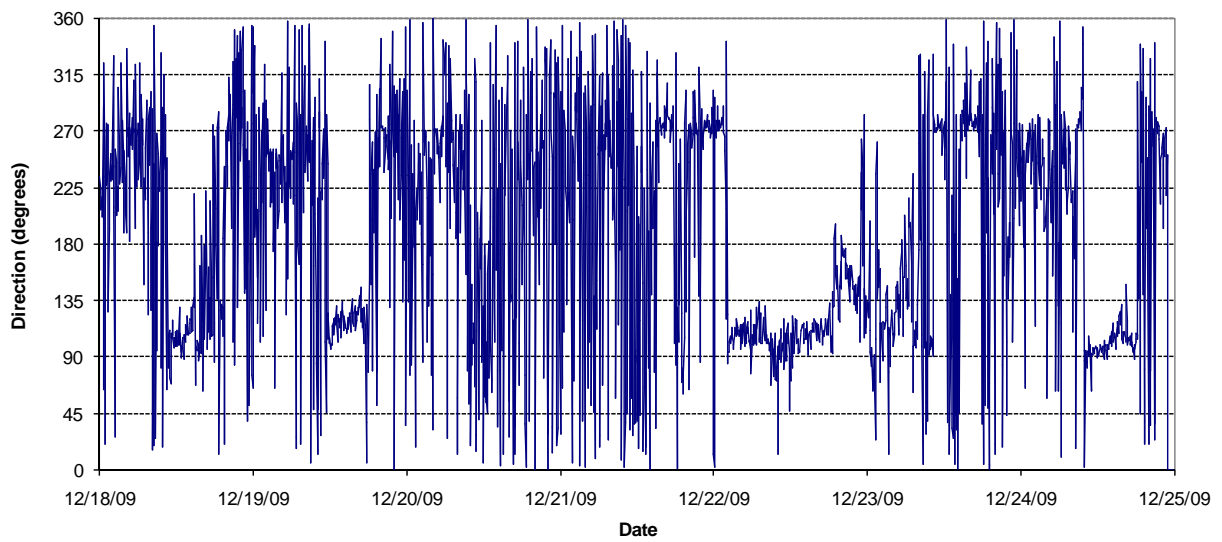
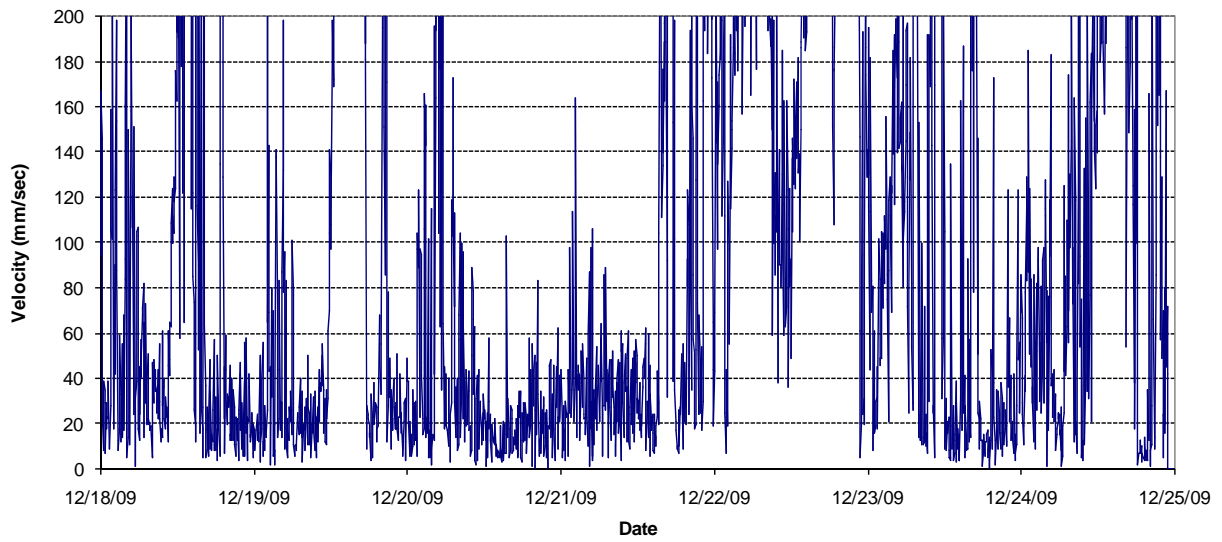
Figure A-14



Week 5 – Bin 3 Current Measurements at Inside Gage



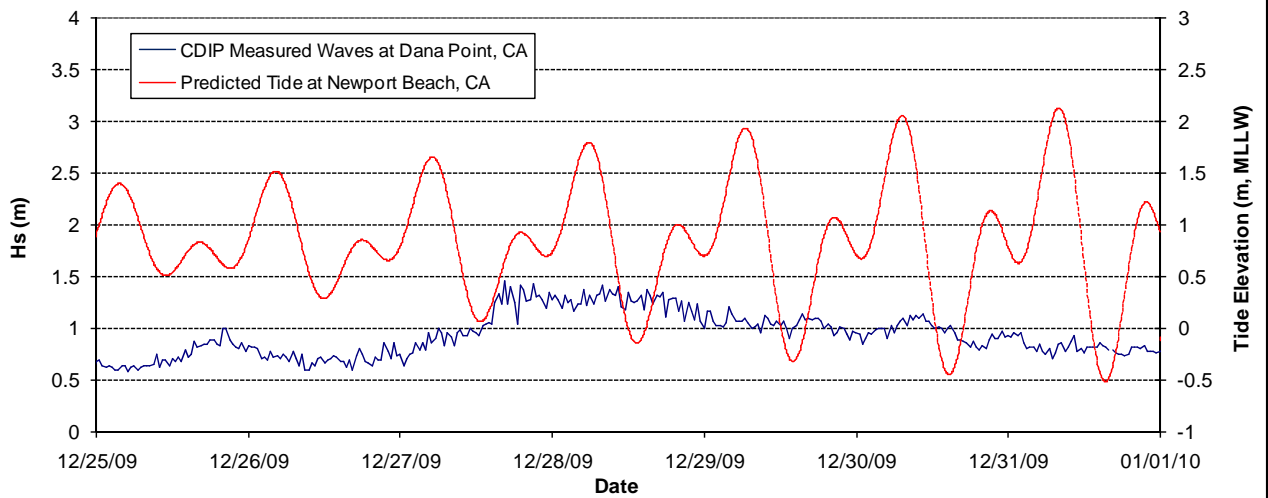
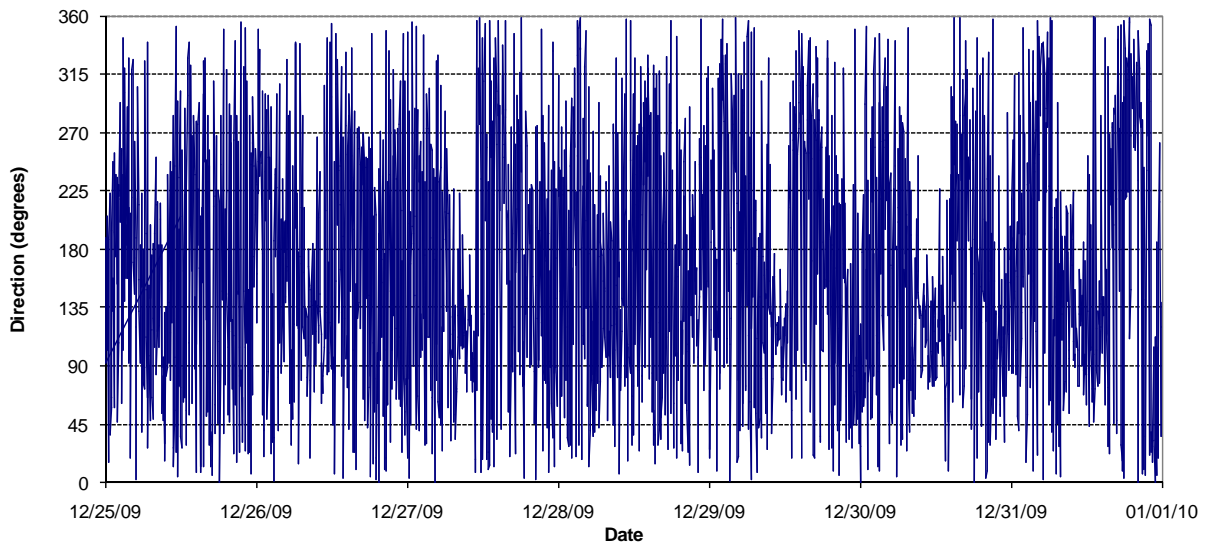
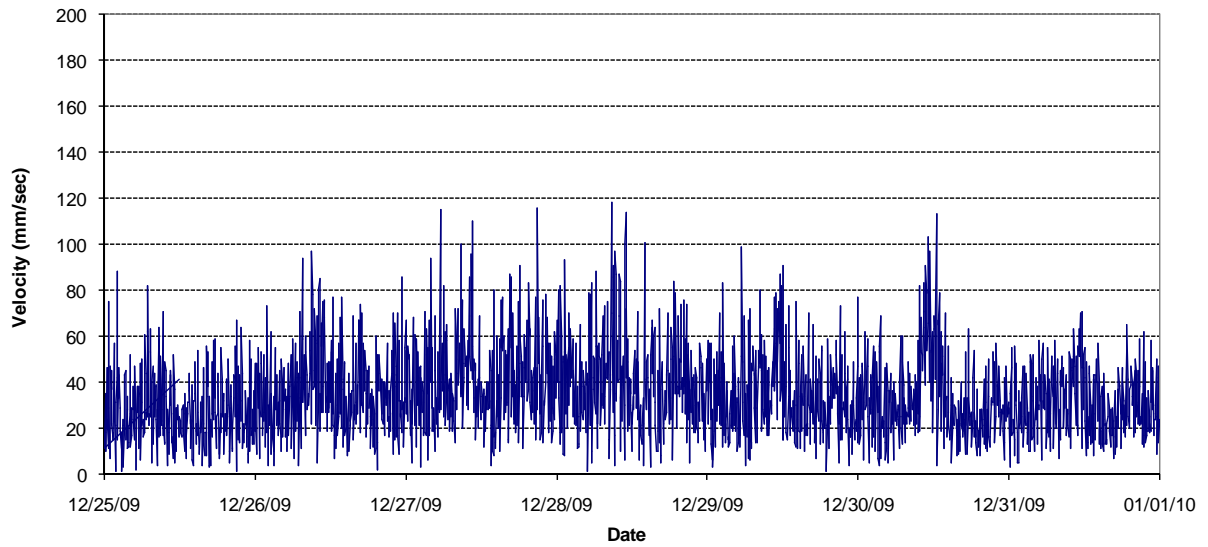
Figure A-15



Week 5 – Bin 4 Current Measurements at Inside Gage



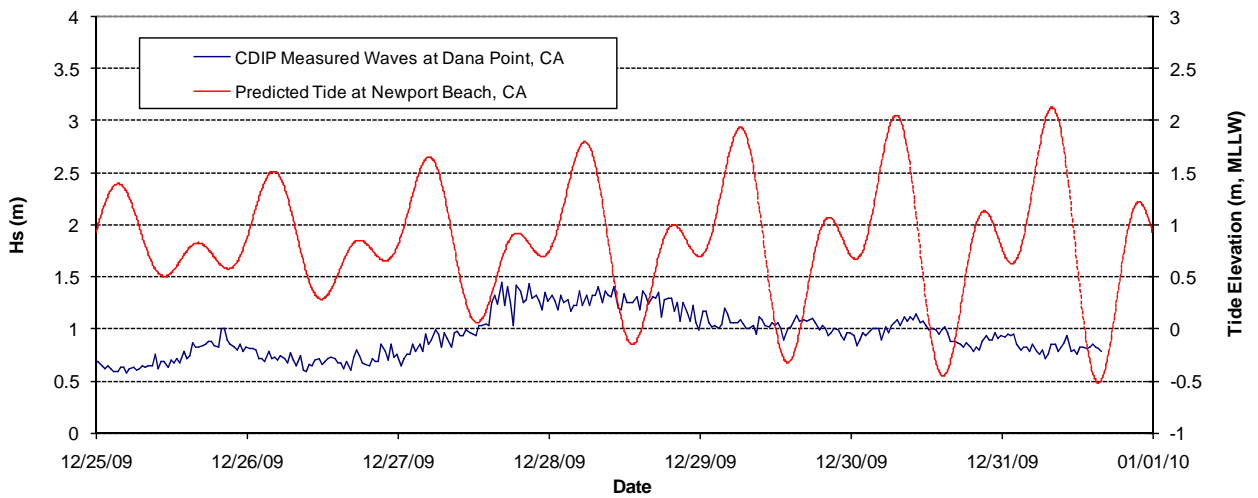
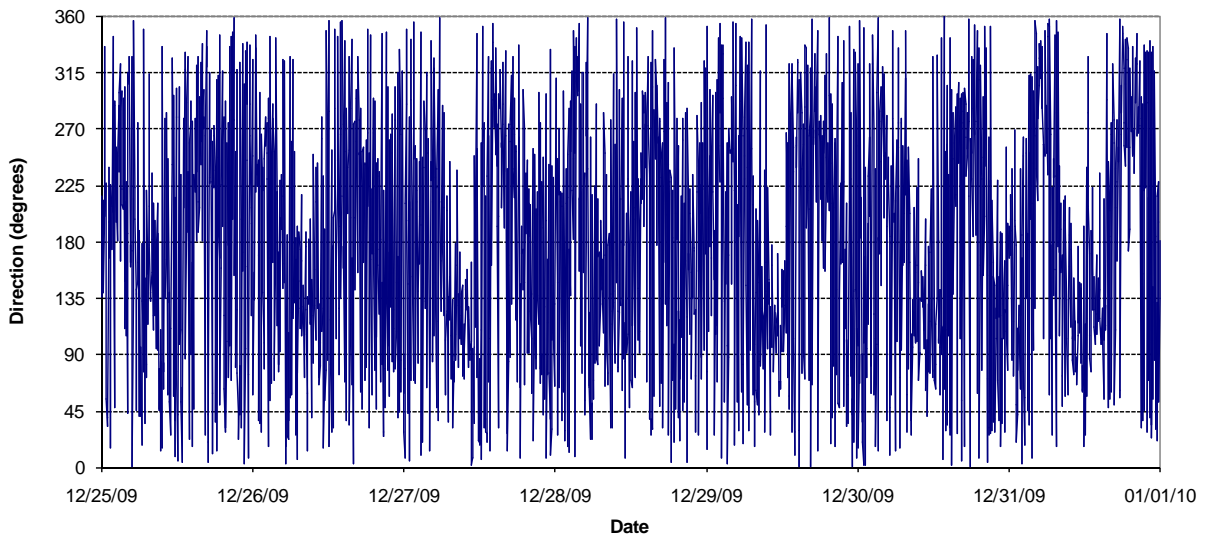
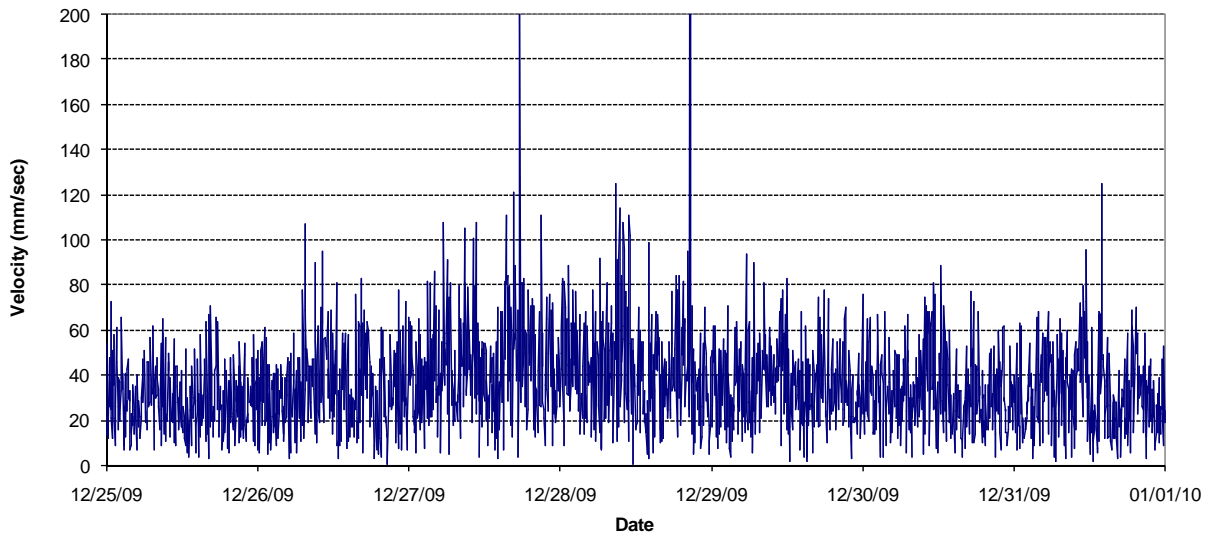
Figure A-16



Week 6 – Bin 1 Current Measurements at Inside Gage



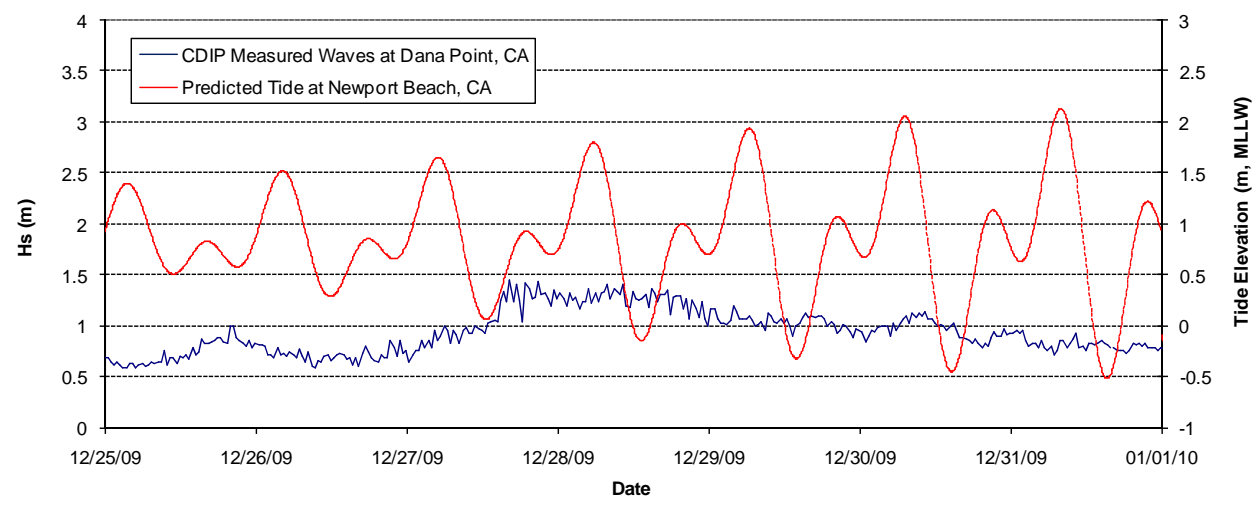
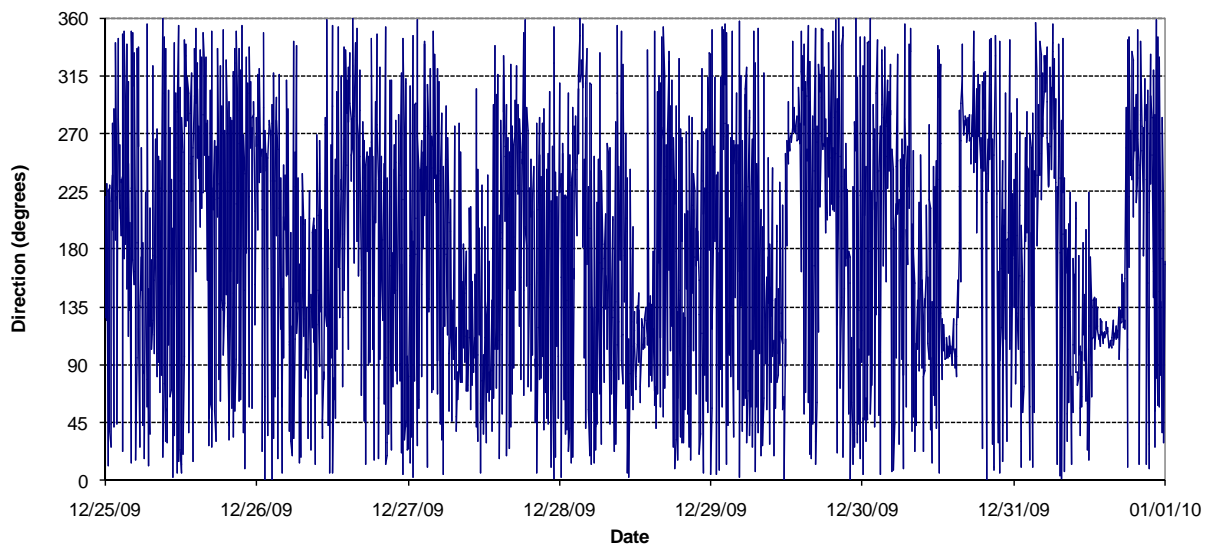
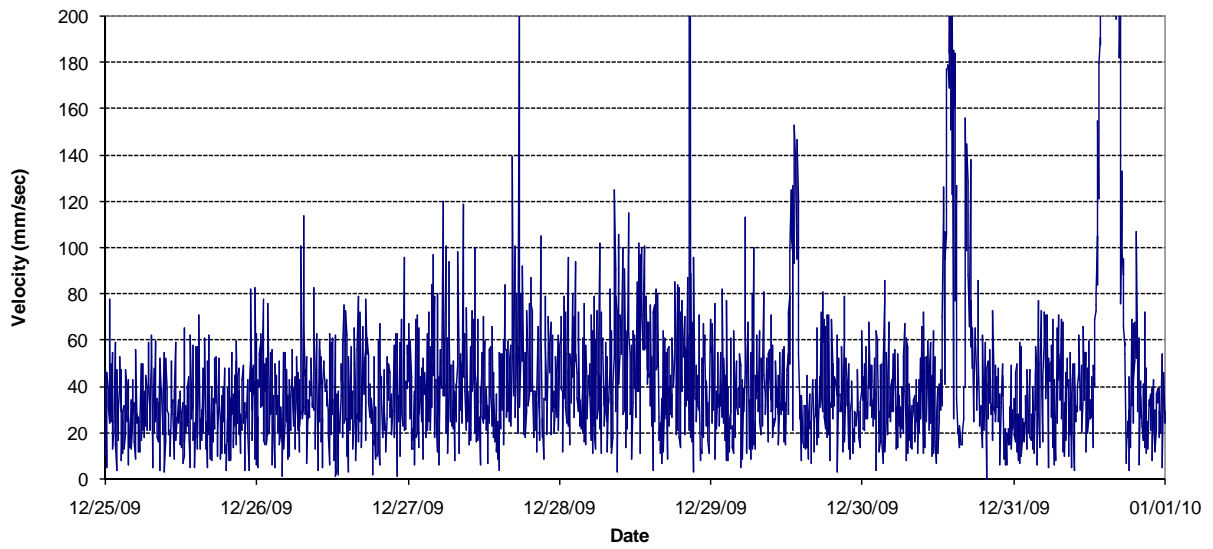
Figure A-17



Week 6 – Bin 2 Current Measurements at Inside Gage



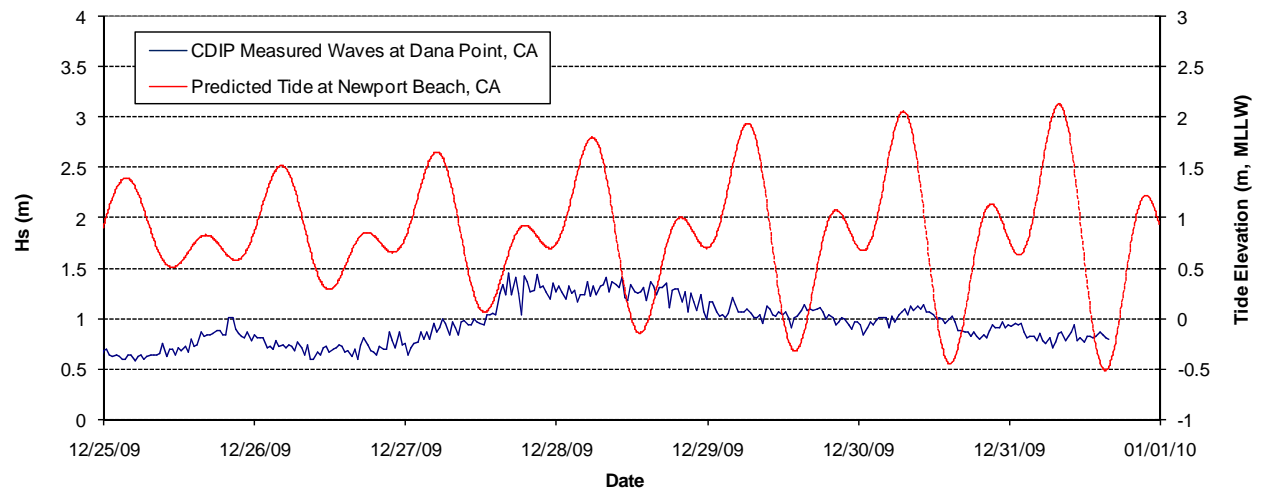
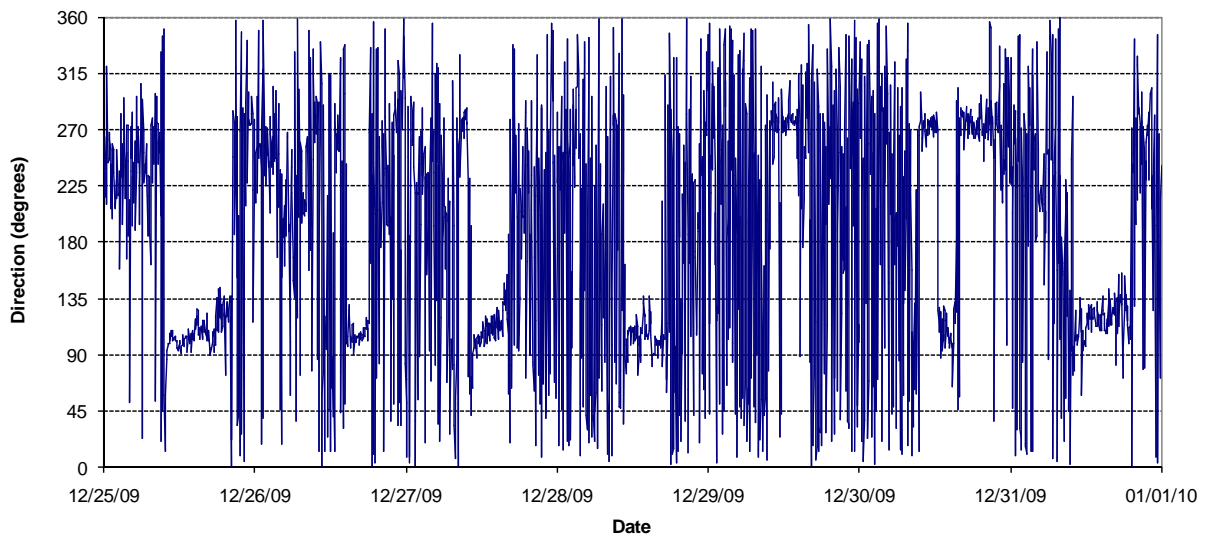
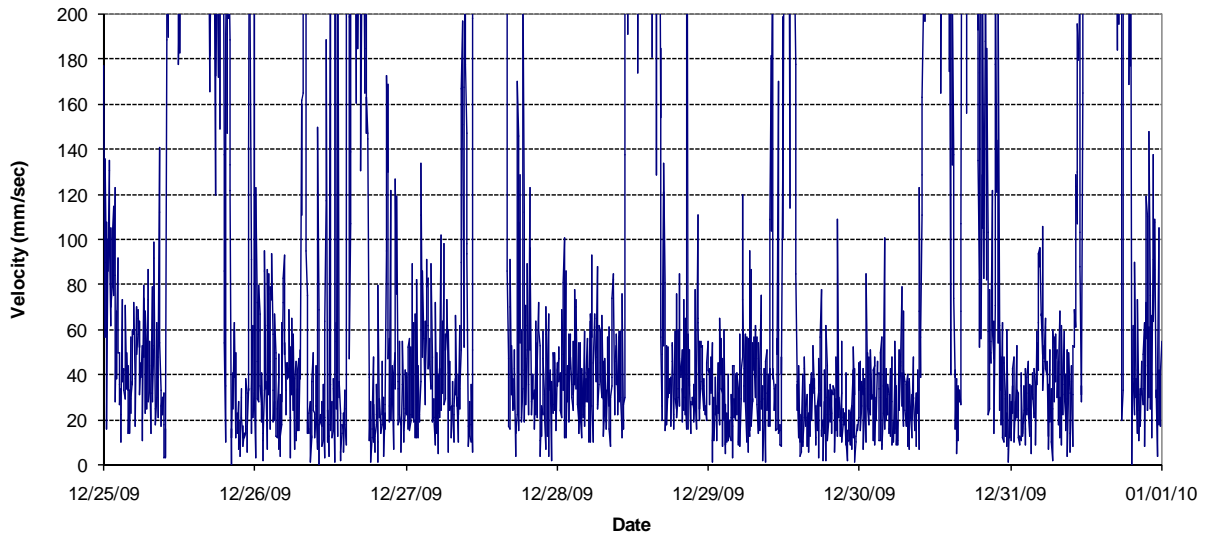
Figure A-18



Week 6 – Bin 3 Current Measurements at Inside Gage



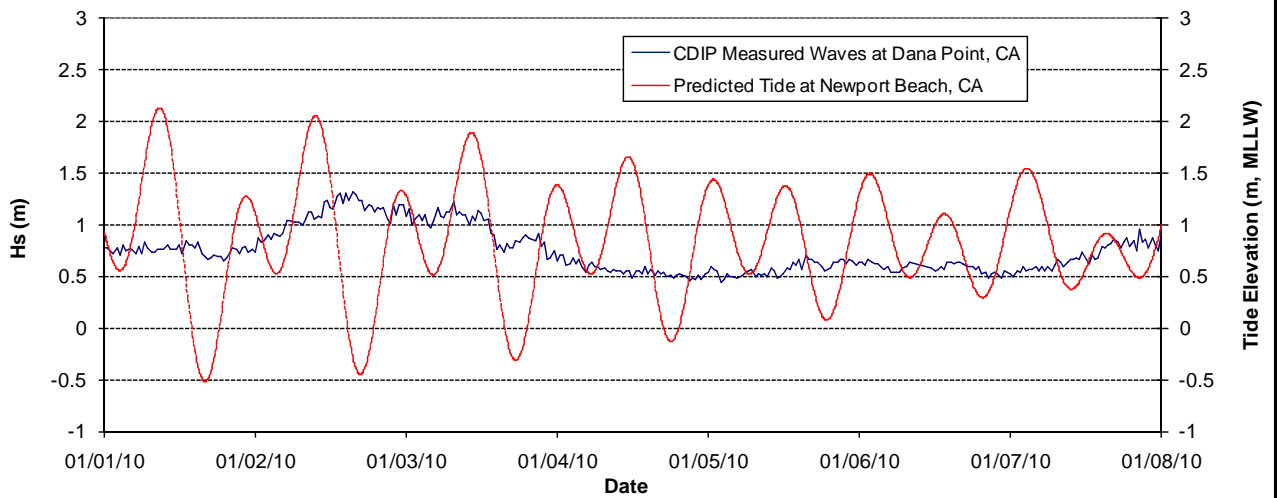
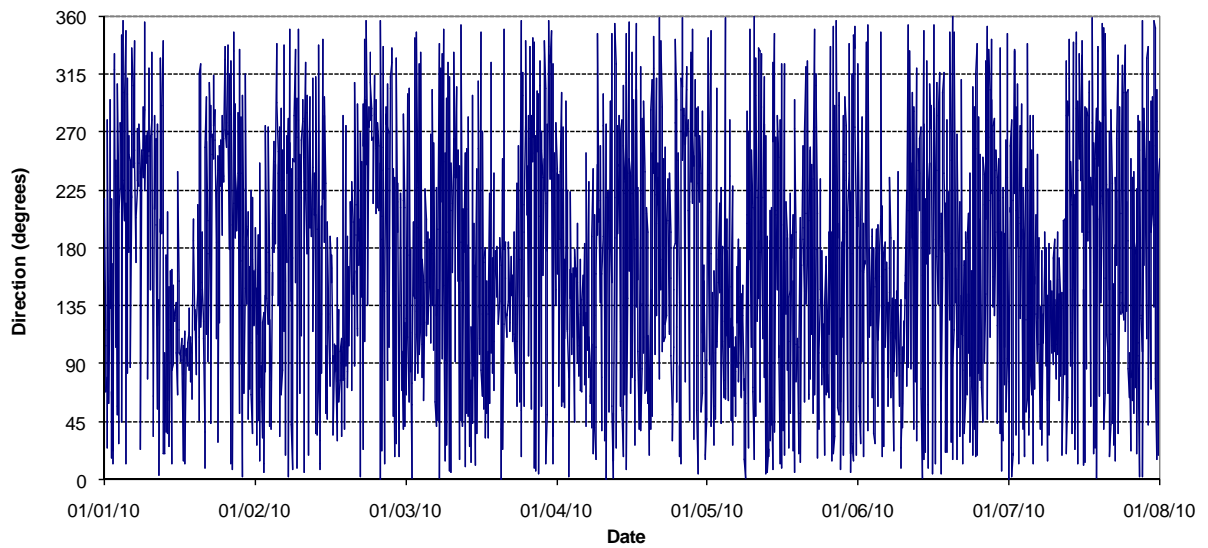
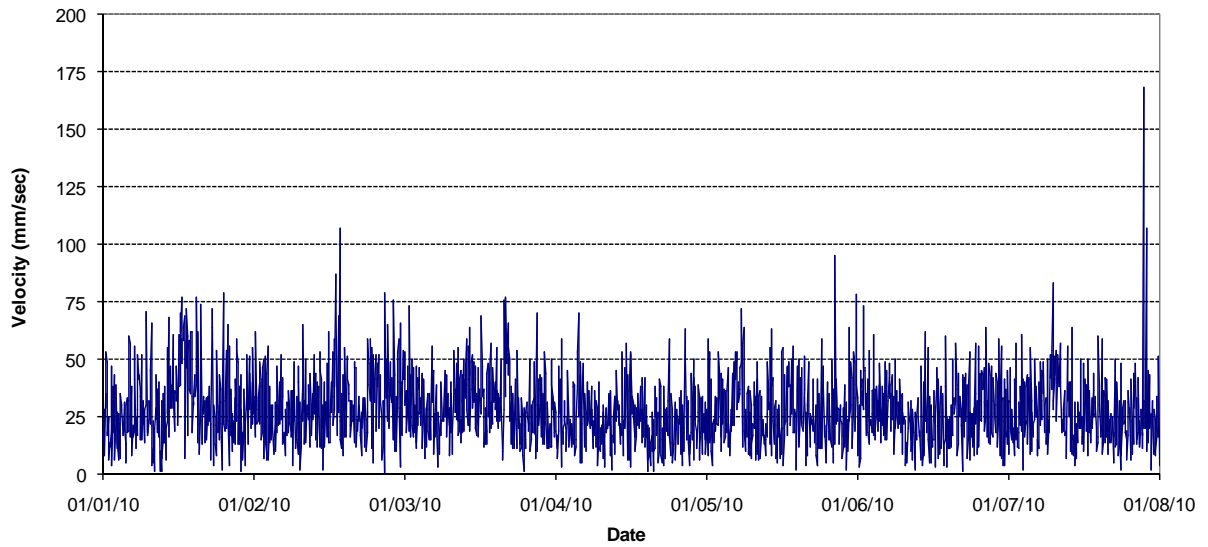
Figure A-19



Week 6 – Bin 4 Current Measurements at Inside Gage



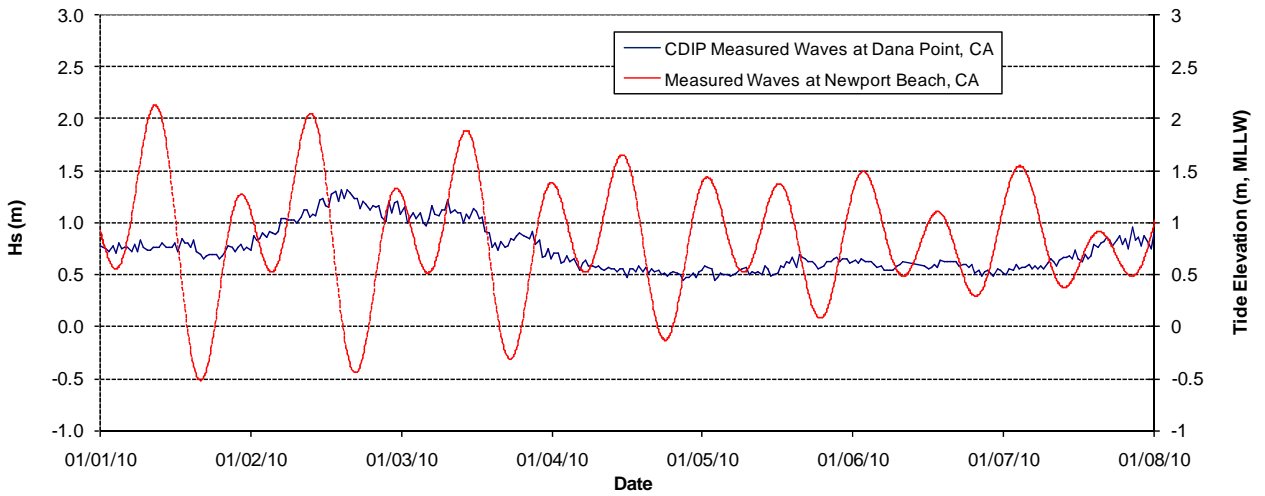
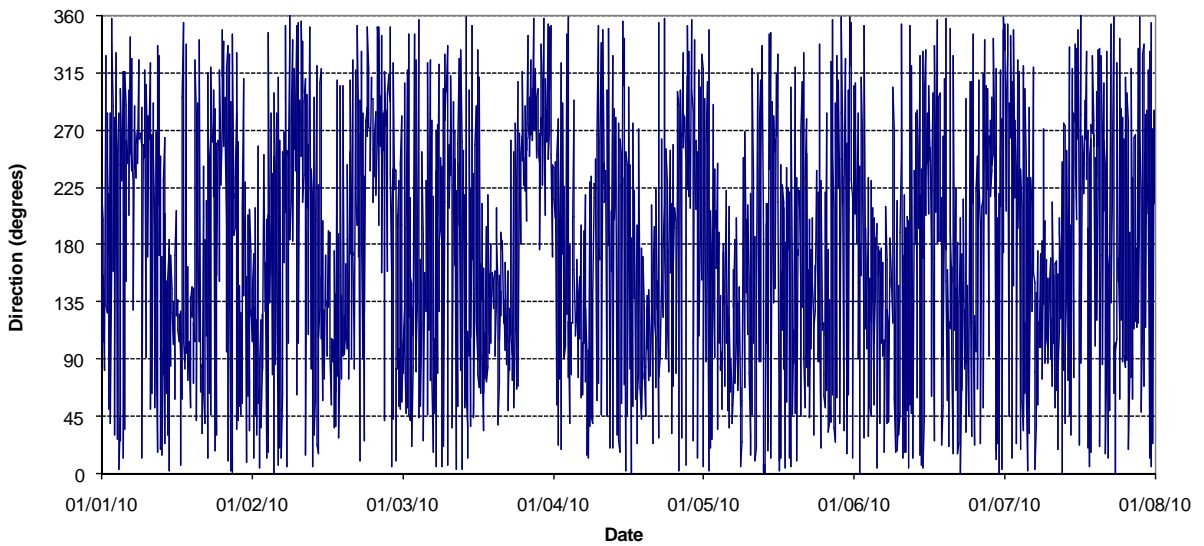
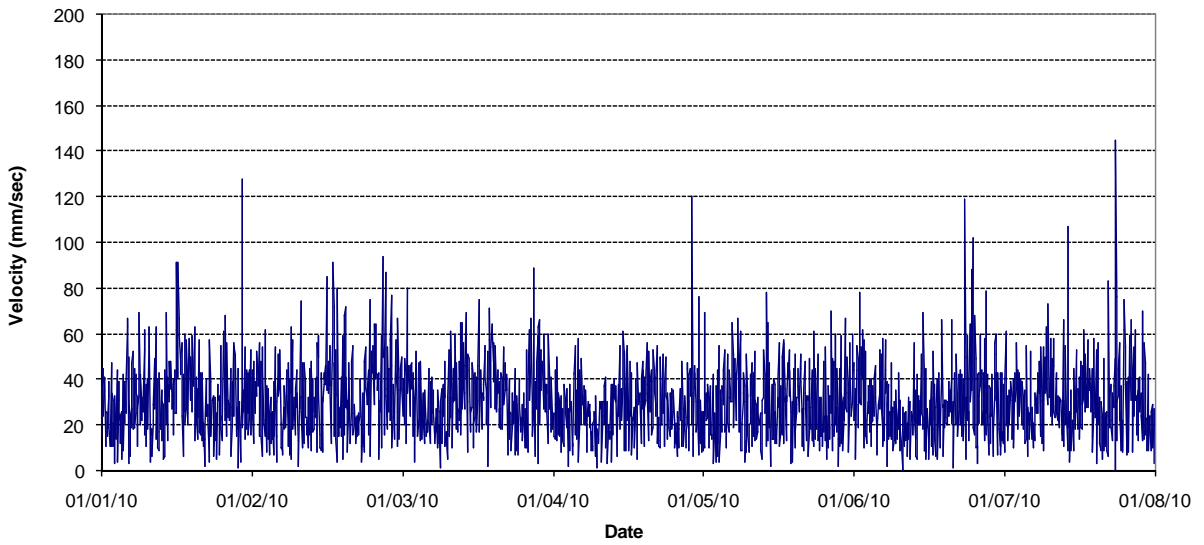
Figure A-20



Week 7 – Bin 1 Current Measurements at Inside Gage



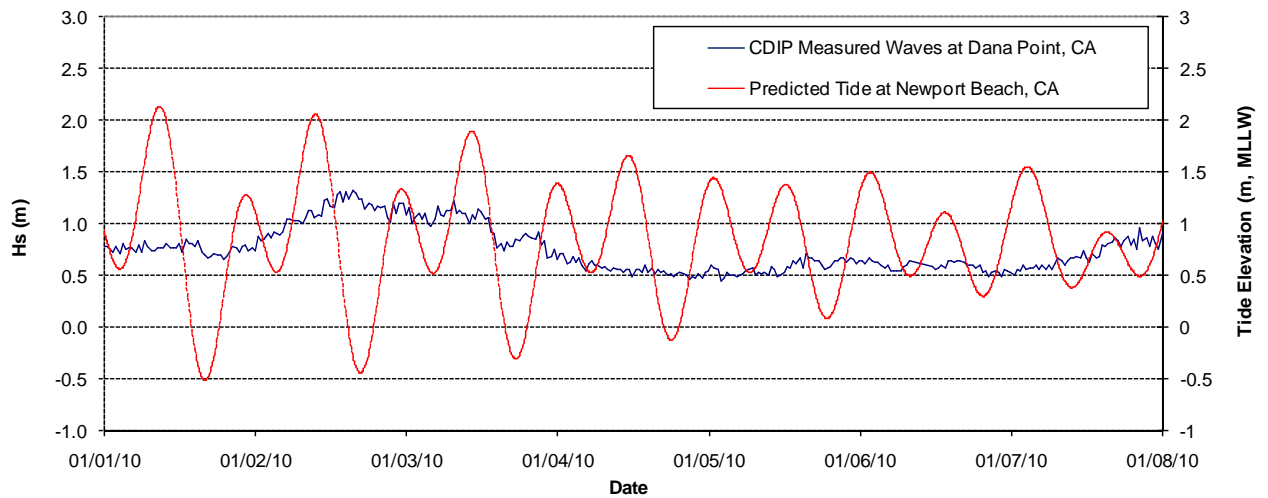
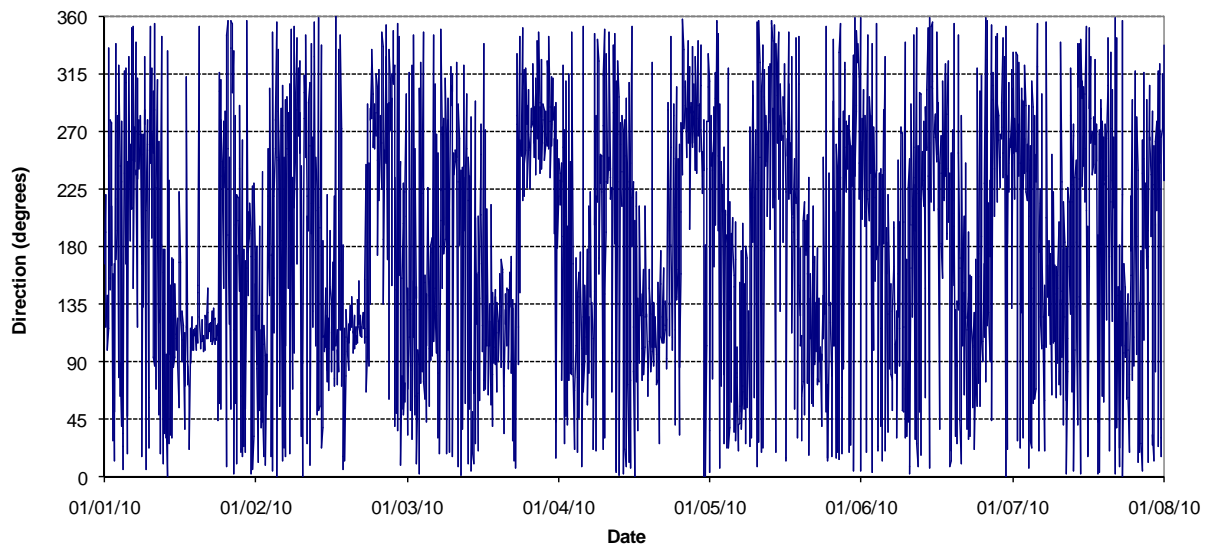
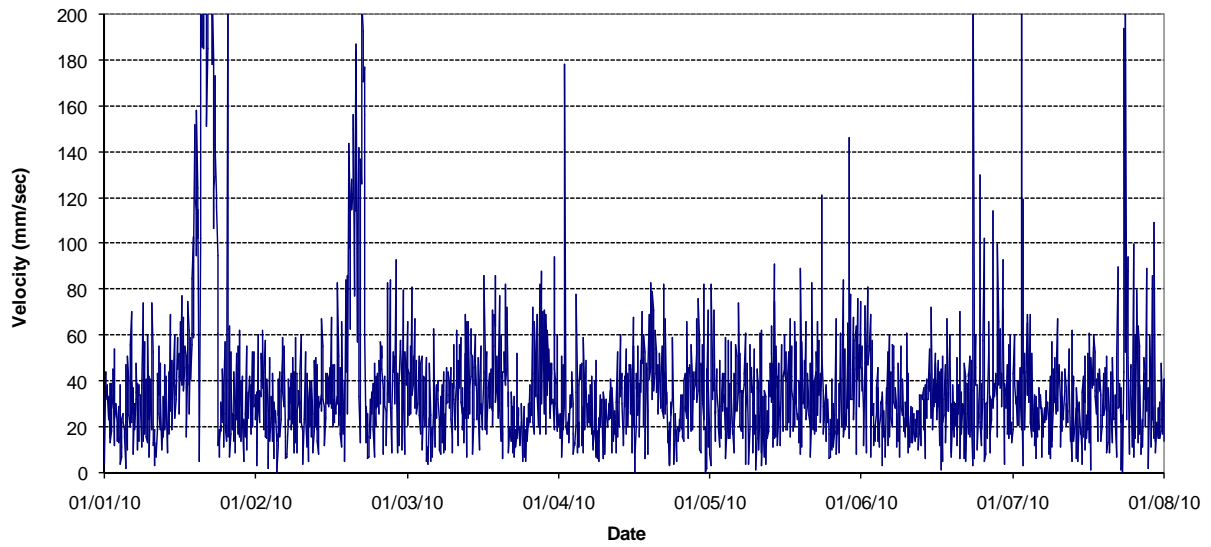
Figure A-21



Week 7 – Bin 2 Current Measurements at Inside Gage



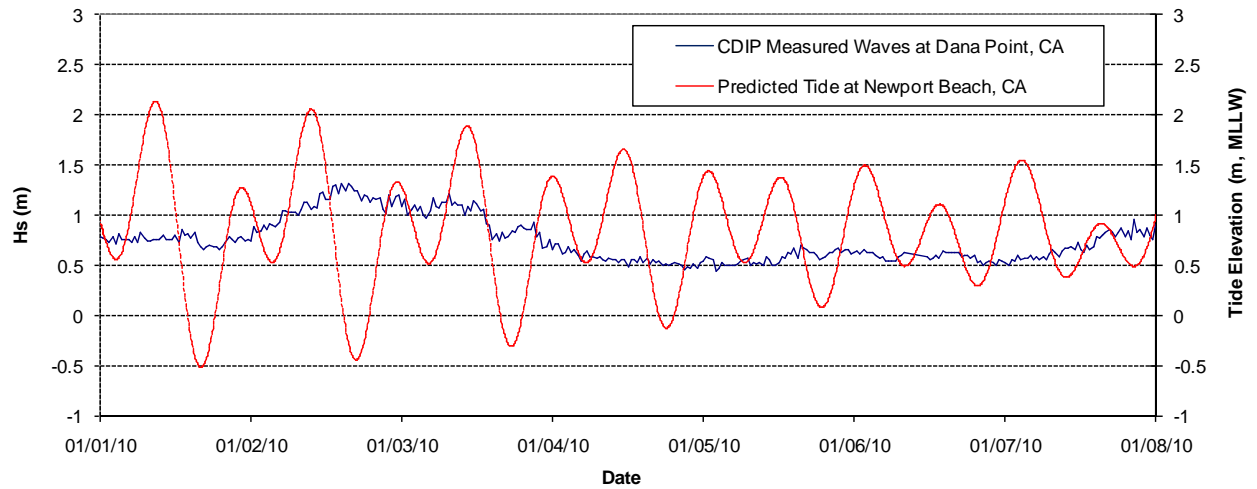
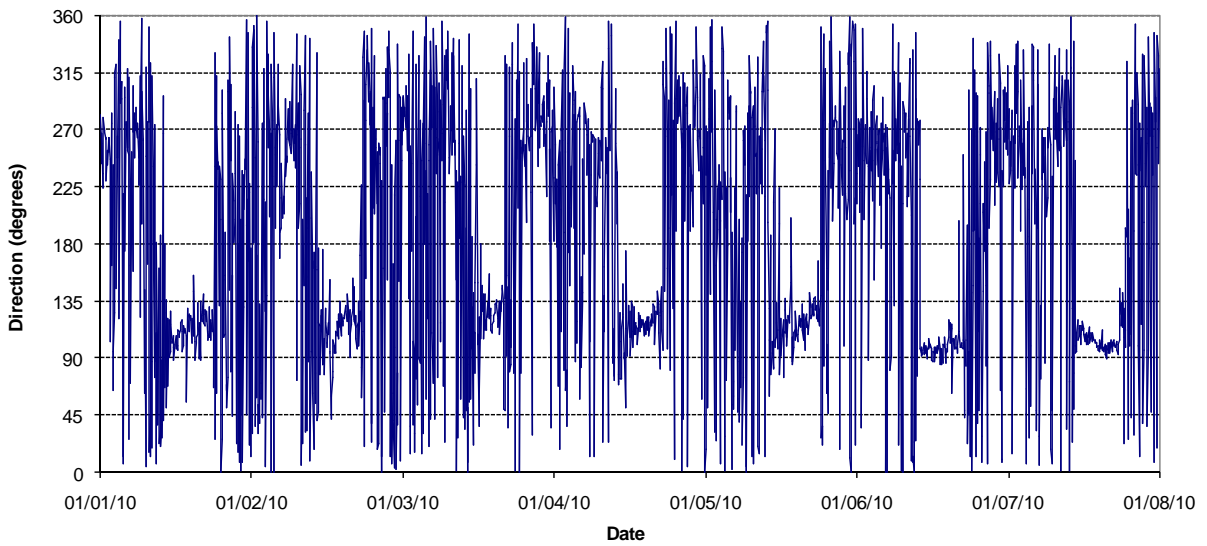
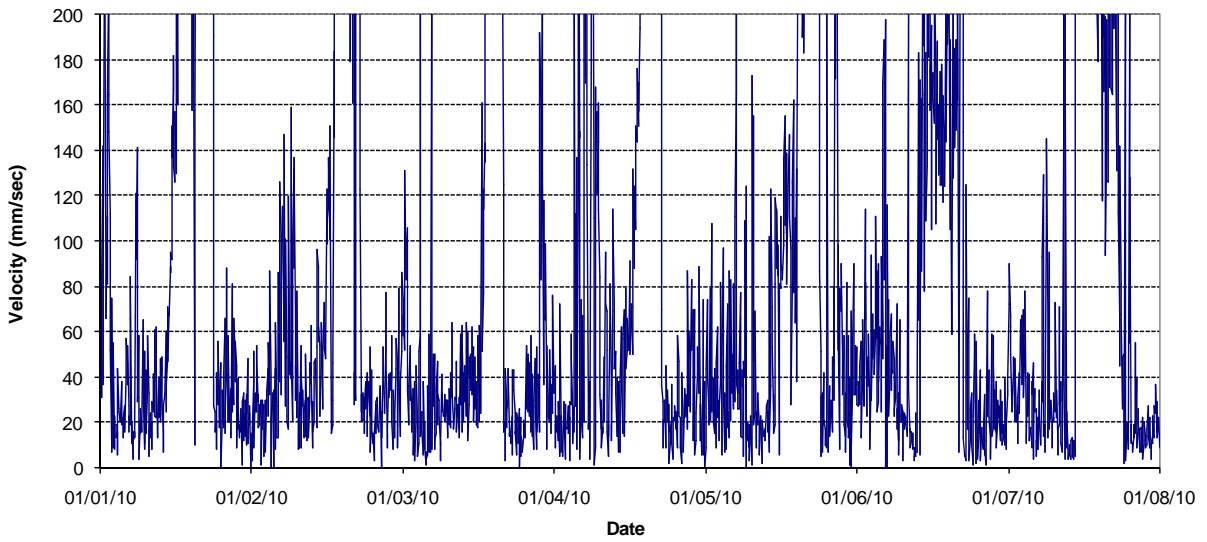
Figure A-22



Week 7 – Bin 3 Current Measurements at Inside Gage



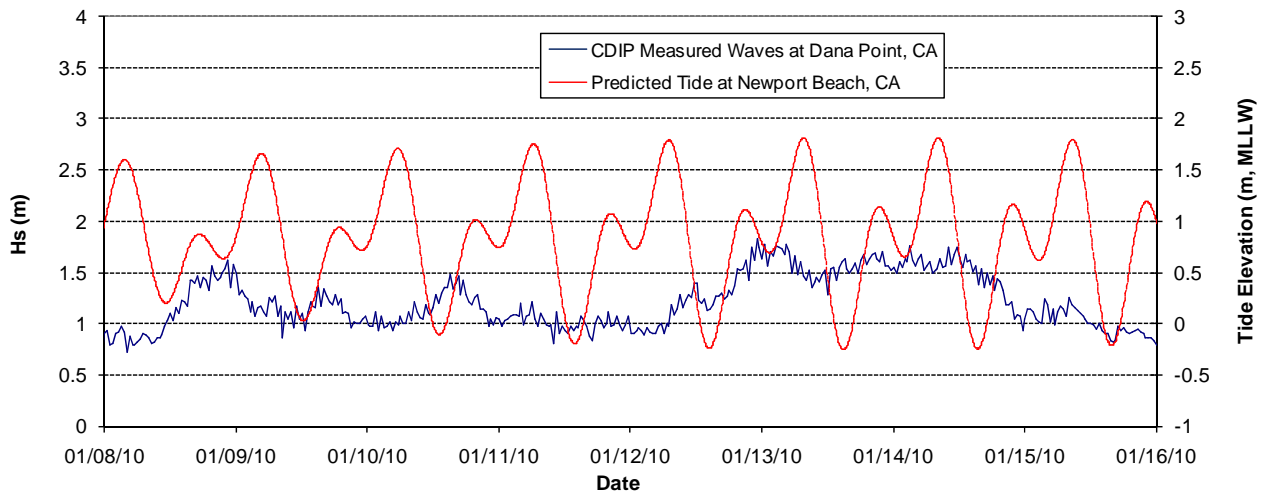
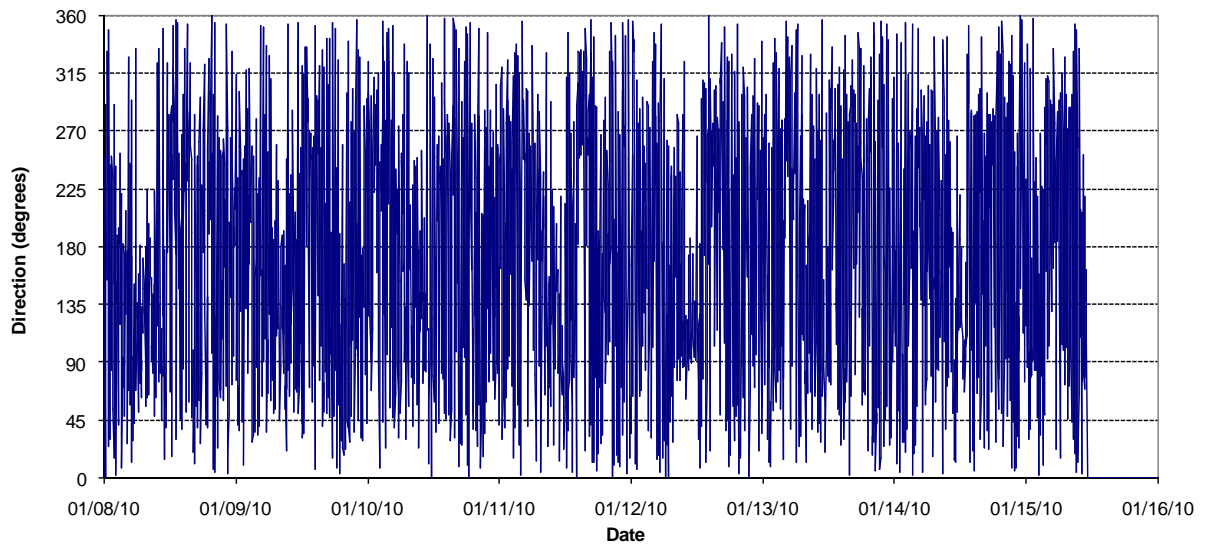
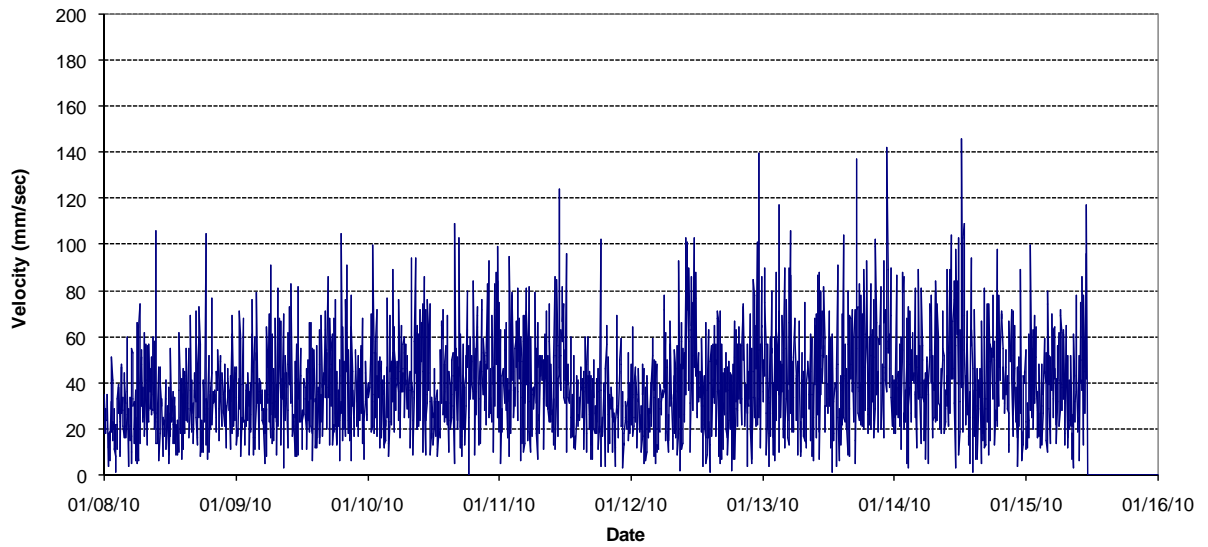
Figure A-23



Week 7 – Bin 4 Current Measurements at Inside Gage



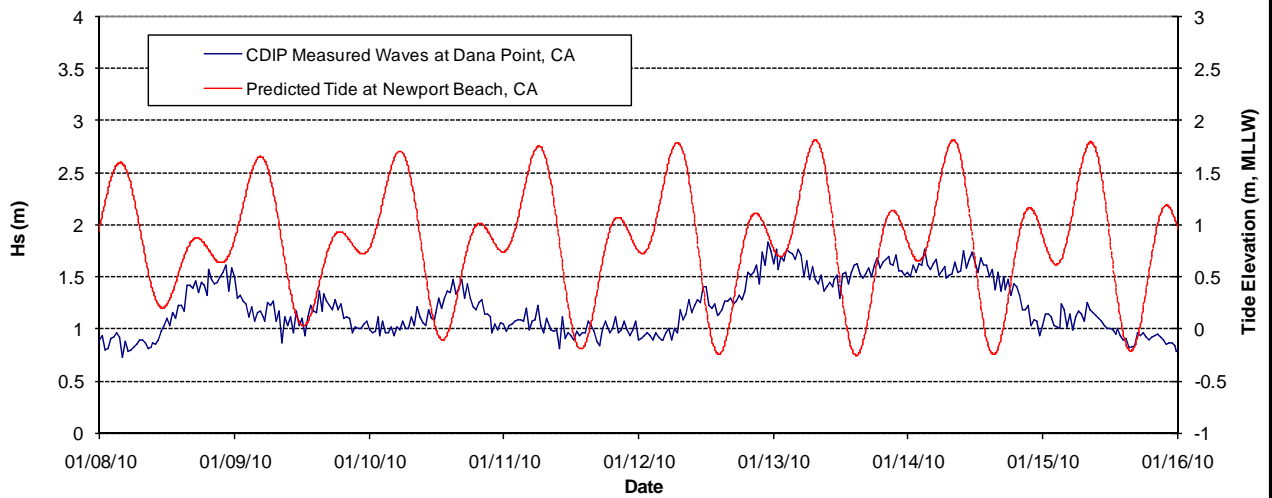
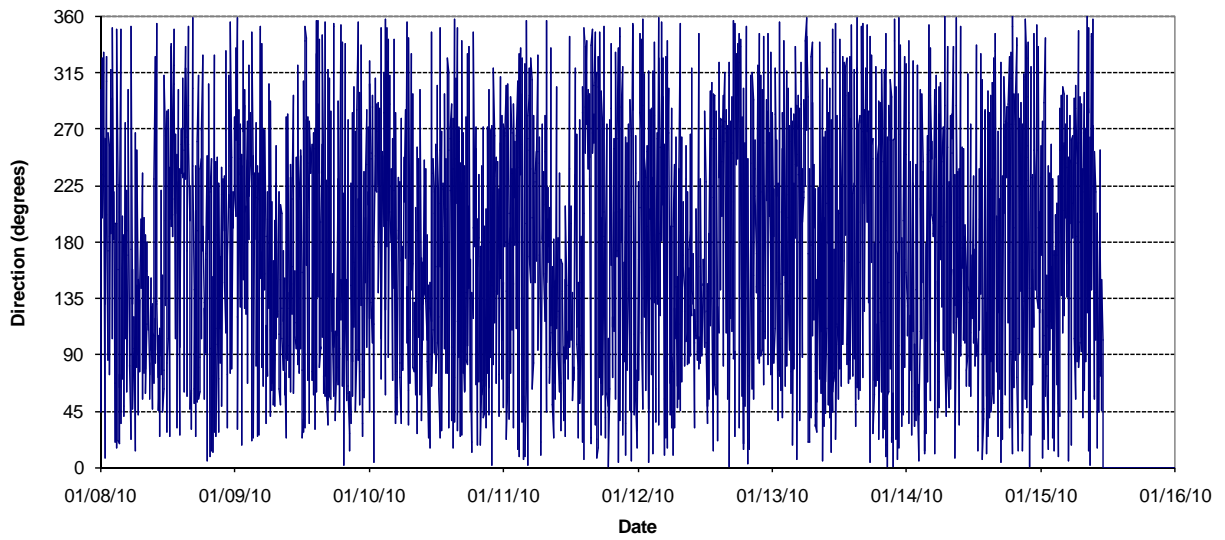
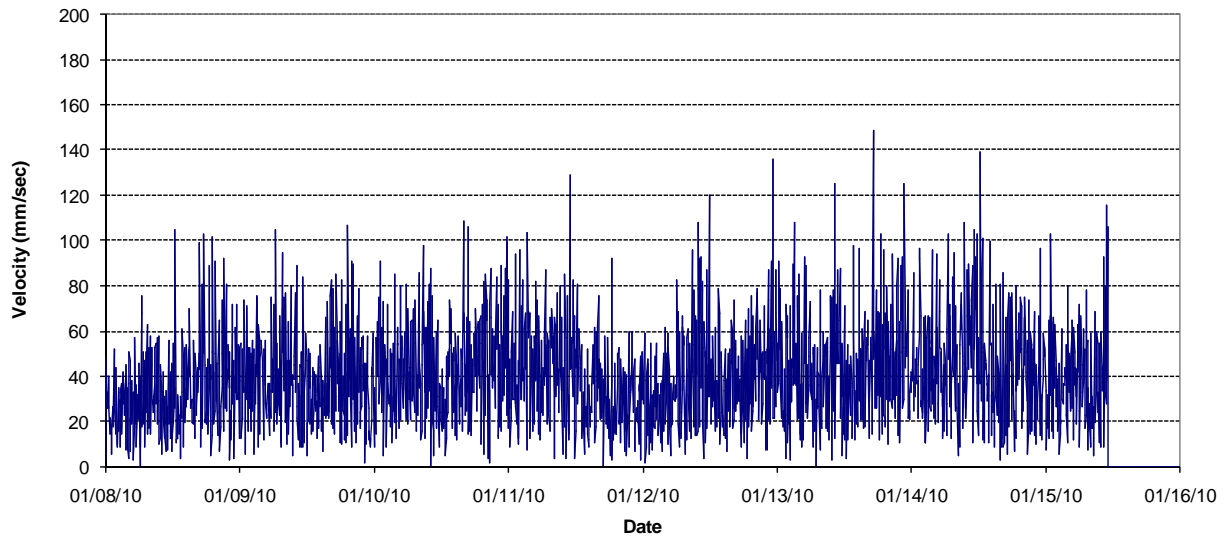
Figure A-24



Week 8 – Bin 1 Current Measurements at Inside Gage



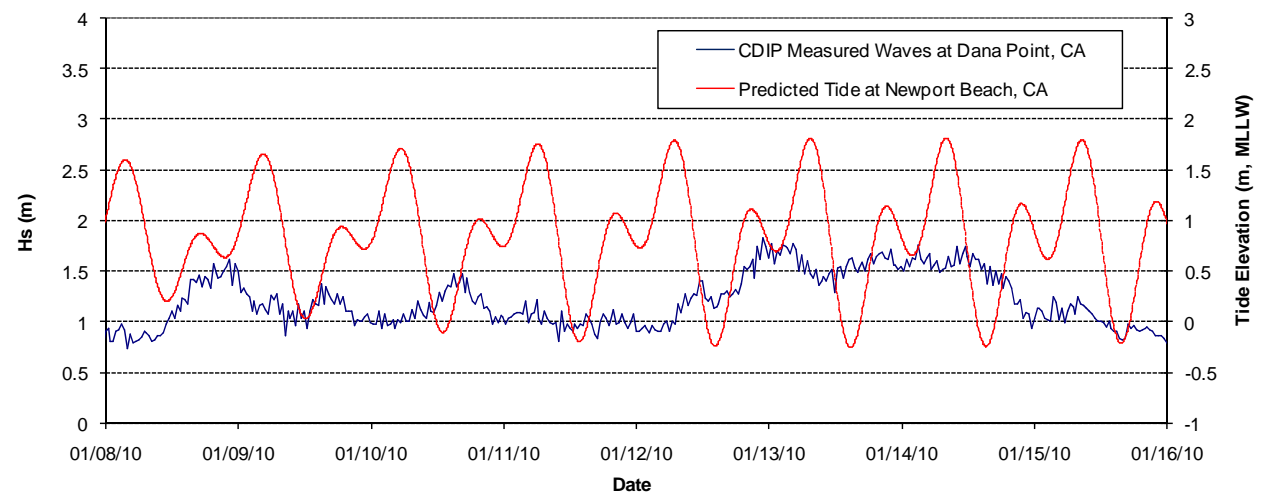
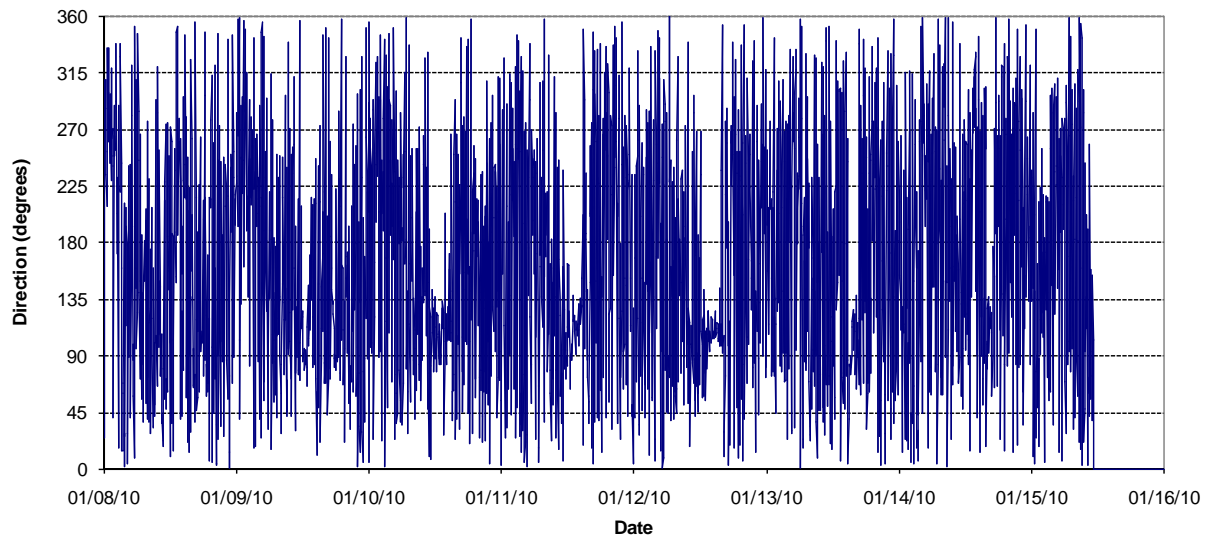
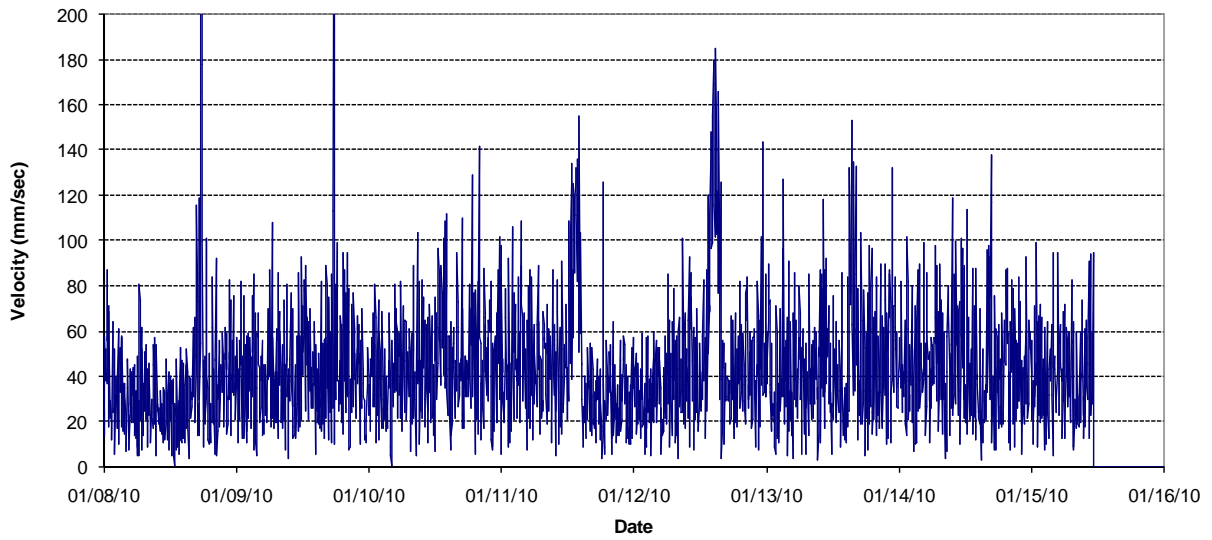
Figure A-25



Week 8 – Bin 2 Current Measurements at Inside Gage



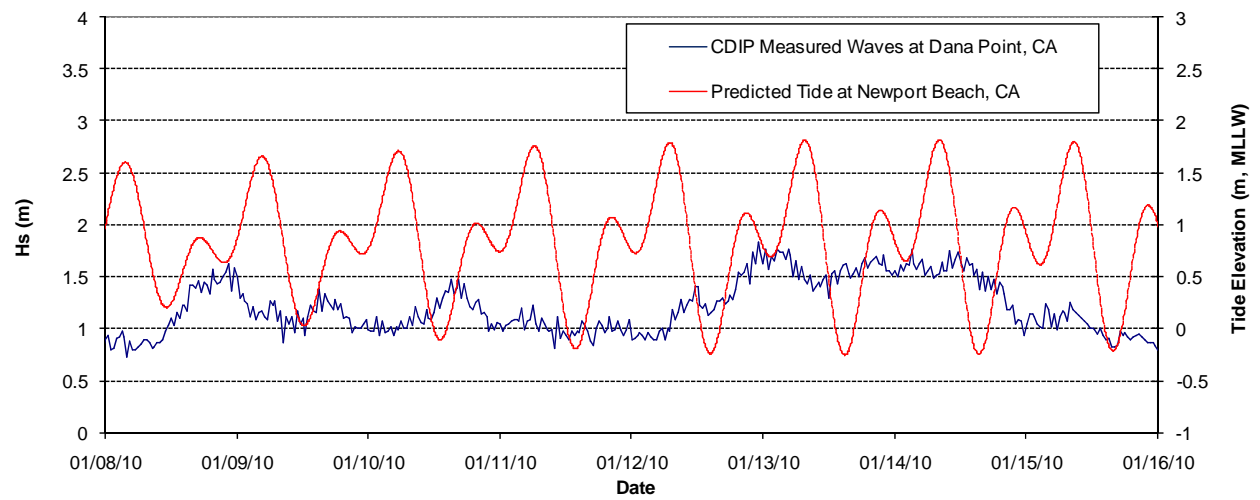
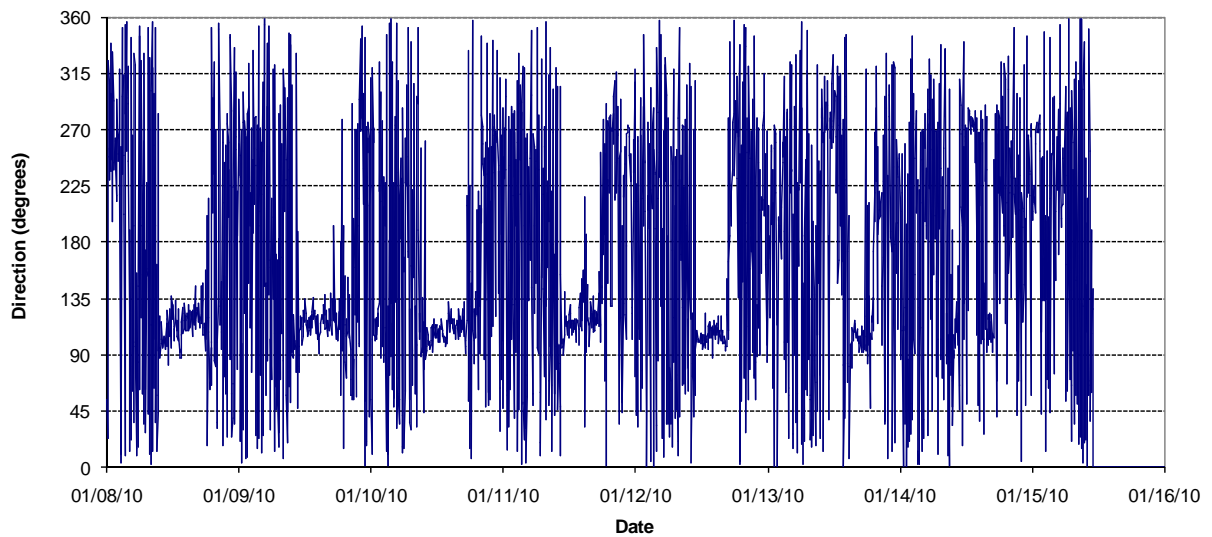
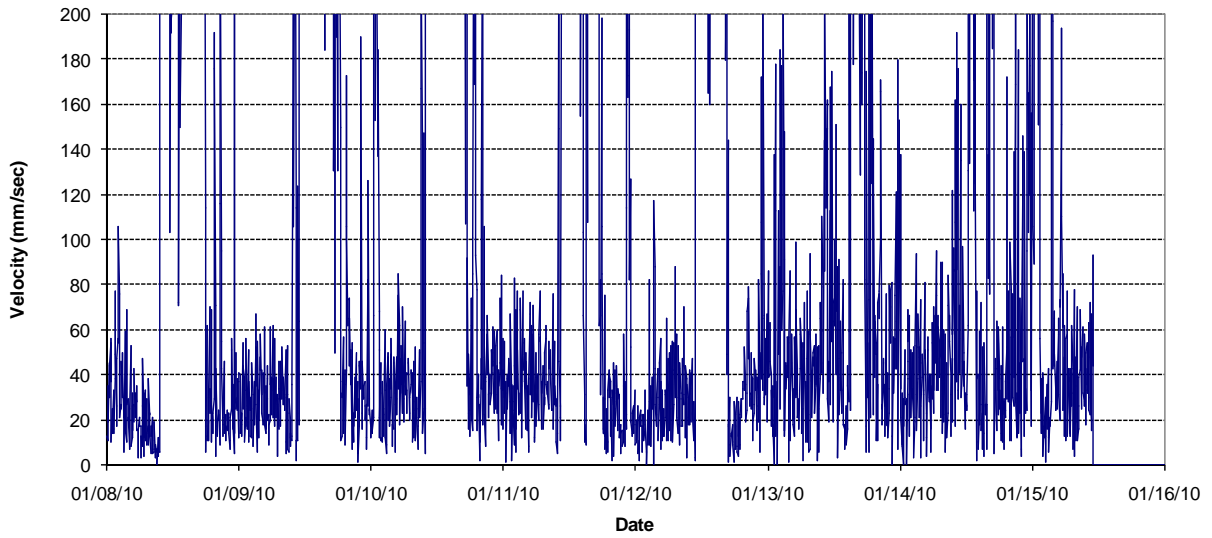
Figure A-26



Week 8 – Bin 3 Current Measurements at Inside Gage

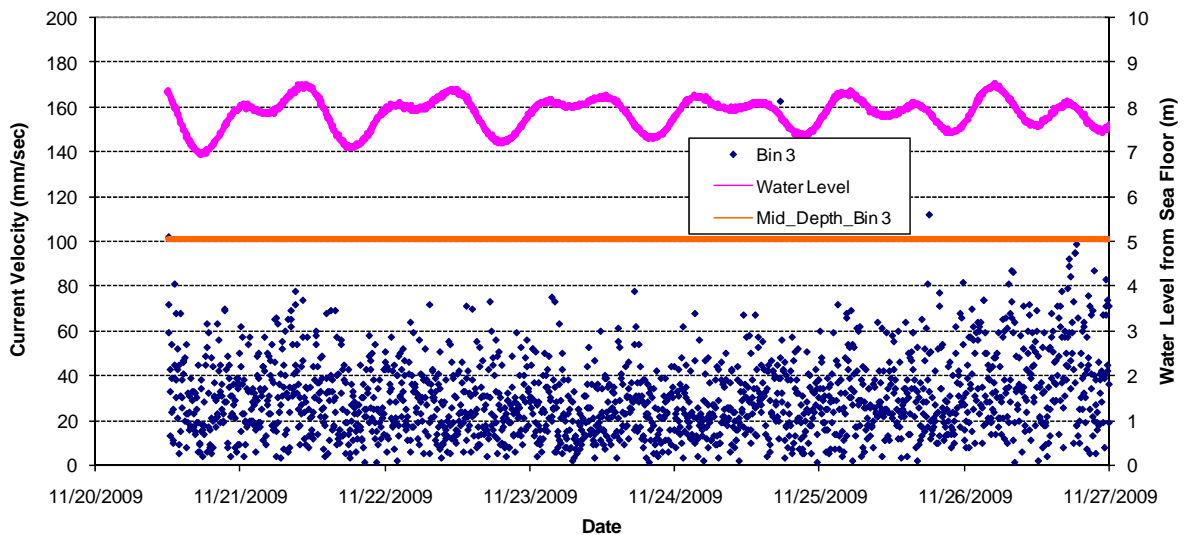
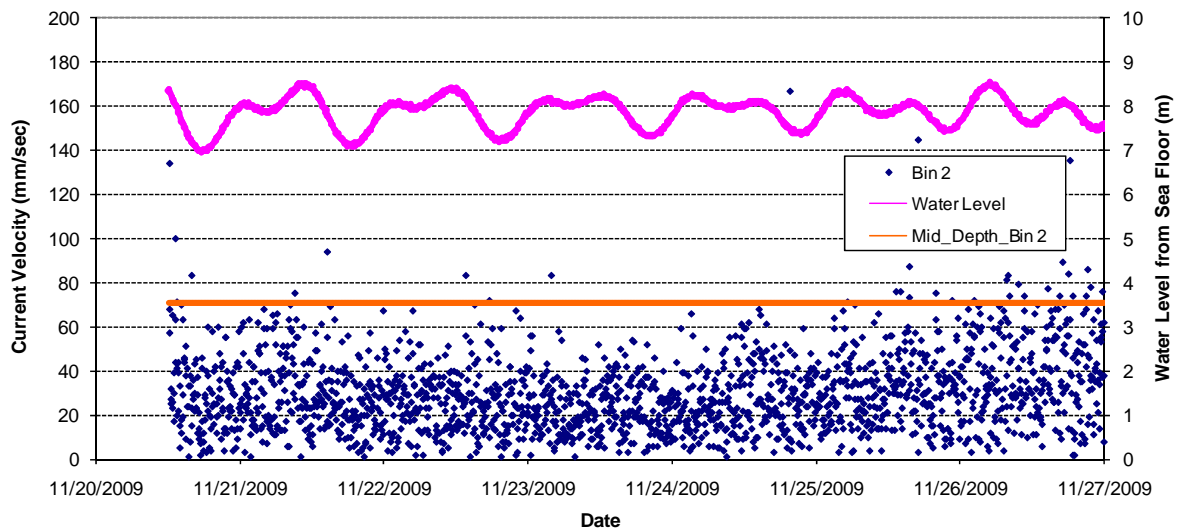
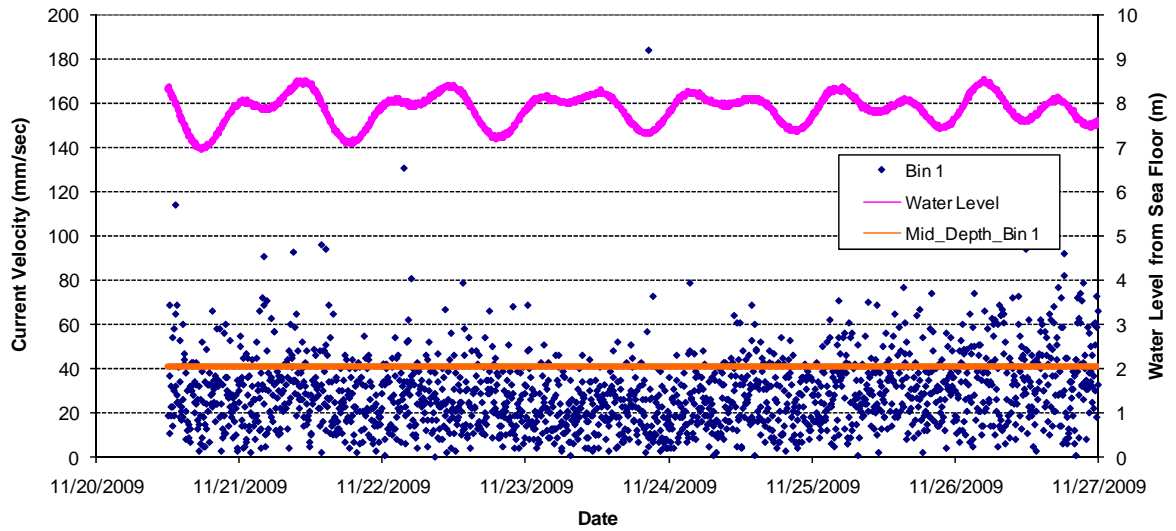


Figure A-27



Week 8 – Bin 4 Current Measurements at Inside Gage

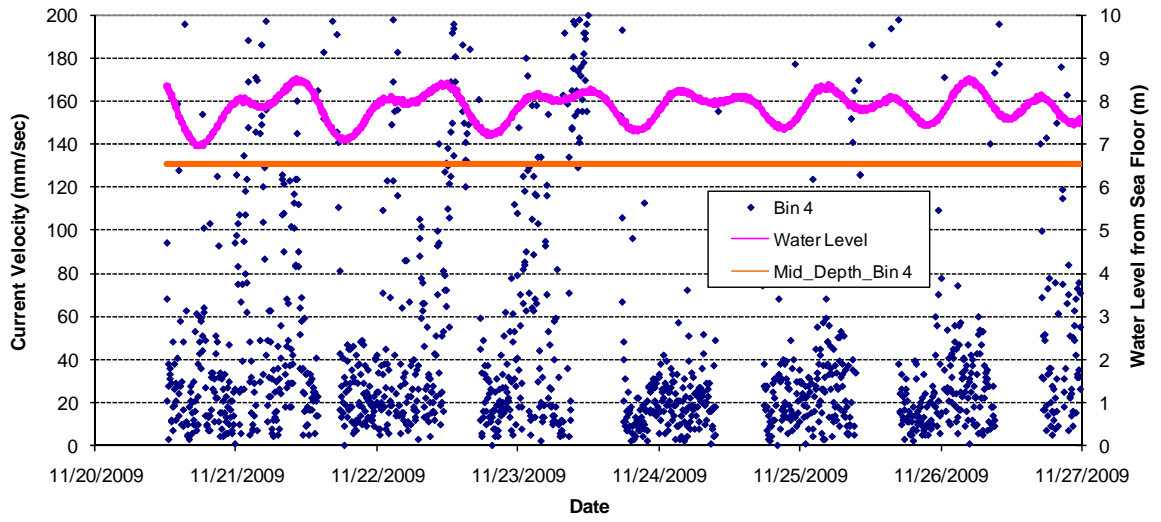




Week 1 - Bin 1, 2, & 3 Measurements at Inside Gage



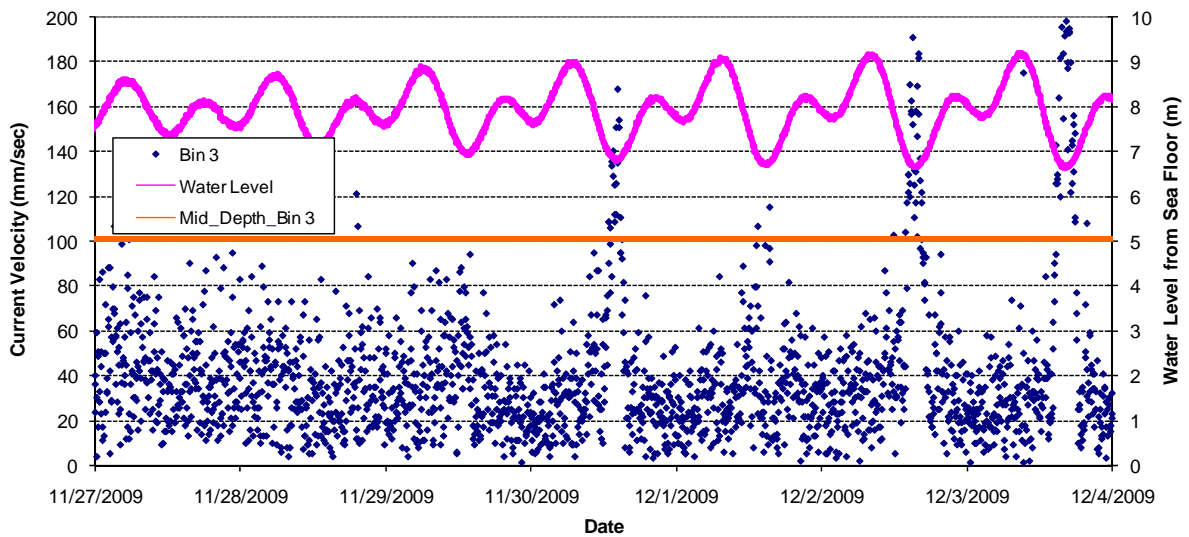
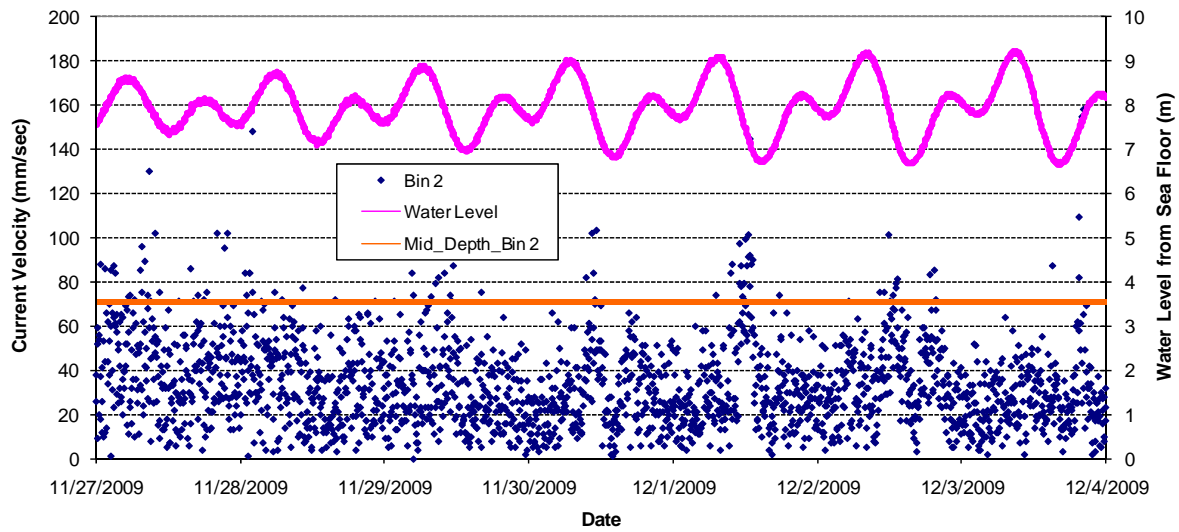
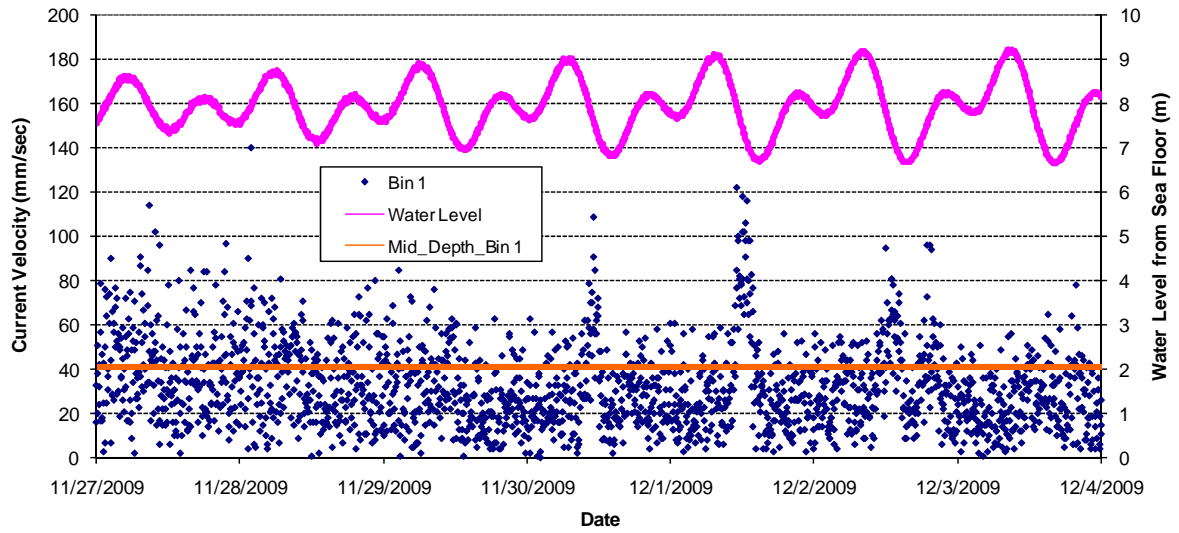
Figure A-29



Week 1 – Bin 4 Measurements at Inside Gage



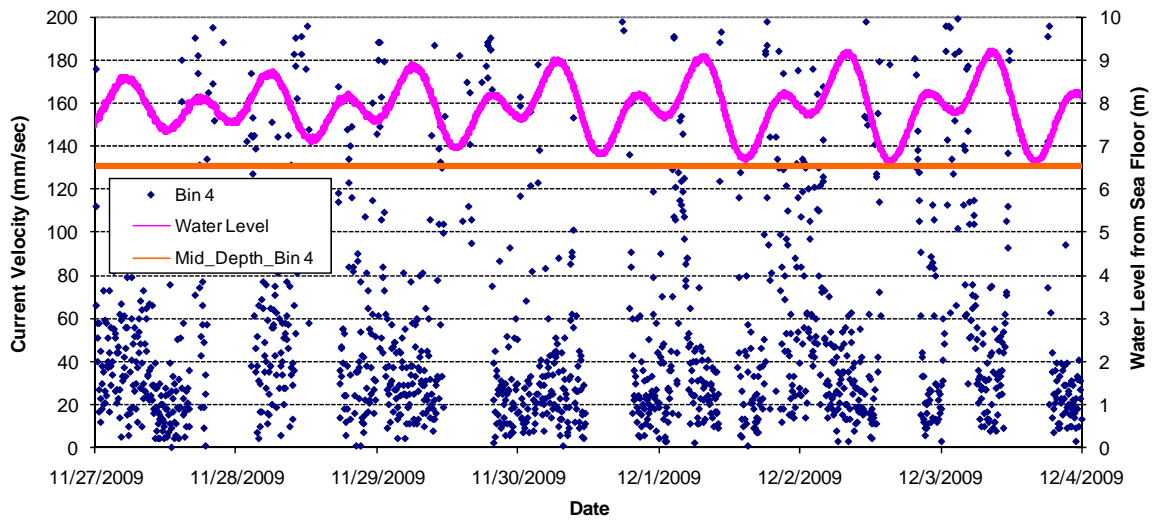
Figure A-30



Week 2 – Bin 1, 2, & 3 Measurements at Inside Gage



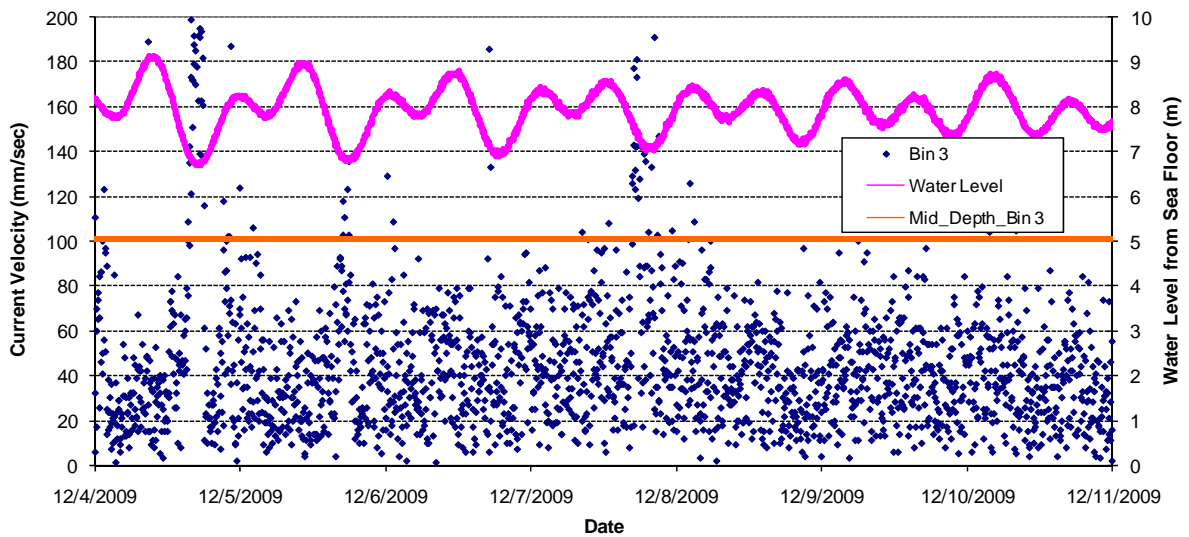
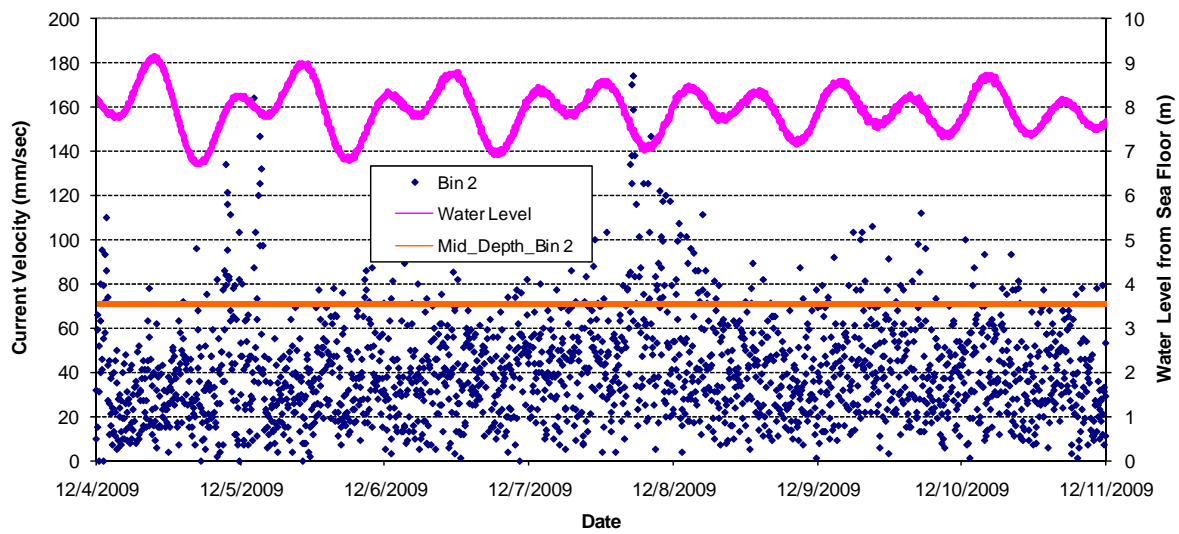
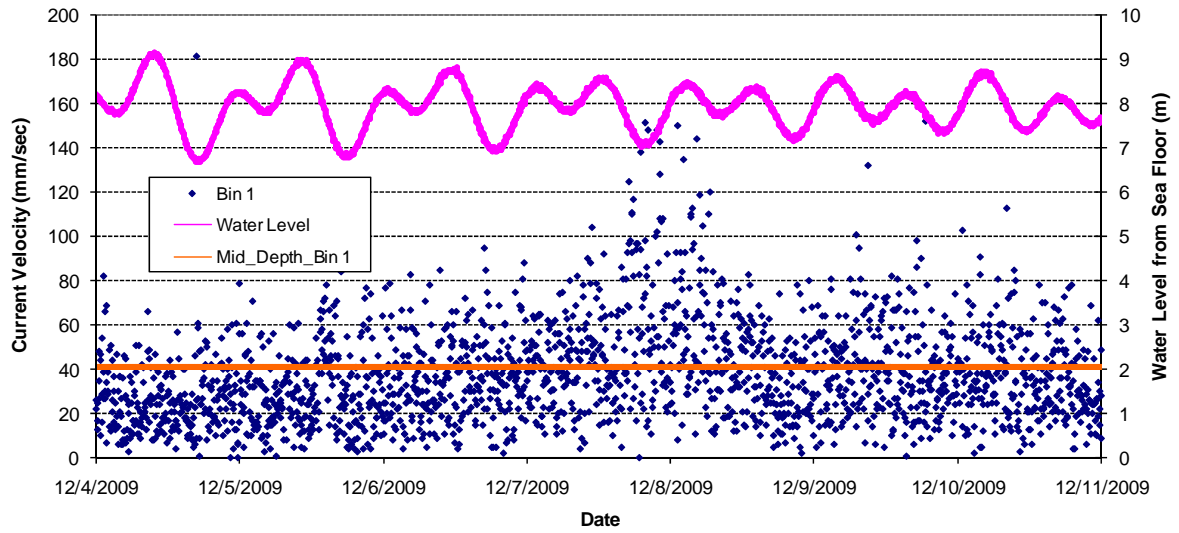
Figure A-31



Week 2 – Bin 4 Measurements at Inside Gage



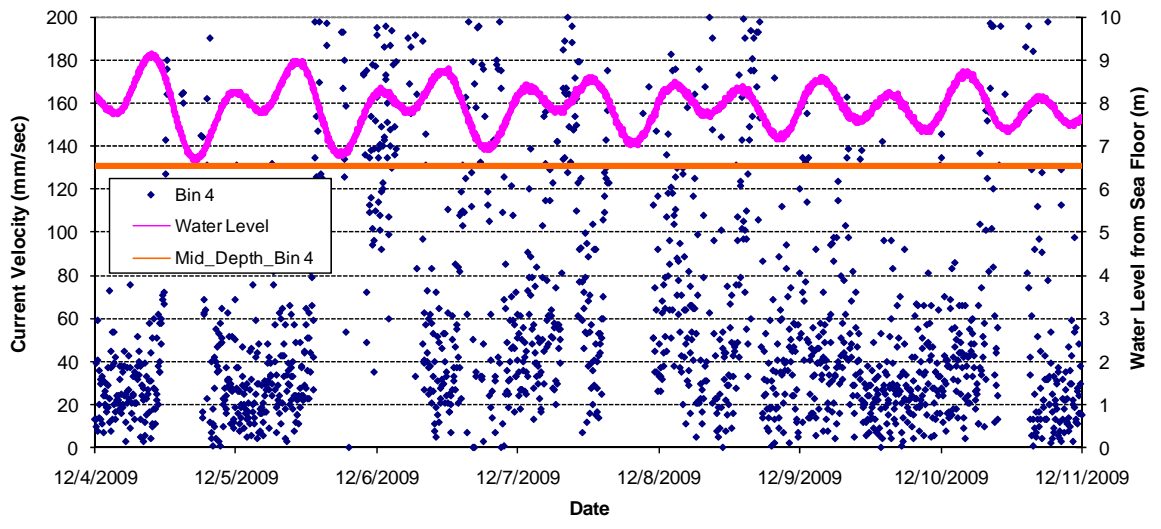
Figure A-32



Week 3 – Bin 1, 2, & 3 Measurements at Inside Gage



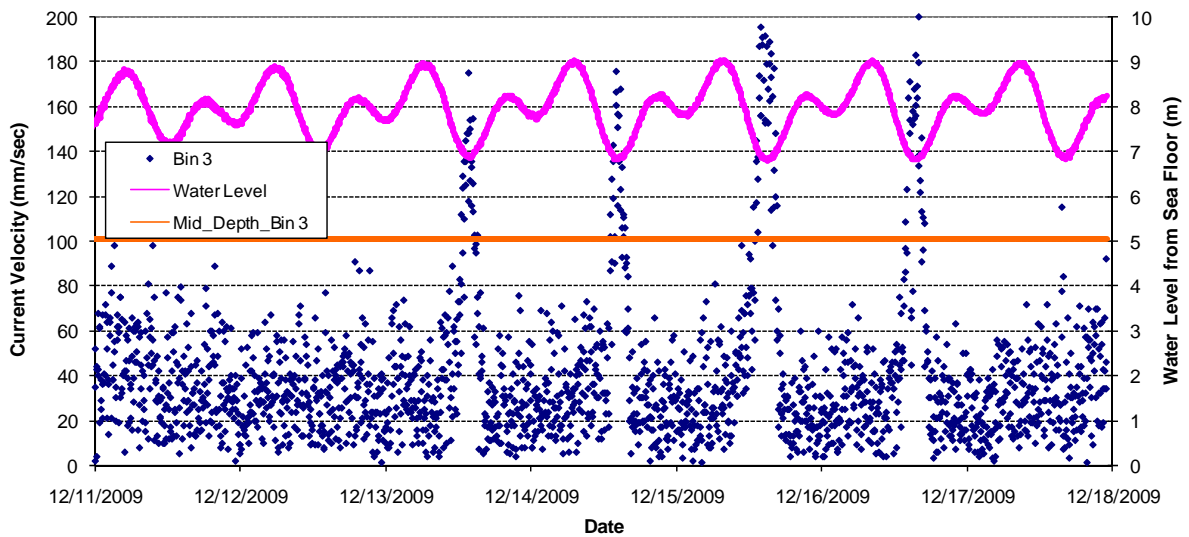
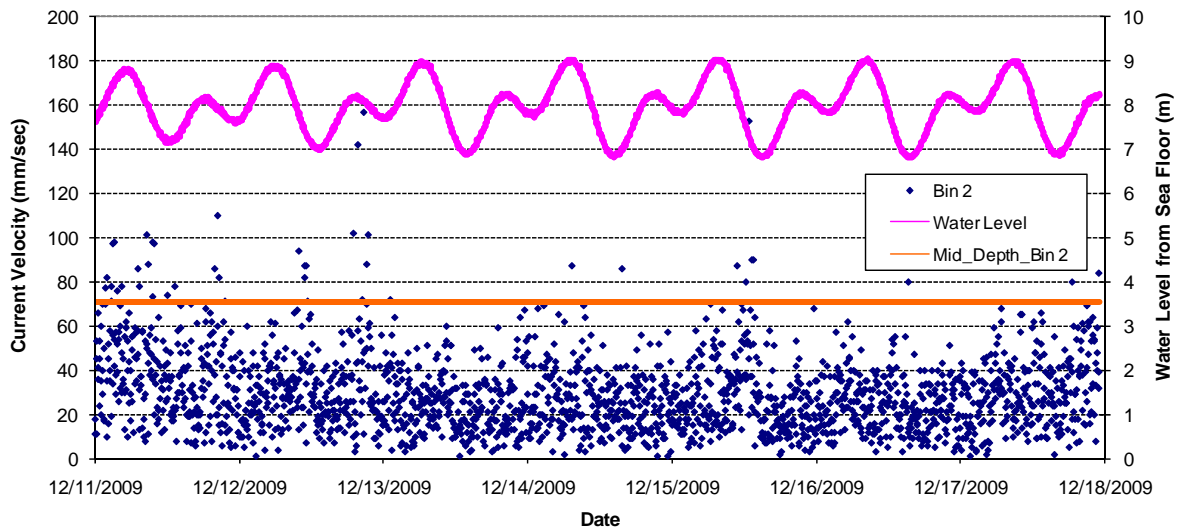
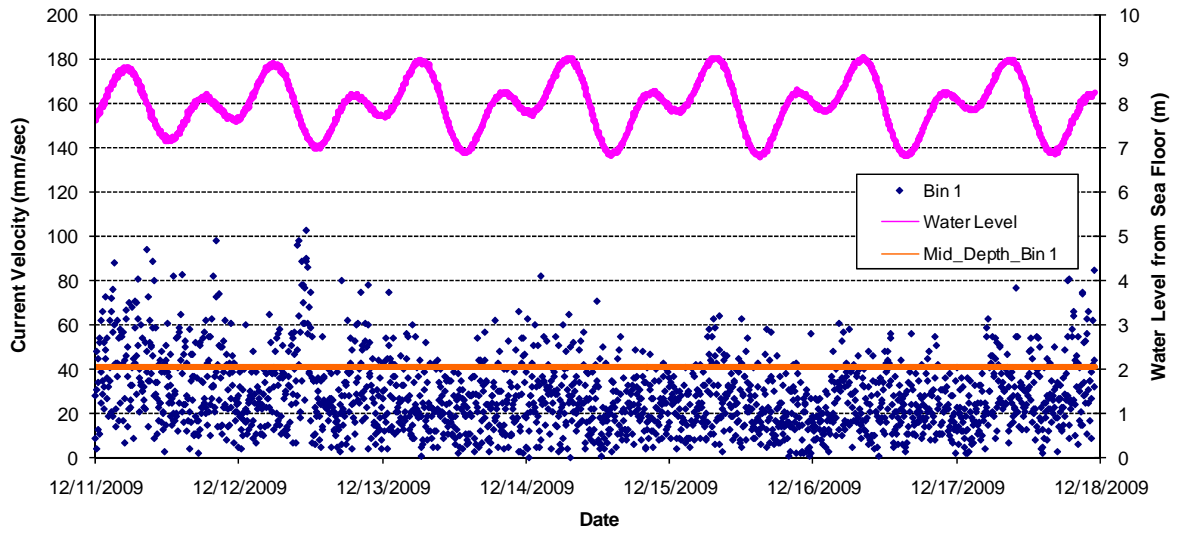
Figure A-33



Week 3 – Bin 4 Measurements at Inside Gage



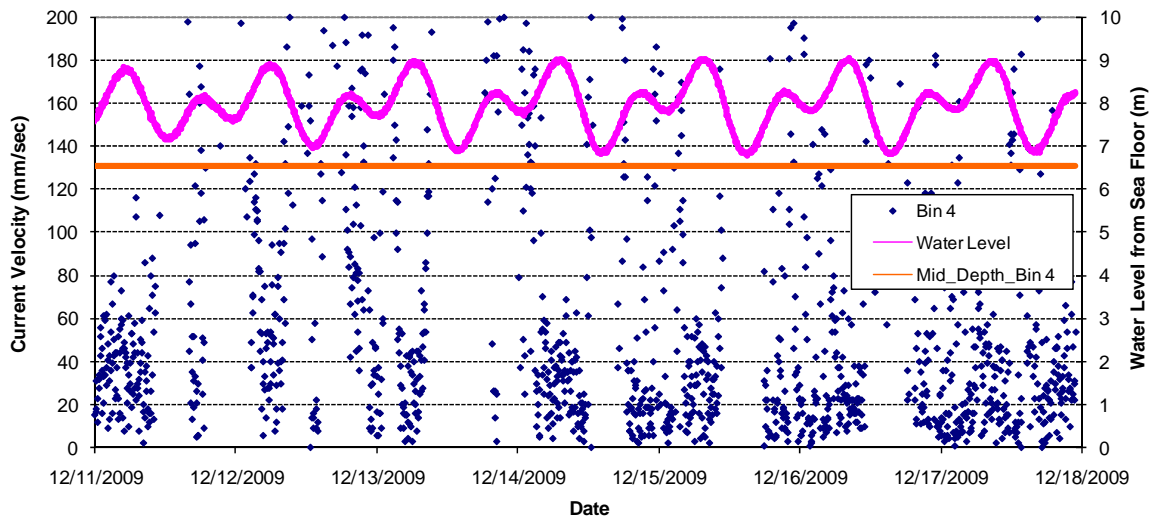
Figure A-34



Week 4 – Bin 1, 2, & 3 Measurements at Inside Gage



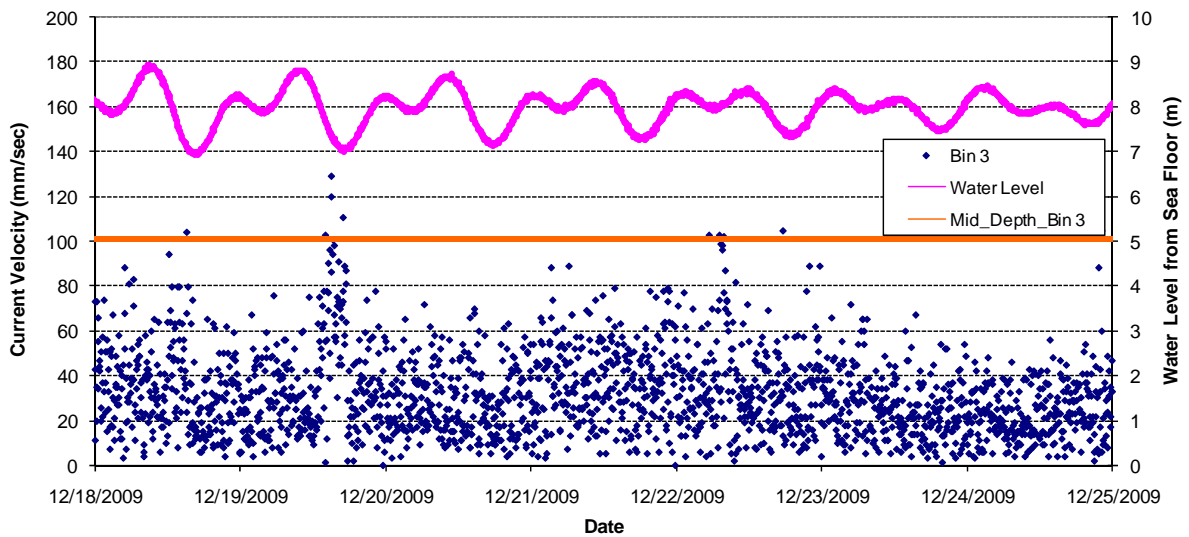
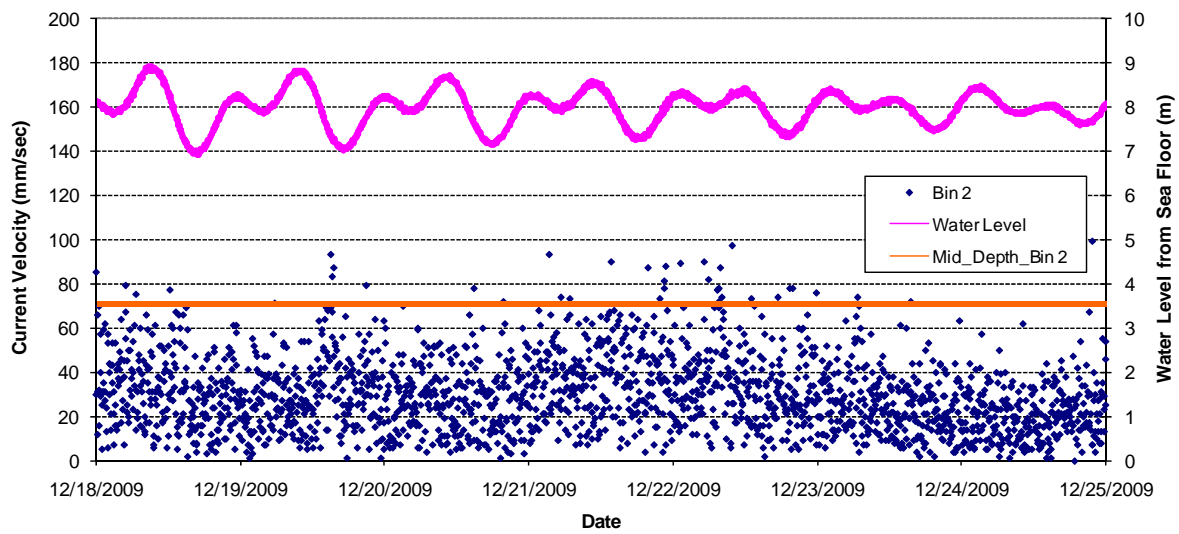
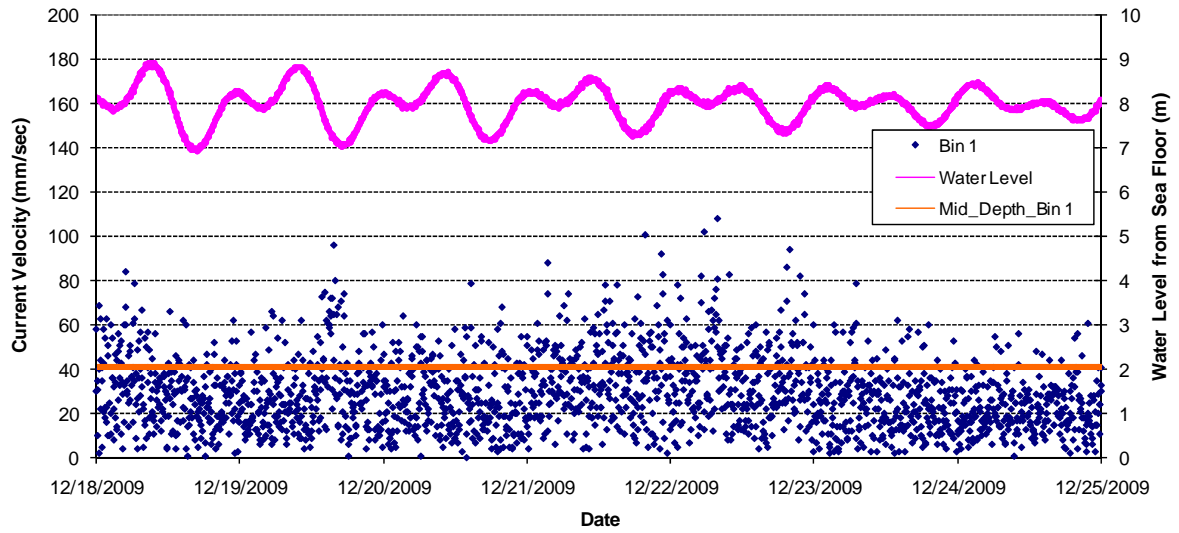
Figure A-35



Week 4 – Bin 4 Measurements at Inside Gage



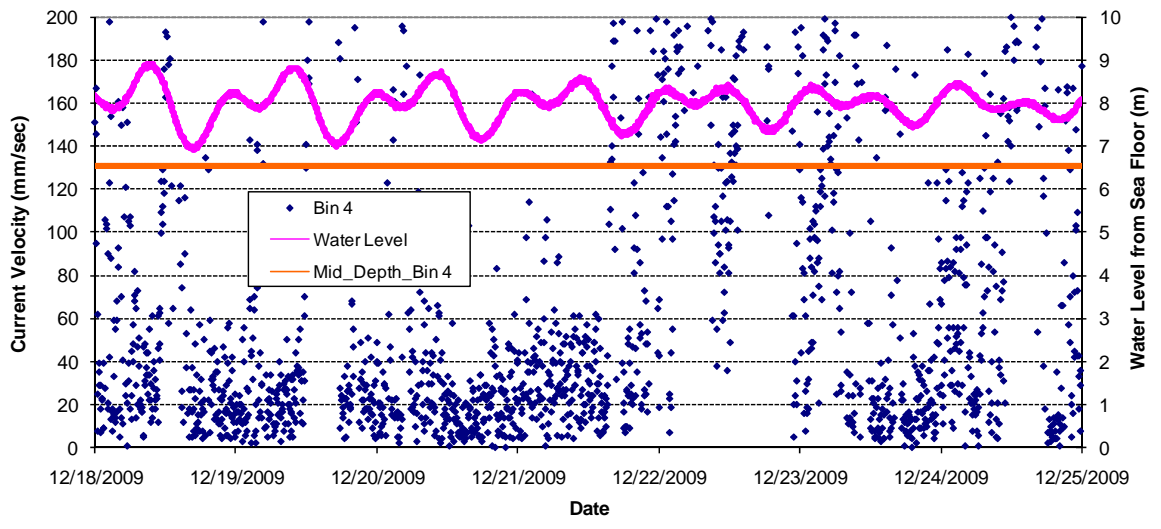
Figure A-36



Week 5 – Bin 1, 2, & 3 Measurements at Inside Gage



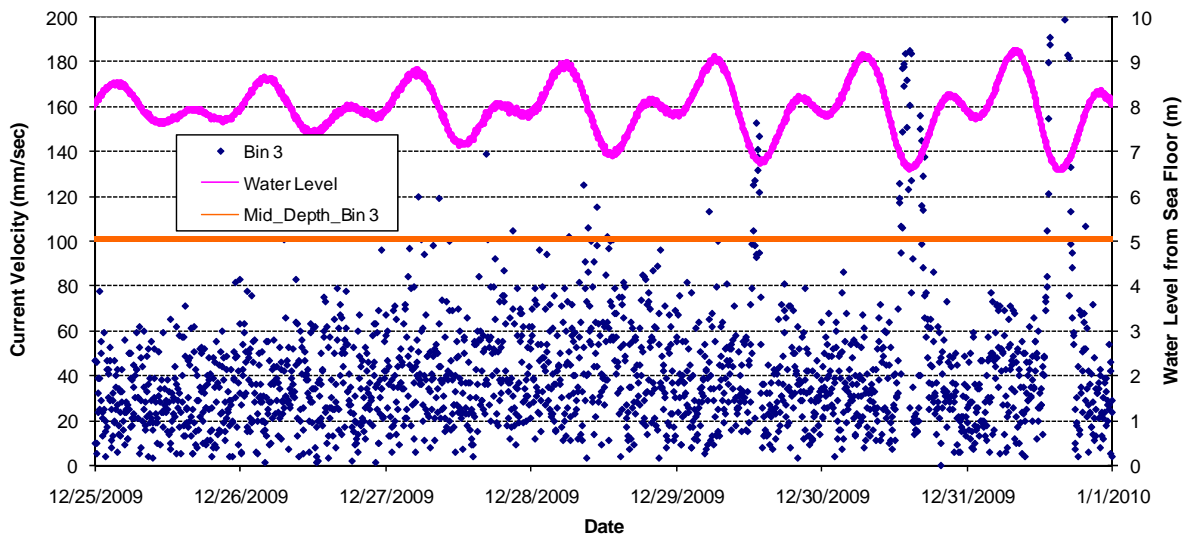
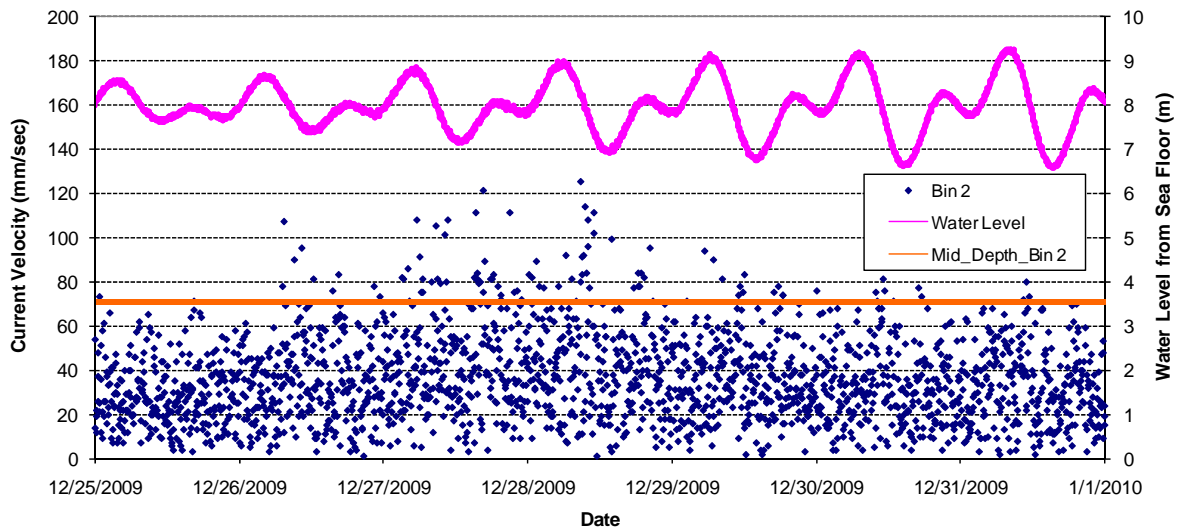
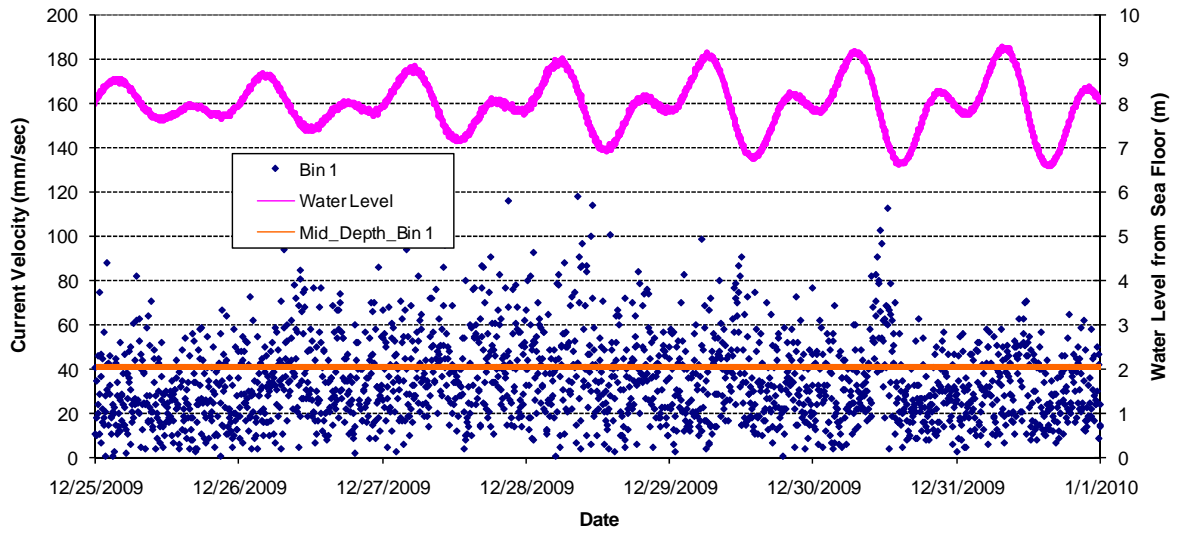
Figure A-37



Week 5 – Bin 4 Measurements at Inside Gage



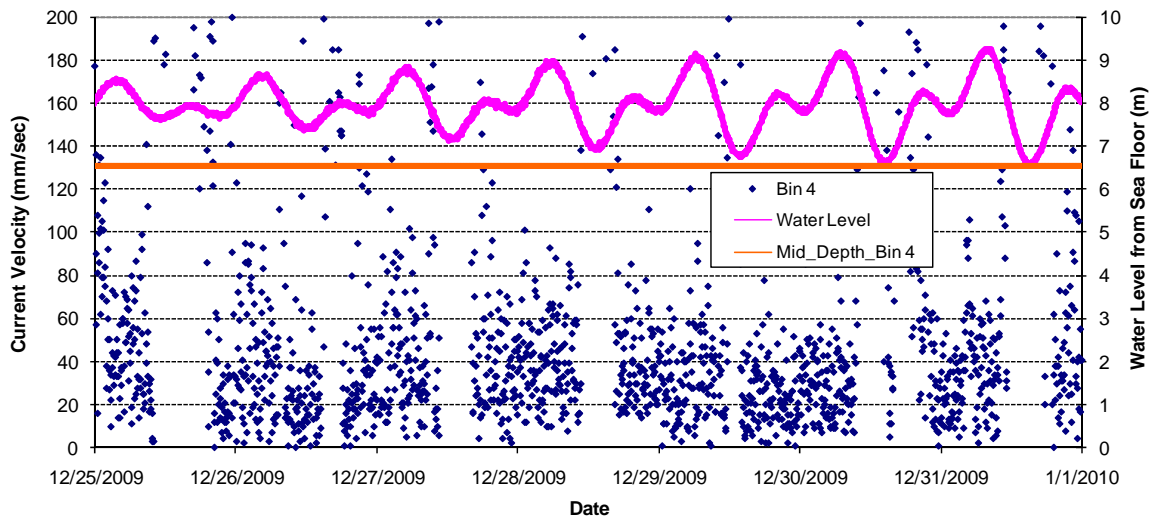
Figure A-38



Week 6 – Bin 1, 2, & 3 Measurements at Inside Gage



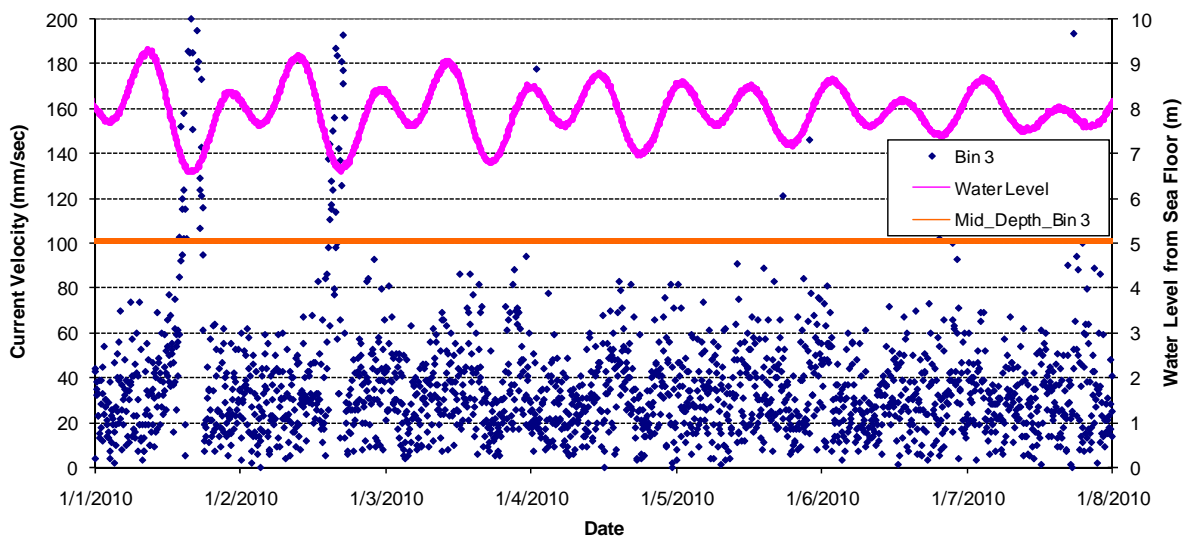
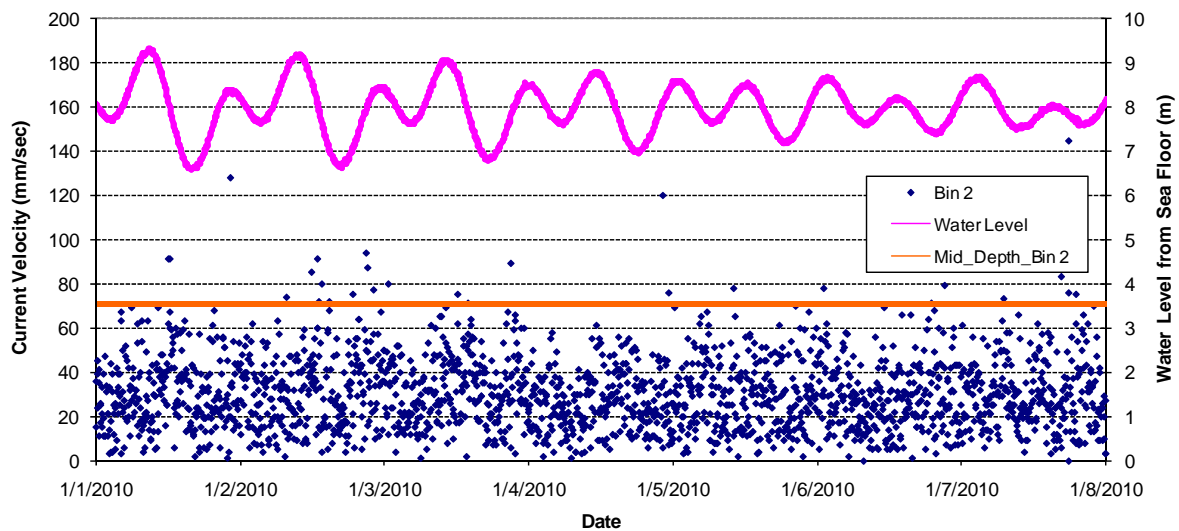
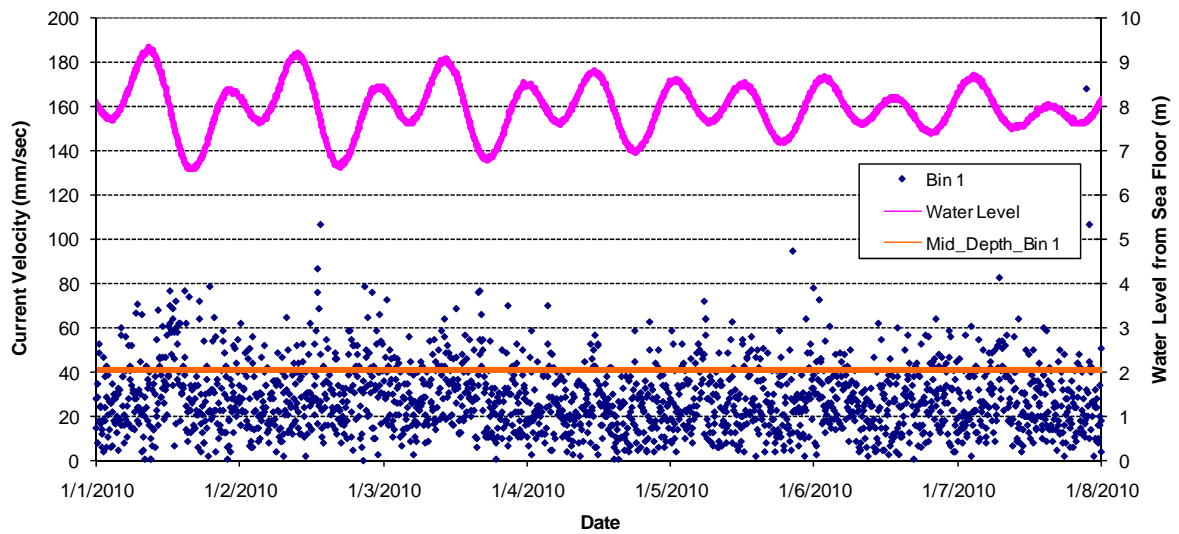
Figure A-39



Week 6 – Bin 4 Measurements at Inside Gage



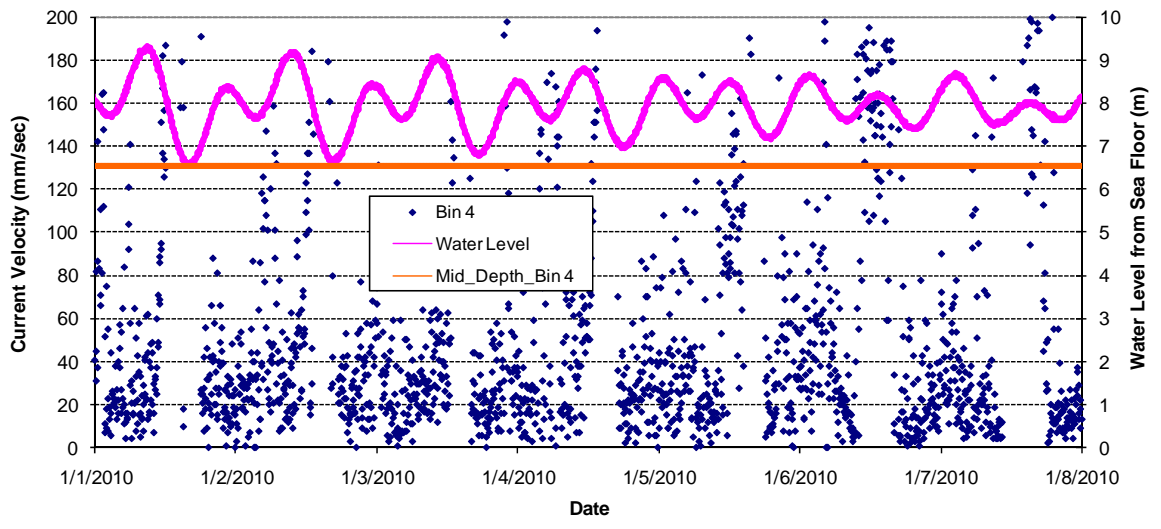
Figure A-40



Week 7 – Bin 1, 2, & 3 Measurements at Inside Gage



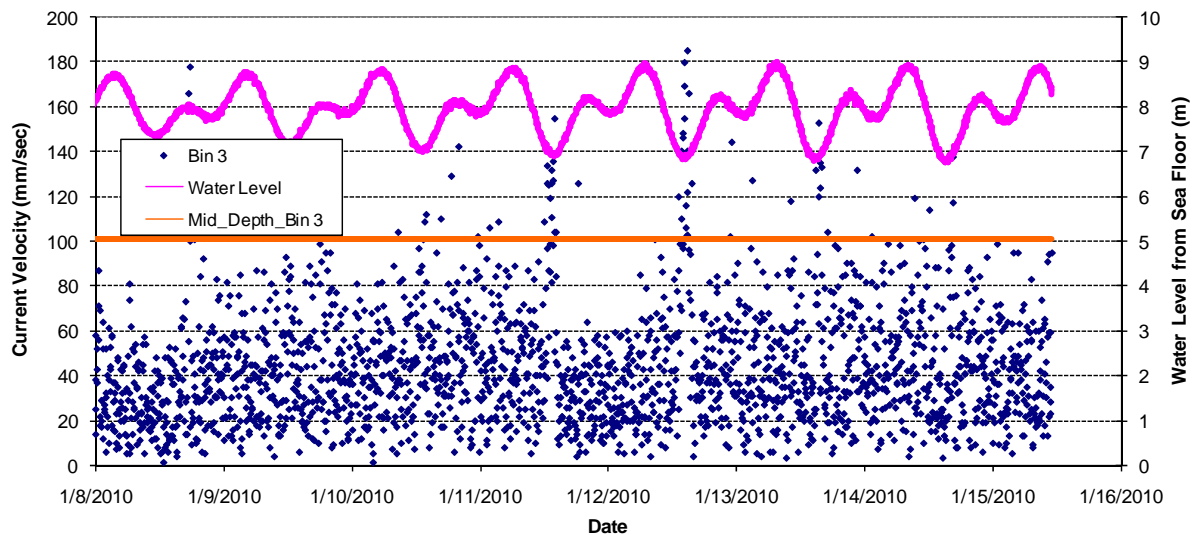
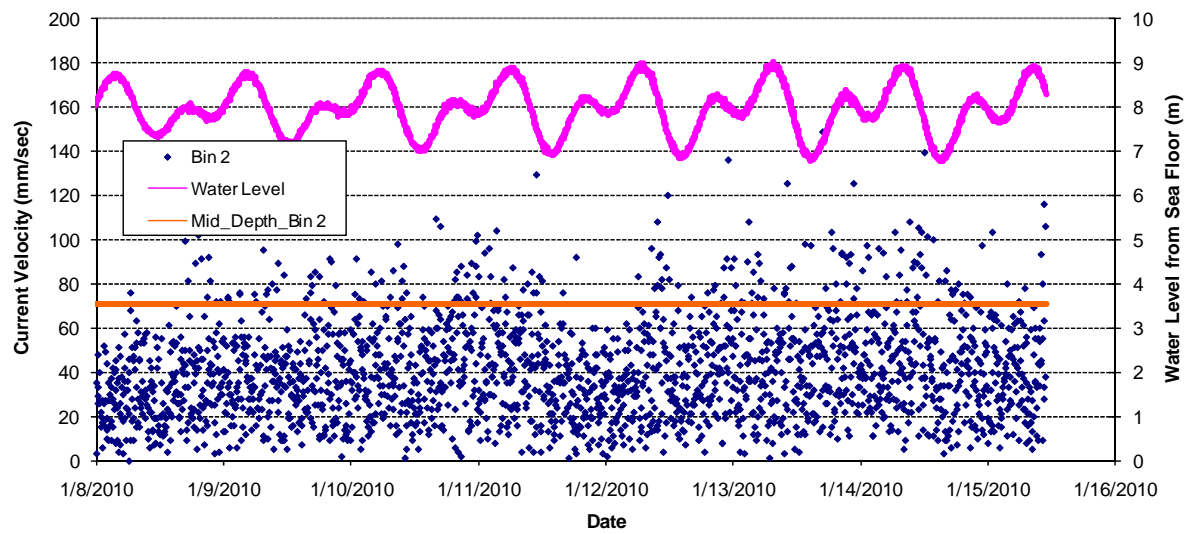
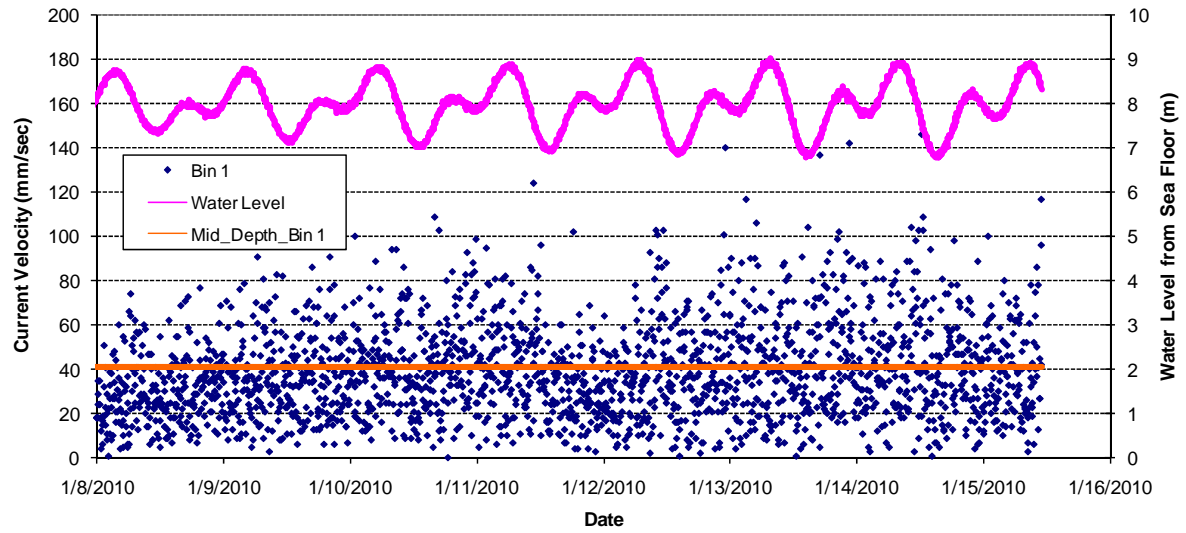
Figure A-41



Week 7 – Bin 4 Measurements at Inside Gage



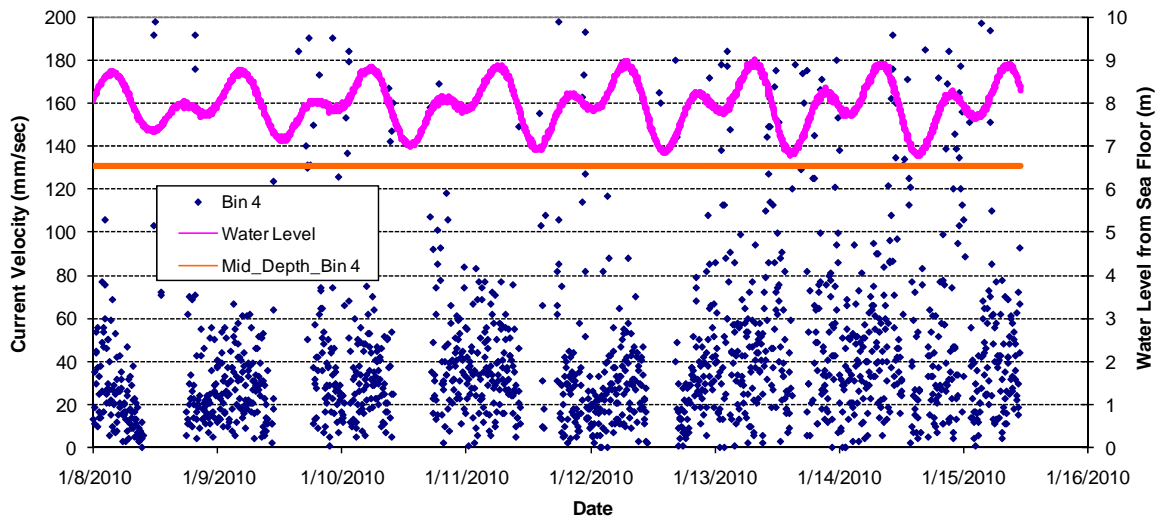
Figure A-42



Week 8 – Bin 1, 2, & 3 Measurements at Inside Gage



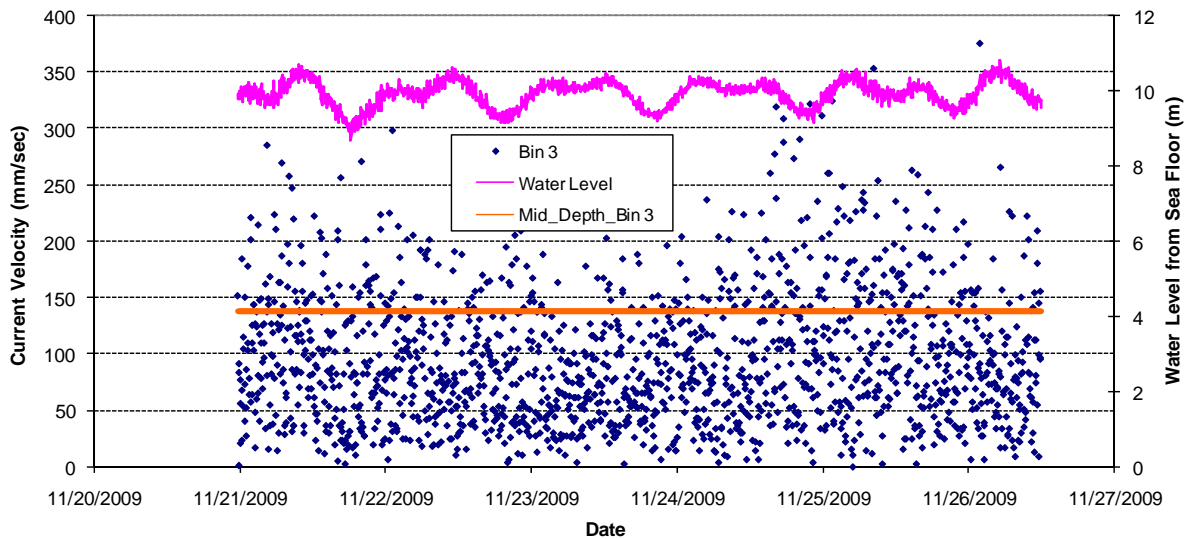
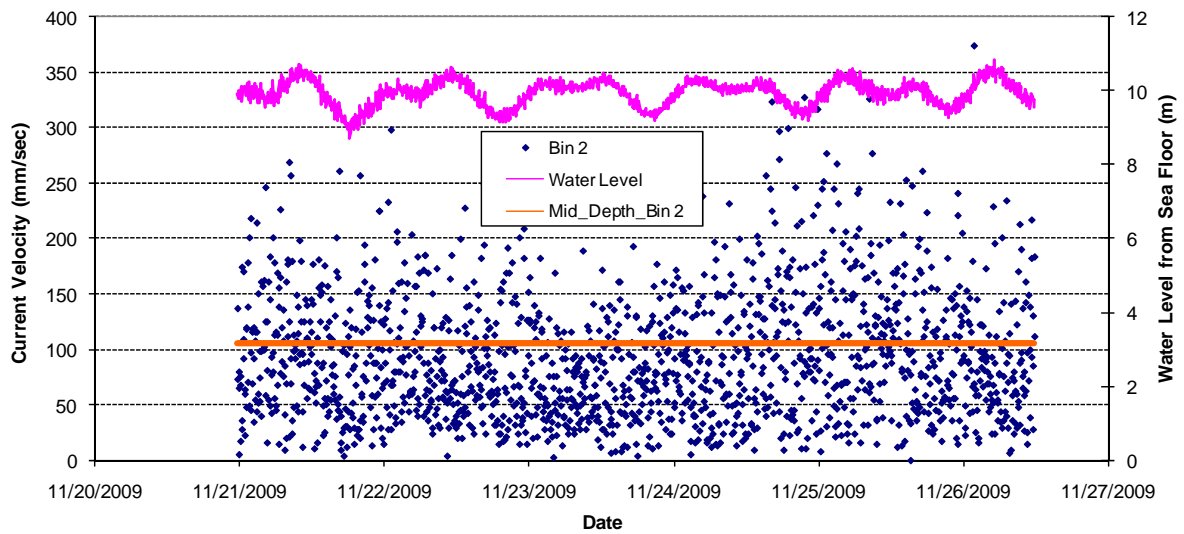
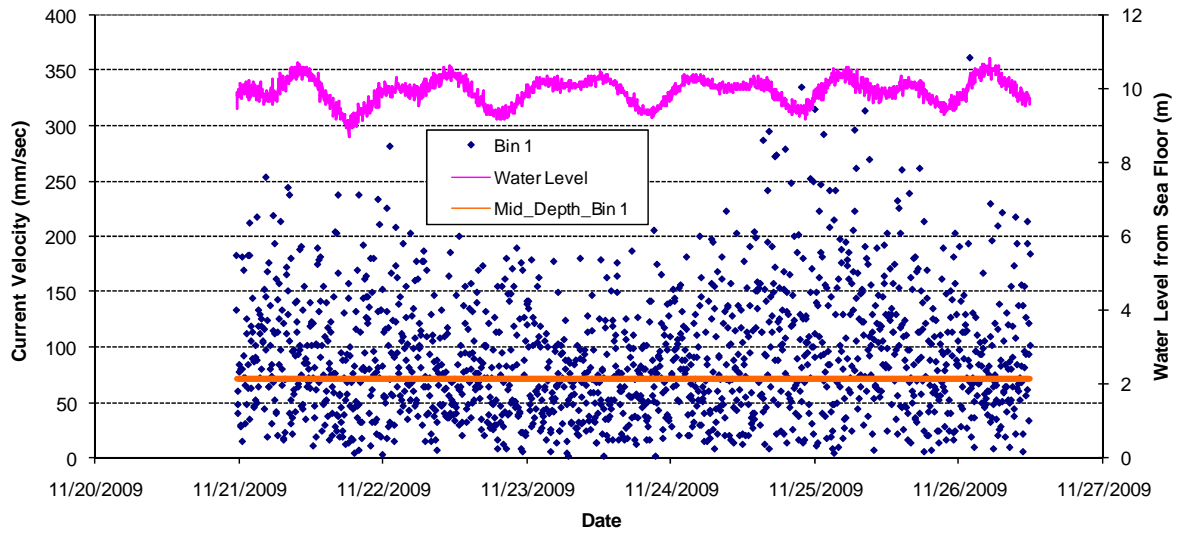
Figure A-43



Week 8 – Bin 4 Measurements at Inside Gage



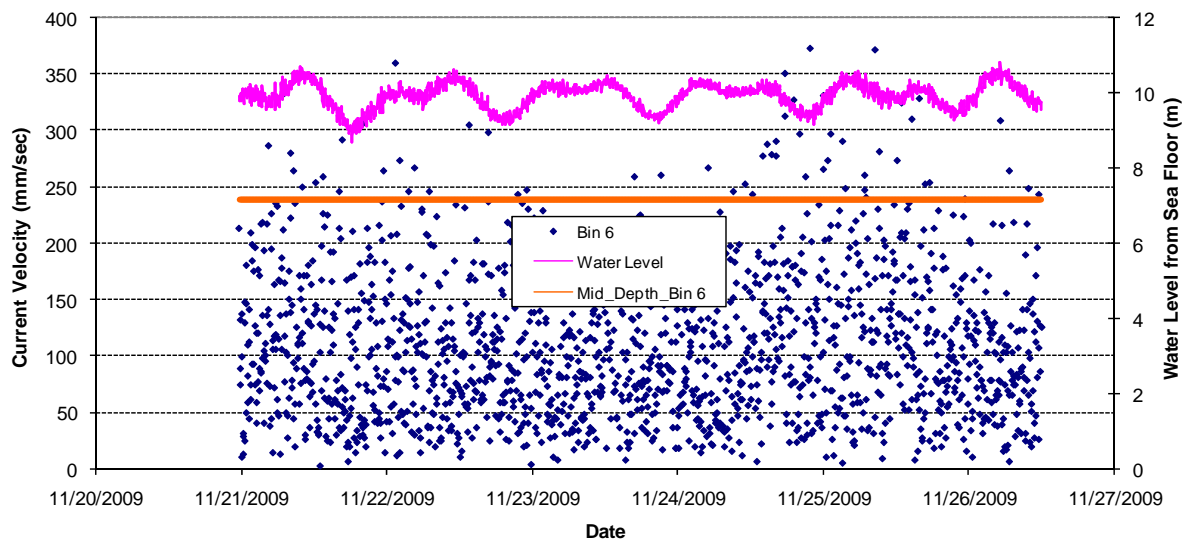
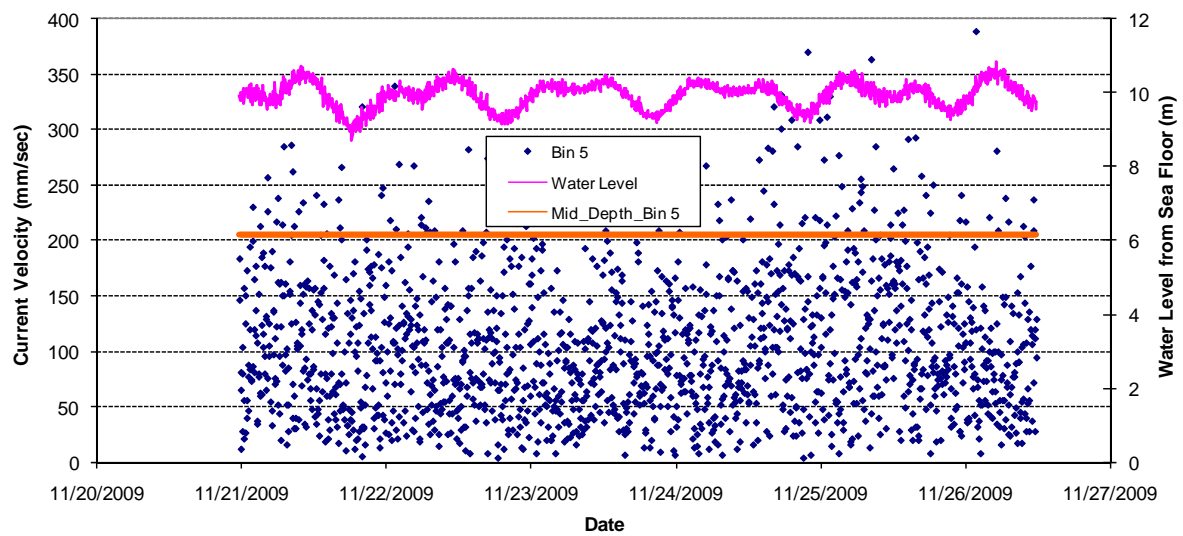
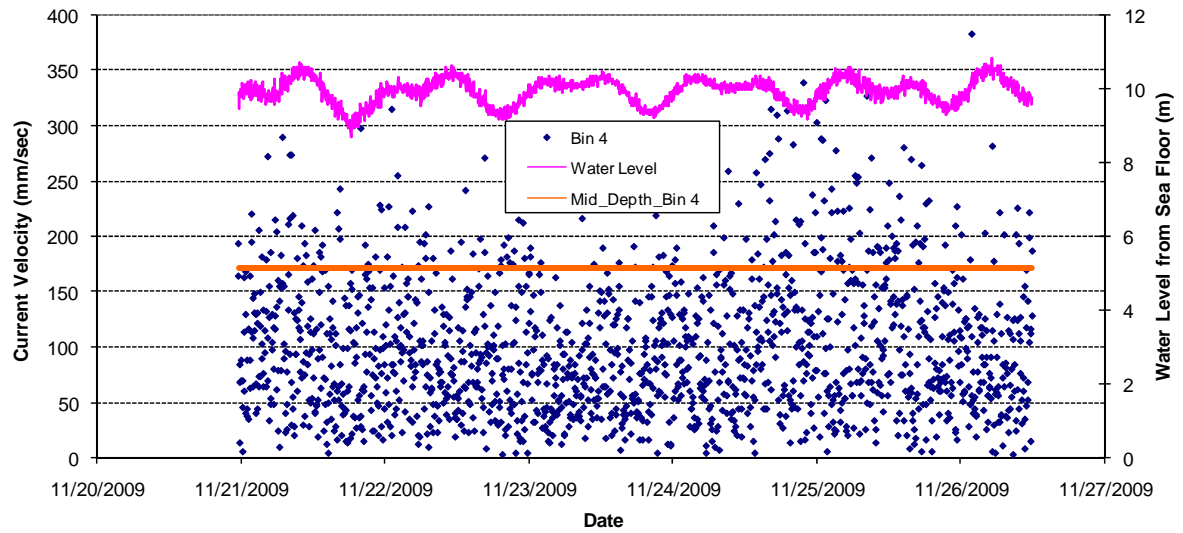
Figure A-44



Week 1 – Bin 1, 2, & 3 Measurements at Outside Gage



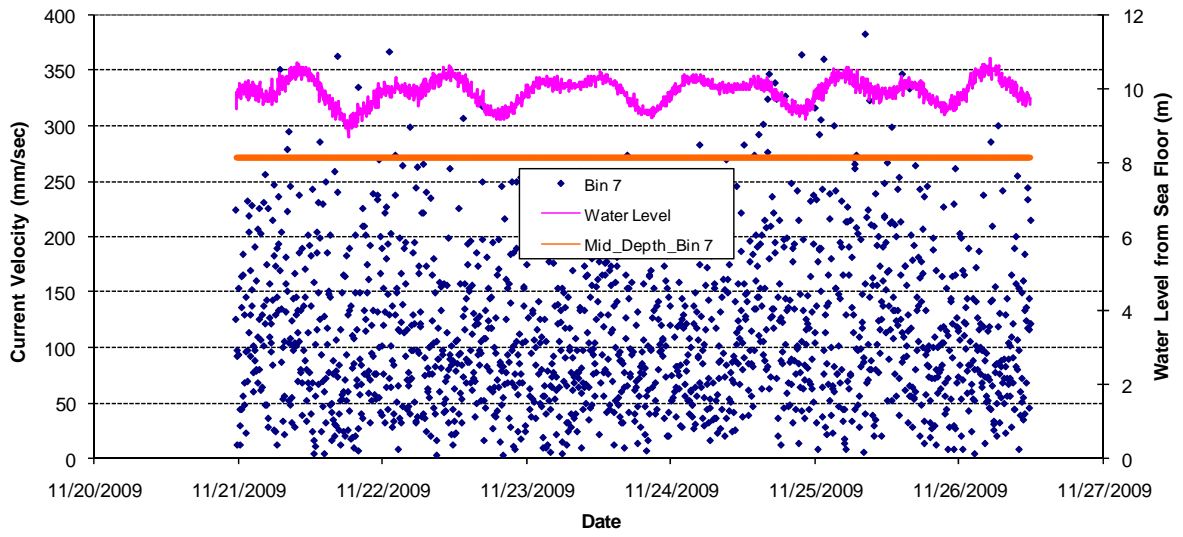
Figure A-45



Week 1 – Bin 4, 5, & 6 Measurements at Outside Gage



Figure A-46



Week 1 – Bin 7 Measurements at Outside Gage



Figure A-47